

Characterizing The Role Of Atrial Natriuretic Peptide Signalling In The Development Of
The Embryonic Ventricular Conduction System

by

Arun Govindapillai

Submitted in partial fulfilment of the requirements
for the degree of Doctor of Philosophy

at

Dalhousie University
Halifax, Nova Scotia
August 2017

© Copyright by Arun Govindapillai, 2017

Dedicated to my parents, Govi and Varatha, my uncle, Dr. Elagu, and my sister, Sindu for their continued support and encouragement.

TABLE OF CONTENTS

LIST OF TABLES	xi
LIST OF FIGURES	xii
ABSTRACT	xix
LIST OF ABBREVIATIONS AND SYMBOLS USED	xx
ACKNOWLEDGEMENTS.....	xxv
CHAPTER 1: INTRODUCTION	1
1.1 Thesis Overview	1
1.2 Embryonic Heart Development	4
1.2.1 Formation of the Primitive Heart Tube	4
1.2.2 Cardiac Cell Gene Programming	7
1.2.3 The Four-Chambered Heart.....	8
1.3 Development of the Cardiac Conduction System	9
1.3.1 Development of the Sinoatrial (SA) Node	12
1.3.2 Development of the Atrioventricular (AV) Node.....	13
1.3.3 Development of the Ventricular Conduction System: The His-Purkinje Network.....	14
1.3.4 Cardiac Action Potentials.....	18
1.4 Notch Signalling and Trabecular Development	20
1.5 Role of Neuregulin-1 in the Development of the Ventricular Conduction System	22

1.6	Role of Endothelin-1 in the Development of the Ventricular Conduction System	25
1.7	Comparative Effects of Neuregulin-1 and Endothelin-1 on the Development of the Ventricular Conduction System	28
1.8	Cardiac Conduction System Markers	30
1.8.1	Role of Cx40 in the Cardiac Conduction System.....	30
1.8.2	Role of HCN4 in the Cardiac Conduction System	33
1.9	Genetic Models Used to Study Development of the Cardiac Conduction System	37
1.10	Cell Lineage Tracking of Nkx2.5+ Myocardial Cells: Cardiac Progenitor Cells	39
1.11	MicroRNAs and Regulation of Cx40 and HCN4 Gene Expression	41
1.11.1	The Functions and Mechanisms of MicroRNAs	41
1.11.2	MicroRNAs Regulating Gene Expression of Cx40 and HCN4	43
1.12	The Genetic Mechanisms of Congenital Heart Diseases	45
1.13	Role of Atrial Natriuretic Peptide in Physiology and Cell Biology	47
1.13.1	Synthesis and Storage of Atrial Natriuretic Peptide	47
1.13.2	Gene Expression and Regulation of Atrial Natriuretic Peptide.....	50
1.13.3	Natriuretic Peptide Receptors	51
1.13.4	Role of Atrial Natriuretic Peptide in Cardiovascular Physiology.....	56
1.13.5	Regulation of Cell Growth and Proliferation by Atrial Natriuretic Peptide.....	58
1.13.6	Role of Atrial Natriuretic Peptide in Cardiac Development.....	60

1.14	The Potential Role of Atrial Natriuretic Peptide in the Development of the Cardiac Conduction System	61
1.15	Characterizing the Specific Roles of Atrial Natriuretic Peptide in Cell Biology: A Paradigm Shift	64
CHAPTER 2: MATERIALS AND METHODS.....		72
2.1	Animal Maintenance and Mouse Strains	72
2.2	Genomic DNA Extraction.....	73
2.3	Genotyping by Polymerase Chain Reaction (PCR)	73
2.4	Timed Pregnancies for Female Mice	77
2.5	Ventricular Cell Cultures.....	77
2.6	Drug Treatments and Dosage Protocols.....	78
2.7	Fluorescence Activated Cell Sorting and Tetramethylrhodamine Methyl Ester Perchlorate Staining	84
2.8	Immune Cytochemistry	84
2.9	Total RNA Extraction from Cells and Tissues.....	87
2.10	RNA Quality Control.....	88
2.11	Real Time Quantitative Polymerase Chain Reaction (RT-qPCR)	88
2.12	MicroRNA Analysis.....	92
2.13	Cx40 ^{egfp} Whole Embryo Culture and Imaging	94
2.14	Second Messenger Assays: cGMP and cAMP	96

2.15	Measurement of Cell Size	101
2.16	Generation of Cx40 Promoter Construct	101
2.17	Transfections	104
2.18	Secrete-Pair Dual Luminescence Luciferase Assay	105
2.19	Statistical Analysis	106
	CHAPTER 3: CHARACTERIZING THE AUTOCRINE/PARACRINE ROLE OF ATRIAL NTRIURETIC PEPTIDE IN THE DEVELOPMENT OF THE VENTRICULAR CARDIAC CONDUCTION SYSTEM	108
3.1	Background and Hypothesis	108
3.2	Specific Aims	110
3.3	Results	110
3.3.1	Effects of ANP on Percent Distribution of Cells Expressing HCN4 and Cx40 in E11.5 Mouse Ventricular Cells	110
3.3.2	Effects of ANP on Gene Expression of HCN4 and Cx40 in E11.5 Mouse Ventricular Cells.....	127
3.3.3	Effects of ANP and/or A71915 on Intracellular Production of cGMP in Mouse E11.5 Ventricular Cells	134
3.3.4	Determination of the Bioactivity of Exogenously Added ANP in E11.5 Ventricular Cell Cultures	138
3.3.5	Gene Expression of HCN4 and Cx40 in NPRA-KO mice at E14.5.....	140
3.3.6	Effects of ANP on Cx40 reporter gene expression in E11.5 Cx40 ^{egfp} Ventricles	142
3.3.7	Visualization and Quantification of Ventricular Cardiac Conduction System Development in Newborn Mice Lacking NPR-A Using the Cx40 ^{egfp} Mouse Model.....	147

3.3.8	Determining the Effects of ANP on Intracellular cGMP Production in Cardiac Progenitor Cells and Ventricular Cells at E11.5	150
3.3.9	Effects of Exogenous cGMP (8-Br-cGMP) on Gene Expression of HCN4 and Cx40 in Mouse E11.5 Ventricular Cells.....	153
3.3.10	Cardiomyogenic Differentiation is Enhanced in Embryonic Ventricular Cells Treated with 8-Br-cGMP.....	158
3.3.11	Effects of Rp-8-pCPT-cGMPS, a Protein Kinase G Inhibitor, on Gene Expression of HCN4 and Cx40 in E11.5 Ventricular Cells in The Presence and Absence of ANP.....	163
3.3.12	Effects of ANP on MicroRNA Regulation of HCN4 and Cx40 in E11.5 and E14.5 Mouse Ventricular Cells	166
3.3.13	Effects of the NPRA-KO Genotype on MicroRNA Regulation of HCN4 and Cx40 in E14.5 and Neonatal Mouse Heart Tissue	170
CHAPTER 4: CHARACTERIZING THE PHARMACOLOGICAL PROPERTIES OF THE NPR-A ANTAGONIST A71915 IN EMBRYONIC MOUSE VENTRICULAR CELLS		174
4.1	Background and Hypothesis	174
4.2	Specific Aims	175
4.3	Results	175
4.3.1	Generation of Dose-Response Plots for ANP in E11.5 Ventricular Cells.....	175
4.3.2	Generation of Dose-Response Plots for A71915 in E11.5 Ventricular Cells in the Absence of Exogenous ANP.....	178
4.3.3	Effects of A71915 on ANP-Induced cGMP Production in E11.5 Ventricular Cells.....	180
4.3.4	Determining the Type of Antagonism of A71915	182
4.3.5	Effects of A71915 Dosage on ANP-Induced Changes in Ventricular Conduction System Gene Expression	185

4.3.6	Determining the Natriuretic Peptide Receptor Selectivity for A71915	188
CHAPTER 5: CHARACTERIZING THE POTENTIAL FOR SIGNALLING INTERACTIONS BETWEEN ATRIAL NATRIURETIC PEPTIDE, ENDOTHELIN-1, AND NEUREGULIN-1 SIGNALLING PATHWAYS IN THE DEVELOPMENT OF THE VENTRICULAR CONDUCTION SYSTEM.....		193
5.1	Background and Hypothesis	193
5.2	Specific Aims	194
5.3	Results	194
5.3.1	Effects of ET-1 and NRG-1 on Percent Distribution of Cells Expressing HCN4 and Cx40 in E11.5 Ventricular Cultures	194
5.3.2	Effects of ET-1 and NRG-1 on Gene Expression of HCN4 and Cx40 in E11.5 Ventricular Cells	206
5.3.3	Effects of ET-1 and NRG-1 on Intracellular Production of cGMP in E11.5 Mouse Ventricular Cells	228
5.3.4	Comparative Effects of ANP, ET-1 and NRG-1 on Cardiomyocyte Hypertrophy in E11.5 Mouse Ventricular Cells	236
5.3.5	Effects of Rp-8-pCPT-cGMPS on Gene Expression of HCN4 and Cx40 in E11.5 Ventricular Cells in Combination with ET-1 or NRG-1	240
5.3.6	Determining the Luciferase Activity of a Cx40-Promoter Construct Upon Addition of ANP, ET-1, or NRG-1	247
 CHAPTER 6: DISCUSSION		250
6.1	Summary of Results	250
6.2	Characterizing the Role of Atrial Natriuretic Peptide Signalling in the Development of the Embryonic Ventricular Conduction System	251

6.2.1	Context	251
6.2.2	Effects of ANP on Protein and Gene Expression of HCN4, Cx40 and Cardiac Transcription Factors	253
6.2.3	Determination of Natriuretic Peptide Receptor Signalling Mediators Involved in the Regulation of Ventricular Conduction System Specific Marker Gene Expression and Formation of the Ventricular Conduction System	258
6.2.4	Effects of Exogenous ANP on Cell Survival and Growth, Proliferation and Differentiation of Cardiac Progenitor Cells and Cardiomyocytes.....	261
6.2.5	Characterization of the Effects of ANP/NPR-A Signalling on Embryonic Ventricular Conduction System Development using the Cx40 ^{egfp} Mouse Model	264
6.2.6	Post-Transcriptional and Transcriptional Mechanisms Responsible for Changes in HCN4 and Cx40 Gene Expression in Response to Modulation of the ANP/NPR-A Signalling Pathway	266
6.3	Characterizing the Pharmacological Properties of the NPR-A Antagonist A71915.....	270
6.3.1	Context	270
6.3.2	Determining the Antagonistic Nature of A71915	271
6.4	Characterizing the Potential for Signalling Interactions Between ANP, ET-1 and NRG-1 Signalling Systems in the Development of the Ventricular Conduction System	273
6.4.1	Context	274
6.4.2	Characterizing the Potential for Signalling Interactions Between ANP, ET-1 and NRG-1 Signalling Systems by Examining Changes to HCN4/Cx40 Protein and Gene Expression and Intracellular cGMP Production	277
6.4.3	Effects of ET-1 and NRG-1 on Cardiomyocyte Cell Growth/Hypertrophy in the Embryonic Heart.....	285

6.5	Clinical Significance	286
6.6	Limitations and Future Directions	292
6.7	Conclusions.....	293
	REFERENCES	294
	APPENDIX I: Copyright permissions for Figure 1.1.....	318
	APPENDIX II: Copyright permissions for Figure 1.2.....	321
	APPENDIX III: Copyright permissions for Figure 1.3.....	323
	APPENDIX IV: Copyright permissions for Figure 1.4.....	324
	APPENDIX V: Copyright permissions for Figure 1.7.....	325

LIST OF TABLES

Table 1.1:	Summary of the reported biological effects of exogenous ANP on cardiovascular cell types.....	67
Table 1.2:	Reported concentrations of ANP in the circulation (plasma or serum) in different species and different developmental stages vs. concentrations of ANP measured from organs (tissue)	68
Table 1.3:	Summary of reported biological effects of exogenous ANP on non-cardiovascular cell types	70
Table 2.1:	List of primers utilized for genotyping and their expected band sizes	75
Table 2.2:	List of primary antibodies and corresponding dilutions used For immune cytochemistry experiments.....	86
Table 2.3:	List of primers and corresponding primer sequences for real time quantitative PCR experiments and expected amplicon sizes.....	91

LIST OF FIGURES

Figure 1.1	Schematic diagram depicting development of the embryonic mouse heart	6
Figure 1.2	Development of the cardiac conduction system in the embryonic mouse heart	11
Figure 1.3	First heart field and second heart field progenitor cells contribute toward formation of the ventricular cardiac conduction system in the embryonic mouse heart	17
Figure 1.4	Expression Pattern of Cx40 and HCN4 in the mouse embryonic heart at E14.5	36
Figure 1.5	Structure and processing of the paracrine factor, atrial natriuretic peptide	49
Figure 1.6	Structures of natriuretic peptide receptors and binding affinities for natriuretic peptides	55
Figure 1.7	Model depicting potential signalling interactions of three paracrine factors: atrial natriuretic peptide, neuregulin-1, and endothelin-1, and their cognate receptors to induce formation of the ventricular cardiac conduction system within the ventricular trabecular myocardium of the mouse embryonic heart	63
Figure 1.8	Primary sequences of species expressing biologically active atrial natriuretic peptide and structure of NPR-A inhibitor A71915	71
Figure 2.1	Expected band sizes (bp) from the genotyping of various mouse strains.....	76
Figure 2.2	Dosing protocol for addition of exogenous ANP and/or A71915 in primary and embryonic cell cultures.....	83
Figure 2.3	Schematic diagram depicting the principle behind the second messenger competitive immunoassays for cGMP and cAMP	100
Figure 2.4	Schematic depicting sequence of mouse Cx40 promoter construct.....	103

Figure 3.1	Expression of HCN4 protein in E11.5 mouse ventricular cells following addition of exogenous ANP treatment (1000 ng/ml) over 48 hours.....	117
Figure 3.2	Percentage of HCN4+/MF20+ and HCN4+/MF20- cells in E11.5 mouse ventricular cells following addition of exogenous ANP	118
Figure 3.3	Calculated ratios of HCN4+/MF20+ cells to HCN4+/MF20- cells in E11.5 mouse ventricular cells following addition of exogenous ANP treatment	119
Figure 3.4	Number of Hoechst stained nuclei per field and number of MF20+ cells per field in E11.5 cells immunolabelled with anti-HCN4 antibody following addition of exogenous ANP	120
Figure 3.5	Expression of Cx40 protein in E11.5 mouse ventricular cells following addition of exogenous ANP (0, 10, 100 and 1000 ng/ml)	121
Figure 3.6	Percentage of Cx40+/MF20+ and Cx40+/MF20- cells in E11.5 mouse ventricular cells following addition of exogenous ANP	122
Figure 3.7	Calculated ratio of Cx40+/MF20+ cells to Cx40+/MF20- cells in E11.5 mouse ventricular cells following addition of exogenous ANP	123
Figure 3.8	Number of Hoechst stained nuclei per field and number of MF20+ cells per field in E11.5 cells immunolabelled with anti-Cx40 antibody following addition of exogenous ANP	124
Figure 3.9	Comparison of HCN4+/MF20+ cell percentages in ventricular cell cultures from various developmental stages following addition of exogenous ANP	125
Figure 3.10	Comparison of Cx40+/MF20+ cell percentages in ventricular cell cultures from various developmental stages following addition of exogenous ANP	126
Figure 3.11	RT-qPCR analysis of HCN4 and Cx40 gene expression in E11.5 mouse ventricular cells following addition of exogenous ANP (1000 ng/ml), and in the presence of an NPR-A inhibitor (A71915) over 48 hours	130
Figure 3.12	Comparison of HCN4 gene expression changes across embryonic	

	stages of heart development upon addition of exogenous ANP and/or A71915 over 48 hours	131
Figure 3.13	Comparison of Cx40 gene expression changes across embryonic stages of heart development upon addition of exogenous ANP and/or A71915 over 48 hours	132
Figure 3.14	RT-qPCR analysis of various cardiac transcription factors in E11.5 mouse ventricular cells following addition of exogenous ANP (1000 ng/ml) over 48 hours	133
Figure 3.15	Generation of the standard curve for cGMP	136
Figure 3.16	The effects of exogenous ANP and A71915 on cGMP production in E11.5 ventricular cells.....	137
Figure 3.17	Determination of the bioactivity of exogenous ANP (1000 ng/ml) upon addition to E11.5 ventricular cells.....	139
Figure 3.18	Gene expression of HCN4 and Cx40 in NPR-A-KO mice in E14.5 stage ventricles	141
Figure 3.19	Visualization of EGFP fluorescence in Cx40 ^{egfp+/-} (heterozygous) whole embryos cultured in the presence or absence of ANP	144
Figure 3.20	Visualization of EGFP fluorescence in Cx40 ^{egfp+/-} (heterozygous) whole hearts treated with ANP and/or A71915 for 24 hours, at E11.5.....	145
Figure 3.21	Quantification of green pixels (%) to determine reporter gene expression in Cx40 ^{egfp+/-} ventricles at E11.5 treated with ANP and/or A71915	146
Figure 3.22	Quantification of ventricular conduction system development in neonate day 1 hearts of wild-type and NPR-A-KO ^{+/-} mice using Cx40 ^{egfp+} approach.....	149
Figure 3.23	The effects of exogenous ANP on intracellular cGMP production in cardiac progenitor cells and ventricular cardiomyocytes at E11.5.....	152
Figure 3.24	Effects of exogenous addition of 8-Br-cGMP on gene expression of Cx40 and HCN4 in E11.5 ventricular cells.....	155
Figure 3.25	Generation of standard curve using 8-Br-cGMP	156

Figure 3.26	Intracellular permeability of 8-Br-cGMP in E11.5 ventricular cells	157
Figure 3.27	Conditional activation of the <i>LacZ</i> reporter gene allowing for cells of the Nkx2.5 cell lineage to be genetically labelled	160
Figure 3.28	Cellular differentiation of cardiac progenitor cells is influenced by addition of exogenous cGMP (8-Br-cGMP) in E11.5 Nkx2.5 Cre-Rosa <i>LacZ</i> (NCRL) mouse ventricular cells, as denoted by changes in protein expression obtained via immunofluorescence.....	161
Figure 3.29	Cellular differentiation of cardiomyocytes is influenced by addition of exogenous cGMP (8-Br-cGMP) in E11.5 Nkx2.5 Cre-Rosa <i>LacZ</i> (NCRL) mouse ventricular cells, as denoted by changes in protein expression obtained via immunofluorescence.....	162
Figure 3.30	Effects of protein kinase G inhibitor – Rp-8-pCPT-cGMPS on gene expression of HCN4 and Cx40 in the presence or absence of ANP, in E11.5 ventricular cells.....	165
Figure 3.31	Effects of exogenous ANP (1000 ng/ml) and/or A71915 (1 μ M) on microRNA levels in E11.5 mouse ventricular cells.....	168
Figure 3.32	Effects of exogenous ANP (1000 ng/ml) and/or A71915 (1 μ M) on microRNA levels in E14.5 mouse ventricular cells.....	169
Figure 3.33	Effects of the NPRA-KO genotype on microRNA levels in E14.5 ventricles of NPRA-KO mice.....	172
Figure 3.34	Effects of the NPRA-KO genotype on microRNA levels in neonate (ND1) hearts of NPRA-KO mice.....	173
Figure 4.1	Dose-response for ANP on cGMP production in E11.5 ventricular cells.....	177
Figure 4.2	Dose-response for A71915 on cGMP production in E11.5 ventricular cells	179
Figure 4.3	Dose-response for ANP on cGMP production in E11.5 ventricular cells, using fixed concentrations of A71915 (0.1, 0.5, 1, 2, 5 μ M).....	181
Figure 4.4	Determining the type of antagonism of A71915 through	

	dose-response curves with varying concentrations of ANP (1, 10, 100, 1000 ng/ml) in the absence or presence of A71915 (1 μ M).....	184
Figure 4.5	RT-qPCR analysis of HCN4 gene expression in E11.5 mouse ventricular cells following addition of exogenous ANP (1000 ng/ml) in combination with varying concentrations of A71915 (0.1, 0.5, 1, 2 and 5 μ M) over 48 hours.....	186
Figure 4.6	RT-qPCR analysis of Cx40 gene expression in E11.5 mouse ventricular cells following addition of exogenous ANP (1000 ng/ml) in combination with varying concentrations of A71915 (0.1, 0.5, 1, 2 and 5 μ M) over 48 hours.....	187
Figure 4.7	Determining selectivity of A71915 for NPR-A by measuring changes in cGMP production that occur with partial genetic ablation of the NPR-A receptor (NPR-A-KO ^{+/-}).....	191
Figure 4.8	Determining selectivity of A71915 for NPR-C by measuring changes in cAMP signalling.....	192
Figure 5.1	Expression of HCN4 protein in E11.5 mouse ventricular cells following addition of ET-1 or NRG-1 over 48 hours.....	199
Figure 5.2	Percentage of HCN4+/MF20+ and HCN4+/MF20- cells in E11.5 mouse ventricular cells following addition of ET-1 or NRG-1 over 48 hours.....	200
Figure 5.3	Calculated ratio of HCN4+/MF20+ cells to HCN4+/MF20- cells in E11.5 mouse ventricular cells following addition of ET-1 or NRG-1 over 48 hours	201
Figure 5.4	Expression of Cx40 protein in E11.5 mouse ventricular cells following addition of ET-1 or NRG-1 over 48 hours.....	202
Figure 5.5	Percentage of Cx40+/MF20+ and Cx40+/MF20- cells in E11.5 mouse ventricular cells following addition of ET-1 or NRG-1 over 48 hours.....	203
Figure 5.6	Calculated ratio of Cx40+/MF20+ cells to Cx40+/MF20- cells in E11.5 mouse ventricular cells following addition of ET-1 or NRG-1 over 48 hours.....	204
Figure 5.7	Number of nuclei per field and number of MF20+ cells per	

	field in E11.5 cells immunolabelled with anti-HCN4 or anti-Cx40 antibody following addition of ANP, ET-1 or NRG-1 over 48 hours.....	205
Figure 5.8	RT-qPCR analysis of HCN4 gene expression in E11.5 mouse ventricular cells following addition of ET-1 or NRG-1 over 48 hours.....	218
Figure 5.9	RT-qPCR analysis of HCN4 gene expression in E11.5 mouse ventricular cells following addition of combination treatments of ANP, NRG-1 and/or ET-1 over 48 hours	219
Figure 5.10	RT-qPCR analysis of HCN4 gene expression in E11.5 mouse ventricular cells following addition of ET-1 or NRG-1 in combination with A71915 over 48 hours	220
Figure 5.11	RT-qPCR analysis of Cx40 gene expression in E11.5 mouse ventricular cells following addition of ET-1 or NRG-1 over 48 hours.....	221
Figure 5.12	RT-qPCR analysis of Cx40 gene expression in E11.5 mouse ventricular cells following addition of combination treatments of ANP, NRG-1 and/or ET-1 over 48 hours	222
Figure 5.13	RT-qPCR analysis of Cx40 gene expression in E11.5 mouse ventricular cells following addition of ET-1 or NRG-1 in combination with A71915 over 48 hours	223
Figure 5.14	RT-qPCR analysis of HCN4 gene expression in E11.5 mouse ventricular cells following addition of ErbB receptor antagonist AG1478, and ANP or ET-1 in combination with AG1478, over 48 hours.....	224
Figure 5.15	RT-qPCR analysis of Cx40 gene expression in E11.5 mouse ventricular cells following addition of ErbB receptor antagonist AG1478, and ANP or ET-1 in combination with AG1478, over 48 hours.....	225
Figure 5.16	RT-qPCR analysis of HCN4 gene expression in E11.5 mouse ventricular cells following addition of non-selective ET-1 receptor antagonist PD145065, and ANP or NRG-1 in combination with PD145065, over 48 hours.....	226
Figure 5.17	RT-qPCR analysis of Cx40 gene expression in E11.5 mouse	

	ventricular cells following addition of non-selective ET-1 receptor antagonist PD145065, and ANP or NRG-1 in combination with PD145065, over 48 hours	227
Figure 5.18	The effects of ET-1 on cGMP production in E11.5 ventricular cells	232
Figure 5.19	The effects of NRG-1 on cGMP production in E11.5 ventricular cells	233
Figure 5.20	The effects of AG1478 on cGMP production in E11.5 ventricular cells	234
Figure 5.21	The effects of PD145065 on cGMP production in E11.5 ventricular cells	235
Figure 5.22	Effects of ANP, ET-1, and NRG-1 on cardiac hypertrophy of CMs of E11.5 ventricular cells	239
Figure 5.23	RT-qPCR analysis of HCN4 gene expression in E11.5 mouse ventricular cells following addition of Rp-8-pCPT-cGMPS in combination with ET-1 or NRG-1 over 48 hours.....	245
Figure 5.24	RT-qPCR analysis of Cx40 gene expression in E11.5 mouse ventricular cells following addition of Rp-8-pCPT-cGMPS in combination with ET-1 or NRG-1 over 48 hours.....	246
Figure 5.25	Effects of ANP, ET-1 and NRG-1 on luciferase activity of mouse Cx40-promoter clone in E11.5 ventricular cells.....	249
Figure 6.1	Complex cellular network involving ANP, ET-1 and NRG-1 signalling pathways may be involved in signalling interactions to promote formation and development of the ventricular conduction system in the embryonic mouse heart.....	291

ABSTRACT

Ventricular arrhythmias occur as a result of impairment in the conduction of the electrical impulse in the ventricular conduction system (VCS), and present prominently among the complications encountered by patients with congenital heart disease (CHF) and heart failure. Atrial natriuretic peptide (ANP), a paracrine factor produced and stored in the atria, has been shown to be transiently expressed in the ventricular trabeculae of the embryonic heart, which is the main site for the formation of future components of the VCS. We hypothesized that ANP, along with paracrine factors endothelin-1 (ET-1) and neuregulin-1 (NRG-1), interact in a complex cellular signalling network to guide differentiation of non-conduction system cardiac cell types such as cardiac progenitor cells (CPCs) and/or working cardiomyocytes (CMs) toward a VCS cell lineage, thereby promoting formation and development of the VCS.

The present study examined the potential impact of ANP on formation of the VCS in the embryonic mouse heart and showed that ANP induces protein and gene expression of important VCS markers such as HCN4 and Cx40 *in vitro*, through the natriuretic peptide receptor-A (NPR-A)/cGMP/PKG signal transduction pathway. Genetic ablation of NPR-A revealed significant decreases in VCS marker gene expression and defects in Purkinje fiber arborisation. Additional experiments revealed that the NPR-A antagonist A71915 behaves as a competitive antagonist at a specific concentration in E11.5 mouse ventricular cells. Lastly, this study provides evidence that the ANP, ET-1, and NRG-1 signalling systems interact in a cooperative manner to induce development of the VCS in the embryonic mouse heart.

Results from this thesis provide new insights into the molecular mechanisms that guide development of the VCS, specifically the potential role of ANP and the complex interplay between ANP, ET-1, and/or NRG-1 signalling pathways in the formation of the VCS. Collectively, results from these studies may facilitate the development of clinical strategies to aid in the treatment of children and patients born with arrhythmia-associated CHDs.

LIST OF ABBREVIATIONS AND SYMBOLS USED

~	Approximately
Δ	Change
$^{\circ}$	Degree
μ l	Microliter
μ m	Micrometer
μ M	Micromolar
nM	Nanomolar
pM	Picomolar
#	Number
%	Percent
14 C-Phe	[14 C]-phenylalanine
8-Br-cGMP	8-Bromoguanosine 3',5'-cyclic monophosphate sodium salt
AP2	Activating protein 2
ATP	Adenosine triphosphate
AC	Adenylyl cyclase
α	Alpha
ANOVA	Analysis of Variance
Ang II	Angiotensin II
Ab/Am	Antibiotic/antimycotic
ANP	Atrial natriuretic peptide
AS	Atrial septum
AV	Atrioventricular
AVB	Atrioventricular bundle
AVC	Atrioventricular canal
β	Beta
β -gal	β -galactosidase
β -MHC	β -myosin heavy chain
BMP	Bone morphogenetic protein
BSA	Bovine serum albumin
BTAEC	Bovine transformed aortic endothelial cells
Ca^{2+}	Calcium
PKA	cAMP-dependent protein kinase
PKG	cGMP-dependent protein kinase
CCS	Cardiac conduction system
CPC	Cardiac progenitor cell
SCN5A	Cardiac sodium channel $\text{Na}_v1.5$
CM	Cardiomyocyte
C/EBP	CCAAT-enhancer-binding protein
C	Celsius
cGATA-6	Chicken-GATA6
cDNA	Complementary DNA

CHD	Congenital heart disease
CHF	Congestive heart failure
Cx	Connexin
Cntn2	Contactin-2
Cre	Cre-recombinase
cAMP	Cyclic adenosine monophosphate
cGMP	Cyclic guanosine monophosphate
Cha	β -cyclohexyl-alanine
DTic	D-1,2,3,4-tetrahydroisoquinoline-3-carboxylic acid
DNA	Deoxyribonucleic acid
DMF	Dimethyl formamide
DMSO	Dimethyl sulfoxide
ID2	DNA-binding protein inhibitor
dd	Double distilled
NCRL	Double transgenic Nkx2.5-Cre/Rosa-LacZ
Drosha	Drosha RNase III endonuclease
DMEM	Dulbecco's Modified Eagle media
ECG	Electrocardiogram
E	Embryonic day
ES	Embryonic stem
ET-1	Endothelin-1
ECE-1	Endothelin-converting enzyme 1
ET-A	Endothelin receptor type A
ET-B	Endothelin receptor type B
Ednra	Endothelin receptor type A gene
Ednrb	Endothelin receptor type B gene
EGFP	Enhanced green fluorescent protein
Erk	Extracellular signal-regulated kinase
FBS	Fetal bovine serum
FGF	Fibroblast growth factor
FHF	First heart field
FACS	Fluorescence activated cell sorting
I _f	Funny/pacemaker current
GPCRs	G-protein-coupled receptors
Gja	Gap junction-alpha
GATA4	GATA4 transcription factor
GLuc	Gaussia luciferase
rhGGF2	Glial growth factor 2
GAPDH	Glyceraldehyde 3-phosphate dehydrogenase
G _q - α	G _q alpha subunit
g	Gram
Grb	Growth factor receptor-bound protein
GDP	Guanosine diphosphate
GTP	Guanosine triphosphate

GC	Guanylyl cyclase
HEY	Hairy/enhancer-of-split related with YRPW motif protein
EC ₅₀	Half-maximal effective concentration
HAND	Heart and neural crest derivatives-expressed transcript
HFD	High-fat diet
Hopx	Homeodomain-only protein homeobox
HTRF	Homogeneous time resolved fluorescence
Hrs	Hours
hESC	Human embryonic stem cell
HEK293	Human embryonic kidney epithelial cell
HCN4	Potassium/sodium hyperpolarization-activated cyclic nucleotide-gated channel 4
IFT	Inflow tract
G _i	Inhibitory heterotrimeric G-protein
IP3	Inositol triphosphate
IRES	Internal ribosomal entry sequence
IVS	Interventricular septum
Irx	Iroquois-class homeobox factor
ISO	Isoproterenol
k	Kilo
kb	Kilo bases
KO	Knockout
IBMX	3-Isobutyl-1-methylxanthine
LTCC	L-type calcium channel
LA	left atrium
LV	left ventricle
Luc	Luciferase
MAML	Mastermind-like transcriptional coactivator
mRNA	Messenger ribonucleic acid
MRE	Metal responsive element
MV	Mitral valve
microRNA	miRNA
mg	Milligram
ml	Milliliter
mm	Millimeter
minK	Minimal potassium channel subunit
MAPK	Mitogen activated protein kinase
MEK	Mitogen activated protein kinase kinase
M	Molar
mAb	Monoclonal antibodies
MEF	Myocyte enhancer factor
MyBP-C	Myosin binding protein-C
ng	Nanogram
nm	Nanometer

nM	Nanomolar
Nppa/b	Natriuretic peptide precursor A/B gene
NPR	Natriuretic peptide receptor
NPRA-KO	Natriuretic peptide receptor A knockout
ND1	Neonatal day 1
NEP	Nepilysin
NRG-1	Neuregulin-1
NO	Nitric oxide
Nkx2.5	NK2 transcription-factor related, locus 5
NC	Nkx2.5-Cre
NICD	Notch intracellular domain
N	Number
OFT	outflow tract
PBS	Phosphate buffered saline
PI3K	Phosphatidylinositol 3-kinase
PDE	Phosphodiesterase
K	Potassium
K	Potassium chloride
PCR	Polymerase chain reaction
PAS	Primary atrial septum
PHT	Primitive heart tube
P-bodies	Processing bodies
Akt	Protein kinase B
PKC	Protein kinase C
Src	Proto-oncogene tyrosine-protein kinase Src
qPCR	Quantitative polymerase chain reaction
RAN	RAs-related nuclear protein
RbJK	RbJK/CSLSu(H) transcription factor
RT-qPCR	Real time quantitative polymerase chain reaction
RGS2	Regulator of G-protein signalling 2
RLU	Relative light units
RAA	Renin-angiotensin II-aldosterone system
RT	Reverse transcription
RPM	Revolutions per minute
RNA	Ribonucleic acid
RA	Right atrium
RV	Right ventricle
RISC	RNA-induced silencing complex
RL	Rosa- <i>LacZ</i>
SERCA	Sarco/endoplasmic reticulum Ca ²⁺ -ATPase
MF20	Sarcomeric myosin heavy chain
SHF	Second heart field
SEAP	Secreted alkaline phosphatase
ShcA	Shc-transforming protein A/1

Shox	Short stature homeobox
SA	Sinoatrial
sMHC	Slow twitch muscle myosin heavy chain
siRNA	small interfering RNA
Na ⁺	Sodium
NaCl	Sodium chloride
NaOH	Sodium hydroxide
SP1	Specificity protein 1 transcription factor
SEM	Standard error of mean
TMRM	Tetramethylrhodamine methyl ester perchlorate
Tbx	T-box transcription factor
Bry	T-box transcription factor Brachyury
C _T	Threshold cycle
dRN	Threshold fluorescence
X	Times
TGF-β	Transforming Growth Factor-β
TRPC	Ca ²⁺ -permeable transient receptor potential canonical cation channel
TV	Tricuspid valve
U	Unit
USA	United States of America
UTR	Untranslated region
VCS	Ventricular conduction system
v/v	Volume per volume
H ₂ O	Water
w/v	Weight per volume
WT	Wild-type
X-Gal	5-Bromo-4-Chloro-3-Indolyl-β-D-Galactopyranoside

ACKNOWLEDGEMENTS

First and foremost, I would like to thank my PhD supervisor, Dr. Kishore Pasumarthi for his guidance, patience and support throughout my doctoral studies. His passion and dedication for science is admirable, and I enjoyed our lengthy scientific discussions together over the years. I am thankful for his advice, insight and encouragement, and approachability.

I would also like to extend my thanks to all of the members of the Pasumarthi lab, both past and present, for their support and friendship. Special thanks to Dr. Adam Hotchkiss and Dr. Tiam Feridooni who helped me get started in the lab, and to Brittney Allen, who all helped to create memorable moments filled with laughter. Thank you to Dr. Mark Baguma and Sarita Chinni for all of your guidance in the lab. I would like to thank the members of my advisory committee, Dr. Denis Dupre and Dr. George Robertson for their valuable insight, advice and constructive feedback to improve my skills as a scientist. Thank you to the administrative staff in the Department of Pharmacology, Sandi Leaf, Luisa Vaughan, and Cheryl Bailey for all of their assistance over the years. I would also like to express my appreciation to my thesis examining committee, Dr. Keith Brunt, Dr. Scott Grandy, and Dr. Bradley W. Doble for reviewing my thesis work.

I would like to thank my colleagues and friends, for their constant moral support and encouragement throughout my graduate studies. Lastly, I would like to extend my deepest thanks to my father, mother and sister, for their patience and unwavering support throughout my doctoral studies.

CHAPTER 1: INTRODUCTION

1.1 Thesis Overview

In a normal lifespan, the human heart can beat almost 2 billion times, a feat that is only made possible by the cardiac conduction system (CCS). The CCS refers to a complex network of cells within the heart that generates and conducts electrical impulses, enabling rhythmic and coordinated contraction of the heart. Each heartbeat is initiated in the sinoatrial (SA) node, which acts as the intrinsic pacemaker for electrical conduction. The electrical impulse travels as a depolarizing wave through the atrial myocardium before converging at the atrioventricular (AV) node. From the AV node, the electrical impulse travels into the ventricles through the Bundle of His, and then is transmitted through the bifurcating left and right branches of the Bundle of His, which then arborize extensively to form the Purkinje fiber network. The Purkinje fiber network distributes the electrical impulse into the ventricular myocardium. Heart function begins as early as embryogenesis and is essential to supply the embryo with sufficient nutrients and oxygen (Weerd and Christoffels, 2016). The development of the CCS results in coordinated contractions of the heart and allow it to efficiently pump blood to the rest of the body.

Arrhythmias occur as a result of impairment in conduction of the electrical impulse. Arrhythmias present prominently among the complications encountered by patients with congenital heart disease (CHD) and/or heart failure. CHD is the most common type of birth defect, affecting approximately 1-2% of newborns, and is the leading cause of birth defect-related deaths (Khairy and Balaji, 2009). In CHDs, impaired

cardiac function results from structural malformation of the heart and/or components of the CCS during embryonic development, which can in turn lead to the development of life-threatening arrhythmias that require medical or surgical intervention. Although progress has been made to understand the electrophysiological components of the CCS, less is known about the molecular mechanisms governing development of the CCS.

In the past, the paracrine factors endothelin-1 (ET-1) and neuregulin-1 (NRG-1), which are both transiently expressed in the trabeculae of embryonic ventricles, have been shown to play an important role in the development of the CCS in the embryonic chick and mouse hearts respectively (Gourdie et al., 1998; Rentschler et al., 2002). Recent knockout studies involving endothelin receptors (Hua et al., 2014) and species-specific differences related to the ability of ET-1 to induce CCS (Gourdie et al., 1998; Patel and Kos, 2005) suggest that additional factors may be involved in the formation and maturation of CCS. **Atrial natriuretic peptide (ANP), a paracrine factor produced and stored in the atria, has been shown to be transiently expressed in the ventricular trabeculae of the embryonic heart, which is the main site for the formation of future components of the ventricular conduction system (VCS) (i.e. the Purkinje fiber network and bundle branches). However, a definitive role for ANP in the formation of the VCS has yet to be explored.** Since ET-1, NRG-1 and ANP are highly expressed in ventricular trabeculae, there exists a possibility that a complex cellular signalling network involving these three paracrine factors could be guiding the differentiation of non-conduction system cardiac cell types such as cardiac progenitor cells (CPCs) and/or working cardiomyocytes (CMs) toward a VCS cell lineage.

Thus, the first hypothesis addressed in my doctoral work was that ANP induces formation of the cardiac Purkinje fiber network of the VCS in the embryonic mouse heart. Toward this aim, my objectives were, (i) to investigate the potential impact of ANP on protein and gene expression of the important VCS markers, hyperpolarization-activated cyclic nucleotide-gated channel 4 (HCN4) and connexin-40 (Cx40), in embryonic mouse ventricular cells, (ii) to determine if the ANP/NPR-A/cGMP signal transduction pathway was biologically active in the embryonic mouse heart and contributed toward formation and development of the VCS, (iii) to visualize the gross morphology of embryonic ventricles and assess the progress of Purkinje fiber formation in the absence or presence of ANP or with genetic ablation of the cognate receptor for ANP, natriuretic peptide receptor-A (NPR-A), (iv) to determine the effects of ANP and the NPR-A knockout (KO) genotype on microRNA (miRNA) regulation of HCN4 and Cx40 mRNA expression in embryonic ventricular tissue and cells, and (v) to determine if the second messenger cGMP signalling could impact differentiation of CPCs and/or CMs in the embryonic mouse heart.

The second hypothesis addressed in my doctoral work was that the NPR-A antagonist A71915 may behave as an inverse agonist and/or a competitive antagonist in a dose dependent manner in embryonic mouse ventricular cells. Toward this aim, my main objective was to characterize the pharmacological properties of the NPR-A antagonist A71915 in embryonic mouse ventricular cells by generating (i) dose-response plots for ANP in the presence or absence of varying concentrations of A71915 (ii) dose-response plots for A71915 alone by measuring endogenous cGMP in embryonic day 11.5

(E11.5) ventricular mouse cells, and (iii) by determining the type of antagonistic behaviour of the A71915 compound.

The third hypothesis addressed in my doctoral work was that the three distinct signalling systems of ANP, NRG-1, and ET-1, interact in a cooperative manner, to form a complex cellular signalling network that guides the development of the VCS in the embryonic mouse heart. To address this aim, my objectives were (i) to investigate the potential impact of ET-1 and NRG-1 on protein and gene expression of the important VCS markers, HCN4 and Cx40, in embryonic mouse ventricular cells, (ii) to determine if ET-1 and/or NRG-1 signalling pathways involve the second messenger molecule cGMP in cell signalling associated with the development of the VCS, and (iii) to determine if exogenous ANP, ET-1, or NRG-1 induce activity of a mouse Cx40-promoter-driven reporter construct.

Results from this thesis provide new insights into the molecular mechanisms that guide development of the cardiac conduction system, specifically the potential role of ANP and the complex interplay between ANP, ET-1 and/or NRG-1 signalling pathways in the formation of the VCS. Results obtained from these studies may facilitate the development of clinical strategies to aid in the treatment of children and patients born with arrhythmias.

1.2 Embryonic Heart Development

1.2.1 Formation of the Primitive Heart Tube

During mouse embryogenesis, the earliest known cardiac cells, referred to as cardiac progenitor cells (CPCs), are present, and are found on each side of the midline in

the mouse epiblast by embryonic day 7 (E7) stage (Tam et al., 1997; Kirby, 2007, **Figure 1.1 A**). Cells from the epiblast migrate through the primitive streak, to form a mesodermal germ layer (Tam et al., 1997). From the primitive streak, mesodermal cardiac precursor cells move both laterally and cranially. The movement of cells in these directions generates bilateral cardiogenic fields in the regions of the anterior lateral plate mesoderm (Kirby, 2007). As more and more cells move from the primitive streak toward the midline and laterally, bilateral fields merge together cranially, to form a structure known as the cardiac crescent at E7.5 (Tam et al., 1997; Kirby, 2007, **Figure 1.1 B**). At E8, the lateral portions of the cardiogenic fields migrate toward the ventral midline, fusing together, and forming the linear heart tube (Tam et al., 1997; **Figure 1.1 C**). Cells from the first heart field (FHF) generate the primitive heart tube (PHT) and cells from the second heart field (SHF) migrate into the heart tube from both sides of the heart to allow the heart to loop (Gessert and Kuhl, 2010, **Figure 1.1 D**). The primitive heart tube is composed of two distinct layers: an outer layer of myocardium, and an inner layer of endothelial cells. During the process of cardiogenesis, the primitive heart tube elongates and expands in order to form the four-chambered heart structure (**Figure 1.1 E-H**). As this developmental process occurs, the heart continues to carry out its function in pumping blood containing oxygen and nutrients to meet the metabolic demands, which continue to increase with development.

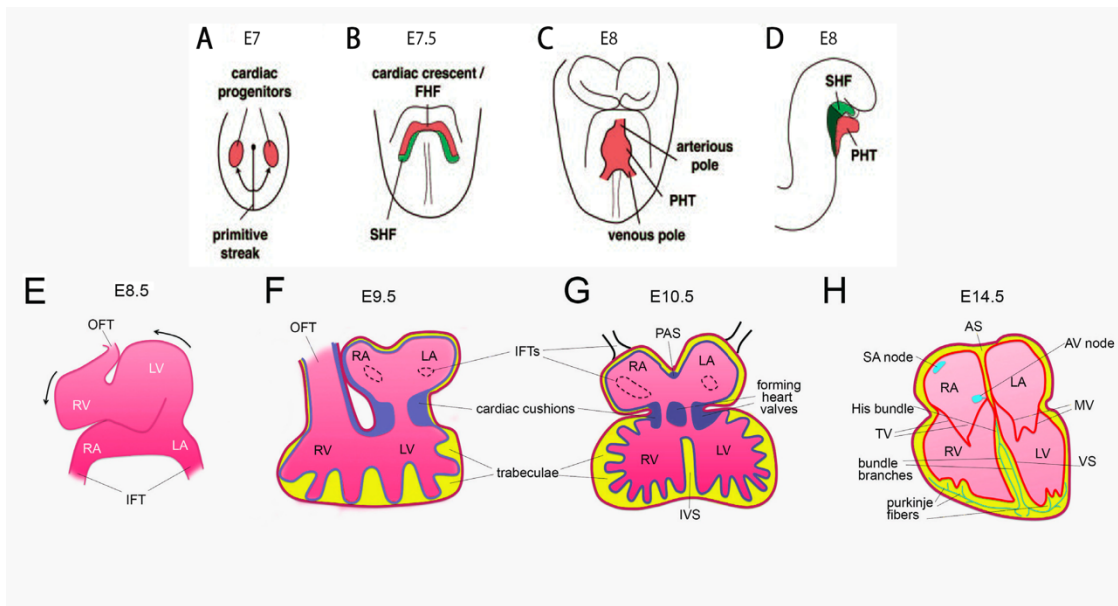


Figure 1.1. Schematic diagram depicting development of the embryonic mouse heart.

A) At E7, cardiac progenitor cells are found on each side of the midline in the epiblast. Cells from the epiblast migrate through the primitive streak to form a mesodermal germ layer. Then, the mesodermal cardiac precursor cells move both cranially and laterally, generating bilateral cardiogenic fields in the regions of the anterior lateral plate mesoderm. **B)** Eventually, bilateral cardiogenic fields merge together to form the cardiac crescent at E7.5. **C)** At E8, the linear heart tube is formed when the lateral portions of the cardiogenic fields migrate toward the ventral line, fusing together. **D)** Cells originating from the FHF generate the primitive heart tube (PHT) while SHF cells contribute toward looping of the heart. **E)** The linear heart tube begins to balloon and loop. The heart loops to the right (black arrows) as the outflow tract and inflow tract develop from the arterial and venous poles, respectively. **F-H)** Transverse cross-section of the embryonic heart during development. **F)** At E9.5, the heart is composed of the epicardium (pink), myocardium (yellow) and endocardium and cardiac jelly (blue). Through the process of epithelial-mesenchymal transformation, epicardial cells make up the cells of cardiac jelly, which is a thick layer between endocardium and myocardium. **G)** At E10.5, trabeculae begin to develop within the cardiac chambers and the cardiac jelly and endocardium extend into the lumen of the heart to form heart valves. **H)** At E14.5, the heart chambers are formed and are separated by the atrial septum and ventricular septum, along with the mitral valve and tricuspid valve. At this stage, the CCS is half-formed, with the SA node capable of transmitting the electrical impulse to the AV node, then through the Bundle of His and bundle branches to the Purkinje fibers. FHF, first heart field; SHF, second heart field; PHT, primitive heart tube, OFT, outflow tract; IFT, inflow tract; RA, right atrium; RV, right ventricle; LA, left atrium; LV, left ventricle; PAS, primary atrial septum; IVS, interventricular septum; SA, sinoatrial; AV, atrioventricular; AS, atrial septum; TV, tricuspid valve; MV, mitral valve; VS, ventricular septum. Figures adopted from (Fishman and Chien, 1997 and Gessert and Kuhl, 2010) and modified and recoloured minimally with permission from the publishers (see **APPENDIX I**).

1.2.2 Cardiac Cell Gene Programming

Induction of cardiomyogenic cells occurs from the mesodermal cells that have moved through the primitive streak, due to the activity of proteins from the family of transforming growth factor (TGF) β , secreted from the hypoblast (in chick hearts) or from the anterior visceral endoderm (mice) (Chapman et al., 2003). It has been shown that inhibition of the Wnt pathway in cardiogenic mesoderm by factors secreted from the endoderm is essential for heart specification in the anterior mesoderm (Yamaguchi, 2001). Wnt genes encode for a large family of cysteine-rich glycoproteins that are secreted in order to regulate cell behaviours during metazoan embryonic development (Yamaguchi, 2001). Wnt1 receptors transduce signals through the canonical Wnt/ β -catenin pathway, where β -catenin is a transcriptional co-activator that acts as the primary effector for this pathway (Yamaguchi, 2001). By inhibiting this pathway, induction of the mesoderm is tightly regulated.

Following the induction of cardiomyogenic cells from the mesodermal cells, differentiation occurs, which is a process by which cells change morphologically in appearance and begin to specialize in their functions (Kirby, 2007). When cardiomyogenic cells differentiate into CMs, they gain specific morphological properties, including the presence of contractile proteins, transmembrane ion channels and gap junction proteins. The endoderm secretes proteins to enable differentiation of cardiomyogenic cells into CMs, which includes the bone morphogenetic protein (BMP) and fibroblast growth factor (FGF) families (Srivastava and Olson, 2000; Alsan and Schultheiss, 2002). Proteins from these families initiate expression of the transcription

factor Nkx2.5, and other transcription factor families including T-box (Tbx), Iroquois (Irx), GATA, MEF2, and HAND. These transcription factors work collectively to further differentiate CMs by activating the working CM gene programme (Srivastava and Olson, 2000). In order to ensure that the differentiating CMs do not expand outside of the cardiogenic field, Wnt is secreted from the ectoderm (Kirby, 2007).

1.2.3 The Four-Chambered Heart

In the mouse, until E9, the primitive heart tube elongates with the addition of myocytes to the ends of the tube, and the tube itself then undergoes looping to form a “C” shaped structure. This “C” structure contains a broad outer curvature, and a narrow inner curvature (Olson and Srivastava, 1996). As the tube continues to loop, the primordial ventricles become visible and expand outward from the outer curvature (**Figure 1.1 F**). The atrial chambers also begin to expand and develop, bringing the inflow and outflow tracts of the primitive heart tube close to each other (Kirby, 2007). At the same time, as the heart continues to loop and expand, the primordia of the valves and the septa begin to form. The trabeculae, which are sheets of CMs that form muscular ridges and are lined by endocardial cells, begin to form along the inner surface of the ventricles and the interventricular septum, which is also forming at this time (de la Pompa and Epstein, 2012). At E10.5, the four-chambered heart has formed. This is followed by a process known as septation whereby the interventricular septum forms, which is the wall separating the left and right ventricles of the heart (Buckingham et al., 2005; Harvey, 2002; **Figure 1.1 G**).

1.3 Development of the Cardiac Conduction System

The CCS refers to a specialized network of tissues in the heart that is responsible for initiating and coordinating the heart beat (Boyett, 1994; **Figure 1.2**). There are several components of the CCS that play a crucial role in initiating and conducting the electrical impulse throughout the heart, which allows for coordinated contraction of the chambers (Weerd and Christoffels, 2016). The components of the CCS include: the sinoatrial node (SA node, also known as the pacemaker), the atrioventricular node (AV node), and the His-Purkinje system. Specialized pacemaker myocytes in the SA node generate the impulse, which is then rapidly propagated through the atrial myocardium travelling to the AV node, where conduction is slowed down, allowing the atria to contract while also allowing the ventricles to fill, before the ventricles themselves are able to contract (Weerd and Christoffels, 2016). The His-Purkinje system consists of the Bundle of His and a network of Purkinje fibers arising from bundle branches. The purpose of this system is to conduct the impulse to all parts of the ventricles and to ensure that both chambers contract simultaneously (Boyett, 1994). Hence, the His-Purkinje system is frequently referred to as the ventricular conduction system (VCS). Each component of the CCS uses its own distinct set of ion channels, channel-associated proteins, and gap junction proteins or connexins (Mikawa and Hurtado, 2007).

During the early stages of heart development, myocytes can be electrophysiologically characterized as being automatic, in that they are able to spontaneously depolarize. These myocytes conduct the impulse slowly. They are also characterized by their inability to contract adequately, due to their underdeveloped

sarcomeres and sarcoplasmic reticulum (Weerd and Christoffels, 2016). Following elongation of the heart tube, activation of gene expression in myocardial cells allows for proper conduction of the impulse. These include genes encoding for the gap junction proteins connexin 40 and connexin 43 (Cx40 and Cx43) through expression of the Gja5 and Gja1 genes, respectively, and the cardiac sodium channel SCN5A (or Na_v1.5). Additionally, genes encoding for components of the sarcomeres and mitochondria are activated, allowing for CMs to assume a phenotype that is capable of conducting rapid conduction of the impulse and is able to contract sufficiently. In contrast, the components of the CCS begin to develop as genes suppress the CM gene programme in myocytes of the developing sinus venosus and the atrioventricular canal (AVC), which allows for myocytes in these regions to continue to possess automaticity and be able to slowly conduct the impulse (Weerd and Christoffels, 2016). At the same time, the direction of the propagation of the impulse in ventricles changes, from base-to-apex to apex-to-base (Mikawa and Hurtado, 2007).

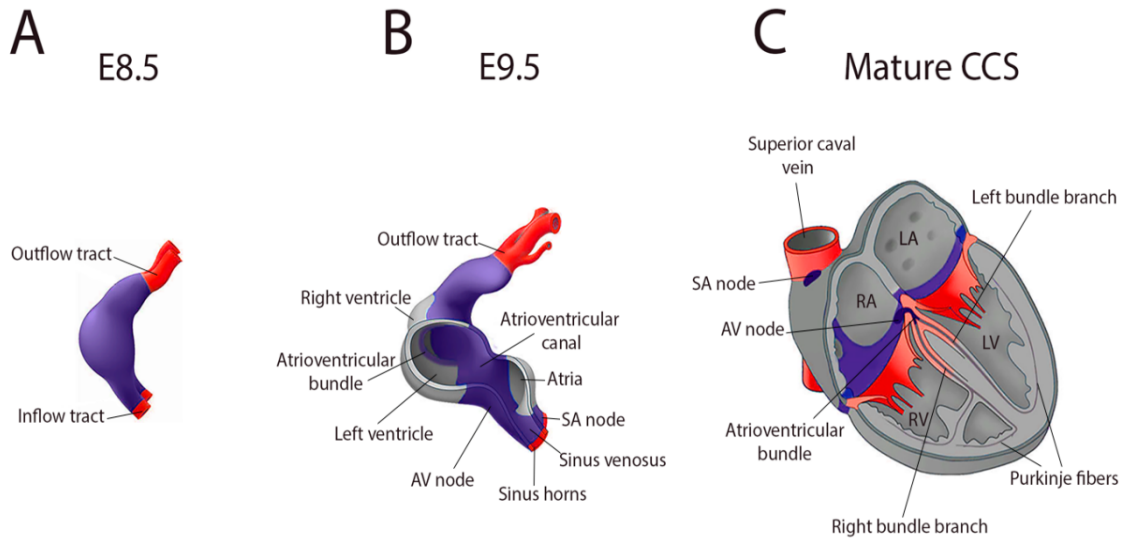


Figure 1.2. Development of the cardiac conduction system in the embryonic mouse heart. **A)** The primitive heart tube is initially formed during folding of the embryo. Myocardial tissue is depicted in purple, whereas non-myocardial tissue in the outflow and inflow tracts regions is depicted in red. **B)** The heart tube elongates through the addition of myocytes to both ends of the heart and begins to loop to form and expand the atrial and ventricular chambers. The SA node develops from the sinus venosus, and the AV node develops from the atrioventricular canal. Ventricular trabeculations give rise to the bundle branches and Purkinje fibers as the heart continues to mature. The myocardium of the chambers is depicted in grey and non-chamber myocardium is depicted in purple. **C)** The mature cardiac conduction system (CCS) is fully formed postnatally, and is composed of specialized CMs called CCS cells that are capable of conducting and propagating the electrical impulse that is necessary for the heart to contract. The SA node generates the electrical impulse, which depolarizes the atria and allows them to contract, and then travels to the AV node. Then, the impulse is propagated through the left and right bifurcating bundle branches and through the Purkinje fibers in order to depolarize the ventricles and allows them to contract. SA, sinoatrial; AV, atrioventricular; RA, right atria; LA, left atria; RV, right ventricle; LV, left ventricle; CM, cardiomyocyte. Figure adopted and minimally modified from (Weerd and Christoffels, 2016) with permission from publishers (see **APPENDIX II**).

1.3.1 Development of the Sinoatrial (SA) Node

The SA node develops from the sinus venosus myocardium in the developing heart and it can be histologically distinguished by the E11.5 stage in embryonic mouse hearts (Viragh and Challice, 1977). The cardiac homeobox transcription factor Nkx2.5 is expressed in the forming heart tube (Komuro and Izumo, 1993), but is largely absent from the developing areas of the SA node gene programme. Between E9-E9.5 and E11.5-E12.5, Nkx2.5⁻ sinus venosus myocardium (Note: Nkx2.5⁻ [minus] indicates lack of transcription factor, whereas Nkx2.5⁺ [plus] indicates presence of transcription factor) is developed from the venous pole of the heart containing the inflow tract, by specialized cells known as Tbx18+/Nkx2.5⁻ progenitor cells (Christoffels et al., 2006). The HCN4 gene is activated in this region of Nkx2.5⁻ sinus venosus myocardium, and is downregulated in the surrounding Nkx2.5⁺ myocardium. (Garcia-Frigola et al., 2003). HCN4 channels elicit the funny current/pacemaker current (I_f), and this current plays an important role in helping conduction cells to establish automaticity (Musso and Vassalle., 1982).

The transcription factor Tbx5 is important in the development of the SA node. Tbx5 is expressed in the sinus venosus and atria during heart development and targets Nkx2.5 to regulate expression of several key regulators of SA node function: short stature homeobox 2 (Shox2), Tbx3, and BMP4 (Mori et al., 2006). Tbx3 is involved in directing the gene expression program of SA node by repressing factors that promote the working myocyte phenotype. Tbx3 suppresses Cx40, Cx43, SCN5A and the natriuretic peptide precursor A and B genes (*Nppa* and *Nppb*).

1.3.2 Development of the Atrioventricular (AV) Node

During heart development, the AVC eventually forms the AV node and AV ring bundles. The AV node can be histologically distinguished by E11.5 in embryonic mouse hearts (Viragh and Challice, 1977). Transcription factors involved in the development of the AVC include BMP2, Tbx2, and Tbx3 (Weerd and Christoffels, 2016). The AVC contains cells that possess a slow conducting phenotype (Weerd and Christoffels, 2016). The AVC has been shown to be originally derived from Tbx2+ cells of the inflow tract (Aanhaanen et al., 2009). Tbx2 and Tbx3 act to repress the expression of factors that are involved in promoting the chamber myocardium gene programme, including suppression of *Nppa*, Cx40 and SCN5A; this allows the AVC/AV node cells to retain the slow conduction phenotype (Weerd and Christoffels, 2016). BMP2 is required for development of the AVC and regulates expression of Tbx2 and Tbx3 (Ma et al., 2005). Tbx20, which is necessary for formation of the heart tube and development of the chambers, is also involved in regulation of the expression of Tbx2, acting to confine activation of Tbx2 to the AVC (Singh et al., 2009). Notch signalling is involved in establishing the boundary between the AVC and the chambers. In the chick heart, within the myocardium, Notch signalling has been shown to activate Hairy/enhancer-of-split related with YRPW motif protein 1 and 2 (HEY1 and HEY2), which in turn suppress BMP2, which then helps to develop the AVC (Rutenberg et al., 2006). It has been shown that inhibition of Notch signalling resulted in underdeveloped AV nodes in mice (Rentschler et al., 2011).

1.3.3 Development of the Ventricular Conduction System: The His-Purkinje Network

The ventricular myocardium conducts the electrical impulse rapidly due to its high expression of Cx40 and SCN5A. The Purkinje fiber network is derived from trabecular myocardium by E14.5 and continues to mature throughout fetal and neonatal stages of heart development (Viragh and Challice, 1982). The trabecular myocardium expresses several factors including Cx40, Iroquois homeobox protein 3 (Irx3), Notch, NRG-1 and its receptor ErbB (de la Pompa and Epstein, 2012). Rentschler et al. (2012) found that activation of Notch in the embryonic ventricular myocardium can promote conversion of CMs to CCS cells with a conduction phenotype. They utilized a CCS reporter mouse line (CCS-*lacZ*) and demonstrated increased expression of CCS marker genes such as Contactin-2 (Cntn2), HCN1 and SCN5A as well as the β -galactosidase (β -gal) reporter gene expression after activation of Notch pathway. The same group determined that administration of NRG-1 to embryonic hearts in this CCS-*lacZ* reporter line resulted in increased β -gal expression (Rentschler et al., 2002), indicating that NRG-1 may be involved in the formation of CCS cells in the mouse heart. It has also been hypothesized that ET-1 may also be involved in the formation of the VCS. In the chick heart, addition of ET-1 was shown to induce CMs to differentiate into Purkinje fiber cells (Gourdie et al., 1998).

A complex transcriptional network consisting of Nkx2.5, Tbx5, Tbx3, Irx3, homeodomain-only protein homeobox (Hopx), and DNA-binding protein inhibitor (ID2) regulate AV bundle, bundle branch, and Purkinje fiber development (Weerd and Christoffels, 2016). Tbx3 plays a similar role in the VCS as in the development of the AVC

and AV node (see Section 1.3.2), by acting to suppress the working myocardium gene programme (by suppressing Cx40 and Cx43), while also stimulating the pacemaker gene programme through induction of HCN4 (Weerd and Christoffels, 2016). Tbx5 is expressed throughout the ventricles, and promotes cells to elicit rapid conduction, through induction of Cx40 and SCN5A.

Retrospective clonal analysis and genetic tracing experiments using the Cx40^{egfp} mouse transgenic model were performed in the embryonic mouse VCS and identified the presence of two different progenitor cell lineages that comprise the VCS (Miquerol et al., 2013). This finding was later validated in a separate mouse model system involving HCN4, using several HCN4 knock-in mouse lines (Liang et al., 2015). One progenitor cell lineage forms the right Purkinje fiber network, and most likely originates from the first heart field (FHF) whereas the other progenitor cell lineage forms the left bundle branch and most likely originates from the second heart field (SHF). Both cell lineages were shown to contribute toward the AV bundle and right bundle branch (Miquerol et al., 2013). Retroviral labeling studies in chick hearts showed that CCS cells originate from two distinct myocardial lineages (Mikawa and Fischman, 1996). Before or during gastrulation, cardiogenic mesodermal cells become a part of either the first or second lineage that will give rise to either the FHF or SHF. The FHF is derived from the first myocardial lineage and is composed of the first myocardial cells to differentiate into the cardiac crescent. Later in development, cells from the FHF will develop into the primitive heart tube, left ventricle, and sections of the atria (Liang et al., 2015). The SHF is derived from the second myocardial lineage, and will give rise to the outflow tract,

right ventricle, and the majority of the atria (Buckingham et al., 2005; Evans et al., 2010; Cai et al., 2003). Thus, there appears to be a dual contribution of FHF and SHF progenitor cells in the development of the VCS (**Figure 1.3**).

Many of the experiments described in this thesis occur at the E11.5 stage of development, since this is when the components of the VCS (bundle branches and Purkinje fibers) have started to form (Viragh and Challice, 1977; Viragh and Challice, 1982). At E11.5, our lab has previously identified a population of undifferentiated cells (CPCs) that exist in the myocardium (Hotchkiss et al., 2015) using a cell tracking method involving the crossing of two knock-in mouse strains: *Nkx2.5-cre* (NC) and *Rosa-LacZ* (RL). It is highly likely that these CPCs, found in the E11.5 myocardium, may give rise to both working CMs and Purkinje cells (McMullen et al., 2009). It has been suggested that the trabecular myocardium houses important myogenic precursors of the cardiac Purkinje fiber network, as well as paracrine factors like ET-1, NRG-1 and their cognate receptors, which are thought to play an important role in recruiting undifferentiated cardiac precursors and other cell types in the heart toward becoming CCS cells (Gourdie et al., 1998; Rentschler et al., 2002; Christoffels and Moorman, 2009).

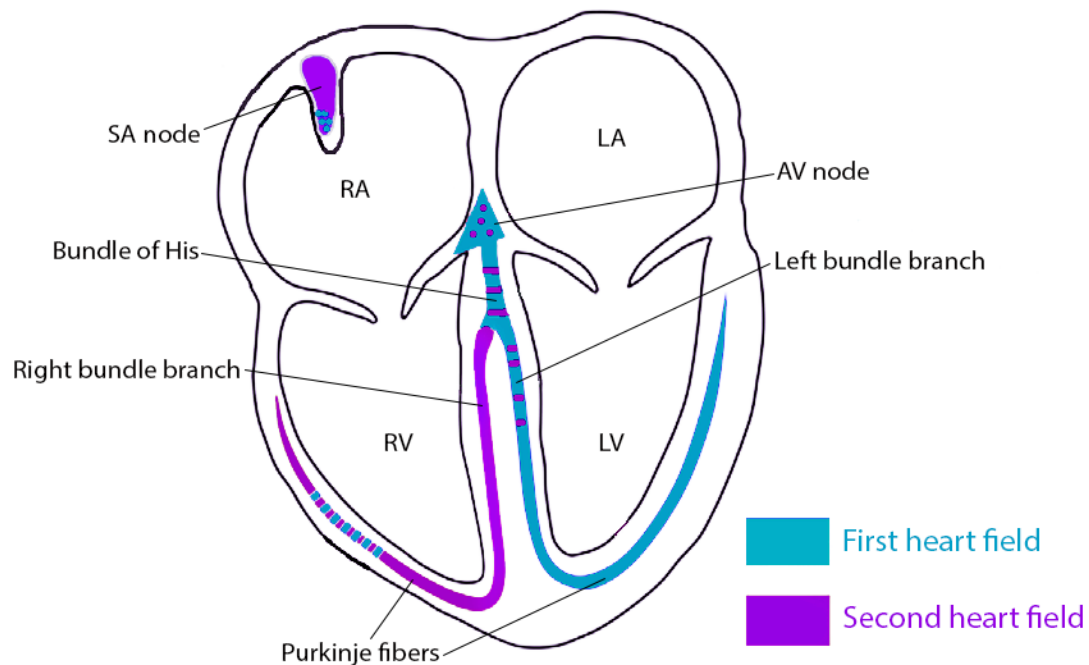


Figure 1.3. First heart field (FHF) and second heart field (SHF) progenitor cells contribute toward formation of the ventricular cardiac conduction system (VCS) in the embryonic mouse heart. Retrospective clonal analysis and genetic tracing experiments using $Cx40^{egfp}$ and HCN4 mouse model systems reveal that two distinct progenitor cell lineages, one from the first heart field (FHF) and the other from the second heart field (SHF), contribute toward development of the VCS in the embryonic mouse heart (Miquerol et al., 2013; Liang et al., 2015). FHF progenitor cells give rise to the atrioventricular (AV) node, Bundle of His, and left VCS (left bundle branch and Purkinje fibers; blue). SHF progenitor cells give rise to the sinoatrial (SA) node and right VCS (right bundle branch and Purkinje fibers; purple). A small subset of cells in the SA node and right Purkinje fibers are derived from the FHF, and a small subset of cells in the AV node, Bundle of His, and left bundle branch are derived from the SHF. SA, sinoatrial; AV, atrioventricular; RA, right atria; LA, left atria; RV, right ventricle; LV, left ventricle; FHF, first heart field; SHF, second heart field. Figure adapted and minimally modified from (Liang et al., 2015) with permission from the publishers (see **APPENDIX III**).

1.3.4 Cardiac Action Potentials

The cardiac action potential is a change in membrane potential across the cell membrane of a cardiac cell caused by the movement of ions into and out of the cardiac cell. Cardiac action potentials propagate through the heart from cell to cell through gap junction proteins (connexins, such as Cx40), in order to trigger excitation-contraction coupling (Boron et al., 2009). There are two types of cardiac action potentials that exist: one for non-nodal cells such as atrial and ventricular cardiomyocytes and Purkinje fiber cells of the VCS, and another for nodal cells such as SA node or AV node cells (Boron et al., 2009). Non-nodal cell action potentials have a resting potential, a rapid depolarization phase, and a prolonged plateau phase and consist of four phases. In Phase 0, rapid depolarization occurs due to the opening of voltage-gated fast Na^+ channels, resulting in rapid upstroke (Boron et al., 2009). In Phase 1, partial repolarization occurs due to the closing of sodium channels and opening of a transient outward K^+ current combined with reduced conductance through the inward rectifier K^+ current. Phase 2 is known as the plateau phase, due to influx of Ca^{2+} through L-type Ca^{2+} channels (LTCCs) as K^+ continues to efflux out of the cell. This phase prolongs the duration of the action potential, distinguishing cardiac action potentials from much shorter action potentials as found in both neurons and skeletal muscle cells (Boron et al., 2009). In Phase 3, repolarization occurs, when LTCCs inactivate and Ca^{2+} influx halts, as K^+ continues to leave the cell through delayed rectifier K^+ currents. In this phase, the fast Na^+ channels, which were inactivated (but open) at the end of Phase 1, now remain in their resting state as closed channels (which can be subsequently activated in the

next action potential cycle). Phase 4 refers to the resting membrane potential which is characterized by a stable membrane voltage at approximately -90 mV. This is due to a balance in the flux of ions leaving the cell (potassium, chloride) and ions entering the cell (sodium, calcium; Boron et al., 2009).

Nodal cell action potentials, as found in SA node and AV node cells, display automaticity or pacemaker activity due to the ability of these cells to spontaneously depolarize. These cells display shorter and slower action potentials than non-nodal cells, and do not have a Phase 1 or Phase 2 (Boron et al., 2009). In Phase 4, spontaneous depolarization occurs due to the presence of I_f currents that provide a slow, inward, depolarization Na^+ current, allowing the nodal cell to depolarize. These currents are generated by HCN channels such as the HCN4 isoform. When the resting membrane potential reaches approximately -50 mV, a second channel is triggered to open, known as transient or T-type Ca^{2+} channels. These channels provide an additional influx of Ca^{2+} to further depolarize the cell, and then triggers opening of LTCCs which further contribute toward Ca^{2+} influx and depolarization (Boron et al., 2009). Together, these channels allow for the threshold voltage to be reached, resulting in the propagation of an action potential. Hyperpolarization in nodal cells is a requirement for HCN channels to activate and elicit the I_f current leading to spontaneous depolarization. In Phase 0, depolarization results due to Ca^{2+} influx from LTCCs, and T-type Ca^{2+} and HCN channels close. This is in contrast to Phase 0 of non-nodal cells, whereby fast sodium channels largely contribute toward the initial upstroke of the action potential. Lastly, Phase 3 or repolarization

occurs when K^+ channels open allowing for K^+ efflux, while LTCCs inactivate and close, decreasing Ca^{2+} influx (Boron et al., 2009).

Within the VCS, Purkinje fiber cells have action potentials that have longer duration than ventricular myocyte action potentials (Dun et al., 2008). Additionally, Purkinje fiber cells display very rapid, maximal upstroke velocities during Phase 0 and can conduct electrical signals faster than all other cardiac tissues (Dun et al., 2008). This is due to the contribution of several sodium currents that are unique to Purkinje fiber conduction (Dun et al., 2008). The cardiac sodium channel isoform known as $Na_v1.5$ elicits a fast sodium current I_{Na} which is exclusive to Purkinje cells and does not exist in nodal cells. There is also a late sodium current (I_{NaL}), which exists in Purkinje fiber cells. Both of these sodium currents are responsible for inducing the rapid upstroke of the action potential in Purkinje fiber cells (Boron et al., 2009).

1.4 Notch Signalling and Trabecular Development

Developing myocardium differentiates into two distinct layers: one being an outer compact zone, while the other is the inner trabecular zone (de la Pompa and Epstein, 2012). This inner trabecular zone continues to become remodeled and becomes the home for components of the VCS (i.e. the His-Purkinje network). Notch signalling plays a vital role in trabecular development (Grego-Bessa et al., 2007). Trabeculae refer to sheets of CMs that form muscular ridges and are lined by endocardial cells (de la Pompa and Epstein, 2012). Early in heart development, as the coronary vessels begin to develop, trabeculae serve as the active zones for CM proliferation and differentiation

(Sedmera et al., 2000). Notch refers to a group of transmembrane receptors (named Notch 1-4 in mammals) that contain an extracellular domain and an intracellular domain (NICD). In the developing embryonic ventricles, Notch1 is highly expressed in the trabecular endocardium and as development continues, Notch1 is highly concentrated at the base of the trabeculae (Grego-Bessa et al., 2007). Membrane-bound ligands that are part of the Delta or Serrate/Jagged families are capable of binding to the extracellular regions of Notch1 (Grego-Bessa et al., 2007). Subsequently, a fragment of the receptor is cleaved by γ -secretase, resulting in release of NICD, which then translocates to the nucleus to bind to the transcription factor RBJK/CSLSu(H) (abbreviated as RBJK). The binding of NICD to RBJK is followed by recruitment of the transcriptional coactivator Mastermind-like (MAML); this complex leads to transcriptional activation of target genes (de la Pompa and Epstein, 2012).

Notch signalling can affect important gene targets found in the trabeculae such as BMP10, NRG-1/ErbB, and EphrinB2/EphB4 (Chen et al., 2004). BMP10 is highly expressed in the trabecular myocardium in order to promote cellular proliferation (Chen et al., 2004). Inactivation of Notch1 resulted in a significant reduction in the activity of BMP10, which was correlated with decreased proliferation of trabecular myocytes (Grego-Bessa et al., 2007). The EphrinB2/EphB4 ligand-receptor complex is necessary for trabecular development. Mutant mice with the Notch1 gene knocked out resulted in a significant reduction in the activity of EphrinB2/EphB4 (Grego-Bessa et al., 2007). NRG-1 is also required for trabeculation. NRG-1 interacts with ErbB2 and ErbB4 receptors in the myocardium and stimulates cellular differentiation and proliferation in the trabeculae

(de la Pompa and Epstein, 2012). NRG-1 is a downstream gene target of Notch signalling. In mutant mice with the Notch1 gene knocked out, the activity of NRG-1 was shown to be reduced (Grego-Bessa et al., 2007). Thus, the activities of EphrinB2/EphB4, NRG-1 and Notch are closely related. Taken together, Notch signalling targets increased activity of NRG-1 and EphrinB2, which promote CM differentiation in the trabeculae, and Notch signalling simultaneously promotes BMP10 activity to induce CM proliferation in the trabeculae (de la Pompa and Epstein, 2012).

1.5 Role of Neuregulin-1 in the Development of the Ventricular Conduction System

Neuregulins refer to a family of growth factors containing an epidermal growth factor-like (EGF-like) domain. In mammals, there have been four identified neuregulin genes: NRG 1-4. Among these genes, NRG-1 is the most studied in the heart since it has been detected both in the embryonic myocardium and in the adult heart and coronary vasculature (Parodi and Kuhn, 2014). The receptors for NRG-1 are known as ErbB receptors, with only ErbB2-4 expressed in the heart. ErbB2 and ErbB4 are expressed in both the pre- and postnatal heart, and are found in both the developing and adult ventricles, whereas ErbB3 is found only in atrioventricular regions of the developing heart (Parodi and Kuhn, 2014). Neuregulins are presented on the cell surface and are then subject to proteolytic cleavage by metalloproteinases. Following their release into the extracellular space, neuregulins are capable of binding to ErbB receptors on target cells (Parodi and Kuhn, 2014).

In the heart, endocardial cells release NRG-1 into the extracellular space, binding to ErbB4 receptors expressed in the myocardium, which then dimerizes with ErbB2 receptors, in order to promote proliferation and differentiation of CMs (Parodi and Kuhn, 2014). In adult CMs, phosphatidylinositol 3-kinase (PI3K), proto-oncogene tyrosine-protein kinase Src (Src), and Shc-transforming protein A/1 (ShcA) are important effector molecules of ErbB2/ErbB4 signalling that regulate proliferation and hypertrophy (Wadugu and Kuhn, 2012). Extracellular signal-regulated kinase (Erk) 1/2 are downstream targets of ErbB receptor stimulation and modulate CM cell growth/hypertrophy and proliferation as well as sarcomeric organization, while Akt acts as another downstream target of ErbB stimulation to prevent apoptosis (Yin et al., 2015). Stimulation of Erk 1/2 by NRG-1 is modulated by growth factor receptor-bound protein 2 and 7 (Grb2 and Grb7) and Snc, which are downstream targets of ErbB2 receptor signalling, and have been shown to play a role in regulating CM hypertrophy (Zhang et al., 2003; Pero et al., 2007; Yoshizumi et al., 2001).

NRG-1/ErbB2/ErbB4 signalling has been shown to be essential for cardiac development. Disruption of the NRG-1 gene or genes of ErbB2 and ErbB4 receptors, led to unexpected death of mice during mid-gestation due to aborted development of the trabeculae in the ventricles of the fetal myocardium. In these mice, the inner trabecular layer of myocardium was found to be very thin (Meyer and Birchmeier, 1995; Gassmann et al., 1995; Lee et al., 1995; Kramer et al., 1996, Marchionni, 1995). NRG-1 may also stimulate the differentiation of CMs from undifferentiated stem cells and progenitor cells, since it was shown that NRG-1 stimulated the generation of CMs from embryonic

stem cell cultures (Sun et al., 2011; Wang et al., 2009; Zhu et al., 2010). Currently, the signalling pathway by which NRG-1 regulates differentiation of various cell types to CMs is not known. Overexpression of NRG-1, ErbB4 or ErbB2 receptors has been shown to promote hyper-trabeculation, leading to ventricular non-compaction, which could potentially lead to the development of congenital heart diseases (Hertig et al., 1999; Stollberger and Finsterer, 2004; Parodi and Kuhn, 2014).

One group utilized a *CCS-lacZ* reporter line in mice to study the effects of exogenous NRG-1 on cultured embryonic hearts isolated from this line (Rentschler et al., 2002). The *CCS-lacZ* reporter line is capable of delineating the entirety of the CCS including the early ventricular trabeculae. Addition of exogenous NRG-1 to these hearts resulted in increased β -gal expression, providing evidence that NRG-1 is capable of stimulating proliferation and/or differentiation of CMs into CCS cells (Rentschler et al., 2002). In this study, addition of exogenous NRG-1 (2.5 nM) induced ectopic *lacZ* expression in E9.5 embryonic hearts vs. no treatment. Additionally, ectopic expression of *lacZ* increased in response to the addition of NRG-1 in a dose-dependent manner, utilizing doses ranging from 25 pM to 2.5 nM (Rentschler et al., 2002). *LacZ* expression was also measured in hearts ranging from E8.5 to E12.5, with *lacZ* expression continuing to increase as the heart matured up until E12.5, whereby *lacZ* expression within the CCS seemed similar in both control and NRG-1 treated E12.5 hearts. Another important finding from this study was that induction by NRG-1 was shown, in embryonic ventricular tissue sections, to not only increase *lacZ* expression but this was also correlated with cells displaying electrophysiological characteristics that were consistent

with tracts of conduction tissue (Patel and Kos, 2005). It was suggested that patterning of the tissue was largely completed by E12.5 (Rentschler et al., 2002). Additionally, the group hypothesized that NRG-1 provided a paracrine signal to induce differentiation of CMs into CCS cells that declined in its paracrine effect as development of the embryo proceeded and as the conduction system became fully mature, since it became difficult to detect differences in *lacZ* expression between control and NRG-1 treated hearts at E12.5 (Rentschler et al., 2002). This raises the possibility that other paracrine factors may be involved in the development of the CCS, in the mid to late stages of embryonic development, where NRG-1 expression begins to decline as the heart continues to mature.

1.6 Role of Endothelin-1 in the Development of the Ventricular Conduction System

The paracrine factor ET-1 was initially discovered to be a potent vasoconstrictor that was found in endothelial cells, epithelial cells of the kidneys, lungs, and colon. Within the cardiovascular system, ET-1 was found in all types of vessels including arteries, arterioles, veins and venules (Davenport et al., 2016). The ET-1 gene encodes for a 212-amino acid precursor known as prepro-ET-1. A signal peptidase then removes 17 amino acids from the polypeptide to generate pro-ET-1. Pro-ET-1 is cleaved at both C and N terminals by furin enzymes to yield Big ET-1. Endothelin converting enzyme -1 (ECE-1) hydrolyzes the tryptophan-valine bond in Big-ET-1 to yield ET-1 (Davenport et al., 2016). ET-1 can be synthesized from endothelial cells and be secreted to interact

with ET-A and ET-B receptors to induce vasoconstriction in nearby smooth muscle cells (Davenport et al., 2016).

In CMs, the ET-A receptor is more abundant (90% of total ET-1 receptors) and is considered to elicit most of the cardiac effects of ET-1 whereas the ET-B receptor may be more responsive to physiological stress (Kedzierski and Yanagisawa, 2001). When ET-1 binds to ET-A/B receptors, this induces a conformational change in the receptor that allows for GTP to bind to the G_q - α subunit of the trimeric receptor associated G_q -protein. G_q - α activates and dissociates from the $\beta\gamma$ -complex and initiates downstream G-protein signalling, including activation of the mitogen activated protein kinase (MAPK) pathway (Schorlemmer et al., 2008). Alternatively, G_q - α can activate protein kinase C (PKC), which activates Ras, and Ras undergoes conformational changes that allow for the exchange of Ras-bound GDP for GTP. GTP-bound Ras recruits Raf, which becomes phosphorylated and subsequently activated. Activated Raf phosphorylates mitogen activated protein kinase kinase (MEK) 1/2 or MAPK, leading to activation of Erk 1/2. ET-1 can also activate the PI3K/Akt pathway to prevent apoptosis of CMs (Schorlemmer et al., 2008). All together, these pathways lead to regulation of CM cell growth, hypertrophy, proliferation and survival. Currently, the signalling pathway by which ET-1 modulates differentiation of various cell types to CMs is not known.

Gourdie et al. (1998) demonstrated that exogenous ET-1 added to chick ventricular CMs was capable of converting them into Purkinje fiber cells. Upon addition of ET-1 (10 nM) to chick ventricular CMs at E3, it was observed that after 1, 3 and 5 days, there was a gradual conversion of CMs to CCS cells shown by a decline in

expression of cardiac myosin binding protein-C (cMYBP-C) which is exclusively expressed in contractile CMs, and subsequent increase in expression of slow twitch muscle myosin heavy chain (sMHC) which is uniquely present in Purkinje cells (Gourdie et al., 1998). Addition of ET-1 also resulted in increased expression of the conduction system markers Cx40 and Cx42 (Gourdie et al., 1998). However, some controversy exists as to the specific role that ET-1 may play in forming the cardiac conduction system. Another study demonstrated that mice with genetic ablation of *Ednra* and *Ednrb*, which encode for the ET-A and ET-B receptors, did not show any significant abnormalities in the function of the CCS (Hua et al., 2014).

It has been suggested that the expression pattern of ECE-1, the enzyme involved in generating ET-1 from Big ET-1, in the embryonic heart coincides with the timing and localization of Purkinje fiber differentiation (Sedmera et al., 2008). ECE-1 expression is present in some areas of the endocardium and coronary arterial endothelium, but is absent from myocytes and endothelium of cardiac veins and capillaries (Mikawa and Hurtado, 2007). The localized distribution of endogenous ECE-1 may account for the localized ET-1 dependent induction of embryonic CMs to become Purkinje fiber cells. It was shown that viral-mediated ectopic co-expression of ECE-1 and prepro-ET-1 in the embryonic ventricular myocardium resulted in significant ectopic expression of Purkinje fiber markers in the trabecular myocardium (Takebayashi-Suzuki et al., 2000).

Using a *CCS-lacZ* mouse model, it was shown that ET-1 did not significantly alter *CCS-lacZ* expression (Rentschler et al., 2002). While ET-1 signalling might stimulate Cx40 expression in chick embryos, it may not be sufficient to induce conversion or lineage

specification of the entire Purkinje fiber network (Christoffels et al., 2009). In the avian heart, a Purkinje fiber network exists in the subendocardium along with a periarterial Purkinje network, both of which express Cx40. It has been shown that recruitment of Purkinje fiber cells from contractile myocytes occurs both periarterially and subendocardially in the avian heart, suggesting that paracrine interactions of myocytes with endocardial and arterial cells may play a role in the formation of CCS cells (Mikawa and Hurtado, 2007). Additionally, suppressing the development of coronary arteries in the chick heart led to a decrease in Purkinje fiber differentiation, further providing evidence that coronary arterial beds may be necessary to recruit myocytes to become CCS cells (Hyer et al., 1999). In contrast to Purkinje fiber network distribution in chick hearts, mouse hearts possess only a subendocardial Purkinje fiber network (Weerd and Christoffels, 2016).

1.7 Comparative Effects of Neuregulin-1 and Endothelin-1 on the Development of the Ventricular Conduction System

Although the literature has described a role for both NRG-1 and ET-1 to contribute toward the development of the CCS in the embryonic heart, there are some important differences in their effects. One notable study sought to determine the effects of adding exogenous NRG-1 or ET-1 to embryonic CMs and to assess formation of the CCS through measurement of expression of several CCS markers, including Cx40, Nkx2.5, GATA4, Irx4, Cx45, HF-1b, and minimal potassium channel subunit (MinK) (Patel and Kos, 2005). Both NRG-1 (2.5 nM) and ET-1 (1.5 nM) increased CCS marker gene expression as measured by semi-quantitative RT-PCR, in embryonic mouse CMs at E9.5

(Patel and Kos, 2005). However, this effect was not synergistic. Interestingly, this study was able to show that ET-1 may have inductive effects on the CCS in not only the avian heart, but also the mouse heart, as Rentschler et al.'s (2002) study previously suggested that the ET-1 inductive effects may be exclusive to the avian heart due to the unique distribution of the Purkinje fiber network, both periarterially and subendocardially.

Additionally, Patel and Kos' (2005) study suggested that induction of the CCS by ET-1 may occur through ET-A and/or ET-B receptor signalling, since adding selective ET-A and ET-B receptor antagonists (BQ123 and BQ786, respectively) to embryonic mouse CMs resulted in a significant decline in the number of cells expressing Cx40 (Patel and Kos, 2005). This is in contrast with the results of another study wherein mice with deletions in *Ednra* and *Ednrb*, encoding for ET-1 receptors, did not appear to show deficits in the CCS suggesting that the ET-1 signalling pathway may be dispensable in mouse CCS development (Hua et al., 2014). With respect to NRG-1, the results of Patel and Kos' (2005) study coincide with the results of Rentschler et al.'s (2002) study.

Upregulation of Nkx2.5 was found in the CCS of avian and mouse embryos and in the fetal human heart (Takebayashi-Suzuki et al., 2001; Thomas et al., 2001). However, in the avian heart, ET-1 induced Purkinje fibers did not show upregulation of Nkx2.5 (Takebayashi-Suzuki et al., 2001). In contrast, Patel and Kos' (2005) study demonstrated that in the embryonic mouse heart, addition of ET-1 and NRG-1 both upregulated Nkx2.5. It was hypothesized that the upregulation of Nkx2.5 may be required to regulate CCS-specific genes such as Cx40, in the mouse embryonic heart (Patel and Kos, 2005). Consistent with this notion, another study found that hearts of transgenic mice that

overexpressed a DNA non-binding mutant of Nkx2.5 under control of the β -myosin heavy chain (β -MHC) promoter, had reduced levels of Cx40 expression (Kasahara et al., 2001).

1.8 Cardiac Conduction System Markers

1.8.1 Role of Cx40 in the Cardiac Conduction System

Connexins are a family of proteins capable of forming gap junctions, which are required to maintain cellular homeostasis and function (Seul et al., 1997). There are 20 different connexin genes found in mice, and 21 different connexin genes found in humans (Condorelli et al., 1998). Most connexin genes share a common gene structure, comprised of 2 exons separated by 1 intron sequence. By forming gap junctions, connexins allow for the direct exchange of small molecules between adjacent cells, such as Ca^{2+} or IP3 (Seul et al., 1997). Gap junctions refer to clusters of channels that join two adjacent cells together and consist of building blocks of connexons, that are contributed by each communicating cell (Dbouk et al., 2009). Each connexon is composed of a complex of six connexin proteins (Dbouk et al., 2009). Gap junction channels alternate between “open” and “closed” conformations, which are regulated by various mechanisms including Ca^{2+} concentration, pH and protein phosphorylation (Peracchia et al., 2000; Alev et al., 2008; Peracchia, 2004; Hirst-Jensen et al., 2007; Yahuaca et al., 2000; Anand and Hackam, 2005; Kwak and Jongasma, 1996). The connexin protein is composed of nine main domains, of which the N-terminus, the two extracellular loops (which are stabilized by intramolecular disulfide bridges), and the four transmembrane

domains are highly conserved among the different isoforms (Elfgang et al., 1995; White et al., 1995, Evans and Martin, 2002).

The gap junction protein Cx40 generates channels with high conductance, even in early stages of development (Beblo and Veenstra, 1997). Throughout embryonic heart development, Cx40 is expressed in the fast conducting trabecular myocardium in the ventricles; trabecular myocardium will eventually form the mature CCS (Delorme et al., 1995; Sankova et al., 2012). Cx40 expression is completely absent in the SA node, and is absent in the outer portion of the AV node in mice (Delorme et al., 1995). It was also found to be absent in the AVC wall throughout development (Delorme et al., 1995). Cx40 mRNA was first detected at E11.5 in mice, in both the developing atrium and ventricles. Cx40 mRNA expression in the ventricles was found to be the highest at E14.5, after which there was a sharp decline in expression postnatally. In contrast, in atria, Cx40 mRNA expression remained consistent throughout development and postnatally (Delorme et al., 1995).

At E11.5, distribution of Cx40 protein occurs widely throughout the ventricular trabeculae, with stronger expression occurring in the subendocardial trabeculae than in the subepicardial cells (Delorme et al., 1995). Cx40 is absent from the interventricular septum. At E14.5, immunoreactivity of Cx40 decreases in a gradient from the top of the subendocardial trabeculae to the subepicardial layers (Delorme et al., 1995). The expression pattern of Cx40 in the CCS of the embryonic mouse heart at E14.5 is illustrated in **Figure 1.4**. At E17.5, when the VCS is well organized, Cx40 expression continues to occur in the trabeculae, but is absent from the ventricular wall; Cx40

expression occurs in endothelial cells of blood vessels. At E19, Cx40 expression is highly restricted to the top of the septum, to the Bundle of His extending from the top of the septum and its left and right bifurcating branches, and in the trabeculations which will form the mature Purkinje fiber network (Delorme et al., 1995). At 1-week post-partum, Cx40 expression is increased in the Bundle of His and the bundle branches. At this stage, Cx40 expression is no longer detected in the trabeculae (Delorme et al., 1995).

In the adult mammalian heart, Cx40 is found to be highly expressed in atrial CMs, whereas its expression in ventricular tissue exclusively involves the conduction system and the endothelial cells of blood vessels (Delorme et al., 1995). Cx40 expression is downregulated in the ventricular walls, and has never been detected in adult ventricular CMs (Gros et al., 2004). Cx40 is highly expressed in the AV node, the Bundle of His, bundle branches, and the Purkinje fibers in the adult heart and may contribute toward more rapid propagation of action potentials in these cells compared to working ventricular CMs (Seul et al., 1997; Gros et al., 2004).

In this thesis, we utilized the Cx40^{egfp} knock-in mouse model to visualize Purkinje fiber formation in the embryonic heart (Miquerol et al., 2004). In this model, the vital enhanced green fluorescent protein (EGFP) sequence is inserted upstream of Cx40 coding sequence such that EGFP, but not Cx40, is expressed under the control of the Cx40 promoter (Miquerol et al., 2004). The Cx40^{egfp} knock-in mouse model was initially designed to investigate visualization of the CCS in the adult heart because many other CCS mouse models offered technical limitations at this stage. For example, in the adult heart, in the Hf-1b-*lacZ* model, expression of the reporter gene extends far beyond the

CCS making it difficult to distinguish the CCS from surrounding myocardium; the use of *minK-lacZ* in adult mice allows for clear visualization of the CCS, but the enzymatic activity of *lacZ* used to identify conduction system myocytes was found to be lethal for cells at the adult stage (Miquerol et al., 2004). The Cx40^{egfp} knock-in mouse model offers several advantages over other models because: 1) Cx40 appears to be the best marker for the His-Purkinje system, 2) Cx40 is expressed strongly in atrial CMs, the AV node, the Bundle of His, and distal elements of the CCS and 3) The hyperpolarization activated current/pacemaker current (I_f) is evident in all spontaneously active EGFP positive Purkinje cells. Taken together, the Cx40^{egfp} knock-in mouse model offers the capacity for visualization of live cells and the opportunity to pursue functional analyses of the development of the CCS, as performed by Miquerol et al.'s (2004) group.

1.8.2 Role of HCN4 in the Cardiac Conduction System

The hyperpolarization-activated cyclic nucleotide-gated cation channel (HCN) family generates the pacemaker/funny current (I_f), which provides pacemaker activity in the SA node (Accili et al., 2002; DiFrancesco, 1993; Ludwig et al., 1998). The mammalian genome encodes four HCN channels (HCN 1-4), which are present throughout the heart (DiFrancesco, 1996; Mangoni and Nargeot, 2008). The HCN4 isoform is restricted in its expression in the murine adult SA node (Garcia-Frigola et al., 2003). Therefore, HCN4 is an excellent molecular marker to study cardiac pacemaker function in the adult heart. In the adult SA nodes of rabbit, mouse and dog, the dominant subtype of HCN is HCN4, which accounts for the majority of transcripts present (Schweizer et al., 2009). HCN4

was also found to be the major HCN isoform in adult canine Purkinje cells (Han et al., 2002). It was shown that HCN4 channels contribute toward the majority of the I_f current in E9.5 mouse ventricular CMs, which was significantly downregulated in E18 CMs, presumably to enable pacemaker activity at the SA node (Yasui et al., 2001).

Cardiac pacemaker activity originates early in heart development, at ~E8 in chick embryos and ~E8-8.5 in mouse embryos. Electrical impulses are generated in the forming SA node region and are conducted to the bulboventricular portions of the heart (Garcia-Frigola et al., 2003). It was suggested that this early pacemaker activity was attributed to the presence of HCN4 channels at the embryonic stage, since HCN4 mRNA was detected in dispersed cells in mice throughout the precardiac mesoderm at E7.5 (the cardiac crescent) (Garcia-Frigola et al., 2003). At E8-8.5, HCN4 was detected in the sinus venosus; by E9, HCN4 was detected in the septum transversum; expression continued to expand as the SA node fully developed (Garcia-Frigola et al., 2003). HCN4 mRNA expression was found to be two-fold higher in atria than in ventricles in mice at E9.5 (Schweizer et al., 2009). By E14.5, all components of the CCS, as well as the atria and ventricles, express HCN4, with the SA node having the greatest expression of HCN4, followed by the atria, and then the ventricles (Garcia-Frigola et al., 2003, **Figure 1.4**). Towards birth, HCN4 mRNA expression was found to be downregulated in both the atria and nearly disappeared in ventricles. However, after birth, HCN4 mRNA levels increased in the ventricles (Schweizer et al., 2009). After the postnatal stage, HCN4 became gradually restricted to the SA node (Garcia-Frigola et al., 2003). In human adults, HCN4 was detected in the atria, ventricles, and Purkinje fibers, with the greatest level of

expression being in the SA node (Dobrzynski et al., 2007). In humans, it is suggested that HCN4 may play a significant role in maintaining normal heart rate, since HCN4 mutations were associated with inherited sinus node bradycardia in adult patients (Milanesi et al., 2006; Nof et al., 2007; Schulze-Bahr et al., 2003). However, despite a similar role for HCN4 in generating the I_f current to enable pacemaker activity in the SA nodes of both human and mice, several studies have suggested that, based on the Cre-mediated ablation of HCN4, the HCN4 channel may not be critically important for the acceleration of heart rates in mice (Harzheim et al, 2008; Herrman et al., 2007). In this thesis, we chose to study HCN4 as our VCS marker of choice because it is expressed both prenatally in the ventricular trabeculae, and postnatally becomes restricted to the Purkinje fibers.

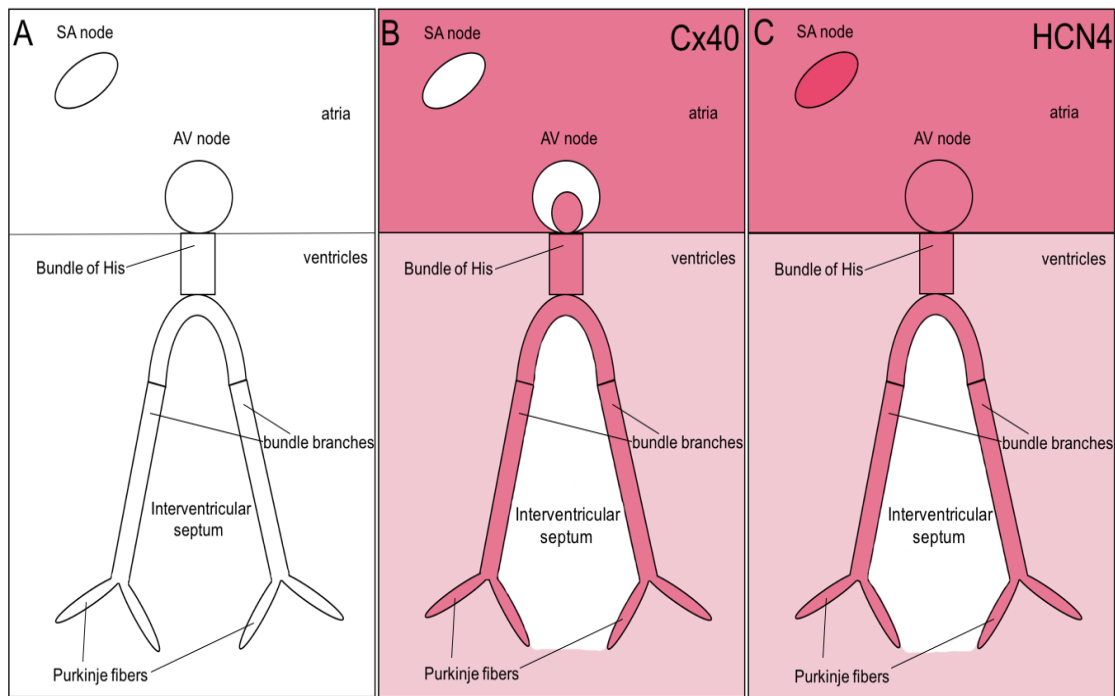


Figure 1.4. Expression Pattern of Cx40 and HCN4 in the mouse embryonic heart at E14.5. At E14.5, in the mouse embryonic heart, the CCS maturation and development is partially completed such that nodal tissue and bundle branches are formed but Purkinje fiber arborisation continues to develop. **A)** Illustration depicts the components of the CCS in the embryonic mouse heart including the SA node, AV node, atria, ventricles, Bundle of His, bundle branches, interventricular septum, and Purkinje fibers. **B)** Expression pattern of Cx40 at E14.5 in the embryonic mouse heart. At this stage, Cx40 is highly expressed in atrial CMs, the inner portion of the AV node, the Bundle of His, bundle branches and Purkinje fibers. Cx40 is expressed to a lesser degree in the ventricular CMs. Cx40 expression is absent in the SA node, the outer portion of the AV node, and the interventricular septum (Delorme et al., 1995). **C)** Expression pattern of HCN4 at E14.5 in the embryonic mouse heart. At this stage, HCN4 is greatly expressed in the SA node. HCN4 is highly expressed in atrial CMs, the AV node, the Bundle of His, bundle branches and Purkinje fibers. HCN4 is expressed to a lesser degree in ventricular CMs. HCN4 expression is absent in the interventricular septum (Garcia-Frigola et al., 2003). The pink gradient depicts relative expression patterns; the stronger the colour, the higher the relative expression. SA, sinoatrial; AV, atrioventricular. Figure redrawn from copyrighted material corresponding to (Gros et al., 2004, see **APPENDIX IV**).

1.9 Genetic Models Used to Study Development of the Cardiac Conduction System

The Cx40^{egfp} transgenic mouse model we employed in our study has been described in Section 1.8.1. Transgenic mice have been used to study CCS development with *lacZ* expression under the transcriptional control of a cardiac-specific enhancer from chicken-GATA6 (cGATA-6), the proximal promoter of regions cardiac troponin-I, or engrailed 2 (CCS-*lacZ*), and also by knocking in the *lacZ* sequence into the coding sequence of the transcription factor HF-1b (reviewed in Myers and Fishman, 2003). The limitations of using cGATA-6 and troponin-I transgenes is that expression of *lacZ* becomes confined to the AVC and is sparse in other components of the CCS, by E9.5 and E10.5, respectively (Di Lisi et al., 2000). HF-1b-*lacZ* model also has limitations in a different sense, because *lacZ* expression occurs broadly throughout the heart, and is not exclusive to components of the CCS, including expression in the right atria, interventricular septum, Bundle of His, bundle branches, and compact myocardium (Nguyen-Tran et al., 2000). MinK-*lacZ* was thought to be an attractive genetic model because of its specificity in delineating the CCS. By E10.5, *lacZ* expression in MinK-*lacZ* mice occurs in the SA node region, parts of the AVC, the interventricular groove, outflow tract, and ventricular trabeculae (Kondo et al., 2003). By E12.5-E13.5, *lacZ* expression is present in the AV bundle, AV node, and bundle branches (Myers and Fishman, 2003). Rentschler et al. (2002) employed a CCS-*lacZ* model utilizing the random insertion of an engrailed-2 enhancer-*lacZ* transgene, which was capable of delineating the entirety of the CCS. Expression of *lacZ* in CCS-*lacZ* mice occurs first at E8.5, where β -gal expression was detected in the region of the right sinus horn where the SA node will eventually

form. By E9.5, *lacZ* expression was detected in the interventricular septum, from which the Bundle of His and bundle branches will be derived from. By E10.5, expression in the AVC was detected. By E12.5, there was a continuous expression of *lacZ* from the SA node, to the AV node, to the developing Bundle of His and bundle branches, and also to the ventricular trabeculae (Rentschler et al., 2002). By E13.5, *lacZ* expression was detected with all components of the CCS labeled, including discrete Purkinje fiber networks (Rentschler et al., 2002). There are some similarities and differences between CCS-*lacZ* and Mink-*lacZ* models. The distinct components of the CCS including the SA node, AV node, and bundle branches, are readily detected by both models (Myers and Fishman, 2003). However, expression of *lacZ* is stronger and broader in CCS-*lacZ* hearts, where expression is also seen along the distinctive Purkinje fibers (Myers and Fishman, 2003).

Several HCN4 knock-in transgenic mouse lines have been established to delineate the entirety of the CCS, including HCN4-CreERT2, HCN4n-*lacZ*, and HCN4-H2BGFP (Liang et al., 2013; Spater et al., 2013; Gros et al., 2010; Horsthuis et al., 2009). Data from these models support the use of HCN4 as a marker to identify development of the CCS, since HCN4 expression was shown to identify distinct components of the CCS at specific developmental stages (Liang et al., 2013). HCN4 was found to be first expressed in the differentiating cells of the cardiac crescent and was transiently expressed throughout formation of the early heart tube, indicating that HCN4 was a good marker for the FHF (Liang et al., 2013). In the FHF, HCN4 expression identified differentiated myocyte precursor cells throughout the CCS. By E16.5, all HCN4

transgenic mouse lines marked all components of the CCS (Liang et al., 2013). Studies to determine the lineage potential and to identify specific contributions of the FHF toward development of the CCS have been very limited due to the lack of appropriate specific markers (Liang et al., 2015).

1.10 Cell Lineage Tracking of Nkx2.5+ Myocardial Cells: Cardiac Progenitor Cells

Although the primitive heart tube in model organisms is miniscule and poses technical limitations when attempting to study cell types in experiments, several groups identified novel cell types present in the embryonic heart known as CPCs (Kirby, 2007; Buckingham et al., 2005; Evans et al., 2010). It is possible that a population of undifferentiated, cardiomyogenic mesodermal precursor cells like CPCs could persist through heart development (presumably derived from the FHF and SHF as described in Section 1.3.3) and be present at later stages in development, and thus, a method was established to assess the ultrastructural characteristics of mouse ventricular cells at the post-chamber stage, at E11.5 (Zhang et al., 2015). This was done using a lineage tracking method that had been previously established to distinguish myocardial cells expressing Nkx2.5, a transcription factor necessary for cardiomyogenesis from non-myocytes (Komuro and Izumo, 1993). This method involves crossing two knock-in mouse strains: Nkx2.5-cre (NC) and Rosa-LacZ (RL). The NC knock-in strain contains an internal ribosomal entry sequence (IRES) and a Cre-recombinase coding sequence (Cre) from bacteriophage P1, inserted within the 3'-untranslated region of the *Nkx2.5* gene (Stanley et al., 2002). When the *Nkx2.5* gene is expressed, this also results in the

expression of Cre recombinase protein. The function of Cre is to mediate site-specific recombination between specific DNA sequences known as LoxP sites (Stanley et al., 2002). The RL knock-in mouse strain was engineered to have a transcriptional terminal stop cassette proximal to the β -gal (*LacZ*) coding sequence (Soriano, 1999). The stop cassette contains a neomycin selection gene and triple polyadenylation sites, and is flanked by LoxP sites. When NC and RL mice are crossed, the double knock-in embryos that result from the cross allow for expression of the *Nkx2.5* gene followed by the co-translation of Cre, which allows for the excision of the floxed stop cassette from the *Rosa-LacZ* transgene. This enables the expression of the *LacZ* reporter gene in all *Nkx2.5*⁺ cells. Therefore, one can detect *Nkx2.5*⁺ cells by immunofluorescent labelling with β -gal antibodies.

Nkx2.5⁺ cells can give rise to cardiac, smooth muscle, endothelial, and conduction system cells (Moretti et al., 2006; Wu et al., 2006). Of the cells that express *Nkx2.5*, we are interested in CPCs and CMs. CPCs give rise to many types of differentiated cells in the embryonic heart, including mature CMs, fibroblasts, smooth muscle cells and endothelial cells (Buckingham et al., 2005; McMullen et al., 2009). We have previously shown that in E11.5 mouse ventricles, there is a population of *Nkx2.5*⁺ CMs and CPCs, and a *Nkx2.5*⁻ nonmyocyte population (McMullen et al., 2009; Zhang et al., 2015). One can use this lineage tracking system combined with sarcomeric myosin staining to differentiate between *Nkx2.5*⁺ CMs and *Nkx2.5*⁺ CPCs, and between these two *Nkx2.5*⁺ populations vs. nonmyocytes (*Nkx2.5*⁻) (Zhang et al., 2015).

1.11 MicroRNAs and Regulation of Cx40 and HCN4 Gene Expression

1.11.1 The Functions and Mechanisms of MicroRNAs

MicroRNAs (miRNAs) are endogenous small non-coding RNAs (~22 nucleotides) that can control gene expression in animals and plants at the post-transcriptional level (Bartel, 2004). MiRNAs induce gene silencing by binding to target sites found within the 3'UTR of the target mRNA, and prevent protein production by either suppressing protein synthesis and/or by initiating the degradation of mRNA (Bartel, 2004). Individual miRNAs can target as many as 100 different mRNAs. MiRNAs are involved in cell cycle control, apoptosis, stem cell differentiation, cardiac and skeletal muscle development, neurogenesis, and many other processes (Bartel, 2004). The short lin-4 RNA (~22 nucleotides) in *C. elegans* was recognized as the founding member of the miRNAs and this was shown to target lin-14 mRNA for degradation during larval development. (Lau et al., 2001; Lagos-Quintana et al., 2001; Lee and Ambros, 2001).

The model for miRNA function can be outlined in seven steps. First, the miRNA gene is transcribed, by RNA polymerase II, to generate pri-miRNA (Wahid et al., 2010). It was recently determined the RNA polymerase II is largely responsible for the transcription of miRNA genes, enabling temporal control such that a specific set of miRNAs can be synthesized for specific conditions or cell types (Wahid et al., 2010, Cai et al., 2004). Second, the Drosha RNase III endonuclease (Drosha) performs nuclear cleavage of pri-miRNA, liberating a ~60-70 nucleotide stem loop intermediate known as the miRNA precursor or pre-miRNA. Drosha cleaves both strands of the stem at the sites near the base of the primary stem loop. In the third step, the pre-miRNA is actively

transported from the nucleus to the cytoplasm by RAN-GTP and the export receptor known as exportin-5 (Bartel, 2004). In the next step, the miRNA is further cleaved in the cytoplasm by the enzyme Dicer. This cleavage performed by Dicer removes the terminal base pairs and the stem loop of the pre-miRNA, leaving behind the 5'-phosphate and a 3'-overhang. The resulting duplex is composed of both the mature miRNA and another fragment that originates from the opposing arm of the pre-miRNA. In step 5, a helicase-like enzyme, samples the end of the duplex many times to unwind the duplex (Bartel, 2004). Next, the cleavage products from Dicer obtained at the end of step 4 are incorporated as single-stranded RNAs into a ribonucleoprotein complex known as the RNA-induced silencing complex (RISC). This complex recognizes targets based on complementarity between the small interfering RNA (siRNA) cleavage products and the target mRNA. RISC contains a protein known as Argonaute, which works with RISC to associate with both strands of the miRNA and then cleaves and discards one of the strands (Wahid et al., 2010). The other strand that remains is used as a guide for RISC to bind to specific mRNAs through base pairing. If the miRNA to RNA match is extensive, Argonaute cleaves the target mRNA, causing its rapid degradation. RISC can then go seek out other target mRNAs with strong complementarity. If there is a less extensive match of miRNA to RNA (weaker complementarity), this results in inhibition of translation of the mRNA, destabilization of the mRNA, shortening of the poly-A-tail, and causes the mRNA to move to structures in the cytosol known as processing bodies (P-bodies). At P-bodies, mRNAs are sequestered, decapped and degraded (Wahid et al., 2010).

1.11.2 MicroRNAs Regulating Gene Expression of Cx40 and HCN4

To study the role of miRNAs in Cx40 expression, we chose miRNA 27b and 208a based on previous evidence published in the literature. To study the role of miRNAs in HCN4 expression, we chose miRNA 133 and 1a, which have been shown to regulate HCN4 gene expression.

The role of miRNA 27b on Cx40 expression and incidence of atrial arrhythmias were analyzed in an obesity animal study (Takahashi et al., 2016). Mice were subjected to high-fat diets (HFDs) to increase their vulnerability to atrial tachycardia. Cx40 gene expression was examined in HFD atria of mice, and was found to be significantly decreased vs. normal chow-fed mice. This was correlated with electrophysiological abnormalities in HFD mice, including decreased conduction velocity. Further analysis revealed that miRNA 27b was the only possible candidate that could directly bind to the 3'UTR of Cx40, and was found to be significantly upregulated in its expression in HFD atria (Takahashi et al., 2016). Therefore, this study demonstrated that miRNA 27b may be a key regulator of increased atrial arrhythmic vulnerability in HFD, by regulating the gene expression of Cx40, which preceded the development of atrial fibrosis (Takahashi et al., 2016).

MiRNA 208a is encoded within an intron of the α -myosin heavy chain (α MHC) gene. It was found that overexpression of miRNA 208a induced cardiac hypertrophy whereas in miRNA 208a knockout mice, it was shown that P waves were absent in the ECGs, and PR intervals were prolonged vs. wild-type (WT) animals (Callis et al., 2009). Further analysis revealed that mRNA and protein levels of Cx40 and its upstream

regulating transcription factor Hop were significantly decreased while protein levels of GATA4 were upregulated in miRNA 208a knockout mice. Although a target site for miRNA 208a in the 3' UTR region of GATA4 mRNA was validated using a reporter gene assay, clear mechanisms underlying the upregulation of Cx40 and Hop levels in miRNA 208a knockout mice were not identified. However, the miRNA 208a knockout mouse study suggests that this miRNA is required for sustained expression of Cx40 and Hop in the heart (Callis et al., 2009).

MiRNA 1 and 133 are co-transcribed as dicistronic messages from the same transcriptional unit and have been shown to play an important role in cardiac development. MiRNA 1 has been implicated to be important for development of the CCS, since a 50% lethality rate was reported for homozygous miRNA 1 knockout offspring by weaning age due to the development of conduction system deficits including ventricular septal defects (Zhao et al., 2007). It was shown that miRNA 1 plays a regulatory role in CM differentiation and electrophysiological maturation in human ES cell cultures by decreasing the I_f current (Fu et al., 2011). Interestingly, it was shown that exercise training produced intrinsic sinus bradycardia as a result of a remodeling of ion channels that govern pacemaking, including decreased HCN4 expression in the SA node, and it was hypothesized that this could have been due to an upregulation in miRNA 1a expression (D'Souza et al., 2014). QPCR analysis revealed that there was significant downregulation of miRNA 1a in the SA node of rats that underwent exercise training compared to the controls (D'Souza et al., 2014). Although a correlation existed in this study between downregulation of miRNA 1a and HCN4 gene expression in rats that

underwent exercise training, they do not prove a causal link by additional validations (D'Souza et al., 2014). MiRNA 1a has also been shown to promote differentiation of CPCs and their exit from the cell cycle in mammals and in flies (Zhao et al., 2005; Kwon et al., 2005). It is possible that miRNA 1a may be important in regulating HCN4 gene expression in the context of the CCS, although this remains to be tested. In cardiogenesis, miRNA 133 has been implicated in early cardiac differentiation of mouse and human embryonic stem cells by repressing non-mesoderm lineages, while enhancing mesoderm specification (Ivey et al., 2008). In another study, elevated levels of HCN2 and HCN4 mRNA and protein were correlated with significant reductions in miRNA 1 and miRNA 133 in atrial biopsies from aged patients with atrial fibrillation compared to those from patients with sinus rhythm (Li et al., 2015).

1.12 The Genetic Mechanisms of Congenital Heart Diseases

The term congenital heart disease (CHD) refers to structural or functional abnormalities of the heart that occur before birth. CHDs are found in 30-50 out of every 1000 live births (Hoffman and Kaplan, 2002). Dysregulation in the development of the heart during embryogenesis leads to the development of CHDs. CHDs are classified into three broad categories: cyanotic heart disease, where infants appear blue due to the mixing of oxygenated and deoxygenated blood, left-sided obstruction defects such as valve stenosis, and septation defects, which affect septation of the atria and/or ventricles (Bruneau, 2008). The severity of CHDs can vary, and therefore, mortality and morbidity is also variable and depends on the specific defects that occur in the patient.

Often, patients and children with CHDs must undergo debilitating surgeries to correct heart defects, and life expectancy and quality of life are greatly reduced.

The majority of CHDs are caused by mutations in the regulators of heart development during embryogenesis (Pierpont et al., 2007). For example, *Tbx5*, a regulator of ANP expression, was shown to be the causative gene in Holt-Oram Syndrome (Basson et al., 1997). In Holt-Oram Syndrome, atrial septal defects occur, along with ventricular septal defects and conduction system deficits. Interestingly, conduction system deficits in this particular CHD have been linked to dysregulation in the spatial expression pattern of ANP (Mori and Bruneau, 2004). *Nkx2-5* mutations have also been shown to be responsible for the incidence of many CHDs, such as ventricular septal defects, Ebstein's anomaly, and Tetralogy of Fallot (Benson et al., 1999). In addition, mutations in *GATA4*, *Tbx1*, *Tbx20*, and many other transcription factors have been implicated in the incidence of CHDs (Garg et al., 2003; Lindsay et al., 2001; Kirk et al., 2007).

Based on the body of knowledge available describing the genetic mechanisms underlying development of CHDs, it is possible that genetic mutations in genes encoding for paracrine factors like ET-1, NRG-1, and ANP and their cognate receptors, or mutations in transcriptional regulators of these paracrine factors, may be involved in contributing toward the incidence of CHDs.

1.13 Role of Atrial Natriuretic Peptide in Physiology and Cell Biology

1.13.1 Synthesis and Storage of Atrial Natriuretic Peptide

ANP is a member of the natriuretic peptide family and the human ANP gene *Nppa* encodes for a prepro-hormone (prepro-ANP) that consists of 151 amino acids (Woodard and Rosado, 2008, **Figure 1.5**). Prepro-ANP is subsequently cleaved proteolytically into a 126-amino acid structure known as pro-ANP. Pro-ANP is stored in secretory granules in atrial myocytes until its release (Woodard and Rosado, 2008). When ANP needs to be secreted by the atria, pro-ANP becomes cleaved by corin, which is a transmembrane cardiac serine protease, generating a mature ANP peptide consisting of 28-amino acids. This product is termed ANP (99-126) (Woodard and Rosado, 2008). Similar to other natriuretic peptides, ANP contains a disulfide-linked ring structure consisting of 17 conserved amino acids, which is necessary for the peptide's biological activity (Inagami et al., 1987; **Figure 1.5**). ANP is released from the atria in response to the stretching of the wall of the atria, which is a result of increased blood pressure and blood volume (Woodard and Rosado, 2008). From there, ANP perfuses into the coronary sinus, and is then distributed to various target organs (Potter et al., 2006). Although ANP is mostly expressed and stored in the atria, it is also present in the ventricles and kidney (Potter et al., 2006).

It appears that a regulatory pathway for ANP secretion exists in the atria, whereas in the ventricles, ANP is released rapidly, as part of a constitutive secretory pathway. The secretion of a protein in a cell can either occur through a cell signal dependent (regulated) or constitutive (unregulated) manner (Burgess and Kelly, 1987).

Atrial CMs of the adult mammalian heart demonstrate features of a regulated secretory cell type. These features include the presence of dense secretory granules, long-term storage for these granules in the cytoplasm, and mechanisms for secretion that are coupled to mechanical stimuli (Burgess and Kelly, 1987). However, in adult ventricles, ANP mRNA expression is nearly ~100-fold lower than in the atria, promoting the idea that secretory granules are not stored in the ventricles but are rapidly released (Nemer et al., 1986). However, there is some evidence to refute the hypothesis that ANP secretion occurs in the ventricles as a part of the constitutive secretory pathway. ET-1 and Ca^{2+} were both shown to stimulate ANP secretion from ventricular CMs, lending support to the idea that perhaps a regulated secretory pathway for ANP may also exist in ventricles (Kinnunen et al., 1991; Irons et al., 1993).

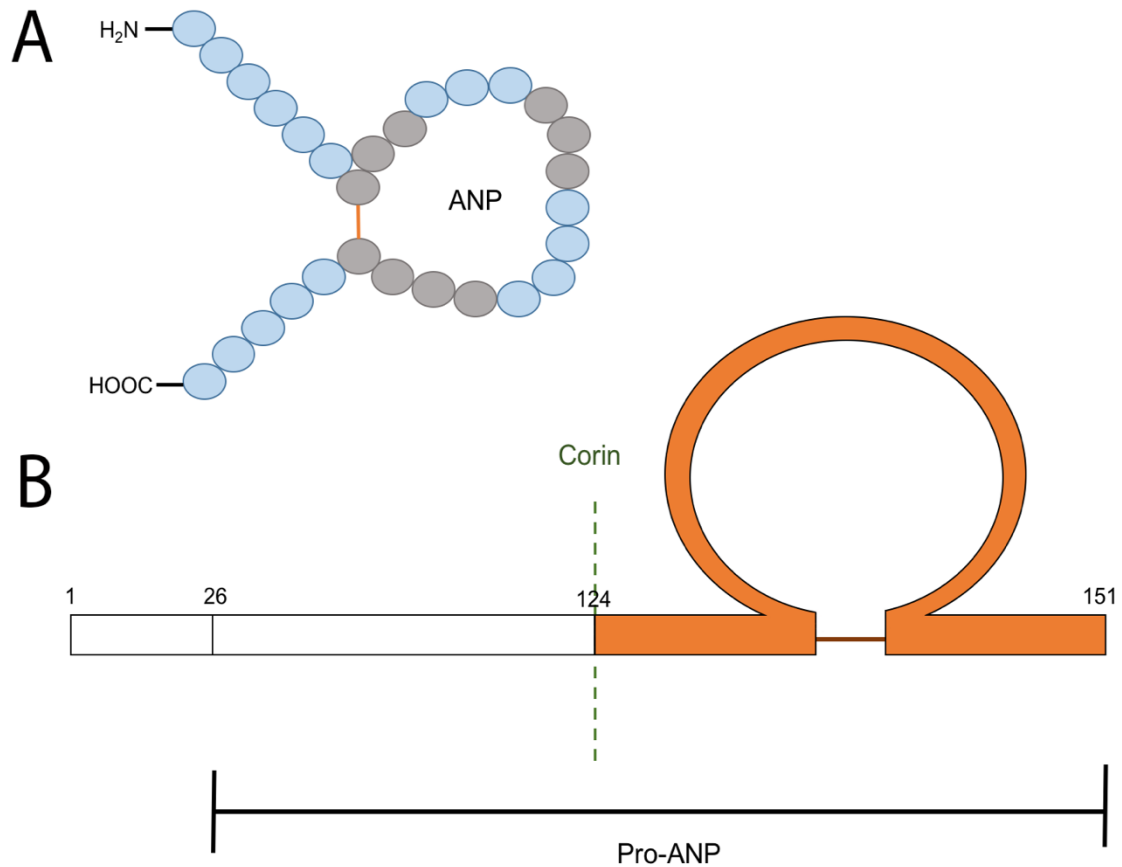


Figure 1.5. Structure and processing of the paracrine factor, atrial natriuretic peptide.

A) Atrial natriuretic peptide (ANP) is a member of the natriuretic peptide family and contains a disulfide-linked ring structure consisting of 17 conserved amino acids, which is necessary for biological activity. Amino acids that are conserved between ANP and the other known natriuretic peptides, BNP and CNP, are depicted as dark grey circles. **B)** ANP is synthesized as a prepro-hormone and is then proteolytically cleaved into a biologically active peptide. At the N-terminal, the signal sequence is cleaved to form the 126-amino acid structure known as proANP (1-126). Corin, a transmembrane cardiac serine protease, processes proANP and the product becomes a mature C-terminal ANP consisting of 28-amino acids, termed ANP (99-126, orange). In this form, ANP is biologically active.

1.13.2 Gene Expression and Regulation of Atrial Natriuretic Peptide

The paracrine factor ANP is encoded by the gene *Nppa*, which contains 3 exons. This gene is found on chromosome 1 in humans and in chromosome 4 in mice (Yang-Feng et al., 1985). ANP mRNA expression can be detected first in the primitive heart tube (Zeller et al., 1987) around the time when atrial and ventricular myocardium first start to differentiate (E8-8.5) (Christoffels et al., 2000). At E10-E12.5, ANP expression is similar in both the myocardium of the primitive atria and ventricles. As the heart continues to mature, ANP expression persists in the atria but declines in the ventricles such that there is a ~100-fold decrease in mRNA expression in the ventricles vs. atria in the adult heart (Nemer et al., 1986). *Cis*-elements present in the *Nppa* promoter are necessary for the heart to acquire the stage specific expression pattern for ANP and are contained within a ~500 bp upstream sequence (Argentin et al., 1994). These *cis*-elements are necessary for the binding of important cardiac transcription factors involved in the development of the embryonic heart, including: GATA4, HAND2, MEF2C, Tbx5, and Nkx2.5. These regulatory elements, in association with cardiac transcription factors, also allow for differential expression of ANP to occur in a cell type specific manner at both developmental or postnatal stages (Small and Krieg, 2003; Durocher and Nemer, 1998; Thattaliyath et al., 2002; Belaguli et al., 2000; Morin et al., 2000; Dai et al., 2002; Morin et al., 2005; Hiroi et al., 2001). Mutations in these regulatory elements and transcription factors have been shown to impair cardiogenesis in experimental animal models and also in humans with CHDs. Mutations in MEF2C have been associated with dysregulation in ANP expression leading to impaired cardiac development in

experimental animal models of disease as well as in human patients with CHDs (Bruneau et al., 2008; Lin et al., 1997; Schott et al., 1998; Molkenkin et al., 1997; Tanaka et al., 1999; Garg et al., 2003; Bruneau et al., 2011). Some CHDs, like Holt-Oram Syndrome, in the mouse, have demonstrated a dysregulated spatial expression pattern of ANP due to a mutation in *Tbx5*, leading to the development of conduction system deficits (Bruneau et al., 2001; Mori and Bruneau, 2004). Despite this body of knowledge, a specific role for ANP in the development of the CCS has not been clearly defined. Therefore, work in this thesis aimed to determine if the ANP-mediated signalling pathway (ANP/NPR-A/cGMP) could play a role in recruiting various cardiac cell types toward the conduction system cell lineage.

1.13.3 Natriuretic Peptide Receptors

Three different natriuretic peptide receptor subtypes exist across species: natriuretic peptide receptor A (NPR-A), natriuretic peptide receptor B (NPR-B), and natriuretic peptide receptor C (NPR-C). ANP is capable of stimulating NPR-A, NPR-B, and NPR-C (Koller et al., 1991). Of all three natriuretic peptides, ANP has the highest affinity for NPR-A (Koller et al., 1991). NPR-A is a guanylyl cyclase (GC) linked receptor (Potter et al., 2006). NPR-A is composed of an extracellular N-terminal ligand binding domain consisting of ~450 amino acids, a single hydrophobic transmembrane domain consisting of ~20-25 amino acids, and a C-terminal intracellular domain consisting of 570 amino acids. This intracellular domain is further subdivided into kinase homology, dimerization and GC domains (Potter et al., 2006; **Figure 1.6**). The gene that encodes for NPR-A,

known as *Npr1*, contains 22 exons and is found in humans and mice, on chromosomes 1 and 3 respectively (Chang et al., 1989). NPR-B has a similar structure and is encoded by the *Npr2* gene, also contains 22 exons, and is found in humans and mice, on chromosomes 9 and 4 respectively (Chang et al., 1989).

Numerous studies have evaluated the biological and physiological effects of ANP in the context of ANP/NPR-A signalling. When ANP binds to NPR-A, cellular responses are induced through elevation of intracellular cGMP levels, and this has been demonstrated in all tissues that express NPR-A. These tissues include those found in kidney, adrenal, terminal ileum, aortic and lung tissues, and the brain, for humans and rats (Potter et al., 2006). When ANP binds to NPR-A, several events occur. First, the normal level of repression that is exerted by the kinase homology domain of the NPR-A receptor is removed. It was hypothesized that this kinase homology domain repressed the activity of NPR-A under basal conditions, since receptors that lacked this kinase homology domain were found to be constitutively active (Potter et al., 2006). Ligand binding leads to the GC domains coming together in a head to tail arrangement. Following this step, the affinity for the ligand-binding domain for ANP decreases, which increases the dissociation rate of the ligand from its receptor (Jewett et al., 1993). Once ANP is completely dissociated from NPR-A, the receptor becomes desensitized and is considered to be in an inactive state, caused by the dephosphorylation of regulatory phosphorylation sites on the kinase homology domain of the receptor (Jewett et al., 1993).

When the GC domains of NPR-A come together and the receptor is thus activated, this leads to production of the second messenger molecule cGMP (Ogawa et al., 2004). Following this, cGMP can then go on to activate several downstream effectors, including cGMP dependent protein kinases like protein kinase G (PKG), cGMP-gated ion channels, and phosphodiesterases (PDEs) (Lincoln and Cornwell, 1993).

ANP is also capable of binding to NPR-C. NPR-C mRNA has been found in atrial, placenta, lung and kidney tissue, in aortic smooth muscle, and in aortic endothelial cells (Suga et al., 1992). An important difference between NPR-C and NPR-A receptors is that NPR-C receptors lack GC activity (Potter et al., 2006). Instead, NPR-C is a disulfide-linked homodimer (Potter et al., 2006). ANP also has the highest affinity for NPR-C, as is the case with NPR-A (Potter et al., 2006). NPR-C is encoded by the gene *Npr3* and contains 8 exons, and is found on chromosome 8 in humans and on chromosome 15 in mice (Chang et al., 1989). The purpose of NPR-C receptors is to act as clearance receptors, to clear natriuretic peptides from circulation, or to clear them extracellularly through receptor-mediated internalization of the ligand/receptor complex, followed by degradation of this complex (Jaubert et al., 1999). The intracellular domain of NPR-C is small, consisting only of 37 amino acids, compared to the larger intracellular domain of NPR-A (Fuller et al., 1988). NPR-C can activate G_i proteins to inhibit adenylyl cyclase (AC) and subsequently reduce the production of the second messenger molecule cAMP (Anand-Srivastava et al., 1987). It is hypothesized that ANP binding to NPR-C may trigger a signal transduction pathway that does not include cGMP signalling, but may include the presence of other secondary messengers like cAMP (Potter et al., 2006), however

the literature investigating ANP/NPR-C signalling is limited, and thus this discussion of the role of ANP in cell biology and cardiovascular physiology will focus on its involvement with NPR-A.

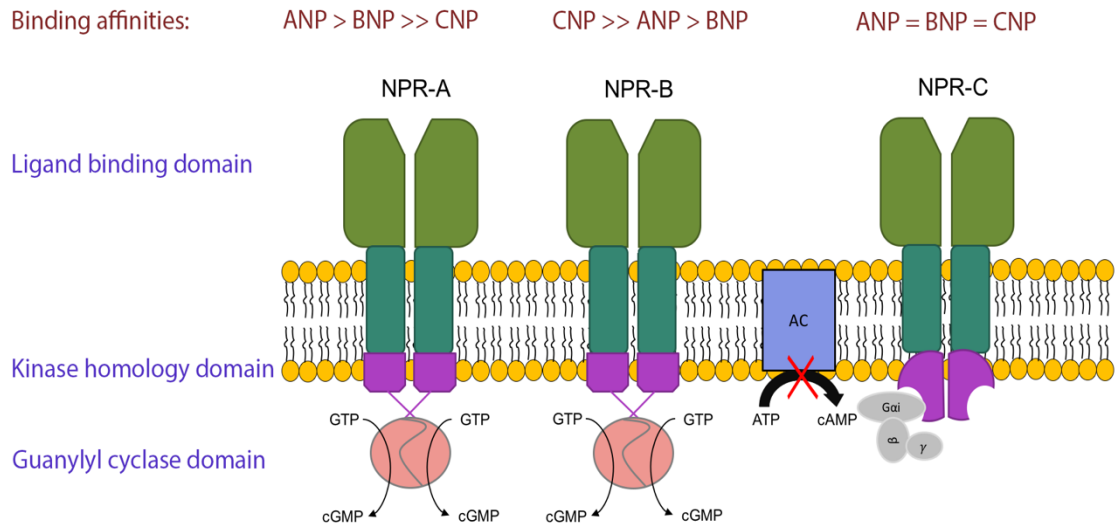


Figure 1.6. Structures of natriuretic peptide receptors and binding affinities for natriuretic peptides. Natriuretic peptides can bind to three subtypes of natriuretic peptide receptors: natriuretic peptide receptor A (NPR-A), natriuretic peptide receptor B (NPR-B), and natriuretic peptide receptor C (NPR-C). NPR-A and NPR-B are guanylyl cyclase (GC)-linked receptors, whereas NPR-C lacks GC activity. NPR-C is a disulfide-linked homodimer and contains activator sequences for the inhibitory heterotrimeric G protein (G_i), which is coupled to inhibition of adenylyl cyclase (AC).

1.13.4 Role of Atrial Natriuretic Peptide in Cardiovascular Physiology

ANP regulates cardiovascular homeostasis, through regulation of blood pressure and volume (Potter et al., 2006). This is achieved through promotion of natriuresis and diuresis, which promotes release of sodium and water from the body, thus decreasing blood pressure and blood volume. ANP can also decrease blood pressure and blood volume by increasing the glomerular filtration rate and reducing renin secretion; these effects are all mediated by binding to NPR-A (Kishimoto et al., 1996). Mutations that disrupt the *Nppa* gene resulted in increased hypertension in these mice, suggesting that ANP has an important role in regulating cardiovascular homeostasis, blood pressure, and blood volume (Kishimoto et al., 1996; John et al., 1995).

ANP can exert specific effects on the systemic vasculature by reducing total peripheral resistance. This is accomplished by having a direct effect on the vessel walls through vasodilation of the renal afferent arterioles, which leads to an increase in glomerular filtration and then diuresis (Woodard and Rosado, 2008). PKG is responsible for mediating the vasodilatory actions of ANP. PKG regulates the opening of ion channels in vascular smooth muscles in order to cause hyperpolarization, which will allow for vasodilation (Dora et al., 2001). Binding of ANP to NPR-A receptors leads to increased intracellular cGMP levels, which can then decrease cytosolic free Ca^{2+} concentrations through a PKG-dependent mechanism, thus leading to further promotion of vasodilation (Rosado et al., 2000). The mechanism of ANP-induced vasodilation has pointed to the involvement of PKGI in this pathway. PKGI is one of two PKG genes and is highly expressed in platelets, smooth muscle, CMs and the brain

(Pfeifer et al., 1998). It was shown that PKGI knockout mice are incapable of vasodilation in response to the addition of cGMP-elevating agents/cGMP-activators such as ANP or nitric oxide (NO) generators (Pfeifer et al., 1998).

PKGI targets several calcium channels; PKGI α phosphorylates and activates calcium-activated potassium channels, leading to potassium efflux and membrane hyperpolarization, which then inhibits calcium influx through nearby voltage-gated calcium channels (Schlossmann et al., 2000). PKGI is also capable of directly inhibiting voltage-gated calcium channels by phosphorylating these channels. PKGI can directly phosphorylate the inositol (1,4,5) triphosphate receptor and the inositol (1,4,5) triphosphate receptor-associated PKGI substrate, at the endoplasmic reticulum, to inhibit the release of calcium from storage vesicles (Schlossmann et al., 2000). PKGI also has been shown to activate calcium/ATPase membrane-associated pumps to pump calcium out of the cell, reducing intracellular calcium levels, and is also capable of phosphorylating phospholamban, which activates the calcium/ATPase (SERCA), resulting in the sequestration of calcium into the sarcoplasmic reticulum (Schlossmann et al., 2000). Thus, downstream signalling of ANP binding to NPR-A can lead to multiple mechanisms that will promote vasodilation in vascular smooth muscle cells.

ANP is thought to have a significant role in maintaining systemic blood pressure, since mice that lacked NPR-A receptors had significantly higher blood pressures, 20 to 40 mm Hg greater, than normal WT mice. Additionally, mice that overexpressed ANP in a transgenic line had blood pressures 20 to 30 mm Hg lower than normal WT mice (Ogawa et al., 2004). Physiological doses of ANP in humans has been shown to suppress

both renin and aldosterone levels, which led to a decrease blood pressure (Potter et al., 2006). ANP has also been shown to directly inhibit the production of aldosterone in the adrenal gland, through activation of PDE2, a cGMP-activated PDE that degrades cAMP. The secondary messenger molecule cAMP is crucial for the synthesis of aldosterone synthesis (Potter et al., 2006).

1.13.5 Regulation of Cell Growth and Proliferation by Atrial Natriuretic Peptide

ANP has been shown to inhibit cell proliferation of several cell types, including vascular smooth muscle cells, through production of intracellular cGMP (Woodard and Rosado, 2008; **Table 1.1 and Table 1.3**). Studies sought to determine the association between ANP and cGMP and its potential anti-proliferative effects on vascular smooth muscle cells when it was first discovered that NO, a cGMP-donor, was capable of exerting anti-proliferative effects on this cell type (Woodard and Rosado, 2008). Indeed, several studies have found that ANP can attenuate cell growth and proliferation of smooth muscle cells, CMs, and fibroblasts (Woodard and Rosado, 2008; Horio et al., 2000; Tsuruda et al., 2002). After hypertrophy was induced in CMs by addition of angiotensin II (Ang II), ET-1, or phenylephrine, the addition of ANP has been shown to inhibit hypertrophy and proliferation of these CMs, both *in vitro* and *in vivo* (Horio et al., 2000; Rosenkranz et al., 2003; Laskowski et al., 2006; Kilic et al., 2007). The exogenous addition of ANP at concentrations between 0.1 and 1 μ M reduced protein synthesis in cultured neonatal rat cardiac myocytes evaluated by incorporation of [14 C] phenylalanine (14 C-Phe) into cells (Horio et al., 2000). Addition of an NPR-A antagonist,

known as HS-142-1, significantly increased protein synthesis due to increased uptake of ^{14}C -Phe and also induced a significant increase in the cell surface area of myocytes (Horio et al., 2000).

Interestingly, genetic ablation of either ANP or NPR-A genes also led to significant increases in cardiac hypertrophy, signifying the importance of the ANP/NPR-A signalling axis in attenuating cardiac hypertrophy (Lopez et al., 1995; John et al., 1996; Oliver et al., 1997). To further clarify if ANP was truly exerting direct anti-hypertrophic effects on CMs or whether this was an indirect effect due to the natriuretic and diuretic properties of this paracrine factor which decreases blood pressure and blood volume, NPR-A knockout mice were given anti-hypertensive drugs to normalize blood pressure, and despite becoming normotensive, these mice still demonstrated hypertrophy and fibrosis, providing a convincing argument that ANP had a direct anti-hypertrophic effect in the heart (Knowles et al., 2001).

Not only does ANP exert anti-hypertrophic effects on CMs, but these effects also extend to other cell types found in the heart, including cardiac fibroblasts, vascular smooth muscle cells, and mesangial cells (Cao and Gardner 1995, Sharma et al., 2002, Tripathi and Pandey, 2012). NPR-A knockout embryonic hearts of mice were shown to be significantly enlarged at mid-gestation, providing evidence that normal functioning of the receptor may be important for regulating cardiac growth during embryonic heart development (Ellmers et al., 2002).

1.13.6 Role of Atrial Natriuretic Peptide in Cardiac Development

The transient expression of ANP in the ventricles during cardiac ontogeny suggests that ANP could be important in regulating cellular proliferation and/or differentiation to promote cardiac development. To support this notion, studies have demonstrated that mice lacking NPR-A receptors display reduced survival, experience cardiac hypertrophy at mid to late gestation, and also experience morphological abnormalities like dextrocardia and mesocardia (Cameron and Ellmers, 2003; Lopez et al., 1995; Ellmers et al., 2002; Scott et al., 2009). In both embryonic mice and rats, it has been shown that ANP mRNA is abundantly expressed in trabecular myocardium around mid-gestation (Zeller et al., 1987; Toshimori et al., 1987). The trabecular myocardium has been proven to be the embryonic precursor to Purkinje fibers and the Bundle of His of the mature CCS and serves as the preferred route for electrical conduction prior to the mature CCS forming (Viragh and Challice 1977; Sedmera et al., 2003; Sankova et al., 2012, see Section 1.3.3). However, despite this knowledge, the potential role of ANP in the development of the VCS is poorly understood in literature.

Recently, a potential role for ANP in cardiac development has been identified. At E11.5, mouse/rat ANP significantly decreased cell number and DNA synthesis of CPCs, but not CMs, and this effect was reversible using the NPR-A antagonist A71915 (Hotchkiss et al., 2015; see **Figure 1.8 for the structure of A71915**). Therefore, ANP may play a local paracrine role in regulating the balance between CPC proliferation and differentiation through NPR-A/cGMP mediated pathways (Hotchkiss et al., 2015). Another study showed that addition of human/porcine ANP to fetal sheep CMs inhibited

Ang II-stimulated proliferation (O'Tierney et al., 2010). However, there is some discrepancy in the literature as to whether ANP truly exerts anti-proliferative effects, since exogenous addition of human ANP to embryonic chick CMs resulted in an increase in proliferation of these cells (Koide et al., 1996). Although the primary amino acid sequence of chick NPR-A is not known, chick ANP lacks the well conserved amino acid residues of human ANP (G10, A17, Q18, L21, S25 and F26; **Figure 1.8**) that have been shown to be critical for binding with the extracellular domain of human NPR-A via molecular modeling studies (Parat et al., 2008). Thus, it is possible that results reported by Koide et al. (1996) could be attributed to sequence differences between human and chick ANP and NPR-A receptors.

1.14 The Potential Role of Atrial Natriuretic Peptide in the Development of the Cardiac Conduction System

ANP may play an important role in the development of the VCS. Due to the unique spatiotemporal expression pattern of ANP in the ventricular trabeculae of the developing mouse heart, it has been hypothesized that ANP may be an important paracrine regulator of cardiac growth (Hotchkiss et al., 2015). In a recently published model of VCS development (Weerd and Christoffels, 2016), it has been hypothesized that paracrine interactions between embryonic myocytes and cardiac endothelial cells may play a key role in driving local recruitment of conduction cells from beating myocytes (Mikawa and Hurtado, 2007). Cell lineage studies have demonstrated that periarterial and subendocardial CMs can be recruited into the formation of periarterial and subendocardial Purkinje fiber networks in avian hearts (Mikawa and Fischman,

1996; Mikawa, 1999; Mikawa and Hurtado, 2007). Endothelial cells are the only cell type present in both endocardium and in arterial endothelium, both of which are adjacent to myocytes that are capable of differentiating into Purkinje fibers, and thus it was hypothesized that an endothelial cell-derived signal may play a role in recruitment of conduction system cells (Mikawa and Hurtado, 2007). When Gourdie et al. (1998) studied the effects of ET-1 on embryonic chick CMs, it was found that this paracrine factor, which is released from endothelial cells, was capable of upregulating expression of important CCS markers, *in vitro* (Cx40 and Cx43). This was subsequently validated *in vivo* (Takebayashi-Suzuki et al., 2001). Similarly, NRG-1 is a paracrine factor derived from endothelial cells, and was shown to induce formation of CCS cells during heart development, in a mouse CCS-*lacZ* reporter line employed by Rentschler et al. (2002). The evidence presented thus far sets a strong precedent for the role of a paracrine factor that is secreted from the endocardial/endothelial cells, in specifying the conduction system cell lineage in an autocrine/paracrine fashion. Based on this body of knowledge, it is possible that ANP present in the trabecular myocardium of the developing embryonic heart may interact with NPR-A receptors of nearby cells in the trabeculae to not only modulate cellular proliferation and differentiation, but also may be capable of inducing expression of conduction system markers in an autocrine/paracrine fashion (**Figure 1.7**).

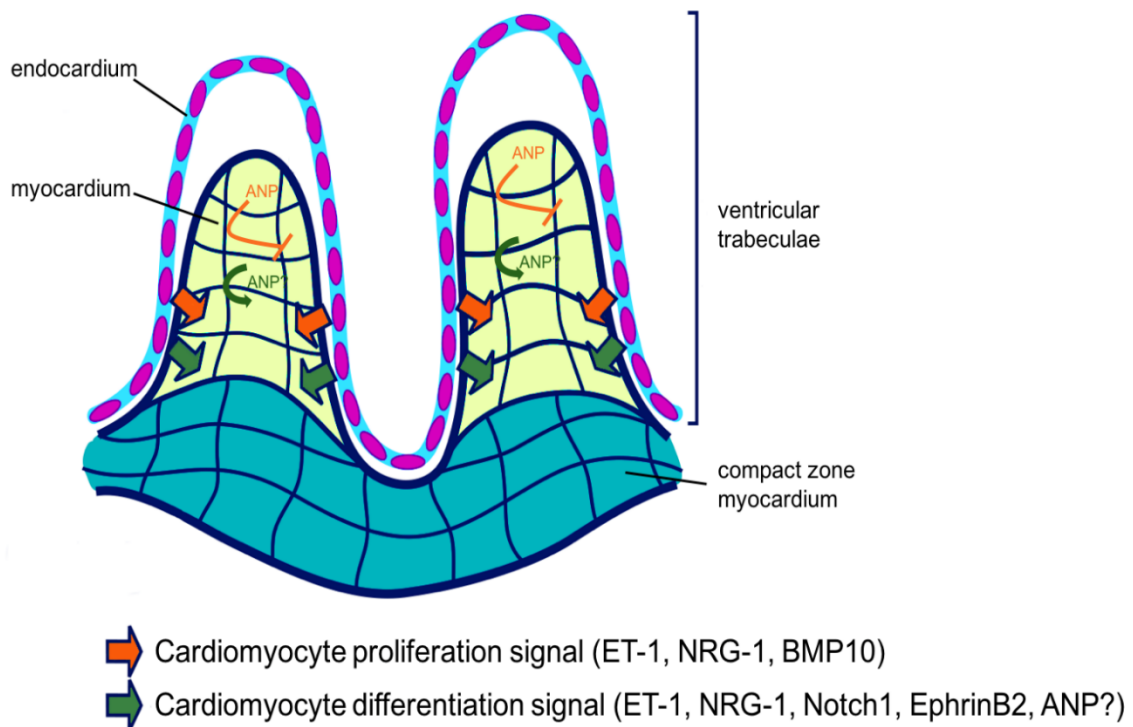


Figure 1.7. Model depicting potential signalling interactions of three paracrine factors: atrial natriuretic peptide (ANP), neuregulin-1 (NRG-1), and endothelin-1 (ET-1) and their cognate receptors to induce formation of the ventricular cardiac conduction system (VCS) within the ventricular trabecular myocardium of the mouse embryonic heart. NRG-1, ET-1 and Notch1 are secreted from endothelial/endocardial cells and have been shown to specify the conduction system cell lineage in an autocrine/paracrine fashion, by promoting differentiation of CMs in the primitive myocardium to trabecular myocardium (green arrows). Some cells in the ventricular trabeculae eventually develop into the bundle branches and Purkinje fibers of the mature VCS. It is possible that ANP may interact with NPR-A receptors present in the primitive myocardium to promote differentiation of CMs into VCS cells, and may also continue to develop ventricular trabeculae in order to form the cardiac Purkinje fiber network of the VCS. NRG-1, ET-1 and BMP10 signals to the trabecular myocardium to promote proliferation of CMs (orange arrows). ANP has been shown to inhibit proliferation of CMs (orange). A complex signalling network involving ANP, NRG-1, and ET-1 may exist in the ventricular trabeculae to promote development of the cardiac Purkinje fiber network. Figure adopted from (de la Pompa and Epstein, 2012) and modified minimally with permission from the publisher (see **APPENDIX V**).

1.15 Characterizing the Specific Roles of Atrial Natriuretic Peptide in Cell Biology: A Paradigm Shift

There is a significant and growing body of literature describing the effects of exogenous ANP on *in vitro* proliferation and differentiation of cardiovascular cell types (i.e. CMs, CPCs, vascular smooth muscle cells and fibroblasts). It is important to recognize that discrepancies between studies in the literature do exist. For example, in various cardiovascular cell types, ANP has been shown to either increase or decrease proliferation. The effects of ANP on cardiovascular and non-cardiovascular cell types as described in the literature have been summarized (**Table 1.1 and Table 1.3**). Primary sequences of ANP from several species as listed in these tables are shown in **Figure 1.8**. As seen from these tables, discrepancies in the biological effects of ANP may be attributed to the varying doses of ANP utilized in each study. An important question to consider is whether ANP is acting in a physiological or pharmacological role to induce biological changes, and whether this is dependent on the concentration of ANP added to treatment groups. Another important question that is raised is whether ANP should be considered as acting in an endocrine or paracrine role in inducing biological effects in the literature. While concentrations of ANP measured in circulation were low, tissue concentrations in specific organs are much higher (**Table 1.2**). We propose a paradigm shift in the way we view the role of ANP, depending on the source of ANP, whereby ANP that is present in plasma or serum that exerts biological effects should be considered to have an endocrine role, whereas ANP that is present in tissue that exerts biological effects should be considered to have a physiological or paracrine role. Local concentrations of ANP can be several orders of magnitude higher than in the general

circulation, as is evidenced by **Tables 1.15.1-1.15.3**, and this may be conducive to a paracrine signalling role for ANP, for example, in the development of the embryonic trabecular myocardium. This concept of viewing the differences in circulatory vs. local ANP concentrations as correlating with whether to assign an endocrine or paracrine role to the hormone draws a similar parallel to the activity of norepinephrine, whereby circulating levels are also generally low (~200-1700 pM), while local concentrations, for example in synaptic clefts are much higher (up to 3.3 nM) (Goldstein et al., 1986).

There are several challenges in searching the literature for a consensus on how to view the impact of ANP in an endocrine or paracrine role. One such limitation is that currently there is no adequate method to measure ANP in fluid compartments, such as the fluid bathing the trabecular myocardium of the developing heart. Furthermore, it may be technically challenging to distinguish the specific biologic effects of the precursors of the ANP hormone, including prepro-ANP, pro-ANP, and mature ANP itself. This leads to several unanswered questions: do the larger molecular-weight forms of unprocessed ANP have signalling functions? And is it possible to distinguish these functions from one another?

We propose that the endocrine functions of ANP require low concentrations of ANP, whereas the paracrine effects of ANP may require a much higher concentration, for example, in localized regions of developing ventricles. It remains to be determined what effects we can consider to be physiological vs. pharmacological in the context of *in vitro* experiments using exogenous ANP. In order to address some of these challenges and limitations, we suggest that it would be highly beneficial to develop methods that

accurately measure local concentrations of ANP. Moreover, assays that detect concentrations of prepro-ANP vs. pro-ANP vs. mature ANP would add significant value to our understanding of the biological effects of ANP. Such methods would certainly help in making distinctions between what effects are pharmacological vs. what effects are physiological, which seems to be a contentious issue across numerous studies.

Type of ANP	Cell Type Used	Con. Range (Reported)	Con. Range (Converted; nM)	Receptor Activated	Downstream Signalling	Biological Effect	Reference/PMID
Mouse (1-28)	E11.5 mouse CPCs and CM	1-100 ng/mL	0.3-30nM	NPRA	cGMP	↓ in CPC prolif. (Thym. inc.) (30nM)	Hotchkiss et al., 2015 25631869
Rat (1-28)	Neonatal rat ventricular CM	0.5-10,000 nM	0.5-10,000 nM	NPRA	cGMP/PKG	↓ in CM prolif. (1000 & 10,000 nM)	Becker et al., 2014 24353062
	Neonatal rat ventricular CM	0.5-10,000 nM	0.5-10,000 nM	NPRC	Gi/AC/cAMP	↑ in CM prolif. (0.5-100nM)	
	H9C2 cells (CM cell line)	0.25-1000nM	0.25-1000nM	NPRA		↓ in prolif (Cyquant) 100-1000 nM	
	H9C2 cells (CM cell line)	0.25-1000nM	0.25-1000nM	NPRC		↑ in prolif (Cyquant) 0.75-1 nM	
Human/Porcine (x-x)	Fetal/Ovine CM	0.003-100 nM	0.003-100 nM	NPRA	cGMP	↓ in CM prolif. (BrdU) (0.003nM in RV) (100 nM in LV)	O'Tierney et al., 2011 20519318
Human (1-28)	Embryonic chick CM	0.1 & 1µM	100-1000 nM	NPRA	NOT cGMP	↑ in CM prolif. (BrdU) (100 & 1000 nM)	Koide et al., 1996 8921580
Rat (1-28)	Cardiosphere Derived Cells (CDC)	1µg/mL-1µg/mL	0.0003-3,000 nM	Not reported	Not reported	↓ in CDC prolif (WST) 0.0003, 300 and 3000 nM	Stasna et al., 2010 20014349
Rat (1-28)	Neonatal Rat Cardiac Fibroblasts	10 ⁻¹¹ -10 ⁻⁶ M	0.001-1000 nM	NPRA/NPRB (implied, did not use antagonist)	cGMP (implied, since ANP stim cGMP production)	↓ in prolif (3H-Thymidine) 0.1-1000nM (AngII stim) 1-1000nM (ET-1 stim)	Fujisaki et al., 1995 7635942
Rat (1-28)	Neonatal Rat Cardiac Fibroblasts	10 ⁻⁷ M	100nM	NPRA/NPRB	cGMP analogue mimicked broad and PDE5 inhibitors enhanced	↓ in prolif (3H-Thymidine) (MTT assay) (basal, GF, vasoactive pep, stretch stim. conditions)	Cao and Gardner 7843772

*Literature survey was conducted in collaboration with Dr. Adam Hotchkiss.

Table 1.1. Summary of the reported biological effects of exogenous ANP on cardiovascular cell types.

Table 1.2. Reported concentrations of ANP in the circulation (plasma or serum) in different species and different developmental stages vs. concentrations of ANP measured from organs (tissue). ANP in the circulation is generally considered to play an endocrine role, whereas ANP in local tissue can be considered to have a physiological/paracrine role.


Species	Developmental Stage	What was measured	Conc. Reported	Conc. Converted	Reference/PMID	
Mouse	E11.5	Ventricular tissue lysate	4.3 ± 0.7 ng/μg	4.3 ng/μg	Hotchkiss et al., 2015 25631869	
	Neonatal	Ventricular tissue lysate	2.3 ± 0.5 ng/μg	2.3 ng/μg		
Rat	E20	Plasma	2.7 ± 0.18 ng/mL ANP 60 ± 12 ng/mL NT-ANP	2.7 ± 0.18 ng/mL ANP 60 ± 12 ng/mL NT-ANP	Wei et al., 1987 2952670	
	Adult	Plasma	0.46 ± 0.05 ng/mL ANP 4.3 ± 0.05 ng/mL NT-ANP	0.46 ± 0.05 ng/mL ANP 4.3 ± 0.05 ng/mL NT-ANP		
	E20	Ventricular tissue lysate Atrial tissue lysate	24.8 ± 1.9 ng/mg 548 ± 43 ng/mg	0.024 ng/μg (1-28 only?)* 0.548 ng/μg (1-28 only?)*		
	Post-natal day 21	Ventricular tissue lysate Atrial tissue lysate	1.2 ± 0.1 ng/mg 2880 ± 216 ng/mg	0.001 ng/μg (1-28 only?)* 2.880 ng/μg (1-28 only?)*		
	Adult	Plasma	158 +/- 15 pg/ml		Ortola et al., 1987 2957390	
	Adult	Atrial tissue lysate	300.0 +/- 14.2 ng/mg		Morii et al., 1986 2937405	
	Adult	Plasma	88 +/- 14 pg/ml		Ruskoaho et al., 1989 2526698	
		Atrial tissue lysate Ventricular tissue lysate	56.2 +/- 7.2 (Total); 141 +/- 14 (Right auricle); 122 +/- 9 (left auricle) ng/mg 69 +/- 8 (Total); 71 +/- 9 (left ventricle); 57 +/- 4 (right ventricle) pg/mg			
	Human	Adult	Plasma	19.6 +/- 1.8 pmol/L		Shenker et al., 1985 2932471
	Adult	Plasma	29.1 +/- 1.7 pmol/L 1199 +/- 53 pmol/L N-ANP		Omland et al., 1996 8640969	
Aged Adult	Plasma	39.5 +/- 2.6 pg/mL		Morita et al., 1993 8319360		
Adult	Plasma	58 +/- 12 pg/mL		Weidmann et al., 1986 2936762		

* Literature survey was conducted in collaboration with Dr. Adam Hotchkiss.

Type of ANP	Cell Type Used	Con. Range (Reported)	Con. Range (Converted; nM)	Receptor Activated	Downstream Signalling	Biological Effect	Reference/PMID
Not known	Granulosa cells from bovine ovaries at various stages of estrus cycle	10^{-8} - 10^{-7} M	10-100 nM	Not reported	Not reported	↓ in GC prolif. (Thym. inc.) (10-100 nM)	Montazer et al., 2015 25500175
Not known	Human gastric adenocarcinoma (AGS) cells	10^{-8} - 10^{-9} M	0.1-1 nM	NPRA	cGMP	↑ in AGS cell prolif. (BrdU. inc.) (0.1-1 nM)	Zhang et al., 2013 24137337
		10^{-7} - 10^{-6} M	100-1000 nM	NPRA	cGMP	↓ in AGS cell prolif. (BrdU. inc.) (100-1000 nM)	Zhang et al., 2013 24137337
Human ANP	Human colorectal cancer (adenocarcinoma) cells	1 μ M	1000 nM	Wtr	Wtr/ β -catenin signaling	↓ in colorectal adenocarcinoma cell prolif. (Assessed by confocal then flow cytometry - mitotic index, BrdU inc.) (1000 nM)	Serifino et al., 2012 22387884
Rat ANP	Rat FC12 cells (embryonic origin in neural crest, with neuroblastic cells)	1-100 nM	1-100 nM	NPRA	cGMP	↑ in FC12 prolif by way of inhibiting DNA fragmentation (apoptosis), prolonged survival (DNA laddering, capillary electrophoresis with laser induced fluorescence CE-LIF) 1, 10, 100 nM	Fiscus et al., 2001 11209918
Rat ANP (1-28)	Rat astroglial cells E16, E17	10^{-12} - 10^{-8} M	0.001-10 nM	NPRC	Not reported	↓ in astroglial cell prolif (Thym inc.)	Levin et al., 1991 163217
Not known	Rat endothelial cells	10^{-7} M	100 nM	Not reported	Not reported	↓ in EC prolif by way of inducing apoptosis (TUNEL) (%), DPA for DNA fragmentation quantification (100 nM)	Suzobu et al., 1999 9888876
Rat ANP (1-28)	Bovine aortic endothelial cells	10^{-7} - 10^{-6} M	100-1000 nM	NPRA, NPR-B implied	cGMP antagonism of bFGF and cGMP	↓ in EC proliferation (Thym inc.) (100, 1000 nM)	Itok et al., 1992 1534317
Human ANP (1-28)	Human coronary arterial endothelial cells	10^{-13} - 10^{-11} M	0.0001-0.01 nM	Not reported	cGMP/cGK	↑ in EC proliferation (Thym inc.) (0.001-0.01 nM)	Koek et al., 2002 1250872
Human ANP (1-28)	Human coronary arterial endothelial cells	10^{-7} - 10^{-5} M	100-10000 nM	Not reported	cGMP/cGK	↓ in EC proliferation (Thym inc.) (100-1000 nM)	
Not known	Rat Cardiac fibroblasts	10^{-7} M	100 nM	NPRA and/or NPRB	cGMP	↓ in fibroblast prolif., also suppresses expression of ET-1, which stimulates fibroblast growth (Thymidine inc.) (100 nM)	Cleyn et al., 2009 19546173
Rat ANP (1-28)	Rat Cardiac fibroblasts	1 μ M	1000 nM	NPRA	cGMP	↓ in fibroblast prolif. (MTT inc.) (1000 nM)	Moharuk et al., 2014 25470517
Rat ANP (99-126)	Vascular smooth muscle cells (Aortic)	1-100 nM	1-100 nM	NPRA, NPRB	cGMP	↑ in VSMC proliferation, indirectly, through amplifying the proliferative effect of growth factor FGF-2. Dhaunis et al., 1996 (Thymidine incorporation) (Significant and relevant concentrations: 10, 50, 100 nM ANP)	8845587
Rat ANP (1-28)	Rat mesangial cells	100 nM	100 nM	NPRA	cGMP	↓ in mesangial cell prolif (Thym inc.) (100 nM)	Pandley et al., 2000 10799905

Table 1.3. Summary of reported biological effects of exogenous ANP on non-cardiovascular cell types.

A**Formatted Alignments**

	N terminus	C terminus
Mouse ANP NP_032751.1		
Mouse ANP NP_032751.1	S L R R S S C F G G R I D R I G A Q S G L G C N S F R Y	
Rat ANP NP_036744.1	S L R R S S C F G G R I D R I G A Q S G L G C N S F R Y	
Ovine ANP NP_001153499	S L R R S S C F G G R M D R I G A Q S G L G C N S F R Y	
Human ANP NP_006163	S L R R S S C F G G R M D R I G A Q S G L G C N S F R Y	
Chick ANP NP_990256	M M R D S G C F G R R I D R I G S L S G M G C N G S R K	

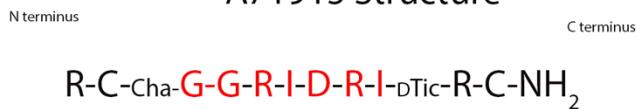
B**A71915 Structure**

Figure 1.8. Primary sequences of species expressing biologically active atrial natriuretic peptide (28 amino acids) and structure of NPR-A inhibitor A71915. A) The alignment of the ANP predicted protein sequence (28 amino acids) which is biologically active, from humans and several other species used commonly in experiments is shown. Shaded boxes correspond to amino acids that are conserved between mouse, rat, sheep, human and chick. This sequence is highly conserved among mammalian species. **B)** Structure of NPR-A inhibitor A71915. Red line in Panel A and amino acids highlighted in red in Panel B correspond to the sequence of amino acids that are conserved in A71915 vs. mouse and rat ANP. Cha, β -cyclohexyl-Ala; DTic, D-1,2,3,4-Tetrahydroisoquinoline-3-carboxylic acid.

CHAPTER 2: MATERIALS AND METHODS

2.1 Animal Maintenance and Mouse Strains

All animal procedures were performed according to the Canadian Council on Animal Care guidelines and were approved by the Dalhousie University Committee on Laboratory Animal Care (CCAC, Ottawa, ON: Vol 1.1.2, 2nd edition, 1993; Vol 2, 1984, Protocol No. 16-048). **CD1** and **C57BL/6 (BL6)** mice were obtained from Charles River Laboratories (Montreal, Canada). The **Nkx2.5-Cre** mouse strain was (abbreviated as NC) initially characterized by Stanley et al. (2002) and was provided by Dr. Richard Harvey (Victor Chang Cardiac Research Institute, University of South Wales, Australia). NC mice were engineered to have an internal ribosomal entry sequence (IRES) and a Cre-recombinase (Cre) coding sequence inserted into the 3' untranslated region of the Nkx2.5 gene. The generation of mice with Cre recombinase inserted into the Nkx2.5 allele was previously described (Stanley et al. 2002). The **R26R** reporter strain (designated as *Rosa-LacZ* and abbreviated as RL) was obtained from Jackson Laboratories (Bar Harbor, Maine, USA). The ***Npr1*^{-/-}** (NPRA-KO) mouse strain, initially characterized by Oliver et al. (1997), was utilized for studying the NPRA-KO genotype. This strain was obtained from Dr. Nobuyo Maeda (University of North Carolina, USA). In *Npr1*^{-/-} mice, exon 1 and intron 1 of the *Npr1* gene which encodes for the NPR-A receptor were replaced with a neomycin resistance cassette. The **Cx40^{egfp+}** mouse strain was utilized to study the formation of the Purkinje fiber network; in this strain, an enhanced green fluorescent protein (EGFP) coding sequence followed by pgk-neo cassette was inserted in frame at the Cx40 start codon (Miquerol et al., 2004). This

strain was received from Dr. Robert Rose (Dalhousie University, Canada). All transgenic lines were maintained in C57BL/6 (BL6) background. Unless otherwise stated, CD1 mice were utilized for all experimental procedures.

2.2 Genomic DNA Extraction

In order to determine the genotype of transgenic mouse strains, ear punch biopsies were obtained for routine genotyping. Extraction of genomic DNA was performed from ear punch biopsy samples using the Sigma REExtract-N-AMP tissue PCR kit (Sigma, Oakville, Ontario, Canada), according to the manufacturer's instructions. Each ear tissue sample was placed in 50 μ l of DNA extraction solution, which was composed of 40 μ l Extraction Solution and 10 μ l Tissue Preparation Solution. Then samples were manually triturated using a sterile pipette tip. After incubation for 10 minutes at room temperature, samples were heated to 95°C in a heating bath. Then, 10 μ l of Neutralization Buffer was added to each sample and samples were mixed briefly by vortexing for a few seconds. Samples were then centrifuged to pellet undigested tissue and the supernatant was used as a template for polymerase chain reaction (PCR).

2.3 Genotyping by Polymerase Chain Reaction (PCR)

PCR was performed using REExtract N-AMP kit (Sigma) with a total reaction volume of 10 μ l. All primers were obtained from Invitrogen (Burlington, Ontario, Canada) and primer sequences are found in **Table 2.1**. Each PCR reaction mixture contained 5 μ l REExtract-N-AMP PCR mix, 0.5 μ l of each primer (50 ng each) and 2 μ l of

tissue extract. Water was added to reach a final volume of 10 μ l. For **Nkx2.5-Cre (NC) genotyping**, PCR reactions were performed for 30 cycles as follows: 30 sec at 94°C, 20 sec at 60°C, and 60 sec at 72°C. Expected PCR products were 583 bp for the knock-in allele and 264 bp for the wildtype allele (**Figure 2.1 A**). No template controls were routinely performed in PCR reactions to rule out false positive results. For **Rosa-LacZ (RL) genotyping**, PCR reactions were performed for 30 cycles as follows: 30 sec at 94°C, 30 sec at 60°C, and 60 sec at 72°C. Expected PCR product sizes were 650 bp for the wildtype and 320 bp for the knock-in allele (**Figure 2.1 B**).

To ensure phenotype integrity of NCRL mice embryos, the atria of E11.5 ventricular cells were stained with X-gal (Goldbio, Missouri, USA). The atria of hearts (whose ventricles were to be used for cell cultures) were placed in X-Gal solution for 1 hour and incubated at 37°C. X-Gal solution was prepared by adding 0.01 g of X-Gal powder to 2.5 mL of N, N-Dimethyl Formamide (DMF, Sigma), and added drop-wise to an 80 mL PBS solution containing 200 μ L of 1M MgCl₂, 0.164g potassium ferricyanide, and 0.212g potassium ferrocyanide. Only ventricles whose corresponding atria stained blue for the presence of β -gal protein were utilized in further experiments.

For ***Npr1*^{-/-} genotyping**, PCR reactions were performed for 34 cycles: 30 sec at 94°C, 60 sec at 55°C, and 60 sec at 72°C. Expected PCR product sizes were 339 bp for the wildtype and 500 bp for the knockout allele (**Figure 2.1 C**). For ***Cx40*^{egfp} genotyping**, PCR reactions were performed for 34 cycles as follows: 30 sec at 94°C, 60 sec at 55°C, and 60 sec at 72°C. Expected PCR product sizes were 380 bp for the WT and 450 bp for the knock-in allele (**Figure 2.1 D**).

Name of Primer	Primer Sequence (5' → 3')	Expected band sizes (bp)	
		WT allele	Knock-in/knockout allele
Nkx2.5-S	GCCCTGTCCCTCGGATTTACACACC	264	583
Nkx2.5-AS	ACGCACTCACTTTAATGGGAAGAG		
Cre-S	GATGACTCTGGTCAGAGATACCTG		
Rosa 1	AAAGTCGCTCTGAGTTGTTAT	650	320
Rosa 2	GCGAAGAGTTTGTCTCAACC		
Rosa 3	GGAGCGGGAGAAATGGATATG		
Npr1-S	GCATGGTTCAGCTCTAAGA	339	500
Npr1-AS	CTAACCTGTGAACTGTAAGC		
Neo-AS	CCTTCAGTTATCTACATCTGC		
Cx40-S	CTCCAATTA ACTCCTTGTGAGCC	380	450
Cx40-AS	AGGCTGAATGGTATCGCACC		
Neo-AS	CTTGCCGAATATCATGGTGG		

Table 2.1. List of primers utilized for genotyping and their expected band sizes. Genotyping by PCR was performed utilizing these primers and primer sequences. Expected band sizes (bp) for WT and transgenic alleles are listed.

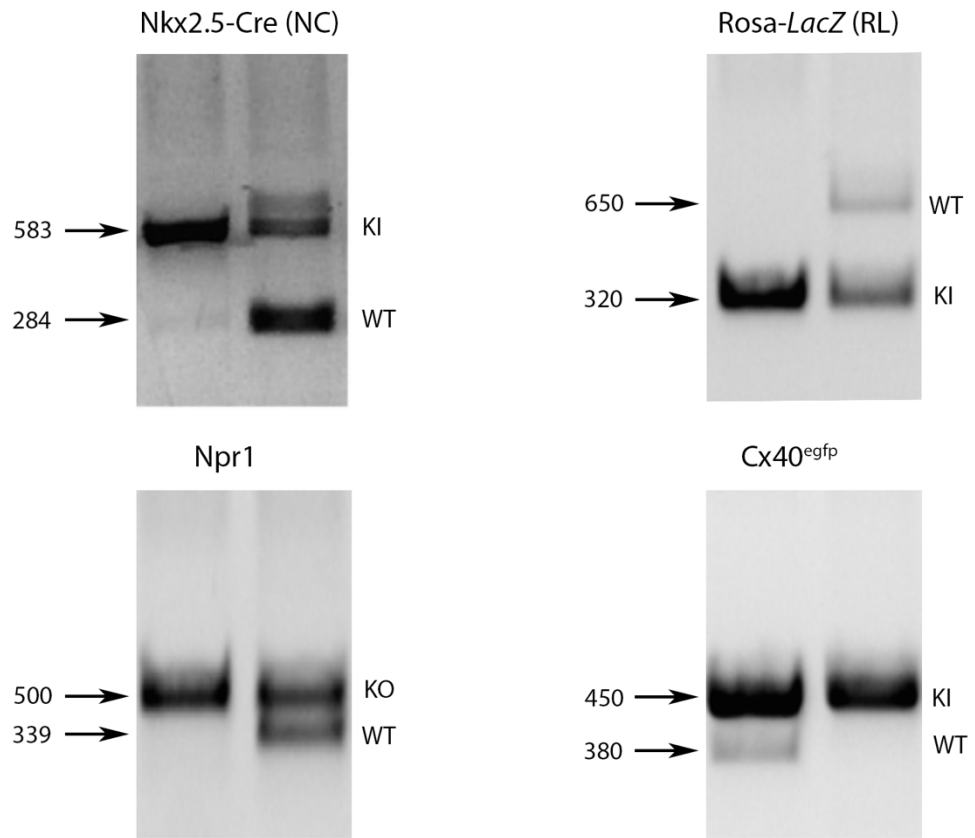


Figure 2.1. Expected band sizes (bp) from the genotyping of various mouse strains. A) Nkx2.5-Cre (NC) B) Rosa-LacZ (RL), C) Npr1 D) Cx40^{egfp}. KI = knockin allele, KO = knockout allele, WT = wild-type allele.

2.4 Timed Pregnancies for Female Mice

Breeding pairs were placed in the same cage overnight, and the following morning, females were examined for the presence of a vaginal plug. Male ejaculate formed a white/yellow fibrous plug in the female vagina and the presence of a vaginal plug was indicative of successful copulation. The morning where the plug was detected was considered to be embryonic day E0.5. Timed pregnant females were anesthetized using 4% isoflurane and were sacrificed by cervical dislocation. Embryos from various developmental stages (E11.5, E14.5 and E17.5) were isolated from the uterine horns and embryonic hearts were dissected using a Leica MZ16SF stereomicroscope (Leica Microsystems, Richmond Hill, Ontario, Canada). In some experiments, 1 day old new born pups (neonates, ND1s) were sacrificed using 4% isoflurane and cervical dislocation and hearts were collected.

2.5 Ventricular Cell Cultures

Mouse embryos were removed from the uterus, followed by removal of the placenta, and the embryos were placed in dishes containing warm PBS (0.138 M NaCl, 0.0027 M KCl, pH 7.4) supplemented with 1x antibiotic/antimycotic (Ab/Am, Gibco, Burlington, Ontario, Canada). Whole hearts were dissected out of embryos and the atria and outflow tracts were removed. Right and left ventricles from each embryo were placed in 0.2% v/v type I Collagenase (Worthington Biochemical Corp., Lakewood, New Jersey, USA) in 1x PBS and incubated for 30 minutes at 37°C to digest ventricular tissues. Following the 30-minute incubation period, tissue was triturated using a 200 µl

pipette tip to mechanically dissociate cells from remaining tissue pieces. Cells were centrifuged at 4,000 rpm for 4 minutes, collagenase was discarded, and the pellet was neutralized with two washes of 10% DMEM (Dulbecco's Modified Eagles Medium; Wisent, Saint Bruno, Quebec, Canada) containing 10% fetal bovine serum (FBS; Wisent, Saint Bruno, Quebec, Canada). Unless otherwise noted, all cell cultures were treated with 10% DMEM (FBS + Ab/Am). The number of cells was determined using a hemocytometer and cells were re-suspended in 10% DMEM to achieve the required cell numbers. Cells were plated at various densities on either fibronectin (Sigma) coated 2- or 4-well chamber slides (250,000 cells/well, Nunc, Rochester, New York, USA), 35 mm dishes (500,000 cells/well, Corning, Corning, New York, USA), or black-walled clear bottom 96-well plates (4000-100,000 cells/well) Greiner Bio-One, North Carolina, USA (Cat#: 655809).

Human embryonic kidney epithelial cells (HEK293) cells were purchased from American Type Culture Collection (ATCC, Virginia). HEK293 cells were trypsinized and re-suspended in culture plates at a density of 300,000 cells per 35 mm dish, and were incubated with DMEM supplemented with 10% FBS and 1x Ab/Am.

2.6 Drug Treatments and Dosage Protocols

ANP (Bachem, King of Prussia, Pennsylvania, USA Cat#: H-2100.0.500) was prepared as a stock solution by dissolving 0.5 mg ANP in 0.5 mg sterile H₂O (Ambion, USA), which was aliquoted and stored at -80°C. Working solutions were prepared at either 1000 ng/μl, 100 ng/μl, 10 ng/μl or 1 ng/μl by serial dilution using sterile H₂O

(Ambion) immediately prior to use on the day of the experiment. For ventricular cell cultures receiving 1000 ng/ml ANP treatment, 1 μ l of 1000 ng/ μ l ANP was added per 1 ml culture medium. Similarly, either 1 μ l of 1 ng/ μ l, 1 μ l of 10 ng/ μ l, or 1 μ l of 100 ng/ μ l ANP working solution was added per 1 ml culture medium to achieve final concentrations of 1, 10, or 100 ng/ml. NPR-A antagonist A71915 stock solution (Bachem, Cat#: H-3048.0500) was prepared by dissolving 0.5 mg A71915 in 0.5 ml H₂O (Ambion) and was then aliquoted and stored at -20°C. For ventricular cultures receiving A71915 treatment, a final concentration of 1 μ M was achieved by adding 2.42 μ l of A71915 stock per 1 ml culture medium. Other concentrations of A71915 were prepared either by serial dilution (0.1 to 0.5 μ M) or by adding the required volume of A71915 stock solution in 1 ml culture media to reach the desired final concentration (2 μ M to 10 μ M). For the addition of combination treatments (ANP + A71915) in all described experiments of this thesis, ANP was added to a 15 or 50 mL Falcon™ conical centrifuge tube containing 10% DMEM (FBS + Ab/Am) first, and then A71915 was added to the tube after 5 minutes. Then, the contents of the tube were distributed to whole embryos/tissue/cells.

The exogenous cGMP compound, 8-Bromoguanosine 3',5'-cyclic monophosphate sodium salt (8-Br-cGMP; Sigma, Cat#: B1381) was prepared as a 100 mM stock solution by dissolving 0.0446g in 1 ml H₂O (Ambion, USA). This compound was added to embryonic ventricular cell cultures at a final concentration of either 100 μ M or 10 μ M. To prepare 100 μ M working solution, 1 μ l of 8-Br-cGMP stock solution was added per 1 ml culture medium. 10 μ M working solution was prepared by dilution of the

100 mM stock solution (1 μ l of 100 mM working solution added to 9 μ l H₂O) and 1 μ l of this working solution was added per 1 ml culture medium.

Isoproterenol (ISO; Sigma, Cat#: I6504) was prepared as a 50 mM stock solution by dissolving 0.0124g in 1 ml H₂O (Ambion, USA). From this 50mM stock, 2 μ l of stock solution was diluted in 98 μ l culture media to prepare a 1mM working solution. From this, 1 μ l of working solution was added per 1 ml culture media to achieve a final concentration of 1 μ M.

ET-1 (Sigma, Cat#: E7764) was prepared as a stock solution by dissolving 10 μ g in 100 μ l of H₂O (Ambion, USA). Aliquots were prepared and stored at -20°C. To achieve a final working concentration of 1.5 nM, 1 μ l of stock solution was added per 20 ml culture media.

NRG-1 (NRG-1 β , R&D systems, Cat#: 396-HB) was prepared by first preparing a solution containing 0.002g BSA dissolved in 2 ml of 1x PBS (the solution was then filtered using a 0.2-micron filter), and then adding 500 μ l of this solution to the 50 μ g powder. Aliquots were prepared and stored at -80°C. To achieve a final concentration of 2.5 nM, 40 μ l of working solution was added per 1 ml culture media.

The PKG inhibitor compound, Rp-8-pCPT-cGMPS (Tocris Bioscience, Cat#: 5524), was prepared as a 1 mM stock solution by dissolving the powder in 1.9 ml H₂O (Ambion, USA). Aliquots were prepared and stored at -20°C. A final concentration of 100 μ M was achieved by adding 100 μ l of stock solution per 1 ml culture media.

The ET-1 non-selective receptor antagonist PD145065 (Sigma, Cat#: SCP0143) was prepared as a 1 mM stock solution by dissolving 1 mg in 1 ml H₂O (Ambion, USA).

Aliquots were prepared and stored at -20°C. To achieve a final concentration of 10 nM, 10 µl of stock solution was added per 1 ml culture media.

The ErbB receptor antagonist, AG1478 (Calbiochem, Cat#: 658552) was prepared as a 16 mM stock solution by dissolving 5mg into 1 ml DMSO. Aliquots were prepared and stored at -20°C. To achieve a final concentration of 10 µM, 1.25 µl of stock solution was added per 2 ml culture media.

Acutely isolated ventricular cells were maintained in 10% FBS-DMEM for approximately 20 hours prior to starting any treatments. For experiments involving CD1 embryonic ventricular cell cultures treated with ANP and/or A71915, cells were treated every 12 hours over a 48-hour period. Cx40^{egfp+} whole embryos were cultured and immediately given a single dose of ANP and/or A71915 for 24 hours. For measurement of intracellular cGMP and cAMP, cells were treated with ANP and/or A71915, ISO, or 8-Br-cGMP for a total period of 2 hours prior to performing the competitive immunoassays.

The exogenous cGMP compound 8-Br-cGMP, and the PKG inhibitor compound Rp-8-pCPT-cGMPS, were added to embryonic cell cultures, every 12 hours over a 24-hour period.

Exogenous ET-1, PD145065, exogenous NRG-1 and AG1478 were added to primary cell cultures, every 12 hours over a 48-hour period.

Exogenous ANP and/or A71915 were added to cell cultures every 12 hours over a 48-hour period (**Figure 2.2**).

Control cultures in all experiments received appropriate vehicle treatment (water, media or DMSO) to match with the conditions used in treatment groups.

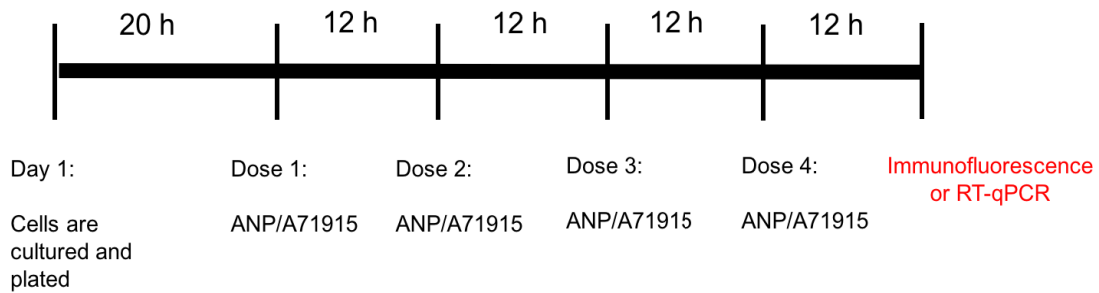


Figure 2.2. Dosing protocol for addition of exogenous ANP and/or A71915 in primary and embryonic cell cultures. ANP and/or A71915 were first added to separate tubes containing 10% DMEM (FBS + Ab/Am), and were then added to cells at appropriate concentrations. Approximately 20 hours following primary cell culture, ANP and/or A71915 were added to cell cultures every 12 hours for a 48-hour period.

2.7 Fluorescence Activated Cell Sorting and Tetramethylrhodamine Methyl Ester Perchlorate Staining

Ventricles from E11.5 CD1 embryos were isolated, pooled, and digested in 0.2% Type I collagenase (Worthington) for 30 min at 37°C. Cell pellets were obtained and neutralized with 10% DMEM as described in Section 2.5. To ensure that a single-cell suspension was obtained, the cells were passed through a 40 µM mesh filter, and centrifuged at 4000 rpm for 4 min. To obtain an adequate number of E11.5 ventricular cells for fluorescence activated cell sorting (FACS), we sacrificed 3-5 pregnant mice and obtained approximately 10 embryonic hearts per pregnancy, resulting in $\sim 4.5 \times 10^6$ cells prior to preparations for FACS analysis.

To stain with tetramethylrhodamine methyl ester perchlorate (TMRM), cells were incubated in 50 nM of TMRM solution (Molecular Probes Inc., 29851 Willow Creek Road, Eugene, OR USA, Cat#: T668) diluted in PBS at 37°C for 30 min, were washed in PBS, and then centrifuged at 4000 rpm for 4 min and reconstituted in FACS Buffer (4% BSA in PBS). Cells were then placed on ice and used for flow cytometry analysis (FACSAria, BD Biosciences). The sorted cells were centrifuged at 4000 rpm for 4 minutes and cultured for further analysis. TMRM fractions contained approximately 1.0×10^6 TMRM-high and 2.5×10^6 TMRM-low cells. Cells sorted based on TMRM staining were processed for measurement of intracellular cGMP using the cGMP *HTRF* assay kit as described in Section 2.14.

2.8 Immune Cytochemistry

Following drug treatment, embryonic CD1 ventricular cell cultures or primary NCRL cultures were fixed with 4% w/v paraformaldehyde (4g paraformaldehyde in 100 ml PBS, pH adjusted to 7.4, using NaOH) for 5 min at room temperature, and were then permeabilized in 0.1% v/v Triton X-100 (Sigma) for 4 min. Following this, cultures were covered in blocking buffer solution [10% v/v goat serum (Gibo), and 1% w/v bovine serum albumin (BSA; Thermo Fisher Scientific) in PBS] for 1 hour at room temperature. After 1 hour, blocking buffer solution was removed and replaced with blocking buffer containing primary antibodies of choice, whose concentrations are listed in **Table 2.2**, for 1 hour at room temperature. Slides were then washed with PBS three times for 3 min each, and were then incubated with secondary goat anti-mouse antibody conjugated to Alexa Fluor 488 (1:200, Invitrogen) and goat anti-rabbit antibody conjugated to Alexa Fluor 555 (1:200, Invitrogen) in blocking buffer for 1 hour. Cells were then washed three times for 3 min each. Cell nuclei were counterstained by immersion of a solution containing 1 µg/ml Hoechst 33258 (Sigma) in PBS. The walls of the chamber slides were removed. The final processing step for immune cytochemistry experiments involved having the slides washed in PBS and mounted with 0.1% propyl gallate (Sigma) solution [0.1% w/v propyl gallate, 50% v/v glycerol (Thermo Fisher Scientific), 50% v/v PBS]. Slides were then examined using the Leica DM2500 fluorescence microscope and images were then captured using a Leica DFC 500 digital acquisition system.

Primary Antibody	Dilution	Source/Catalogue #
β -galactosidase	1:50	Chappel ICN Catalogue #: 55976
Connexin40 (Cx40)	1:100	Alpha Diagnostics Catalogue #: Cx40-A
HCN4	1:100	Alamone Laboratories Catalogue #: APC-052
Sarcomeric myosin (MF20)	1:100	Developmental Studies Hybridoma Catalogue #: MF-20

Table 2.2. List of primary antibodies and corresponding dilutions used for immune cytochemistry experiments.

2.9 Total RNA Extraction from Cells and Tissues

Cultured embryonic ventricular cells (E11.5, E14.5, E17.5) were lysed directly in 35 mm culture dishes by adding 1 ml TRIzol reagent (Invitrogen) to the dish and pipetting the cell lysates through a pipette tip multiple times. For tissue, approximately 20 ventricles (left and right) from E11.5 embryos were collected and pooled from multiple time-pregnant females to obtain sufficient quantity of tissue and then were subjected to RNA extraction using the TRIzol method. Ventricles from embryos at later developmental stages (E14.5 and E17.5) or postnatal stages (neonatal) were minced into smaller pieces (collected from 1-3 ventricles, left and right) and RNA extraction was performed using the TRIzol method. Tissue samples were homogenized in 1 ml TRIzol for approximately 1 min using a power homogenizer. After homogenization/lysis of tissues or cells, all samples were incubated at room temperature for 5 min to allow for dissociation of nucleoprotein complexes. Next, 0.2 ml chloroform was added to the samples and shaken vigorously by hand for 15 seconds. After incubation at room temperature for 3 min, samples were centrifuged at 13,300 rpm for 15 min at 4°C. Following centrifugation, the colourless aqueous phase containing RNA was carefully removed and transferred to fresh tubes. Precipitation of RNA was done by adding 0.5 ml isopropyl alcohol, after which samples were incubated for 10 min at room temperature. Samples were centrifuged at 13,300 rpm for 10 min at 4°C. The resulting pellet was washed with 75% ethanol in nuclease free H₂O (Ambion), air dried and then solubilized in nuclease free H₂O (Ambion). RNA content was quantified by measuring absorbance at 260 nm and 280 nm using a spectrometer (SmartSpecTM Plus, Bio-Rad, Mississauga,

Ontario, Canada). Optimal RNA ratios (A260/A280 values) between 1.8 and 2 indicate ideal and valid assays, therefore, only the samples which had optimal RNA ratios between these values were utilized. Any samples exceeding or were less than this range of ratios were not used for gene expression analysis.

2.10 RNA Quality Control

To ensure a high level of RNA purity, only samples with a 260:280 ratio > 1.8 were used in subsequent gene expression experiments. Also, to ensure a high level of RNA integrity, 2 µg of RNA was electrophoresed on an agarose gel and stained with ethidium bromide, and only samples which displayed two bands corresponding to predominant ribosomal RNAs at ~2kb (18S) and ~5kb (28S) were used. Samples meeting these standards of quality control were then immediately converted into more stable cDNA sequences and stored at -20°C until its use for real time quantitative PCR (RT-qPCR) gene expression analysis experiments.

2.11 Real Time Quantitative Polymerase Chain Reaction (RT-qPCR)

Following RNA extractions, RNA was reverse transcribed into cDNA using SuperScript VILO MasterMix reverse transcriptase kit (Invitrogen). To generate complementary DNA (cDNA) sequences from RNA samples, a reaction mixture was made by combining 1 µg of RNA with 2 µL of SuperScript VILO MasterMix, and RNase/DNAase-free H₂O (Ambion, USA) to a total of 20µl. Reaction mixture samples were gently mixed by tapping Eppendorf tubes and were centrifuged briefly for 30

seconds. All tubes were then incubated at 25°C for 10 min, 42°C for 90 min, and then heat inactivated at 85°C for 5 min.

The cDNA templates were amplified by real time quantitative polymerase chain reaction (qPCR) using the primers listed in **Table 2.3**. The primers for GAPDH, HCN4, Cx40, Tbx5, MEF2C, GATA4, and HAND2 were generated using the NIH primer design tool (<https://mouseprimerdepot.nci.nih.gov/>).

Each of the qPCR reaction mixtures consisted of: 1.0µl of cDNA product, 1.0 µl of the forward and reverse primers (2.5µM), 1.0µl of 5X EVOLution EvaGreen® qPCR mix (Montreal Biotech Inc., Quebec City, Canada) and 2.0µl of RNase/DNase-free H₂O (Ambion, USA). All qPCR reactions were performed using an ECO thermocycler (Illumina, San Diego, California, USA) for 40 cycles: 15 sec at 95°C, 60 sec at 60°C. Once the amplification cycles were complete, melt curves were generated to confirm the amplification of a single primer product, with an extra cycle using the following conditions: 15 sec at 95°C, 15 sec at 60°C and 15 sec at 95 °C. To confirm the expected amplicon sizes, the qPCR amplification products were resolved by electrophoresis on a 1.5% agarose gel.

QPCR analysis was performed on a minimum of 3-6 independent RNA extractions (biological replicates) for each treatment group or as specified in the figure legends. QPCR reactions were performed in duplicate wells for each biological replicate. All gene expression findings were normalized to the control housekeeping gene glyceraldehyde 3-phosphate dehydrogenase (GAPDH) using the $\Delta\Delta C_T$ method (Livak and Schmittgen, 2001). The threshold cycle (C_T) value was determined by setting the threshold of

fluorescence (dRn) to 0.1. The C_T value represents the number of cycles at which the amplification plot for a particular gene intersects the dRn threshold. All treatment conditions did not change the C_T values of GAPDH amplifications, hence GAPDH was used as a reliable housekeeping gene for normalization. In addition, GAPDH transcript levels were shown to be consistent across multiple embryonic ventricular stages (Hotchkiss et al., 2014). To compare the relative expression of a gene of interest between groups, the following calculations were performed and the $2^{-\Delta\Delta CT}$ value was determined for each group. First, to determine the ΔC_T value for each biological replicate or sample, the C_T value of the control (GAPDH) gene was subtracted from the C_T value of the corresponding experimental gene. Next, the ΔC_T values of all samples were averaged. This average was then subtracted from the ΔC_T values for each sample to create $-\Delta\Delta C_T$ values. The $2^{-\Delta\Delta CT}$ values were then determined for each sample and the relative expression for each gene was determined by dividing the $2^{-\Delta\Delta CT}$ obtained for each sample by the average $2^{-\Delta\Delta CT}$ value of the control group. This allowed for data to be expressed as the relative expression of each group compared to the control group, which was set to a value of 1.0. Thus, the QPCR data graphs presented in this thesis represent fold changes in gene expression normalized to GAPDH gene expression and relative to controls.

Table 2.3. List of primers and corresponding primer sequences for real time quantitative PCR (RT-qPCR) experiments and expected amplicon sizes.

Name of Primer	Primer Sequence (5'→3')	Expected Amplicon Sizes (bp)
Cx40-F	CAGAGCCTGAAGAAGCCAAC	137
Cx40-R	GACTGTGGAGTGCTTGTGGA	
HCN4-F	CCTCCTGCGCCTCTTGAGGCTTT	119
HCN4-R	TGCCAATGAGGTTACGATGCGT	
GAPDH-F	TCGTCCCGTAGACAAAATGG	132
GAPDH-R	TTGAGGTCAATGAAGGGGTC	
GATA4-F	CTGGAAGACACCCCAATCTC	100
GATA4-R	CCATCTCGCCTCCAGAGT	
HAND2-F	CGGAGATCAAGAAGACCGAC	96
HAND2-R	TGGTTTTCTTGTCGTTGCTG	
MEF2C-F	TGGAGAGATGAAGTGAAGCG	93
MEF2C-R	GCACAGCTCAGTTCCCAAAT	
TBX5-F	TGGTTGGAGGTGACTTTGTG	101
TBX5-R	GGCAGTGATGACCTGGAGTT	

2.12 MicroRNA Analysis

Following cell culture of embryonic CD1 ventricular cells, dishes were incubated with 1 ml RNAzolRT. Lysate was passed through a pipette several times to ensure lysis, after which samples were incubated in Eppendorf tubes for 5 min at room temperature. To remove protein and DNA, 400 μ l of ddH₂O was added to each sample, and tubes were shaken vigorously by hand for 15 seconds, followed by incubation for 15 min at room temperature. Cells were centrifuged at 12,000 x g for 15 minutes at 4°C and supernatant was transferred to fresh tubes. To remove total RNA, 0.4 ml of 75% ethanol was added to the supernatant and incubated for 10 min at room temperature, and cells were centrifuged at 12,000 x g for 8 minutes at 4°C. Supernatant was transferred to new tubes. To precipitate the miRNA, 100% isopropanol (0.8 ml x total volume per vial) was added to the supernatant, and tubes were incubated at 4°C for 30 min. The tubes were centrifuged at 12,000 x g for 15 minutes at 4°C and decanted. The miRNA, now found in the pellet, was washed and solubilized with 70% isopropanol, and vortexed briefly. Tubes were centrifuged at 8,500 x g for 5 min at 4°C and decanted, and repeated again. The concentration of the miRNA was determined using a spectrometer (SmartSpecTM Plus, Bio-Rad, Mississauga, Ontario, Canada). The miRNA was reverse transcribed using the All-in-One RT-qPCR kit, with miRNAs 1a, 133, 27b, or 208a (GeneCopiaTM, Cat#: QP016). The miRNA was diluted to 100 ng in 18 μ l ddH₂O. A reaction mixture was prepared combining: 1 μ l of 2.5 U/ μ l PolyA polymerase, 1 μ l of RT Enzyme, and 5 μ l of PAP/RT Buffer, per sample. This mix was added to each of the tubes with miRNA from the miRNA extraction step. Samples were gently vortexed and briefly

centrifuged, and were then heated to 37°C for 60 min, 85°C for 5 min. Complementary DNA (cDNA) was processed through quantitative RT-qPCR as described previously, to determine miRNA expression. MiRNA expression for RT-qPCR analysis was normalized to a reference primer (U6) using the $\Delta\Delta C_T$ method. A thermal profile was utilized as follows: 50°C for 2 min, 95°C for 10 min, 95°C for 10 sec, 63°C for 20 sec, 72°C for 10 sec; 40 cycles; then 95°C, 60°C and 95°C for 15 sec each, using an ECO thermocycler (Illumina, San Diego, CA).

MiRNA extraction was also performed on ventricular tissue of NPRA-KO mice at E14.5 and neonates using the RNeasyRNeasy method for extraction of miRNA from tissue. Ventricles obtained from embryos at E14.5 or in neonates were weighed, and 1 ml of RNeasyRNeasy was added per 100 mg of tissue. Ventricular tissue was homogenized on ice, and then transferred to Eppendorf tubes and incubated for 5 min at room temperature. To remove protein, DNA, and other undesired substances, 400 μ l of ddH₂O was added to each 1 ml sample, after which tubes were shaken vigorously by hand for 15 sec and incubated for 15 min at room temperature. Samples were centrifuged at 12,000 x g for 15 min at 4°C and the supernatant was removed and transferred to new tubes. To remove total RNA, 0.4 ml of 75% ethanol was added to the supernatant, and samples were incubated for 10 min at room temperature. Samples were centrifuged at 12,000 x g for 8 min at 4°C, and supernatant was transferred to new tubes. The pellets were stored at -80°C for potential mRNA recovery. To precipitate the miRNA from tissue samples, 100% isopropanol was added to each sample at a volume of 0.8 x the total volume of the tube. Samples were then incubated at 4°C for 30 min. Samples were

centrifuged at 12,000 x g for 15 min at 4°C and decanted. The miRNA was now found in the pellet. To wash and solubilize the miRNA, 0.4 ml of 70% isopropanol was added to the pellet, after which samples were vortexed briefly and centrifuged at 8500 rcf for 5 min at 4°C. Samples were then decanted, and then samples were once again washed and solubilized with 70% isopropanol, vortexed briefly, and centrifuged as before. A volume of 30 µl ddH₂O was added to the pellet, and the samples were gently pipette-mixed. From these samples, 2 µl of the mix was utilized to assay miRNA concentrations using the spectrometer (SmartSpec™ Plus, Bio-Rad, Mississauga, Ontario, Canada) while the remainder of the mixes were stored at -20°C for synthesis of cDNA. The miRNA was reverse transcribed using the All-In-One RT-qPCR kit as described above for cells, and the complementary cDNA was then processed through RT-qPCR using the $\Delta\Delta C_T$ method as described previously.

2.13 Cx40^{egfp} Whole Embryo Culture and Imaging

Timed pregnancies were set up between male Cx40^{egfp+/+} and female BL6 mice to generate Cx40^{egfp+/-} heterozygote whole embryos at E10.5, which were then cultured in 10% DMEM + FBS without Ab/Am. Immediately upon culture, ANP (1000 ng/ml) and/or A71915 (1 µM) were added to culture media for 24 hours. After 24 hours, now at E11.5, whole embryos were imaged for detection of green fluorescence, and then hearts were removed and imaged for detection of green fluorescence using a Leica MZ16SF stereomicroscope fitted with a Leica DFC500 digital camera and corresponding Leica Application Suite software (Leica Microsystems, Richmond Hill, Ontario, Canada). Digital

images were acquired as 1360 x 1024 pixel uncompressed Tiff files at a color depth of 24-bit RGB. Area occupied by green pixels was quantified using a previously described color subtractive image analysis method (Gaspard and Pasumarthi, 2008). Areas occupied by green pixels (Cx40^{egfp} reporter gene expression) and black pixels (non-fluorescence) for each whole embryo and heart were assessed with Image Processing Tool Kit 5.0 software, purchased from Reindeer Graphics (Asheville, NC, USA). The software was installed onto a personal computer in the plug-in folder of Adobe Photoshop 7.0. Upon installation, the software tools appear under the filter window of Adobe Photoshop. First, images taken using the Leica Application Suite were saved as TIFF files and opened in Adobe Photoshop 7.0. To calculate the area of green pixels that corresponds to Cx40^{egfp} reporter gene expression, a new layer labelled “green” was created from the background image. Then, the area occupied by green pixels alone was selected in Photoshop by choosing the SELECT-COLOUR RANGE command. The eyedropper selection tool was used to select the brightest green colour fluorescence in the image, and the command was completed; this step selects the majority of green-stained regions in the image. The area that was selected was filled with white by using the EDIT-FILL command. Bilevel thresholding was performed such that the layer “green” was converted into a binary image, as described in (Gaspard and Pasumarthi, 2008). To measure the area occupied by green pixels, the IP*MEASURE FEATURES-MEASURE REGIONS command was performed under the Filter window in Adobe Photoshop. The MEASURE REGIONS command calculates the filled area, measured in μm^2 , for all green pixels in the binary image. The text file output from Adobe Photoshop was exported into

Microsoft Excel to calculate the area occupied by green pixels. The area occupied by black pixels was also determined by creating a new layer labelled “black” from the background image, filling the black regions with white, converting to binary image and following the same steps as described for green pixels above. The percentage (%) of green pixels was determined for the combined ventricles of each heart using the following formula: % green pixels = [area of green pixels/(area of green pixels + black pixels)] x 100.

Male and female mice double heterozygous for both NPR-A knockout allele and Cx40^{egfp} knock-in allele (NPR-A-KO^{+/-} / Cx40^{egfp+/-}) were crossed to generate neonates in order to visualize arborisation of the Purkinje fiber network. Genotypes of 1 day old newborn pups (ND1s) were determined using tail biopsies as described under Section 2.2. Whole hearts were removed from neonates and imaged for visualization of green fluorescence. Green pixels were quantified as described earlier.

2.14 Second Messenger Assays: cGMP and cAMP

To measure cGMP, competitive immunoassays were performed on embryonic ventricular cells using the two-step protocol of the cGMP *HTRF* assay kit (Cisbio; Cat#: 62GM2PEB). Ventricles from embryos were isolated and digested in Type I collagenase (Worthington) for 30 min at 37°C. Cell pellets were then obtained by centrifugation and neutralized with 10% DMEM + FBS as described earlier (Section 2.5). The competitive immunoassay was based on the competition between endogenous cGMP and a d2-dye

labelled cGMP analogue (d2-cGMP) for binding sites on anti-cGMP monoclonal antibodies that have been labelled with Cryptate (mAb-Cryptate). The specific signal (designated as Delta F) that occurs was a result of the energy transfer between d2-cGMP and Cryptate and was inversely proportional to the concentration of endogenous cGMP contained within the experimental sample (**Figure 2.3**).

In the first step of the protocol for the competitive immunoassay, a volume of 5 μ l cells containing 100,000 cells in 10% DMEM-FBS was added to wells of 96-well plates with 5 μ l of dilution buffer consisting of drug compounds (ex: ANP, ET-1, NRG-1, etc.) diluted in 10% DMEM-FBS; this totaled a volume of 10 μ l/well. Then, the broad substrate PDE inhibitor 3-isobutyl-1-methylxanthine (IBMX, 500 μ M; Sigma) was added to wells in order to prevent the degradation of cGMP. The plate was then sealed and incubated for 1 hour at room temperature. Following incubation, 5 μ l of d2-GMP analogue diluted in lysis buffer was added to each experimental well; d2-cGMP was omitted from the negative control wells in order to determine the presence of any non-specific signal. A volume of 5 μ l of anti-cGMP Cryptate was added to all wells and the plate was incubated for 1 hour at room temperature. The final total volume in each well was 20 μ l. A volume of 20 μ l of media from each well of the 96-well plate was transferred over to a 384-well low volume plate (Greiner Bio-One; Cat#: 784075) just before measurement of cGMP. The d2-cGMP fluorophore was excited at a wavelength of 337 nm and emission was detected at 665 and 620 nm using a POLARstar Omega plate reader (BMG Labtech). The fluorescent ratio 665 nm/620 nm was calculated to minimize photophysical interference due to medium conditions such as the presence of

serum. Results were expressed as delta F values and calculated using the 665 nm to 620 nm ratios, according to the supplier's instructions as described below. First, the 665/620 ratio for each well was multiplied by 10^4 , and then the average values from replicate wells were determined. Next, delta F values were obtained by subtracting the negative control 665/620 ratio value from the experimental sample 665/620 ratio value, then dividing that by the negative control 665/620 ratio value and multiplying by 100. A cGMP standard curve was generated by plotting the delta F values from standards with known cGMP concentrations, using this method, covering a range of 0.49-500 nM final concentration of cGMP per well. Then, cGMP concentrations in experimental samples were determined by extrapolating their corresponding delta F values from the standard curve. A 8-Br-cGMP standard curve was also generated by making up 8-Br-cGMP stock solutions in the range of 0.49-500 nM utilizing a similar protocol as described above. For measuring 8-Br-cGMP uptake, cells were incubated with 8-Br-cGMP for a total period of 2 hours before cGMP levels were measured.

To determine the amount of endogenous cAMP in embryonic ventricular cells, a cAMP competitive immunoassay was performed using a two-step protocol of the cAMP dynamic 2 *HTRF* assay kit (Cisbio, Cat#: 62AM4PEB) according to the manufacturer's instructions. This kit is supplied with d2-dye labelled cAMP analogue (d2-cAMP) and anti-cAMP monoclonal antibodies that have been labelled with Cryptate (mAb-Cryptate). The idea behind how the cAMP immunoassay works is similar to that of the cGMP competitive immunoassay (**Figure 2.3**). The methods for performing the cAMP immunoassay were identical to that of the cGMP immunoassay with one difference:

instead of plating 100,000 cells per well in media, 4,000 cells were added to each well at a volume of 5 μ l, diluted in 10% DMEM. A standard curve for cAMP was generated by plotting calculated delta F values obtained from multiple standards covering known concentrations with an average range of 0.17-712 nM final concentration of cAMP per well.

Therefore, by following these outlined procedures for measurement of cGMP and cAMP levels, all drug compounds tested in this thesis for measurement of cGMP/cAMP levels (ANP, NRG-1, ET-1, etc.) were added to isolated cells for a total period of 2 hours before levels were assayed.

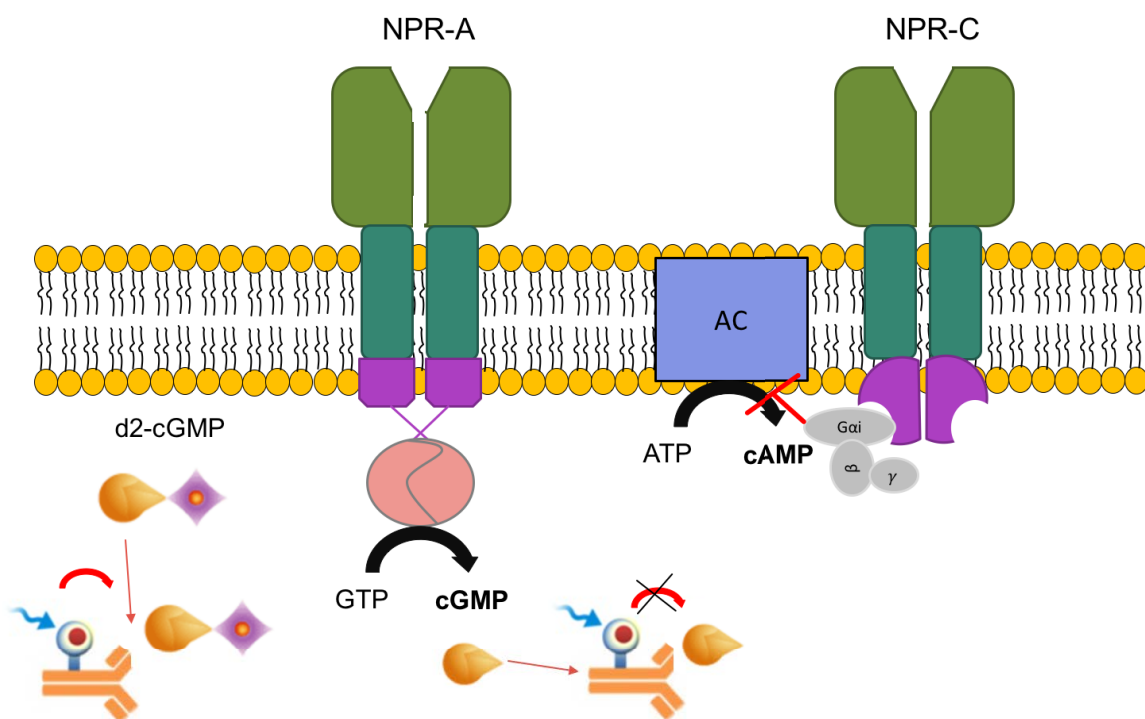


Figure 2.3. Schematic diagram depicting the principle behind the second messenger competitive immunoassays for cGMP and cAMP. Second messenger immunoassays for cGMP and cAMP were performed and rely on the same principle. For simplicity, only the cGMP assay is described here. In the first step, dispersed cells were incubated with drug compounds of choice (ANP, ET-1, NRG-1, etc.). In the second step, competition was initiated between endogenous cGMP and a d2-dye labelled cGMP analogue (d2-cGMP) for binding sites on anti-cGMP monoclonal antibodies labelled with the energy acceptor Cryptate. The specific signal, which is designated as delta F, occurred due to the energy transfer between d2-cGMP and Cryptate. If the drug compound induced stimulation of cGMP, endogenous cGMP would outcompete d2-cGMP for binding sites on antibodies and the energy transfer would decrease. If the drug compound inhibited cGMP production, d2-cGMP would outcompete endogenous cGMP for binding sites on antibodies and the energy transfer would increase. Thus, delta F values were inversely proportional to the concentration of endogenous cGMP measured within the sample. Delta F values could then be extrapolated from a cGMP standard curve to determine cGMP concentrations for each experimental sample.

2.15 Measurement of Cell Size

To determine the cell size/area of CMs at E11.5, cells were cultured as previously described, then after 20 hours, cultures were incubated with various paracrine factors and/or receptor antagonists (ex. ANP, ET-1, NRG-1, etc.) for 48 hours, with a dose provided every 12 hours. Cells were subjected to immune cytochemistry as described in Section 2.8, and were stained with sarcomeric myosin (MF20) primary antibody for detection of CMs, followed by staining with secondary goat anti-mouse antibody conjugated to Alexa Fluor 488 (1:200, Invitrogen) in blocking buffer for 1 hour. Cell nuclei were counterstained by immersion of a solution containing 1 µg/ml Hoechst 33258 (Sigma) in PBS. Slides were then examined using the Leica DM2500 fluorescence microscope and images were then captured using a Leica DFC 500 digital acquisition system. Cell size was determined using the Image Processing Tool Kit 5.0 (Reindeer Graphics, Ashville, NC) and Adobe Photoshop 7.0 software as described earlier with minor modifications (Gaspard and Pasumarthi, 2008). Contours for the cell periphery were marked using the lasso tool and IP* measure feature was used to assess filled areas in 40X magnification images.

2.16 Generation of Cx40 Promoter Construct

The mouse Cx40 5'flanking sequence (1250 bp) subcloned in Bgl II and Hind III sites in pEZX-PG04.1 vector transformed in E. Coli JM109 strain was obtained from GeneCopoeiaTM (Rockville, MD, USA). This construct harbors a coding sequence for Gaussia luciferase under the transcriptional control of mouse Cx40 promoter and a

secreted alkaline phosphatase coding sequence under the control of CMV promoter. The plasmid DNA was amplified using Qiagen midi plasmid kit according to manufacturer's instructions. The purified plasmid is designated as Cx40p-GLuc-CMV-SeAP. To ensure the purity of plasmid DNA, only samples with 260:280 ratios ~ 1.8 were used in subsequent transfection experiments. The fidelity of the purified plasmid DNA was verified by restriction enzyme digestion with Bgl II and Hind III enzymes (GeneCopiaTM, **Figure 2.4**).

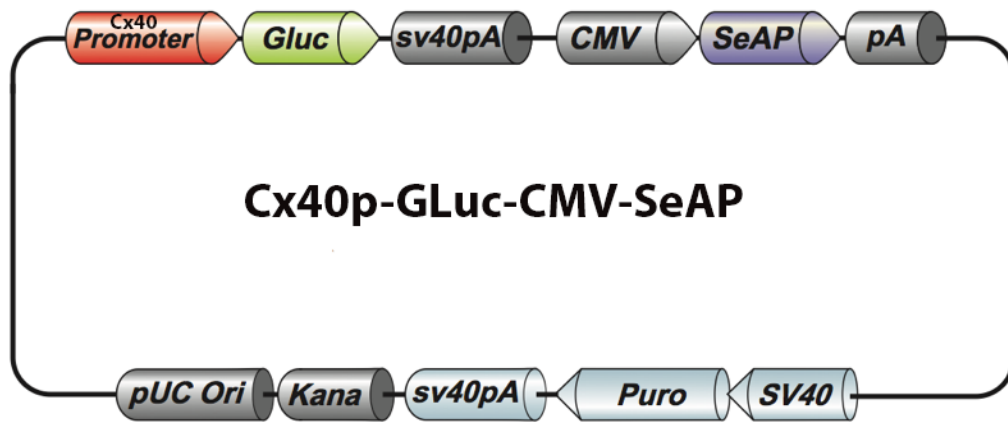


Figure 2.4. Schematic depicting sequence of mouse Cx40 promoter construct.
Modified from GeneCopoeia™, with permission.

2.17 Transfections

CD1 E11.5 ventricular cells were cultured in 10% DMEM-FBS + Ab/Am as described in Section 2.5, with 400,000 cells per 35 mm dish.

For CD1 E11.5 ventricular cells, 20 hours following initial plating of cells, the medium was aspirated and 3 ml of 10% DMEM-FBS (with Ab/Am) was added per 35 mm dish and incubated for 30 min. Then, the transfection cocktail was prepared using Lipofectamine[™] 3000 (Invitrogen) as follows. **1)** 125 μ l of Opti-MEM[®] was added to each of two 1.5 ml microfuge tubes. One tube received 2.5 μ g of plasmid DNA and 5 μ l of P3000 reagent, a necessary component for the cocktail, and was mixed well. The second tube received 7.5 μ l of Lipofectamine[™] 3000. **2)** The contents of the first tube were transferred to the second tube, and the final tube was mixed well and stood at room temperature for 15 min. **3)** The lipofectamine-DNA cocktail was added slowly in a drop-wise fashion to 35 mm culture dishes with 3 ml 10% DMEM-FBS (with Ab/Am). The dishes were then incubated at 37°C for 24 hours. **4)** Media was aspirated and drug treatment occurred now, with either ANP (1000 ng/ml), ET-1 (1.5 nM), or NRG-1 (2.5 nM) diluted in 10% DMEM-FBS (with Ab/Am) being added to dishes for 24 hours, with dosing every 12 hours. **5)** After 24 hours, the medium was collected at this time point and processed with the Secrete-Pair[™] dual luminescence assay kit (GeneCopoeia[™], Rockville, MD, USA) as described below. **6)** After collecting medium for the 24-hour time point, 2 ml of fresh medium (10% DMEM-FBS + Ab/Am) was added to the dishes and cells were maintained for an additional 24 hours to collect medium for the 48-hour time

point luciferase assay as described in Section 2.18. Transfection efficiency in E11.5 cells was found to be 10-15%.

2.18 Secrete-Pair Dual Luminescence Luciferase Assay

Following transfection and drug treatment as described in Section 2.17, 0.2 ml media was collected 24 hours and 48 hours post-treatment to assay using the Secrete-Pair™ Luminescence Assay (GeneCopoeia™, Rockville, MD, USA), and was placed into 1.5 ml Eppendorf tubes per sample at room temperature. The Buffer GL-S solution (10x) was thawed thoroughly at room temperature, and diluted 1:10 in distilled water to make 1x Buffer GL-S solution. Next, the GLuc Assay Working Solution was prepared by adding 10 µl of Substrate GL per 1 ml of 1x Buffer GL-S. This solution was mixed well and incubated at room temperature for 25 min, capped and protected from light. The luciferase assay was performed as follows: **1)** 10 µl of culture media was obtained from sample tubes and pipetted into each well, in triplicate, of a 96-well black plate. **2)** The GLuc Assay Working Solution prepared previously was now added to each well (100 µl per well) and the plate was gently tapped several times to ensure that the sample and substrate were mixed. **3)** The 96-well plate was incubated at room temperature for 1 minute and then measurement of chemiluminescence was determined immediately within 5 minutes after incubation, using the luminescence optics of the POLARstar Omega plate reader (BMG Labtech). This generated GLuc activity values.

To determine secreted alkaline phosphatase (SEAP) activity per sample, a SEAP assay procedure was followed using the Secrete-Pair™ Luminescence Assay Kit. 50 µl of

culture media from samples were aliquoted into 1.5 ml Eppendorf tubes. Then, the SEAP assay procedure was performed as follows. **1)** Collected media samples were heated at 65°C for 10 min, and then were placed on ice. **2)** Buffer AP (10x) was thawed thoroughly at room temperature and diluted 1:10 in distilled water to make 1x Buffer AP. **3)** The SEAP Assay Working Solution was prepared by adding 10 µl of Substrate AP per 1 ml of 1x Buffer AP and the resulting solution was mixed well by inverting the tube several times. **4)** The mix was incubated at room temperature for 5 min, capped and protected from light. **5)** The collected media samples that had been previously heated were now pipetted into the wells of the 96-well plate (10 µl per well, run in triplicate). **6)** The SEAP Assay Working Solution from step 4 was distributed, 100 µl per well, to the samples from step 6. The plate was gently tapped to ensure the sample and substrate were mixed. **7)** The plate was incubated at room temperature for 5 min and then SEAP activity was determined using the luminescence optics of the POLARstar Omega plate reader (BMG Labtech).

The GLuc activity measured in relative light units (RLU) and the SEAP activity measured in RLU were recorded, and the GLuc to SEAP activity ratio (RLU) was determined per each sample. This entire procedure was repeated after another 24 hours (48 hours post-treatment).

2.19 Statistical Analysis

Data are presented as mean \pm standard error of the mean (SEM). A two-tailed unpaired t-test was utilized to compare means between two groups. Multiple group

comparisons were analyzed by ANOVA and Tukey multiple comparison post hoc tests. Significance for all analyses was assigned at $p < 0.05$. For each experiment, the number of experiments/replicates is displayed in the corresponding figure legends. Dose response data were analyzed by nonlinear regression with a four-parameter logistic sigmoidal dose-response (variable slope) curve fit method. All statistical analysis was performed using GraphPad Prism software.

CHAPTER 3: CHARACTERIZING THE AUTOCRINE/PARACRINE ROLE OF ATRIAL NATRIURETIC PEPTIDE IN THE DEVELOPMENT OF THE VENTRICULAR CONDUCTION SYSTEM

3.1 Background and Hypothesis

The cardiac conduction system (CCS) is a complex network of cells within the heart that generates and conducts electrical impulses to enable rhythmic, coordinated contraction of the heart (Gourdie et al., 1998). The main components of the CCS are the SA node, AV node, Bundle of His, bundle branches and Purkinje fibers. The Bundle of His, bundle branches and Purkinje fibers are frequently referred to as the ventricular conduction system (VCS). Lineage-tracing studies within the chick heart have shown that Purkinje fibers, as well as ventricular myocytes are derived from a common CPC lineage (Gourdie et al. 1995). Additional studies have shown that paracrine factors including ET-1 and NRG-1 are involved in the formation of CCS cells (Gourdie et al., 1998, Rentschler et al., 2002). It has been documented that paracrine signals originating from arterial vascular tissues can induce contractile cells in the periarterial sites to form Purkinje fibers in developing chick myocardium (Gourdie et al., 1998). ET-1 is a paracrine factor abundant in the arterial system of the heart and is secreted by endothelial cells in a shear stress-dependent manner. Previous studies reported that ET-1 induces embryonic chick CMs to express several CCS markers both *in vitro* and *in vivo* (Gourdie et al., 1998). NRG-1, a growth and differentiation factor essential for ventricular trabeculation, has been implicated as a key paracrine factor in promoting formation of the mouse CCS. Studies have demonstrated that NRG-1 induces embryonic mouse CMs to differentiate

into cells of the conduction system (Rentschler et al., 2002). However, the inability of NRG-1 or ET-1 to increase CCS reporter gene expression in E10.5-E11.5 CCS-*lacZ* hearts suggests that additional factors may be involved in the development and/or maturation of CCS network in later stages of embryonic heart development.

ANP is a paracrine factor and a member of the natriuretic peptide family, involved in regulating cardiovascular homeostasis (McGrath et al., 2005). Past studies have revealed that although ANP is expressed transmurally in the embryonic ventricular myocardium, its expression is gradually restricted to the VCS (Christoffels and Moorman, 2009). These observations suggest that ANP may be involved in the induction and/or maturation of VCS cells. Trabecular myocardium serves as the preferential route for the conduction of electrical impulses before the mature VCS is formed (Sankova et al., 2012), and has been shown to contain myogenic precursors of the mature Purkinje fiber network (Christoffels, 2009). It was recently shown that exogenous addition of ANP was associated with reduced rates of proliferation in undifferentiated CPCs, and that ANP-rich regions of the trabecular myocardium were characterized by a lower index of proliferation compared to the adjacent compact layer (Hotchkiss et al., 2015). Since trabeculae are known to house cellular progenitors of the VCS, it was speculated that reduced CPC proliferation mediated by ANP/NPR-A signalling could be coupled to recruitment of these cells into the conduction system lineage (Hotchkiss et al., 2015). Currently, it is not known whether ANP plays any inductive role in the formation of the VCS network either directly by acting on CPCs and/or CMs, or in synergy with ET-1 and/or NRG-1. **We hypothesized that ANP secreted from myocardial cells, can act on**

the NPR-A receptors of nearby cells in the embryonic trabecular myocardium and induce expression of conduction system cell markers in an autocrine/paracrine manner.

3.2 Specific Aims

- 1.** To determine the role of ANP/NPR-A/cGMP signalling pathway in inducing VCS marker gene expression using E11.5 mouse embryonic ventricular cell cultures.
- 2.** To determine the effects of genetic ablation of NPR-A on development and maturation of VCS.
- 3.** To utilize a Cx40^{egfp} knock-in embryonic mouse model for visualization of VCS development in the presence or absence of ANP and/or a NPR-A receptor antagonist.
- 4.** To determine the molecular mechanisms underlying ANP/NPR-A mediated changes in VCS marker gene expression in the embryonic ventricles.

3.3 Results

3.3.1 Effects of ANP on Percent Distribution of Cells Expressing HCN4 and Cx40 in E11.5 Mouse Ventricular Cells

Cx40 and HCN4 are expressed in the developing VCS (Delorme et al., 1995; Sankova et al., 2012; Garcia-Frigola et al., 2003). E11.5 ventricles harbor a partially developed Bundle of His and bundle branches with no Purkinje fiber arborisation (Viragh and Challice, 1977; Weerd and Christoffels, 2016). To determine the effects of ANP on the percent distribution of cells expressing Cx40 and HCN4, exogenous ANP was added at varying concentrations to primary ventricular cell cultures prepared from E11.5 stage CD1 embryos. The effects of ANP on VCS marker protein expression were characterized based on co-immunolabelling with antibodies specific for sarcomeric myosin (MF20)

which identified CMs, and with antibodies specific for HCN4 or Cx40 to identify the protein of interest (**Figures 3.1 and 3.5**). MF20+ cells that were HCN4 or Cx40 “positive” were identified as either HCN4+/MF20+ or Cx40+/MF20+ and designated as putative VCS cells. CMs that stained negatively for HCN4 or Cx40 (HCN4-/MF20+ or Cx40-/MF20+) were excluded from cell counts because they are not VCS cells. The percentage of HCN4+/MF20+ cells out of the total number of cells counted per field was determined upon addition of varying concentrations of exogenous ANP (0, 10, 100, or 1000 ng/ml), A71915 alone (1 μ M), or a combination of A71915 (1 μ M) and ANP (1000 ng/ml) (**Figure 3.2 A**). Compounds were added approximately 20 hours after the initial primary culture, every 12 hours over a period of 48 hours, and cells were then processed for immunofluorescence staining. The addition of ANP at concentrations of 10 ng/ml and 100 ng/ml to E11.5 ventricular cells increased the percentage of HCN4+/MF20+ cells, however this increase was statistically not significant vs. control (p=NS). The addition of ANP at 1000 ng/ml resulted in a significant increase in the percentage of HCN4+/MF20+ cells vs. control (86 ± 1.2 % vs. 63 ± 4.6 %, $p < 0.005$). Since endogenous ANP is actively secreted from embryonic ventricular cells (Hotchkiss et al., 2015), we next examined whether blockade of NPR-A receptor was sufficient for changing the percentage of the HCN4+/MF20+ cell population. The addition of A71915 (1 μ M) significantly reduced the percentage of HCN4+/MF20+ cells (21 ± 1.9 % vs. 63 ± 4.6 %, $p < 0.005$, **Figure 3.2 A**). To determine if ANP could rescue this effect, a combination of ANP (1000 ng/ml) and A71915 (1 μ M) were both added to ventricular cells. This combination treatment also led to a significant decrease in the percentage of HCN4+/MF20+ cells when compared to

that of control cultures ($36 \pm 6.4\%$ vs. $63 \pm 4.6\%$, $p < 0.005$, **Figure 3.2 A**) and this reduction was not statistically significant when compared to the percentage of HCN4+/MF20+ cells in cultures treated with A71915 alone ($p = \text{NS}$).

We also determined if the addition of exogenous ANP and/or A71915 had any effect on HCN4+/MF20- cells, that is, cells that stain positive for the VCS marker of interest, but were putative VCS progenitor/non-CM cells at the E11.5 stage. Compared to control, the addition of ANP resulted in a dose-dependent decline in the percent of HCN4+/MF20- cells (Control: $70 \pm 4\%$; 10 ng/ml ANP: $45 \pm 3\%$; 100 ng/ml ANP: $35 \pm 5\%$; 1000 ng/ml ANP: $28 \pm 4\%$, $p < 0.005$; **Figure 3.2 B**). The addition of 1 μM of A71915 increased the percent of HCN4+/MF20- cells vs control ($94 \pm 1\%$, $p < 0.005$). The combination of ANP (1000 ng/ml) and A71915 (1 μM) also resulted in a significant increase in the percent of HCN4+/MF20- cells vs. control ($83 \pm 3\%$, $p < 0.05$). Next, we calculated the ratio of HCN4+/MF20+ cells to HCN4+/MF20- cells to determine the potential impact of ANP and/or A71915 on converting VCS progenitor/non-CM cells (HCN4+/MF20- cells) to differentiated VCS cells (HCN4+/MF20+ cells). Interestingly, we found that the addition of 1000 ng/ml ANP resulted in a cell ratio of 5.0 ± 1.9 vs. control (0.9 ± 0.1) ($p < 0.005$; **Figure 3.3**). Thus, the exogenous addition of ANP at this concentration resulted in a cell distribution where there were 5 times more differentiated VCS cells than VCS progenitor/non-CM cells compared to the control group. The addition of A71915 (1 μM) to cell culture resulted in a significant decrease in this ratio to 0.3 ± 0.02 ($p < 0.05$) vs. 1000 ng/ml ANP treatment (~22-fold reduction). The combination of ANP and A71915 added to cell culture resulted in a decrease in the cell

ratio to 0.4 ± 0.1 ($p < 0.05$) vs. 1000 ng/ml ANP treatment (~11-fold reduction).

Therefore, the addition of the NPR-A antagonist A71915 had the effect of decreasing the percent of VCS cells (HCN4+/MF20+) and increasing the percent of VCS progenitor/non-CM cells (HCN4+/MF20- cells).

We also counted the total number of nuclei present per field upon addition of ANP and/or A71915 to determine if either of these compounds could alter the relative numbers of E11.5 ventricular cells, in slides immunostained with anti-HCN4 antibody. The number of nuclei per field was similar among all treatment groups ($p = \text{NS}$, **Figure 3.4 A**). In order to determine whether ANP and/or A71915 had an effect on the number of CMs, MF20+ cells were counted per field, in slides immunostained with anti-HCN4 antibody. The addition of ANP resulted in a significant increase in the number of MF20+ cells/field vs. control (10 ng/ml ANP: 51 ± 5 cells; 100 ng/ml ANP: 53 ± 2 cells; 1000 ng/ml ANP: 53 ± 3 cells; control: 24 ± 1 cells, $p < 0.00005$, **Figure 3.4 B**). Compared to 1000 ng/ml ANP treatment, the addition of A71915 significantly reduced the number of MF20+ cells (15 ± 1 cells, $p < 0.00005$). Similarly, the combination of ANP and A71915 also reduced the number of MF20+ cells vs. 1000 ng/ml ANP treatment (22 ± 1 cells, $p < 0.00005$).

The percentage of Cx40+/MF20+ cells was determined upon addition of varying concentrations of exogenous ANP, A71915 alone (1 μM), or a combination of A71915 (1 μM) and ANP (1000 ng/ml) (**Figure 3.5**). There was no significant increase in the percentage of Cx40+/MF20+ cells upon addition of varying concentrations of ANP (**Figure 3.6 A**). In contrast, A71915 (1 μM) significantly decreased the percentage of

Cx40+/MF20+ cells compared to that of control cultures ($21 \pm 2.3 \%$ vs. $65 \pm 1.5 \%$, $p < 0.005$; **Figure 3.6 A**). Addition of ANP (1000 ng/ml) in combination with A71915 (1 μ M) also reduced the percentage of Cx40+/MF20+ cells ($32 \pm 3 \%$ vs. $65 \pm 1.5 \%$, $p < 0.005$, **Figure 3.6 A**).

The potential impact of ANP and/or A71915 on Cx40+/MF20- cells was also examined. The addition of ANP to cell culture resulted in a dose-dependent decline in the percentage of Cx40+/MF20- cells vs. control, in a similar manner as with HCN4+/MF20- cells (10 ng/ml ANP: $39 \pm 5 \%$; 100 ng/ml ANP: $35 \pm 6 \%$; 1000 ng/ml ANP: $31 \pm 5 \%$; Control: $68 \pm 5 \%$, $p < 0.005$, **Figure 3.6 B**). The addition of A71915 (1 μ M) increased the percent of Cx40+/MF20- cells vs. control, to $91 \pm 1.7 \%$ ($p < 0.05$). The combination of ANP plus A71915 also resulted in an increase in the percent of Cx40+/MF20- cells vs. control, to $79 \pm 3.4 \%$ ($p < 0.05$). The ratio of Cx40+/MF20+ cells to Cx40+/MF20- cells was also calculated in a similar manner as described above with HCN4. The cell ratio of the control group was 1.1 ± 0.1 cells. Compared to the control group, the addition of both 100 and 1000 ng/ml ANP significantly increased this ratio to 2.5 ± 0.4 and 2.8 ± 0.3 respectively ($p < 0.005$, **Figure 3.7**). The addition of A71915 (1 μ M) significantly reduced the ratio to 0.2 ± 0.02 ($p < 0.05$) and the combination of ANP and A71915 also reduced this ratio (0.4 ± 0.03 , $p < 0.05$).

The total number of nuclei counted per field was similar among all treatment groups in slides immunostained with anti-Cx40 antibody ($p = \text{NS}$, **Figure 3.8 A**). We also counted the number of MF20+ cells present per field in slides immunostained with anti-Cx40 antibody, and found that the number of MF20+ cells increased upon addition of

10, 100 or 1000 ng/ml ANP vs. control (10 ng/ml ANP: 51 ± 5 cells; 100 ng/ml ANP: 51 ± 5 cells; 1000 ng/ml ANP: 53 ± 5 cells; Control: 28 ± 2 cells, $p < 0.05$, **Figure 3.8 B**). The addition of A71915 significantly reduced the number of MF20+ cells vs. 1000 ng/ml ANP (16 ± 1 cells, $p < 0.05$). The combination of ANP plus A71915 significantly reduced the number of MF20+ cells vs. 1000 ng/ml ANP (20 ± 2 cells, $p < 0.05$).

Although the murine ventricular conduction system (VCS) appears to be present by E9.5 using the *CCS-lacZ* reporter model, endogenous VCS specific markers are expressed only after E11.5 and a fully functional VCS appears after E17.5 (Christoffels and Moorman, 2009). In order to determine if there were any differences in the effects of ANP and/or A71915 on HCN4+/MF20+ cells or Cx40+/MF20+ cells across later embryonic stages of development, we also cultured embryonic ventricular cells from embryonic stages E14.5 and E17.5, which represent various stages of VCS development, and treated cells with control, ANP (1000 ng/ml), A71915 (1 μ M), or ANP (1000 ng/ml) + A71915 (1 μ M). Subsequently, we stained cells with either anti-HCN4 or anti-Cx40 antibody for detection of VCS protein expression. The results were compared to the results we found with E11.5 percent distribution of cells. Within each embryonic stage, the percentage of HCN4+/MF20+ cells resulting from the treatment groups were all significantly different from each other, except at E17.5 between A71915 and A71915 + ANP, which were similar (**Figure 3.9**). When comparing potential differences in treatments across embryonic stages, there were no significant differences for any of the treatment groups. Within each embryonic stage, the percentage of Cx40+/MF20+ cells resulting from the treatment groups were all significantly different from each other,

except at E17.5 between A71915 and A71915 + ANP, which were similar (**Figure 3.10**). Interestingly, when comparing potential differences in treatments across embryonic stages, the percentage of Cx40+/MF20+ cells resulting from ANP treatment was significantly greater in E14.5 vs. E11.5 cells and significantly lower in E17.5 cells vs. E14.5 cells (**E11.5**: $77 \pm 5\%$, **E14.5**: $84 \pm 3\%$, **E17.5**: $77 \pm 5\%$, $p < 0.005$). The percentage of Cx40+/MF20+ cells resulting from A71915 treatment was significantly lower in E14.5 vs. E11.5 cells (**E11.5**: $21 \pm 2\%$, **E14.5**: $16 \pm 2\%$, $p < 0.005$). The percentage of Cx40+/MF20+ cells resulting from the ANP + A71915 combination treatment was significantly higher at E11.5 vs. E14.5 and vs. E17.5 (**E11.5**: $32 \pm 3\%$, **E14.5**: $27 \pm 1\%$, **E17.5**: $28 \pm 2\%$, $p < 0.05$).

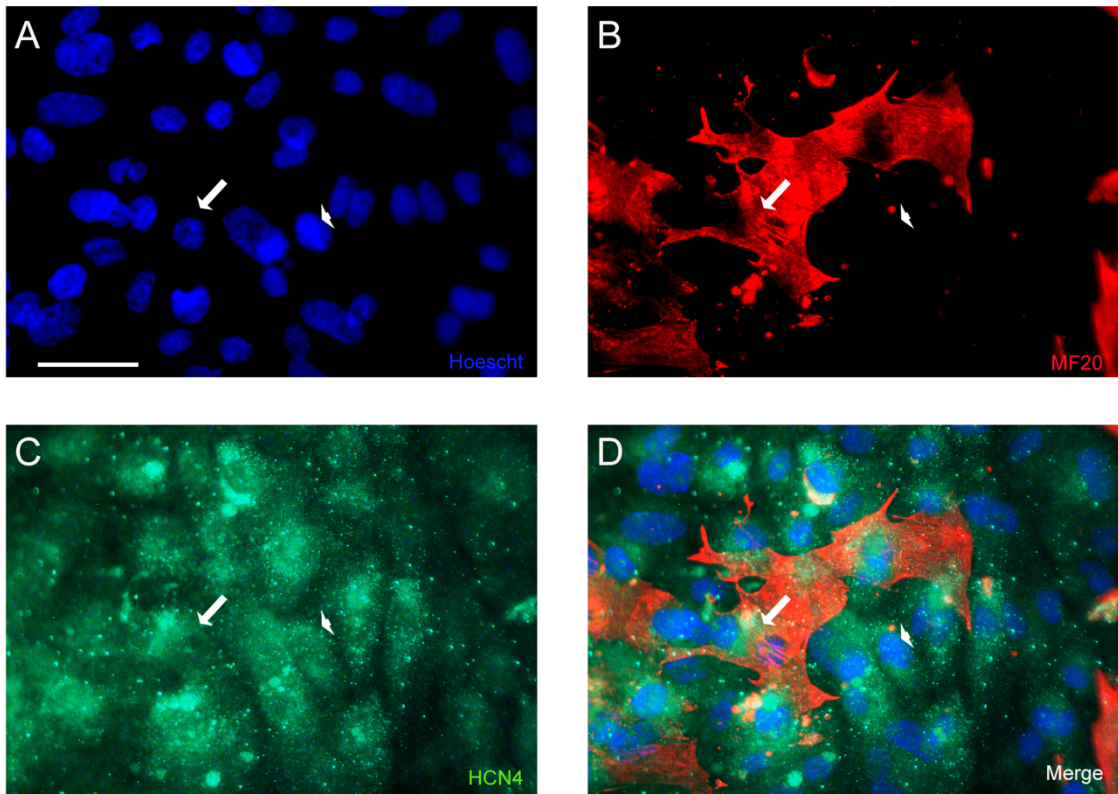


Figure 3.1. Expression of HCN4 protein in E11.5 mouse ventricular cells following addition of exogenous ANP treatment (1000 ng/ml) over 48 hours. A-D: E11.5 ventricular cells were immunolabelled for detection of hyperpolarization-activated cyclic nucleotide-gated channel (HCN4) protein. The same field of cells are labelled with Hoechst nuclear stain (**A**), sarcomeric myosin antibodies MF20 (**B**), HCN4 protein (**C**) and an image overlay (**D**). CMs were identified as MF20+. Ventricular cardiac conduction system (VCS) cells were labelled as those that identified as both HCN4+ and MF20+ (HCN4+/MF20+). Arrows indicate HCN4+/MF20+ cells, arrow-heads indicate HCN4+/MF20- cells. N=5 experiments per group. Scale bar = 100 μ M.

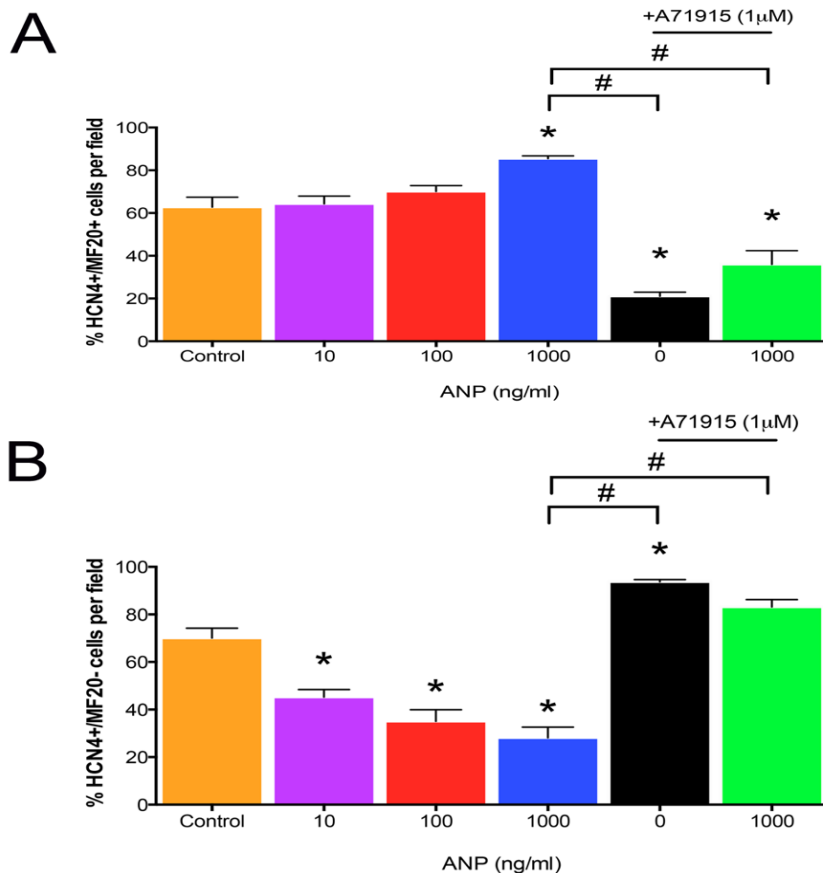


Figure 3.2. Percentage (%) of HCN4+/MF20+ and HCN4+/MF20- cells in E11.5 mouse ventricular cells following addition of exogenous ANP. E11.5 ventricular cells were cultured and ANP was added at varying concentrations every 12 hours over a 48-hour period. Cells were immunolabelled for detection of HCN4 protein. CMs were identified as MF20+. **A)** Bar graph represents the percentage (%) of HCN4+/MF20+ cells per field upon exposure to exogenous ANP at varying concentrations (0, 10, 100 and 1000 ng/ml) and NPR-A inhibitor A71915 (1 μ M) over 48 hours. HCN4+/MF20+ cells were identified as ventricular cardiac conduction system (VCS) cells. ANP (1000 ng/ml) significantly increased the % of HCN4+/MF20+ cells per field vs. control and A71915 (1 μ M) significantly reduced the % of HCN4+/MF20+ cells per field vs. control. **B)** Bar graph represents the percentage (%) of HCN4+/MF20- cells per field upon exposure to exogenous ANP at varying concentrations (0, 10, 100 and 1000 ng/ml) and NPR-A inhibitor A71915 (1 μ M) over 48 hours. HCN4+/MF20- cells were identified as non-CMs expressing HCN4 protein. ANP (10, 100, 1000 ng/ml) significantly decreased the percentage of HCN4+/MF20- cells per field; A71915 (1 μ M) significantly increased the percentage of HCN4+/MF20- cells per field. N=5 experiments per group; ~700-900 cells were counted from 13 fields for each group. Each bar represents mean \pm SEM. * p <0.05 vs. control (no treatment), # p <0.05 vs. ANP (1000 ng/ml), One-way ANOVA with Tukey's multiple comparisons post hoc test.

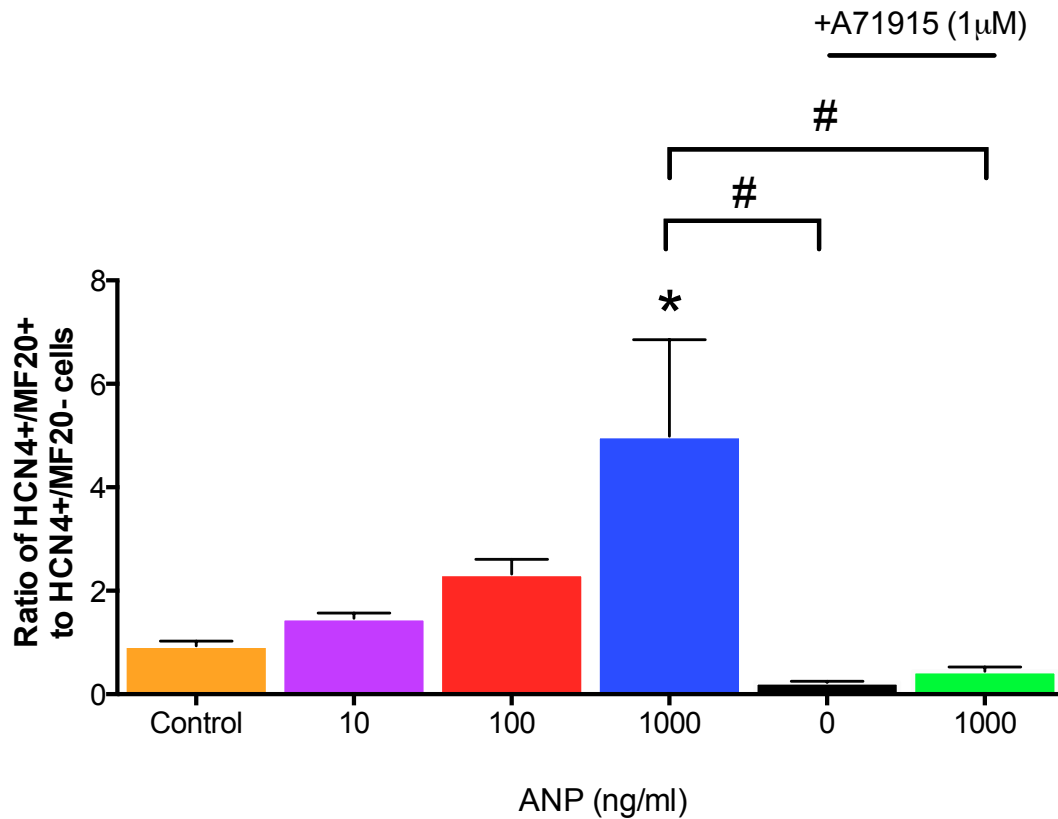


Figure 3.3. Calculated ratios of HCN4+/MF20+ cells to HCN4+/MF20- cells in E11.5 mouse ventricular cells following addition of exogenous ANP treatment. E11.5 ventricular cells were cultured and ANP was added at varying concentrations every 12 hours over a 48-hour period. Cells were immunolabelled for detection of HCN4 protein. CMs were identified as MF20+. Bar graph represents the ratio of VCS cells (HCN4+/MF20+) to VCS progenitor/non-CMs (HCN4+/MF20-) that stained positively for HCN4 upon exposure to exogenous ANP at varying concentrations (0, 10, 100 and 1000 ng/ml) and NPR-A inhibitor A71915 (1 μM) over 48 hours. ANP (1000 ng/ml) significantly increased the cell ratio, favouring differentiation of VCS cells; A71915 (1 μM) significantly decreased the cell ratio, favouring a VCS progenitor/non-CM cell phenotype. N=5 experiments per group; ~700-900 cells were counted from 13 fields for each group. Each bar represents mean ± SEM. *p<0.05 vs. control (no treatment), #p<0.05 vs. ANP (1000 ng/ml), One-way ANOVA with Tukey's multiple comparisons post hoc test.

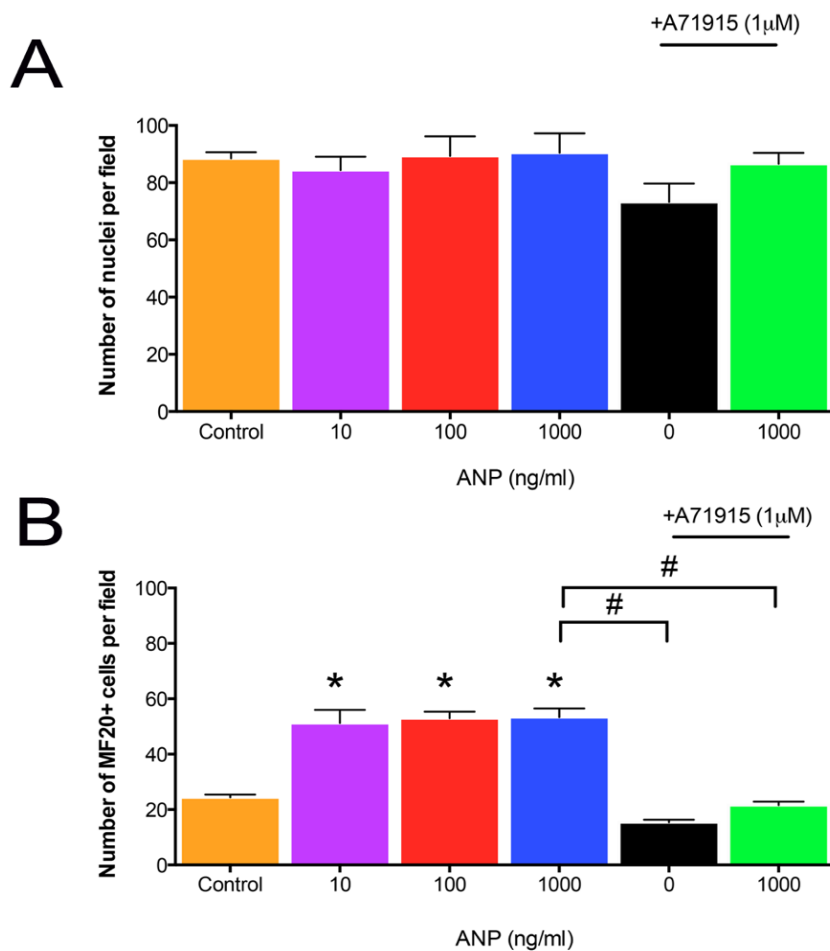


Figure 3.4. Number of Hoechst stained nuclei per field (A) and number of MF20+ cells (B) per field in E11.5 cells immunolabelled with anti-HCN4 antibody following addition of exogenous ANP. E11.5 ventricular cells were cultured and ANP was added at varying concentrations every 12 hours over a 48-hour period. Cells were immunolabelled for detection of HCN4 protein. CMs were identified as MF20+. **A)** The number of Hoechst stained nuclei per field were counted per treatment group; there were no significant differences between groups. **B)** The number of MF20+ cells (CMs) per field were counted. ANP (10, 100, 1000 ng/ml) significantly increased the number of MF20+ cells whereas A71915 significantly decreased the number of MF20+ cells. N=5 experiments per group; ~700-900 cells were counted from 13 fields for each group. Each bar represents mean \pm SEM. * $p < 0.05$ vs. control (no treatment), # $p < 0.05$ vs. ANP (1000 ng/ml) One-way ANOVA with Tukey's multiple comparisons post hoc test.

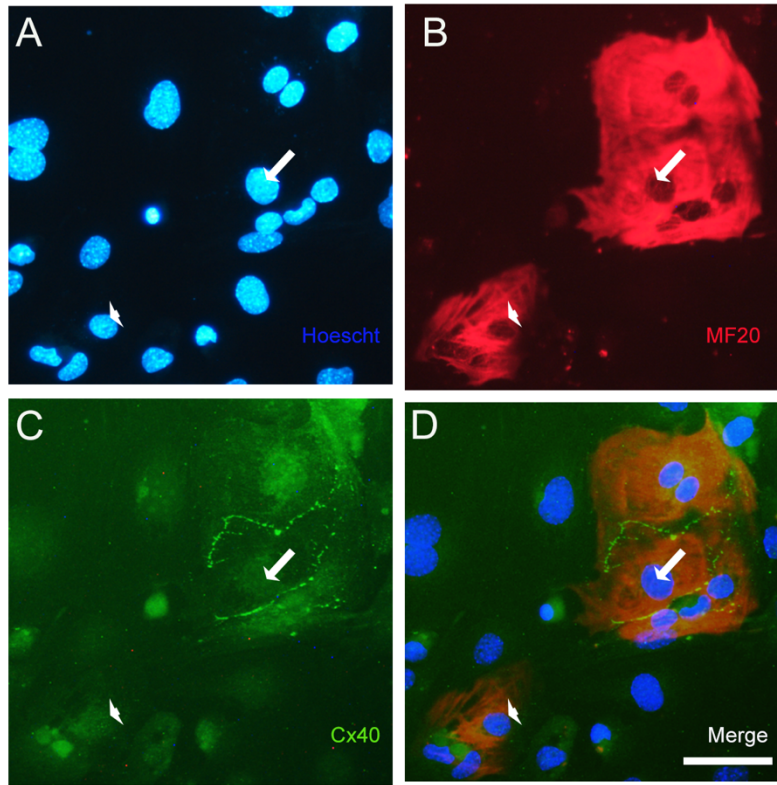


Figure 3.5. Expression of Cx40 protein in E11.5 mouse ventricular cells following addition of exogenous ANP (0, 10, 100 and 1000 ng/ml). A-D: E11.5 ventricular cells were cultured, and ANP at various concentrations were added to cells, every 12 hours over a 48-hour period. The same field of cells were labelled with Hoechst nuclear stain (A), sarcomeric myosin antibodies MF20 (B), Cx40 protein (C) and an image overlay (D). CMs were identified as MF20+. Ventricular cardiac conduction system (VCS) cells were labelled as those that identified as both Cx40+ and MF20+ (Cx40+/MF20+). Arrows indicate Cx40+/MF20+ cells, arrow-heads indicate Cx40+/MF20- cells. N=5 experiments per group. Scale bar = 50 μ M.

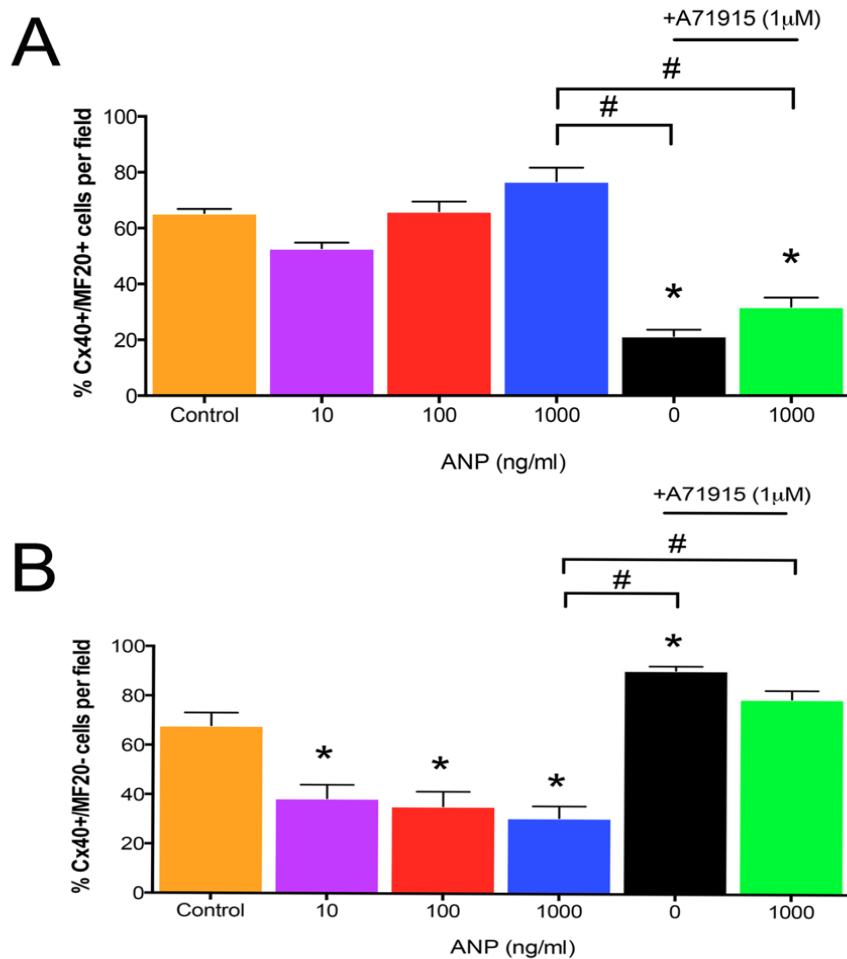


Figure 3.6. Percentage (%) of Cx40+/MF20+ and Cx40+/MF20- cells in E11.5 mouse ventricular cells following addition of exogenous ANP. E11.5 ventricular cells were cultured and ANP was added at varying concentrations every 12 hours over a 48-hour period. Cells were immunolabelled for detection of Cx40 protein. CMs were identified as MF20+. **A)** Bar graph represents the percent (%) of Cx40+/MF20+ cells per field upon exposure to exogenous ANP at varying concentrations (0, 10, 100 and 1000 ng/ml) and NPR-A inhibitor A71915 (1 μ M) over 48 hours. Cx40+/MF20+ cells were not significantly increased by the addition of ANP. A71915 (1 μ M) significantly reduced the % of Cx40+/MF20+ cells per field vs. control. **B)** Bar graph represents the percentage of Cx40+/MF20- cells per field upon exposure to exogenous ANP at varying concentrations (0, 10, 100 and 1000 ng/ml) and NPR-A inhibitor A71915 (1 μ M) over 48 hours. Cx40+/MF20- cells were identified as VCS progenitors/non-CMs expressing Cx40 protein. ANP (10, 100, 1000 ng/ml) significantly decreased the percentage of Cx40+/MF20- cells per field; A71915 (1 μ M) significantly increased the percentage of Cx40+/MF20- cells per field. N=5 experiments per group, ~600-900 cells were counted from 13 fields for each group. Each bar represents mean \pm SEM. * p <0.05 vs. control (no treatment), # p <0.05 vs. ANP (1000 ng/ml), One-way ANOVA with Tukey's multiple comparisons post hoc test.

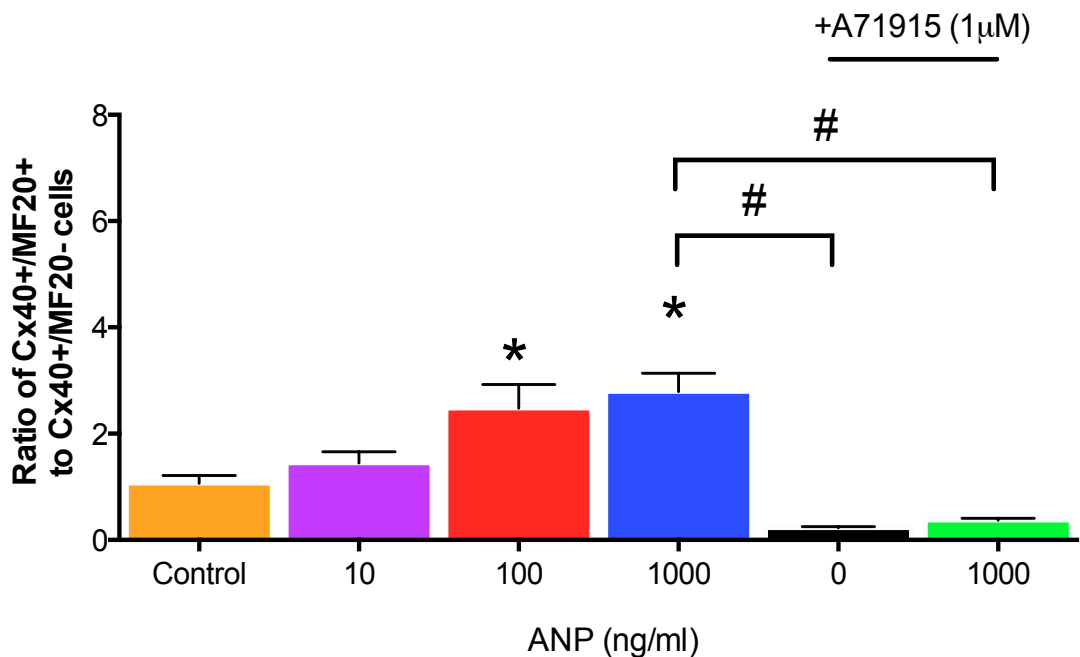


Figure 3.7. Calculated ratio of Cx40+/MF20+ cells to Cx40+/MF20- cells in E11.5 mouse ventricular cells following addition of exogenous ANP. E11.5 ventricular cells were cultured and ANP was added at varying concentrations every 12 hours over a 48-hour period. Cells were immunolabelled for detection of Cx40 protein. Bar graph represents the ratio of VCS cells (Cx40+/MF20+) to VCS progenitor/non-CMs (Cx40+/MF20-) that stained positively for Cx40 upon exposure to exogenous ANP at varying concentrations (0, 10, 100 and 1000 ng/ml) and NPR-A inhibitor A71915 (1 µM) over 48 hours. ANP (100, 1000 ng/ml) significantly increased the cell ratio, favouring differentiation of VCS cells; A71915 (1 µM) significantly decreased the cell ratio, favouring a VCS progenitor/ non-CM cell phenotype. N=5 experiments per group; ~600-900 cells were counted from 13 fields for each group. Each bar represents mean ± SEM. *p<0.05 vs. control (no treatment), #p<0.05 vs. ANP (1000 ng/ml), One-way ANOVA with Tukey's multiple comparisons post hoc test.

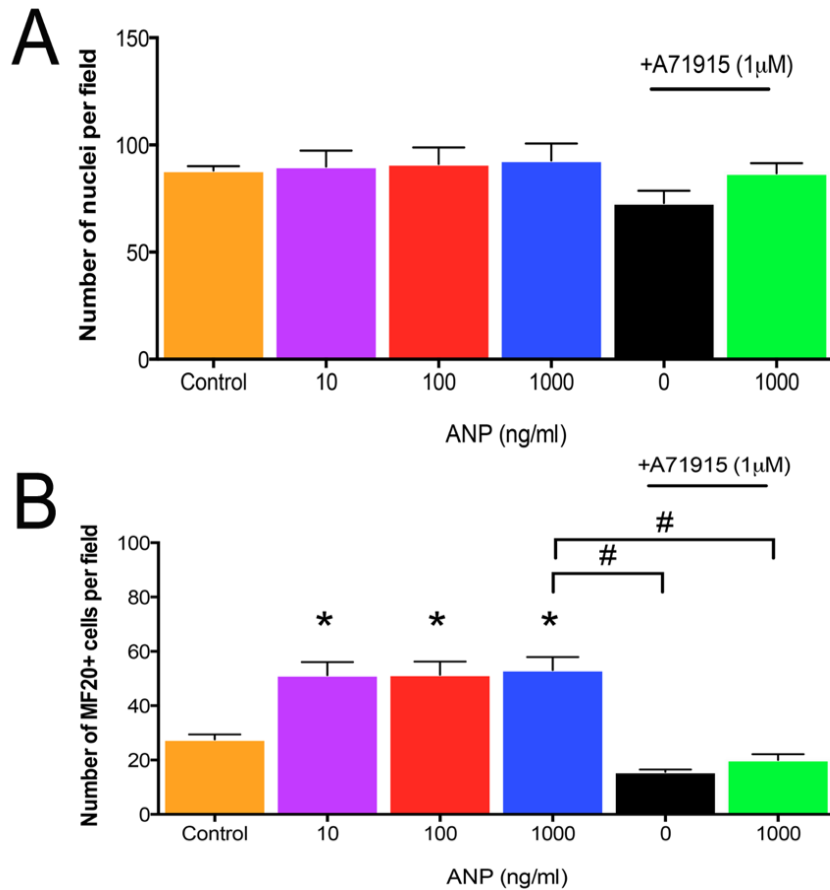


Figure 3.8. Number of Hoechst stained nuclei per field (A) and number of MF20+ cells (B) per field in E11.5 cells immunolabelled with anti-Cx40 antibody following addition of exogenous ANP. E11.5 ventricular cells were cultured and ANP was added at varying concentrations every 12 hours over a 48-hour period. Cells were immunolabelled for detection of Cx40 protein. **A)** The number of Hoechst stained nuclei per field were counted per treatment group; there were no significant differences between groups. **B)** The number of MF20+ cells (CMs) per field were counted. ANP (10, 100, 1000 ng/ml) significantly increased the number of MF20+ cells whereas A71915 significantly decreased the number of MF20+ cells. N=5 experiments per group; ~600-900 cells were counted from 13 fields for each group. Each bar represents mean \pm SEM. * $p < 0.05$ vs. control (no treatment), # $p < 0.05$ vs. ANP (1000 ng/ml), One-way ANOVA with Tukey's multiple comparisons post hoc test.

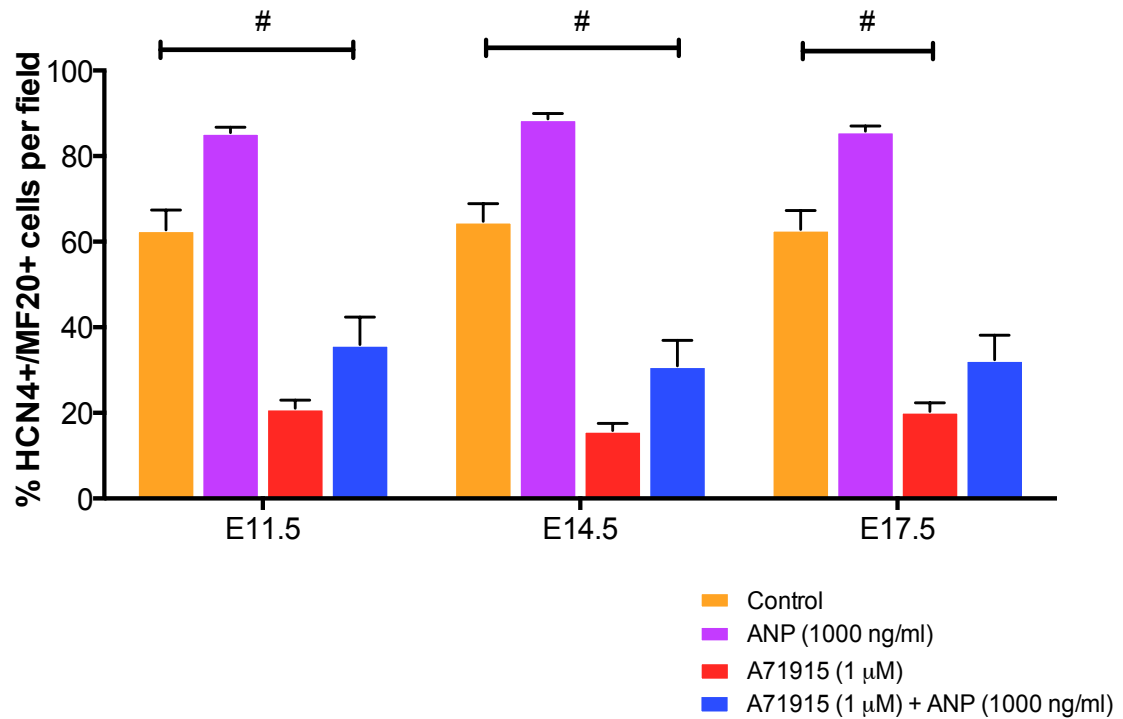


Figure 3.9. Comparison of HCN4+/MF20+ cell percentages in ventricular cell cultures from various developmental stages following addition of exogenous ANP. Ventricular cells at E11.5, E14.5 or E17.5 were cultured and incubated with ANP (1000 ng/ml), A71915 (1 μM), or ANP (1000 ng/ml) + A71915 (1 μM) for 48 hours. Cells were immunolabelled for detection of HCN4 protein. CMs were identified as MF20+. Bar graph represents the percentage (%) of HCN4+/MF20+ cells per field upon exposure to the indicated compounds. Within each embryonic stage, the % of HCN4+/MF20+ cells resulting from the treatment groups were all significantly different from each other, except at E17.5 where there was no significant difference between A71915 and A71915 + ANP. When comparing potential differences in treatments across embryonic stages, there were no significant differences for any of the treatment groups. N=10 experiments per group; ~600-1100 cells were counted from 13 fields for each group. Each bar represents mean ± SEM. #p<0.05 (vs. respective controls per developmental stage), *p<0.05 (between groups as indicated) Two-way ANOVA with Tukey's multiple comparisons post hoc test.

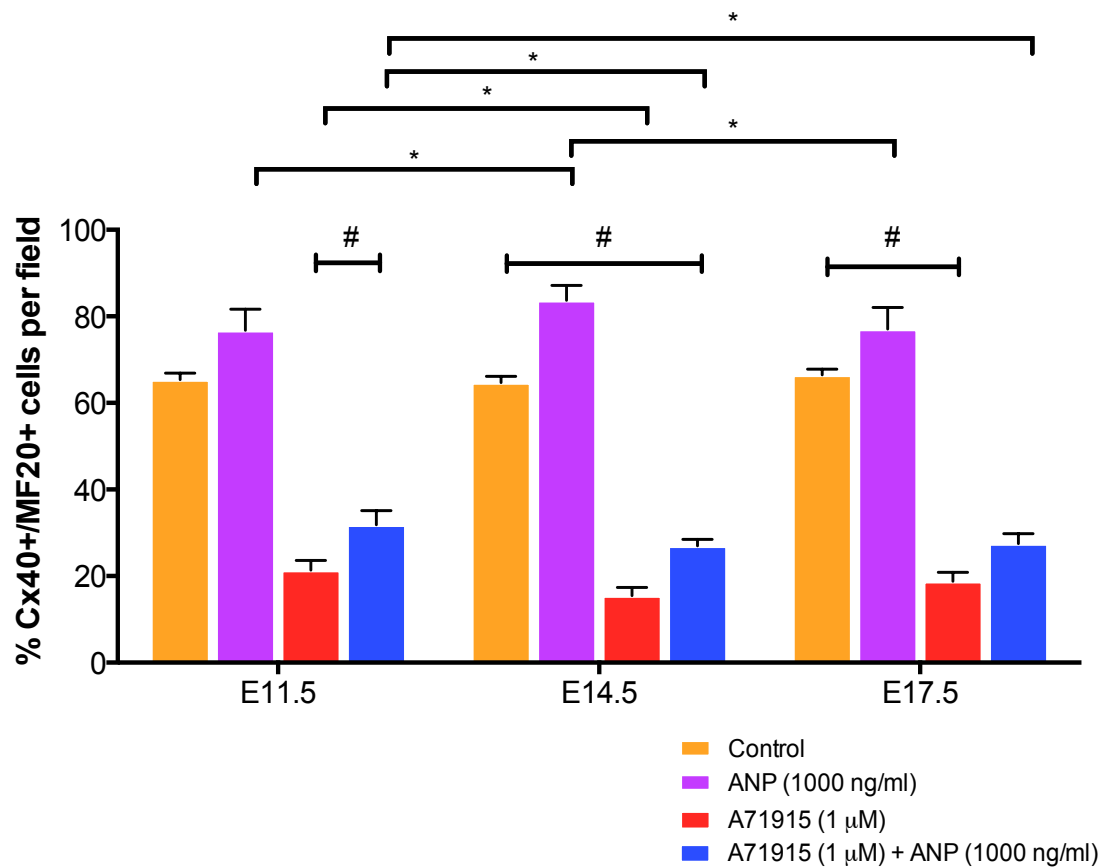


Figure 3.10. Comparison of Cx40+/MF20+ cell percentages in ventricular cell cultures from various developmental stages following addition of exogenous ANP. Ventricular cells at E11.5, E14.5 or E17.5 were cultured and incubated with ANP (1000 ng/ml), A71915 (1 μM), or ANP (1000 ng/ml) + A71915 (1 μM) for 48 hours. Cells were immunolabelled for detection of Cx40 protein. CMs were identified as MF20+. Bar graph represents the percentage (%) of Cx40+/MF20+ cells per field) upon exposure to indicated compounds. Within each embryonic stage, the percentage of Cx40+/MF20+ cells resulting from the treatment groups were all significantly different from each other, except at E11.5 where there was no significant difference between control and ANP, and at E17.5 where there was no significant difference between A71915 and A71915 + ANP. N=10 experiments per group; ~600-1100 cells were counted from 13 fields for each group. Each bar represents mean ± SEM. #p<0.05 (vs. respective controls per developmental stage), *p<0.05 (between groups as indicated) Two-way ANOVA with Tukey's multiple comparisons post hoc test.

3.3.2 Effects of ANP on Gene Expression of HCN4 and Cx40 in E11.5 Mouse Ventricular Cells

The potential effects of exogenous ANP on HCN4 and Cx40 mRNA expression were determined by quantifying the relative abundance of mRNA transcripts at E11.5 by real time quantitative polymerase chain reaction (RT-qPCR). GAPDH was utilized as the housekeeping gene to normalize data because its expression remained unchanged across all treatment groups tested. E11.5 ventricular cell cultures were treated with or without ANP in the presence or absence of A71915, every 12 hours for a total period of 48 hours, and were then processed for extraction of RNA and synthesis of cDNA, followed by RT-qPCR analysis of the genes of interest. The addition of exogenous ANP (1000 ng/ml) to E11.5 ventricular cells resulted in a 1.7-fold \pm 0.1 increase in the gene expression of HCN4 vs. vehicle treated control (Control = 1.0 gene expression) ($p < 0.05$, **Figure 3.11 A**). The addition of A71915 (1 μ M) had the opposite effect in reducing gene expression of HCN4 by 5-fold (0.2 ± 0.04 , $p < 0.005$). The combination of ANP (1000 ng/ml) and A71915 (1 μ M) resulted in a reduction in the gene expression of HCN4 by 2.5-fold (0.4 ± 0.04) ($p < 0.05$).

The effect of exogenous ANP and/or A71915 on Cx40 gene expression was also determined using E11.5 ventricular cells. The addition of ANP (1000 ng/ml) to E11.5 ventricular cell culture resulted in a 1.8-fold \pm 0.1 increase in gene expression of Cx40 vs. control ($p < 0.05$, **Figure 3.11 B**). The addition of A71915 (1 μ M) significantly decreased gene expression of Cx40 by \sim 3-fold (0.3 ± 0.2) ($p < 0.05$). The combination of ANP (1000 ng/ml) and A71915 (1 μ M) resulted in a reduction in the gene expression of Cx40 by \sim 3-fold (0.3 ± 0.04) ($p < 0.005$).

We determined if ANP and/or A71915 could significantly impact HCN4 or Cx40 gene expression across several embryonic developmental stages as the heart continues to mature. Ventricular cells from E11.5, E14.5 or E17.5 hearts were cultured and either ANP (1000 ng/ml), A71915 (1 μ M), or ANP (1000 ng/ml) + A71915 (1 μ M) were added to cells for 48 hours. For HCN4 gene expression, within each embryonic stage group, all treatment groups revealed significant differences from one another, except A71915 alone vs. ANP + A71915, which were similar for all stages (**Figure 3.12**). Across embryonic stages, the induction caused by ANP resulted in significantly higher HCN4 gene expression at E14.5 vs. at E11.5 and higher at E17.5 vs. E11.5 (**E11.5**: 1.7-fold \pm 0.06, **E14.5**: 3.4-fold \pm 0.3; **E17.5**: 3.4-fold \pm 0.3, $p < 0.005$). For Cx40 gene expression, within each embryonic stage group, all treatment groups revealed significant differences from one another, except A71915 alone vs. ANP + A71915, which were similar for all stages (**Figure 3.13**). Across embryonic stages, the induction caused by ANP resulted in significantly higher Cx40 gene expression at E14.5 vs. at E11.5, and higher at E17.5 vs. E11.5 (**E11.5**: 1.8-fold \pm 0.1, **E14.5**: 3.8-fold \pm 0.2, **E17.5**: 3.5 \pm 0.2, $p < 0.005$)

We also determined whether gene expression of important cardiac transcription factors involved in the development of the embryonic heart were affected by the addition of exogenous ANP (1000 ng/ml). The cardiac transcription factors we chose to examine were: GATA4, HAND2, Tbx5, and MEF2C. Tbx5 has been shown to regulate development of the SA node (Mori et al., 2006); MEF2C is essential for formation of the primitive heart tube (Meganathan et al., 2015); GATA4 and HAND2 are essential for normal cardiac morphogenesis *in vivo* (Meganathan et al., 2015). The addition of

exogenous ANP did not significantly alter gene expression of these transcription factors at E11.5 in mouse ventricular cells (p=NS) (**Figure 3.14**).

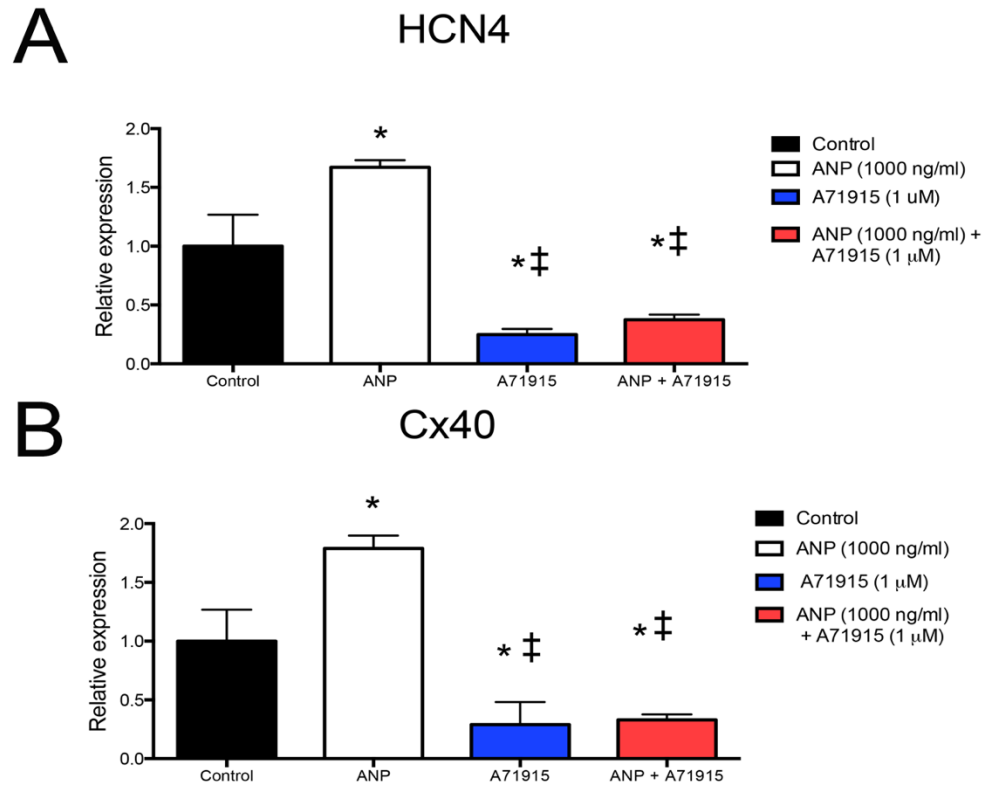


Figure 3.11. RT-qPCR analysis of HCN4 and Cx40 gene expression in E11.5 mouse ventricular cells following addition of exogenous ANP (1000 ng/ml), and in the presence of an NPR-A inhibitor (A71915) over 48 hours. Compared to control, addition of ANP to cell culture resulted in a significant increase in gene expression of HCN4 and Cx40. Addition of A71915 significantly reduced gene expression of HCN4 and Cx40. GAPDH was used as the housekeeping gene. N=6 experiments per group. Each bar represents mean \pm SEM. * $p < 0.05$ vs. H₂O (control), ‡ $p < 0.05$ vs. 1000 ng/ml ANP, One-way ANOVA with Tukey's multiple comparisons post hoc test.

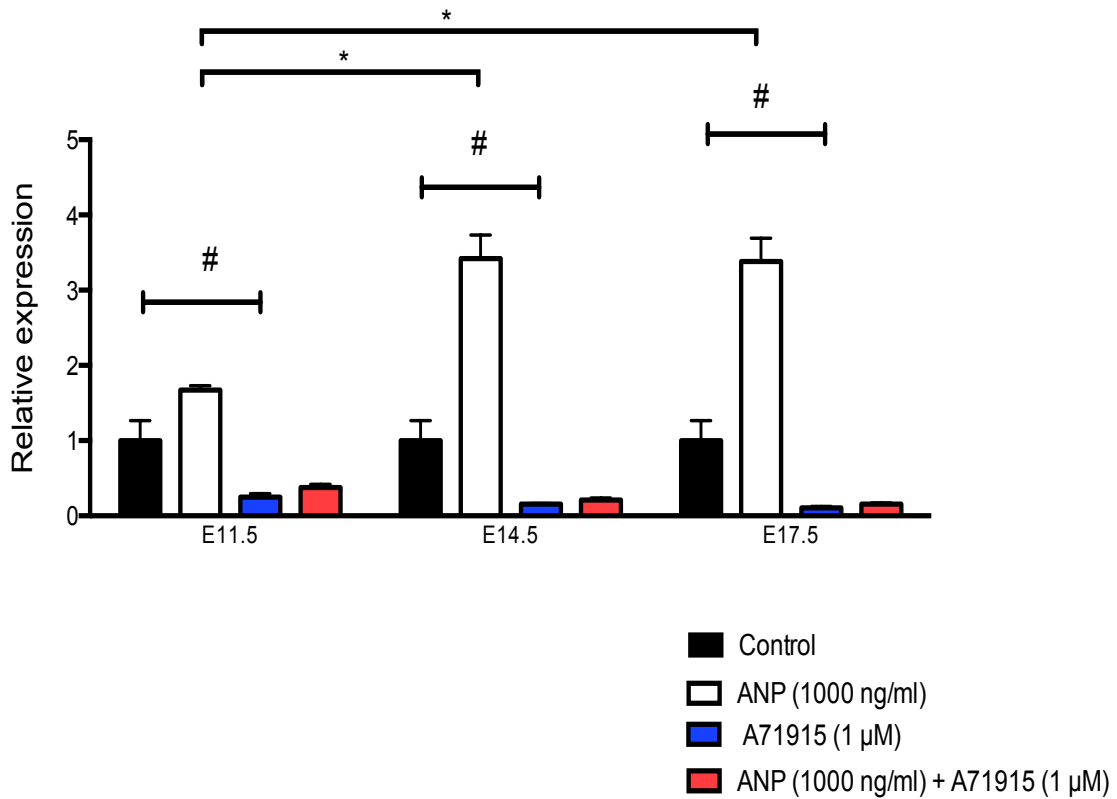


Figure 3.12. Comparison of HCN4 gene expression changes across embryonic stages of heart development upon addition of exogenous ANP and/or A71915 over 48 hours. Ventricular cells at E11.5, E14.5 and E17.5 were cultured and incubated with control, ANP (1000 ng/ml), A71915 (1 μM), or ANP (1000 ng/ml) + A71915 (1 μM). Within each developmental stage, HCN4 gene expression resulting from all treatment groups were significantly different from each other, except between A71915 vs. ANP + A71915. Across developmental stages, ANP significantly increased HCN4 gene expression in E14.5 and E17.5 vs. E11.5 cells. N=6 experiments per group. Each bar represents mean ± SEM. #p<0.05 (within groups), *p<0.05 (across groups), Two-way ANOVA with Tukey's multiple comparisons post hoc test.

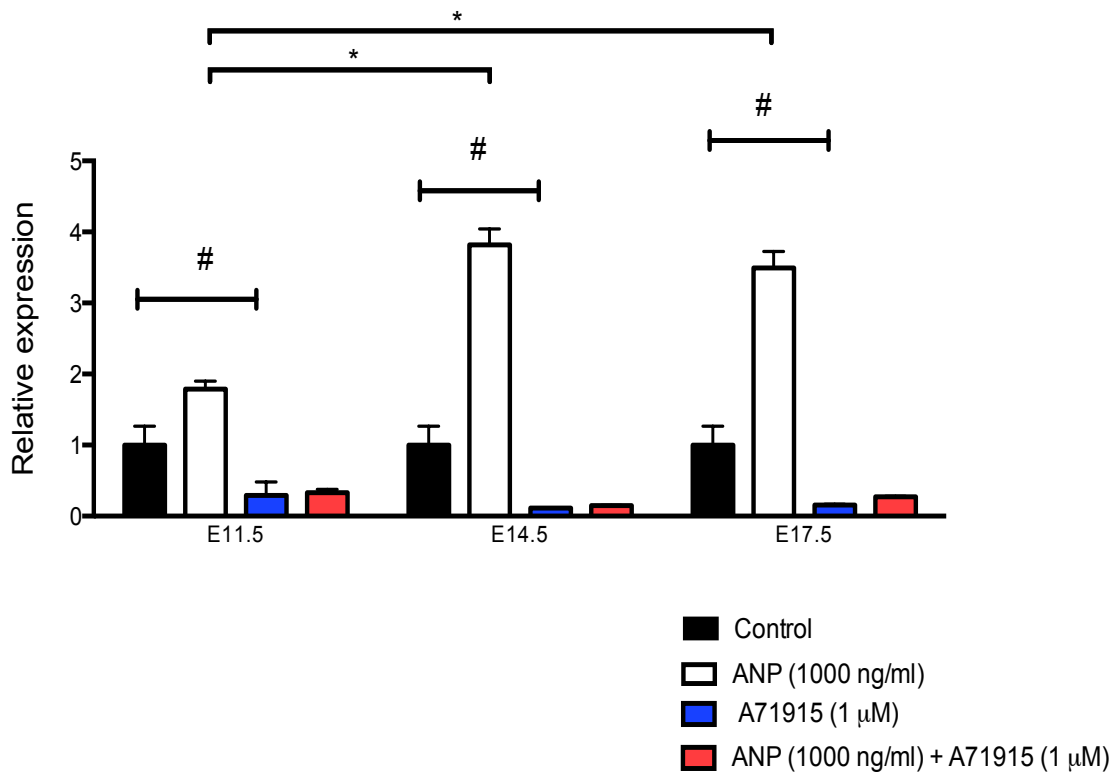


Figure 3.13. Comparison of Cx40 gene expression changes across embryonic stages of heart development upon addition of exogenous ANP and/or A71915 over 48 hours. Ventricular cells at E11.5, E14.5 and E17.5 were cultured and incubated with control, ANP (1000 ng/ml), A71915 (1 μM), or ANP (1000 ng/ml) + A71915 (1 μM). Within each developmental stage, Cx40 gene expression resulting from all treatment groups were significantly different from each other, except between A71915 vs. ANP + A71915. Across developmental stages, ANP significantly increased Cx40 gene expression in E14.5 and E17.5 vs. E11.5 cells. N=6 experiments per group. Each bar represents mean ± SEM. #p<0.05 (within groups), *p<0.05 (across groups) Two-way ANOVA with Tukey's multiple comparisons post hoc test.

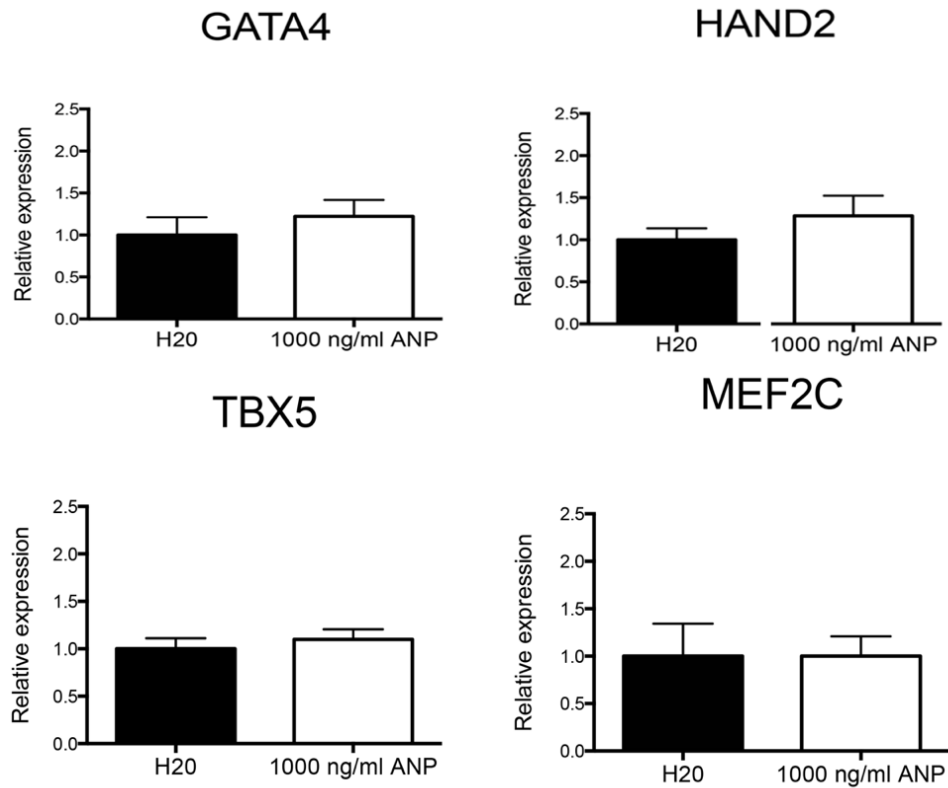


Figure 3.14. RT-qPCR analysis of various cardiac transcription factors in E11.5 mouse ventricular cells following addition of exogenous ANP (1000 ng/ml) over 48 hours. Compared to control, addition of ANP to cell culture had no significant effects on gene expression of GATA4, HAND2, Tbx5, or MEF2C. GAPDH was used as the housekeeping gene. N=6 experiments per group. Each bar represents mean \pm SEM. No significant differences were found between groups. Students unpaired t-test.

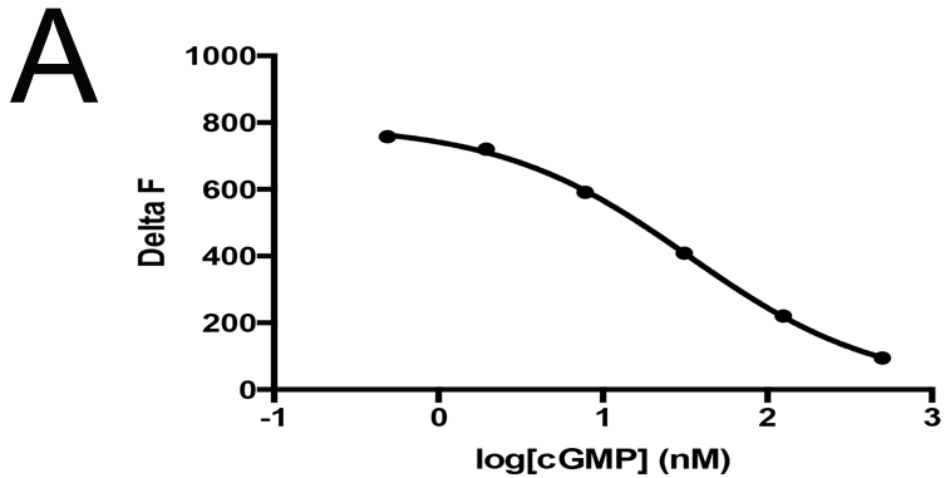
3.3.3 Effects of ANP and/or A71915 on Intracellular Production of cGMP in Mouse E11.5 Ventricular Cells

It has been well established in the literature that the binding of ANP to its high affinity guanylyl cyclase receptor (NPR-A) leads to the production of a second messenger molecule known as cGMP, in several cell types, including CMs (O'Tierney et al., 2010). The potential involvement and biological activity of the ANP/NPR-A/cGMP signalling pathway in the developing embryonic heart has not been well characterized in the literature. Furthermore, significant decreases in gene expression of HCN4 and Cx40 with NPR-A blocker alone warranted further assessment of A71915 effects on intracellular cGMP levels in embryonic ventricular cells. To determine the effects of ANP and A71915 on cGMP levels in E11.5 ventricular, a competitive HTRF based immunoassay was performed as described in Section 2.14.

In the first step of this assay, acutely isolated E11.5 ventricular cells were incubated with ANP and/or A71915 to stimulate the production of intracellular cGMP. In the second step, competition was initiated between endogenous cGMP and d2 dye labeled cGMP for binding sites on anti-cGMP monoclonal antibodies labelled with the energy acceptor Cryptate. The specific signal is recorded as Delta F which occurs due to the energy transfer between the d2-cGMP and Cryptate. Delta F values are inversely proportional to the concentration of endogenous cGMP measured in the sample. Delta F values for known concentrations of cGMP were used to generate a cGMP standard curve, and then, Delta F values from samples were extrapolated using this standard curve (**Figure 3.15**).

To determine the effects of exogenous ANP on intracellular production of cGMP in E11.5 ventricular cells, these cells were stimulated with either no treatment, 1000 ng/ml ANP, 1 μ M A71915, or a combination of ANP (1000 ng/ml) plus A71915 (1 μ M). The basal level of cGMP was measured to be 28.1 ± 0.2 nM per 100,000 cells. The addition of exogenous ANP (1000 ng/ml) significantly increased intracellular cGMP vs control (37 ± 0.2 nM vs. 28 ± 0.2 nM, $p < 0.005$, **Figure 3.16**). Compared to control, there was a significant decrease in cGMP production upon addition of A71915 (1 μ M) to 23 ± 0.4 nM ($p < 0.005$). There was a significant decrease in cGMP production with the addition of the combination of A71915 (1 μ M) and ANP (1000 ng/ml) to 24 ± 0.1 nM ($p < 0.005$). Although cGMP levels in combination treatment were significantly higher compared to A71915 treatment alone ($p < 0.005$), these levels were still significantly lower compared to the levels observed in ANP treatment alone (~1.5 fold, **Figure 3.16**).

Taken together, these results suggest that the ANP/NPR-A/cGMP signalling pathway is biologically active at E11.5 in the embryonic mouse ventricular cells and A71915 can decrease both basal and exogenous ANP induced cGMP levels.



B

Final [cGMP] (nM)	Delta F
500	94
125	221
31.25	409
7.81	591
1.95	720
0.49	758

Figure 3.15. Generation of the standard curve for cGMP. A) The standard curve for cGMP was generated by plotting Delta F values obtained from standards with known cGMP concentrations. These concentrations covered an average range between 0.49-500 nM (concentration of cGMP per well). The experimentally determined Delta F values were obtained utilizing the given standards from the competitive immunoassay kit. **B)** Table displaying the concentration of each of the standards provided in the kit along with their experimentally determined Delta F values. Single point in standard curve represents the mean of three independent experiments.

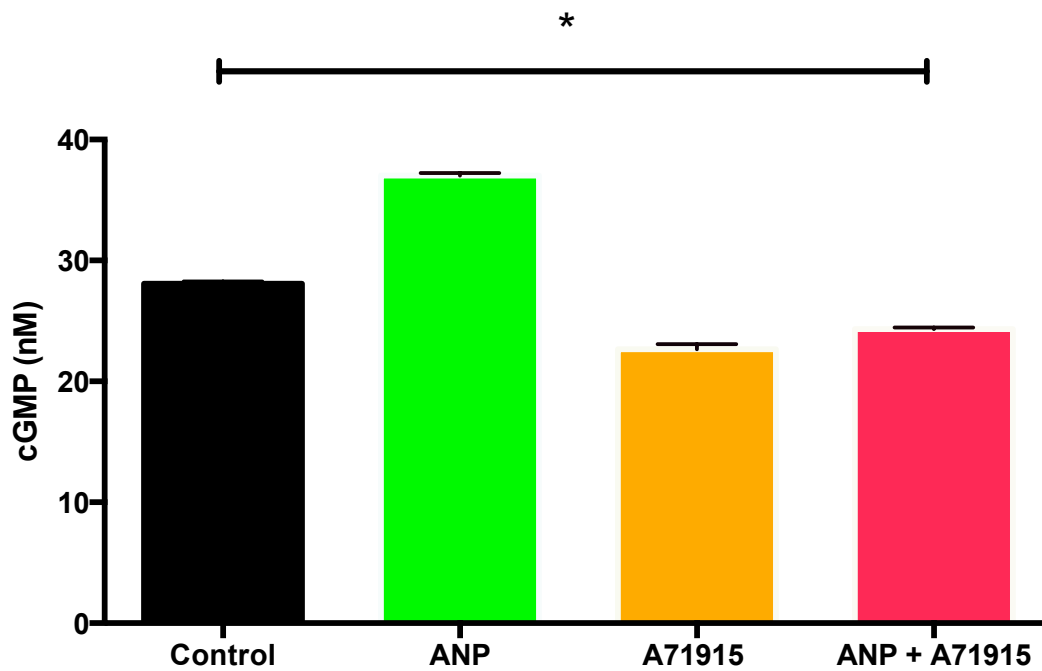


Figure 3.16. The effects of exogenous ANP and A71915 on cGMP production in E11.5 ventricular cells. The effects of exogenous ANP and/or A71915 treatment on intracellular cGMP production was determined by stimulating isolated E11.5 cells with ANP and/or A71915, then measuring cGMP using a competitive immunoassay. The baseline level of cGMP was measured to be 28.1 ± 0.2 nM/ 100,000 cells. Addition of exogenous ANP resulted in a significant increase in cGMP. In contrast, addition of A71915 resulted in a significant decrease in cGMP. N=3 independent experiments, performed in duplicate wells. Each bar represents mean \pm SEM. * $p < 0.0005$, One-way ANOVA with Tukey post hoc test.

3.3.4 Determination of the Bioactivity of Exogenously Added ANP in E11.5 Ventricular Cell Cultures

Secreted ANP is known to be internalized via an NPR-C mediated clearance mechanism as well as subjected for protein degradation by neutral endopeptidases (Potter et al., 2006). Hence, we sought to measure the bioactivity of exogenously added ANP in culture media of E11.5 ventricular cells over a 12-hour period. Media supplemented with ANP (1000 ng/ml) was collected from ventricular cell cultures at 1, 4 or 12 hour durations and transferred to wells containing HEK293 cells which are known to express NPR-A receptors (Airhart et al., 2003). Subsequently, HEK293 cells were incubated at 37°C for 1 hour and intracellular cGMP levels were measured using a competitive HTRF immunoassay. As additional controls, HEK293 cells treated with or without ANP (1000ng/ml) in fresh medium were also included for comparisons (**Figure 3.17**). The baseline level of cGMP in untreated HEK293 cultures was measured to be 29 ± 0.9 nM per 100,000 E11.5 cells (**Figure 3.17**). Addition of exogenous ANP (1000 ng/ml) significantly increased intracellular cGMP compared to untreated cells (37.3 ± 0.2 nM vs. 29 ± 0.9 nM, $p < 0.005$). Furthermore, ventricular cell culture media supplemented with ANP retained significantly higher bioactivity compared to untreated cells at all time points tested (**Figure 3.17**). Although there was a slight but significant decrease in the ability of media at the 12 hour time point to induced cGMP levels compared to that from 1 hour time point (34.1 ± 0.4 nM vs. 36.8 ± 0.3 nM, $p < 0.05$), exogenous ANP was still bioactive at 12 hours since it significantly increased cGMP levels compared to untreated cells (34.1 ± 0.4 nM vs. 29 ± 0.9 nM, $p < 0.005$).

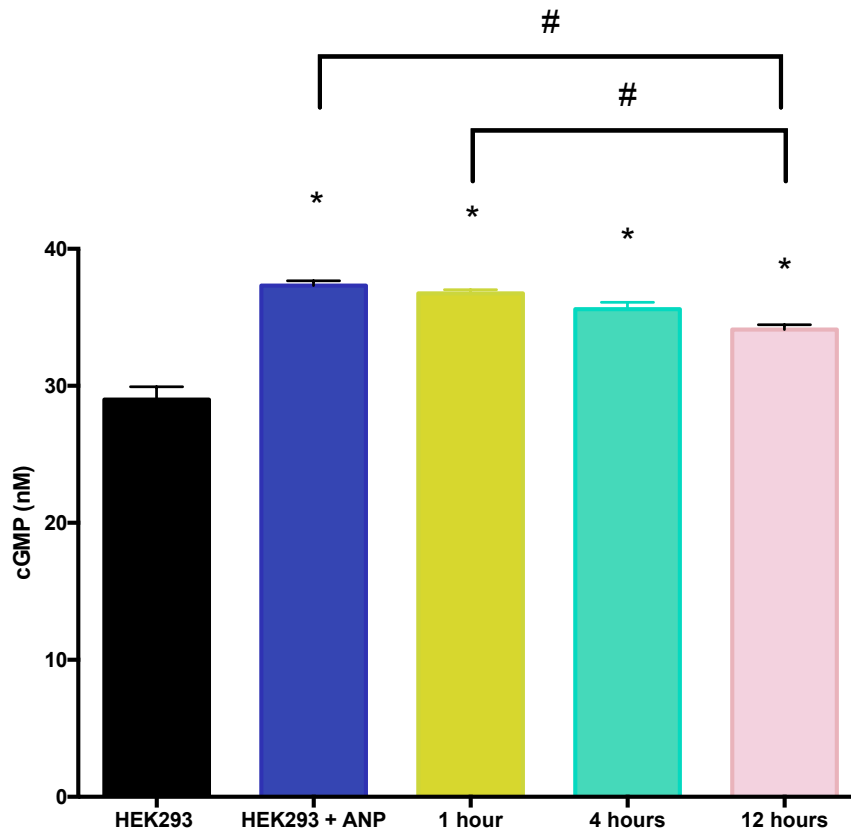


Figure 3.17. Determination of the bioactivity of exogenous ANP (1000 ng/ml) upon addition to E11.5 ventricular cells. To determine if ANP was active in cells 12 hours after the first dose, E11.5 ventricular cells were cultured from CD1 female mice, then ANP was added to cell culture (1000ng/ml). Media was then collected at 1, 4 and 12-hour time points and transferred to HEK293 cells, and intracellular cGMP was immediately measured. As a negative control, intracellular cGMP production was measured in HEK293 cells that were not treated with ANP. As a positive control, intracellular cGMP was measured in HEK293 treated directly with fresh ANP. Over 12 hours, there is a minimal decline in intracellular cGMP. N=4 independent experiments, performed in duplicate wells. Each bar represents mean \pm SEM. * $p < 0.005$ vs. HEK293 control, # $p < 0.05$ between groups as indicated, One-way ANOVA with Tukey post hoc test.

3.3.5 Gene Expression of HCN4 and Cx40 in NPRA-KO mice at E14.5

As an alternative approach to study the effects of the ANP/NPR-A signalling system on the gene expression of HCN4 and Cx40, we utilized NPR-A-KO mice at E14.5 and studied gene expression of whole hearts at this stage (**Figure 3.18**). This developmental stage was selected for gene expression studies due to difficulties with obtaining sufficient number of ventricles for each genotype from early developmental stages such as E11.5. To study the effects of the ANP/NPR-A signalling system on VCS marker gene expression, we extracted total RNA from the ventricles of homozygous and heterozygous NPRA-KO mice as well as WT littermates at E14.5 stage and conducted QPCR analysis for HCN4 and Cx40 gene expression levels. While the gene expression of HCN4 in NPR-A heterozygous ventricles (+/-) revealed a decreasing trend compared to that in WT ventricles (+/+), HCN4 expression levels significantly decreased in homozygous ventricles (-/-) when compared to those in WT samples (2.6-fold reduction vs. WT, $p < 0.005$, **Figure 3.18 A**). Gene expression of Cx40 in heterozygous ventricles was similar to that in WT samples, however the homozygotes had significantly less gene expression of Cx40 compared to WT or heterozygous ventricles (2.5-fold reduction, $p < 0.05$, **Figure 3.18 B**). This data provides further evidence that the ANP/NPR-A signalling axis may be important in the development of the VCS, through expression of HCN4 and Cx40.

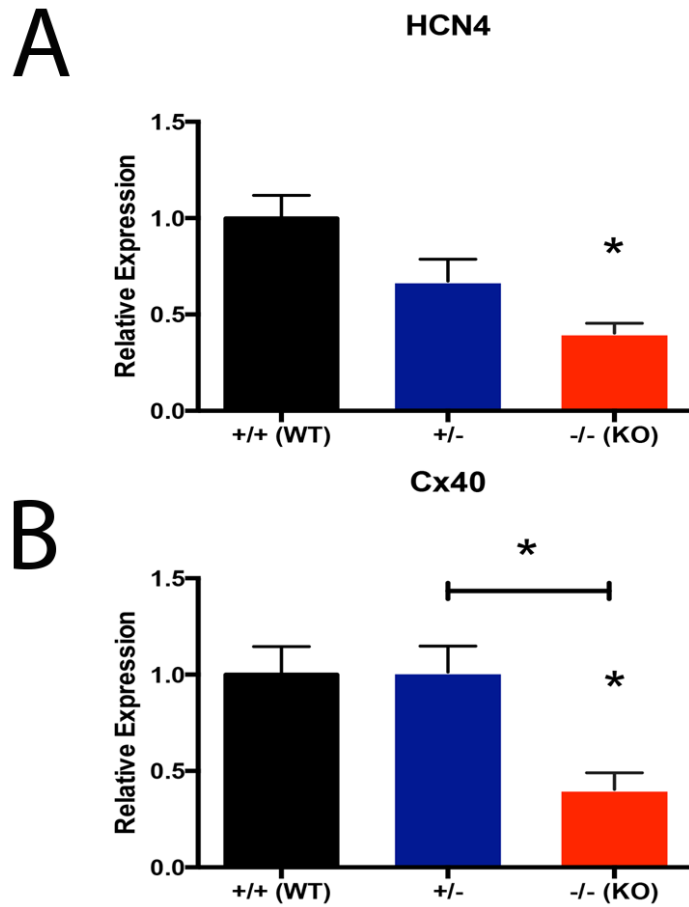


Figure 3.18. Gene expression of HCN4 and Cx40 in NPR-A-KO mice in E14.5 stage ventricles. Gene expression of **A**) HCN4 and **B**) Cx40 decreased in homozygous (-/-) NPR-A-KO mice vs. WT mice. HCN4: N=8 (WT group), N= 12 (heterozygous group), N= 9 (KO group); Cx40: N=8 (WT), N=13 (heterozygous), N = 10 (KO) independent RNA extractions/genotype, with each extraction analyzed in duplicate. GAPDH was used as the housekeeping gene. Each bar represents mean \pm SEM. * $p < 0.05$ vs. WT, One-way ANOVA with Tukey post hoc test.

3.3.6 Effects of ANP on Cx40 Reporter Gene Expression in E11.5 Cx40^{egfp} Ventricles

In the early embryonic heart, Cx40 is expressed transmurally in the ventricular trabeculae. As the heart matures, Cx40 expression becomes gradually restricted to the atria and His-Purkinje network while being excluded from working CMs that surround them in the ventricular myocardium (Miquerol et al., 2004). To further evaluate the role of ANP in Cx40 gene expression at early stages of heart development, we have employed a Cx40^{egfp} reporter mouse model. The Cx40^{egfp} mouse model utilizes the enhanced green fluorescent protein (EGFP) sequence, which is knocked into the 3' untranslated region of the Cx40 gene (Miquerol et al., 2004). This mouse model permits visualization of the His-Purkinje system and has been widely used to monitor development and maturation of the CCS (Tamaddon et al., 2000; Van Rijen et al., 2001; Meysen et al., 2007).

Cx40^{egfp} homozygous knock-in (+/+) mice (designated as Cx40^{egfp+/+}) were bred to WT BL6 mice to generate Cx40^{egfp} heterozygous embryos (designated as Cx40^{egfp+/-}) at E10.5. Whole embryos were cultured with 10% DMEM (no AB/AM) and treated with ANP (1000 ng/ml) and/or A71915 (1 μ M) for 24 hours. Whole embryos and hearts were examined after this 24-hour time point, (now E11.5) for EGFP fluorescence (surrogate marker for Cx40) using stereofluorescence illumination microscopy. Visually, whole embryos incubated with ANP demonstrated greater EGFP fluorescence compared to the fluorescence levels in control embryos (**Figure 3.19**). WT embryos negative for the EGFP knock-in allele do not show any fluorescence under the imaging conditions used. Whole hearts from embryos were imaged under whole mount microscopy to visualize

fluorescence at E11.5. In all groups, the EGFP signal could be detected from the exterior surface in regions of the ventricles, but remained absent from the interventricular septum (**Figure 3.20**). Compared to the controls samples, the hearts treated with ANP (1000 ng/ml) revealed strong EGFP signals in both the atrial chambers and both ventricles, with the left ventricle having the strongest signal of the four chambers (N=5 hearts per group, **Figure 3.20**). A71915 (1 μ M) treated hearts had very weak EGFP signals in both atria and ventricles and in 2 out of 5 hearts the atrial fluorescence was barely visible. In hearts treated with the combination of ANP (1000 ng/ml) + A71915 (1 μ M), both atria and ventricles had very weak EGFP signals as well. In addition, in 3 out of 5 hearts treated with the combination, the atrial fluorescence was barely visible (**Figure 3.20**). We quantified the percentage (%) of green pixels in both left and right ventricles of each heart, either treated with control, ANP, and/or A71915 (**Figure 21**). Compared to control (20 ± 3 % green pixels), ventricles of ANP treated hearts had 42 ± 5 % green pixels, more than double that of control ($p < 0.05$). This was also significantly greater than the green pixel (%) for ventricles of A71915 and ANP + A71915 combination treated hearts ($p < 0.05$). The addition of A71915 to embryos resulted in ventricles having a reduced % of green pixels which was not statistically significant vs. control (13 ± 4 %, $p = \text{NS}$). Similarly, the combination of ANP plus A71915 resulted in ventricles having a reduced % of green pixels although this was not statistically significant vs. control (10 ± 1 %, $p = \text{NS}$) (**Figure 3.21**). Therefore, these results suggest that the addition of ANP can significantly increase reporter gene fluorescence signal in Cx40^{egfp} hearts at E11.5 stage.

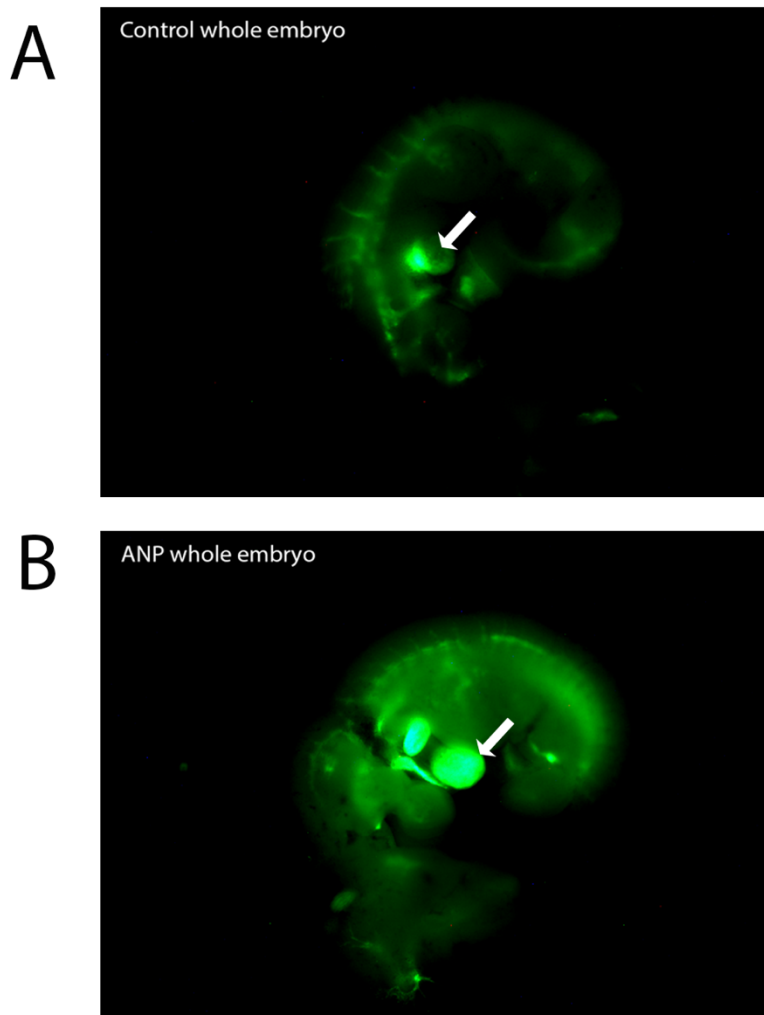


Figure 3.19. Visualization of EGFP fluorescence in $Cx40^{egfp+/-}$ (heterozygous) whole embryos cultured in the presence or absence of ANP. At E10.5, $Cx40^{egfp+/-}$ whole embryos were cultured and incubated with ANP (1000 ng/ml) and/or A71915 (1 μ M), or no treatment (control) for 24 hours. After 24 hours, now at E11.5, whole embryos were visualized for qualitative determination of Cx40 expression. **A)** E11.5 whole embryo with no treatment. **B)** E11.5 whole embryo with ANP (1000 ng/ml) treatment. Visually, ANP-treated whole embryos had stronger green fluorescence throughout, indicating stronger expression of Cx40 vs. control. Arrow indicates labelling of heart. N=5 embryos per group.

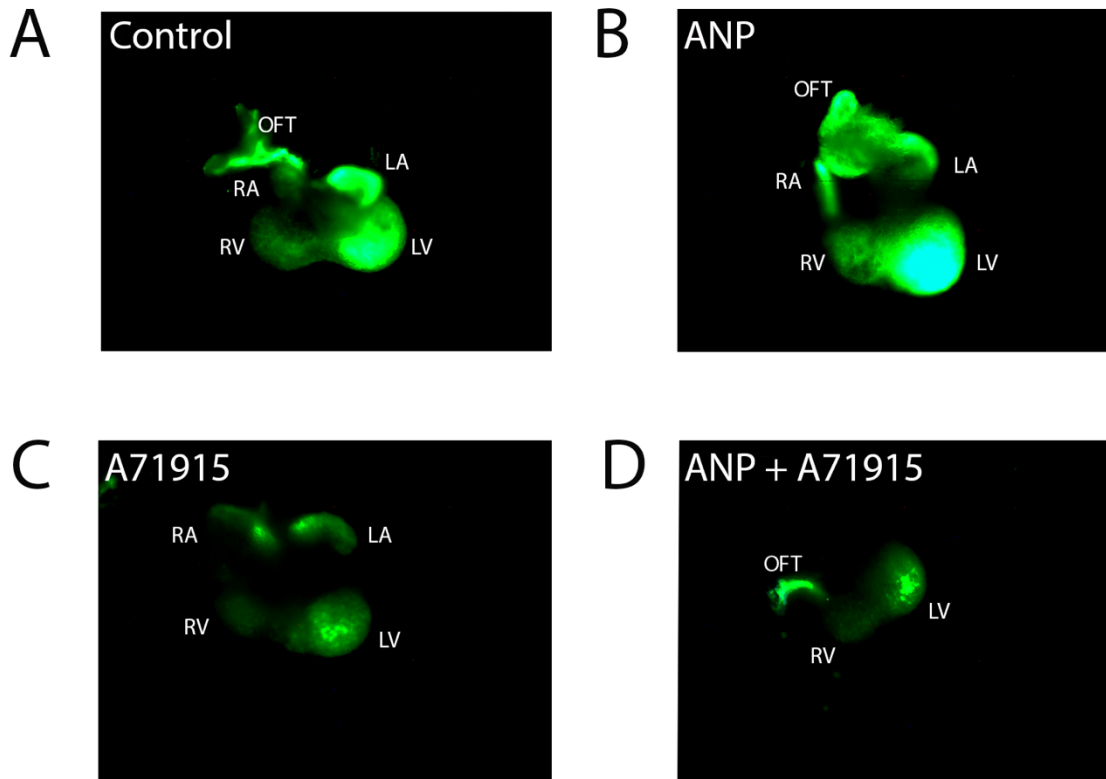


Figure 3.20. Visualization of EGFP fluorescence in $Cx40^{egfp+/-}$ (heterozygous) whole hearts treated with ANP and/or A71915 for 24 hours, at E11.5. At E10.5, $Cx40^{egfp+/-}$ whole embryos were cultured and incubated with ANP (1000 ng/ml) and/or A71915 (1 μ M), or no treatment (control) for 24 hours. After 24 hours, now at E11.5, whole hearts were isolated in order to visualize reporter gene expression. **A)** E11.5 whole heart with no treatment. **B)** E11.5 whole heart with ANP (1000 ng/ml) treatment. **C)** E11.5 whole heart with A71915 (1 μ M) treatment. **D)** E11.5 whole heart with ANP (1000 ng/ml) + A71915 (1 μ M) combination treatment. ANP-treated whole hearts had strong EGFP signals in both atria and ventricles, with the strongest signal coming from the left ventricle. A71915-treated hearts and combination-treatment hearts showed weaker EGFP signals in all four chambers of the heart and were not significant vs. control. RA: right atrium, RV: right ventricle, LA: left atrium, LV: left ventricle and OFT: outflow tract. N=5 hearts per group.

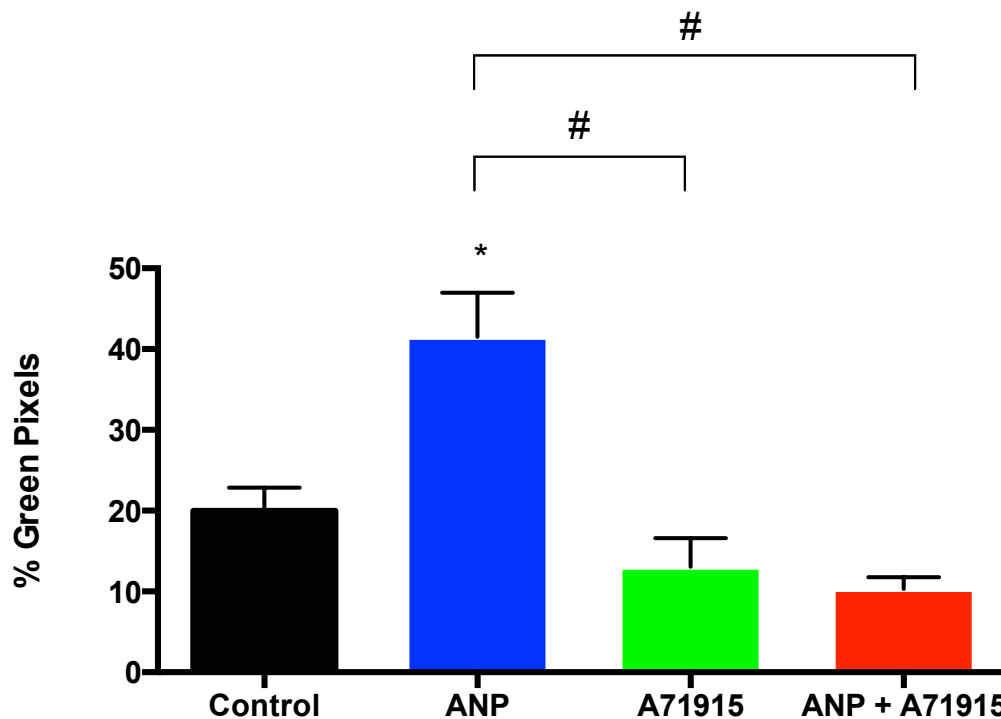


Figure 3.21. Quantification of green pixels (%) to determine reporter gene expression in *Cx40^{egfp+/-}* ventricles at E11.5 treated with ANP and/or A71915. Green pixels were quantified and the percent (%) of green pixels (number of green pixels/(number of green pixels + number of black pixels) x 100%) for both the left and right ventricle (together) of each heart, was calculated. Hearts treated with ANP showed the strongest EGFP signals in the ventricles, whereas hearts treated with A71915 or the combination of A71915 + ANP showed weak EGFP signals in the ventricles (not significantly different vs. control, but significantly less vs. ANP-treated hearts). ANP-treated hearts had significantly higher % green pixels vs. control. N=5 hearts per group. Each bar represents mean \pm SEM. * $p < 0.05$ vs. control, # $p < 0.05$ vs. ANP, One-way ANOVA with Tukey post hoc test.

3.3.7 Visualization and Quantification of Ventricular Cardiac Conduction System Development in Newborn Mice Lacking NPR-A Using the Cx40^{egfp} Mouse Model

The Cx40^{egfp} mouse model was used to visualize mice that were haploinsufficient for the cardiac transcription factor Nkx2.5, which generated hearts that had hypoplastic Purkinje fiber networks (Jay et al., 2004; Meysen et al., 2007). We initiated compound breeding schemes between double heterozygote male and females with a genotype of Cx40^{egfp+/-} and NPR-A^{+/-} to generate 1 day old neonatal pups (ND1) harboring a single copy of Cx40^{egfp+} and lacking one or two copies of NPR-A allele. ND1 pups with a single copy of Cx40^{egfp+} and intact NPR-A alleles (+/+) were used as controls for comparison. Thus far, these crosses have not yielded Cx40^{egfp+/-} pups that were also homozygous knockouts for NPR-A (0 pups from 14 litters).

Crossing the Cx40^{egfp} knock-in line with NPR-A-KO mice as described earlier was done to delineate areas of the neonatal heart that express Cx40 and allowed for us to track the reporter gene expression in WT vs. NPR-A-KO heterozygotes. We analyzed 7 pups with the Cx40^{egfp+/-} / NPR-A^{+/+} genotype, designated as “wild-type (WT)” and 7 pups with the Cx40^{egfp+/-} / NPR-A^{+/-} genotype, designated as “heterozygous NPR-A-KO or NPR-A^{+/-}”. Incisions along the ventricular free wall were made to enable visualization of the inner septal surface as well as the inner free wall of each ventricle (**Figure 3.22 A**). WT hearts revealed extensive arborisation of the Purkinje fiber network. In 5 of the 7 pups in the NPR-A^{+/-} group, these hearts demonstrated significantly less arborisation of the Purkinje fiber network when compared to WT hearts. In several of the NPR-A^{+/-} hearts, the individual fibers appeared thinner and less dense compared to WT hearts (**Figure 3.22 A, B**). Green pixels were quantified in all hearts from both groups to determine if

differences in reporter gene expression existed, and the percentage of green pixels was calculated. Heterozygote NPRA-KO ND1 mice showed a significant decrease in the percentage of green pixels vs. WT mice ($29 \pm 4\%$ vs. $57 \pm 5\%$, $p < 0.05$). (**Figure 3.22 C**).

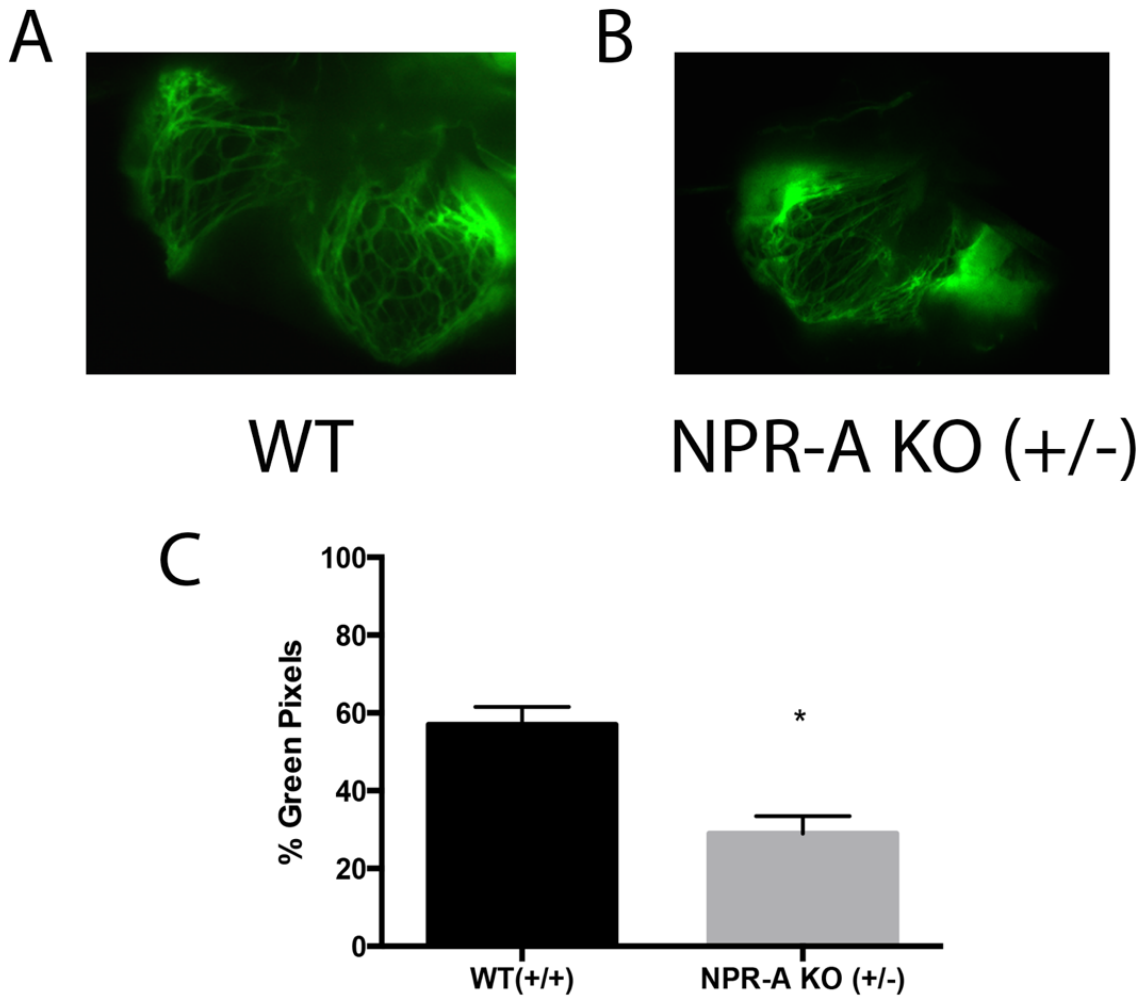


Figure 3.22. Quantification of ventricular conduction system development in neonate day 1 (ND1) hearts of WT and NPR-A-KO^{+/-} mice using Cx40^{egfp+} approach. Green pixels were quantified and the percentage (%) of green pixels (number of green pixels/(number of green pixels + number of black pixels) x 100%) was calculated. Heterozygous NPR-A-KO mice had significantly less arborisation of the Purkinje fiber network, and less % percent green pixels vs. WT mice. Each bar represents mean ± SEM. *p<0.05, unpaired t-test.

3.3.8 Determining the Effects of ANP on Intracellular cGMP Production in Cardiac Progenitor Cells and Ventricular Cells at E11.5

The effects of exogenous ANP were determined on intracellular cGMP production in two different cell populations that exist in the embryonic heart – CPCs and ventricular CMs at E11.5. Earlier findings from our laboratory demonstrated that E11.5 CMs contain a large number of mitochondria compared to the undifferentiated cell population in E11.5 mouse ventricles using transmission electron microscopy (Zhang and Pasumarthi, 2007). A separate study showed that CMs have high mitochondrial content compared to other cell types and can be purified using a fluorescent dye that labels mitochondria (Hattori et al., 2010). In this study, cells were stained with the fluorescent mitochondrial dye tetramethylrhodamine, methyl ester (TMRM) and were sorted by FACS based on their mitochondrial content. ANP was added to cells (1000 ng/ml) and intracellular cGMP was measured immediately. Since CMs possess higher number of mitochondria than CPCs, the group designated “TMRM high” corresponds to the cell population consisting of a majority of CMs, while the “TMRM low” group corresponds to the cell population consisting of a majority of CPCs (Feridooni, 2014; unpublished). The baseline value of cGMP was measured to be 55 ± 0.3 nM in the TMRM high group, and 100 ± 0.5 nM in the TMRM low group. Interestingly, there was a significant difference between these two baseline values ($p < 0.05$). Results were expressed as fold changes over baseline measurement of cGMP for each group. In the TMRM low group (CPCs), the addition of ANP resulted in significant increases in cGMP production at 100 and 1000 ng/ml, 1.6-fold \pm 0.1 and 1.7-fold \pm 0.1, respectively, vs. baseline cGMP ($p < 0.05$) (**Figure 3.23**). In the TMRM high group, only the addition of ANP

at 1000 ng/ml resulted in a 1.2-fold \pm 0.03 increase in cGMP ($p < 0.05$). From these findings, it is possible that CPCs may be more sensitive to ANP-induced increases in cGMP production vs. CMs at E11.5.

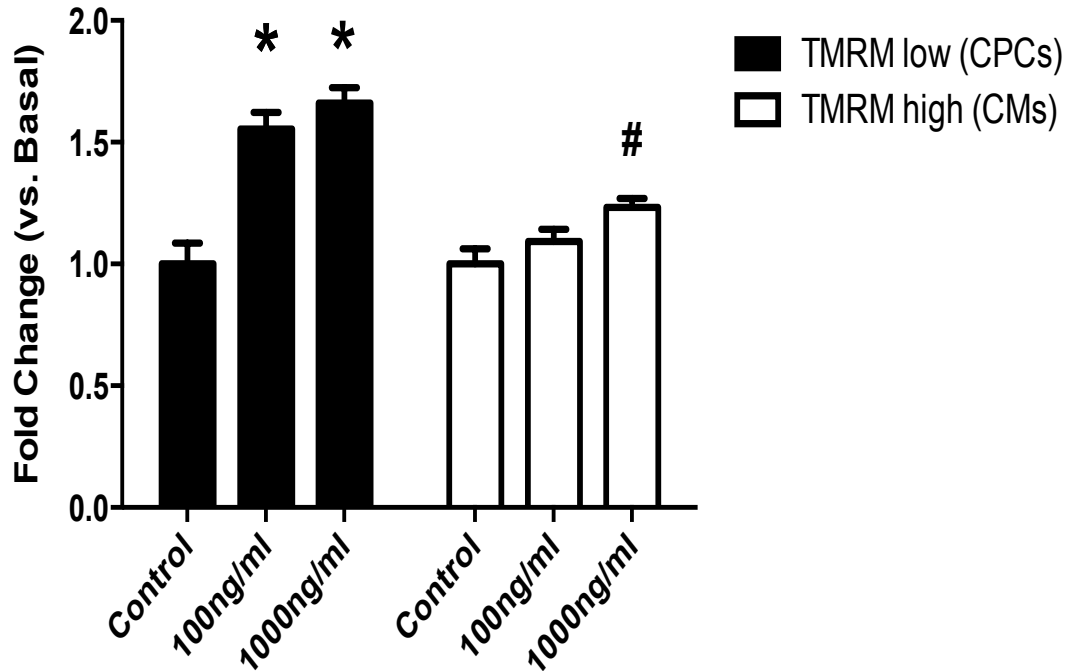


Figure 3.23. The effects of exogenous ANP on intracellular cGMP production in cardiac progenitor cells and ventricular cardiomyocytes at E11.5. Cells were sorted based on mitochondrial content using fluorescent mitochondrial dye staining, (tetramethylrhodamine methyl ester: TMRM), followed by FACS. ANP was added to both cell populations and intracellular cGMP was measured immediately. Results are expressed as the fold change over baseline cGMP measured (given a value of 1). The baseline value of cGMP was measured to be 55 ± 0.3 nM in the TMRM high group, and 100 ± 0.5 nM in the TMRM low group. In the TMRM low group (predominantly CPCs), addition of ANP resulted in significant increases in cGMP production at 100 and 1000 ng/ml. In the TMRM high group, addition of ANP resulted in a significant increase in cGMP production at 1000 ng/ml. N=3 independent experiments, performed in duplicate wells. Each bar represents mean \pm SEM. * $p < 0.05$ vs. control in TMRM low group; # $p < 0.05$ vs. control in TMRM high group, One-way ANOVA with Tukey post hoc test.

3.3.9 Effects of Exogenous cGMP (8-Br-cGMP) on Gene Expression of HCN4 and Cx40 in Mouse E11.5 Ventricular Cells

To determine if the classical NPR-A/cGMP dependent pathway is critical for the regulation of HCN4 and Cx40 gene expression, an exogenous cell permeable cGMP compound (8-Br-cGMP) was added at 10 or 100 μ M concentrations to E11.5 ventricular cells and gene expression levels were determined (**Figure 3.24**). Dosage of 8-Br-cGMP was based on previous reports which showed that only a small fraction of exogenously added 8-Br-cGMP is detectable in the cytoplasm (Li et al., 2012; Yasoda et al., 1998). The addition of 8-Br-cGMP at 10 μ M and 100 μ M significantly increased the gene expression of HCN4 (3.4-fold \pm 0.3 and 5.3-fold \pm 0.3, respectively) vs. control ($p < 0.005$, **Figure 3.24 A**). Similarly, the addition of 8-Br-cGMP at 10 μ M and 100 μ M also significantly increased the gene expression of Cx40 (2.9-fold \pm 0.2 and 5.7-fold \pm 0.8, respectively) vs. control ($p < 0.05$, **Figure 3.24 B**). These results suggest that HCN4 and Cx40 gene expression is regulated by ANP/NPR-A signalling via cGMP.

Since antibodies specific for cGMP also cross-react with 8-Br-cGMP (Li et al., 2012; Yasoda et al., 1998), we employed the competitive HTRF immunoassay to determine the levels of intracellular cGMP after exogenous addition of various concentrations of 8-Br-cGMP to E11.5 ventricular cells. A standard curve for 8-Br-cGMP was generated using the competitive immunoassay, by plotting Delta F values obtained from known concentrations of 8-Br-cGMP (**Figure 3.25**). The baseline level of intracellular cGMP was measured at 27.4 ± 0.6 nM per 100,000 E11.5 ventricular cells which were not treated with 8-Br-cGMP (**Figure 3.26**). The addition of 1 μ M 8-Br-cGMP did not significantly alter cGMP levels vs. control ($p = \text{NS}$). The addition of 10 μ M 8-Br-

cGMP resulted in a measured cGMP level of 77.1 ± 4.2 nM, which corresponds to an approximate 3-fold increase in intracellular cGMP vs. baseline ($p < 0.00005$). Compared to the baseline cGMP level, the addition of $25 \mu\text{M}$ 8-Br-cGMP resulted in a measured cGMP level of 88.5 ± 2.5 nM, which corresponds to an approximate 3-fold increase in intracellular cGMP vs. baseline ($p < 0.005$). The addition of $100 \mu\text{M}$ 8-Br-cGMP resulted in measured cGMP level of 138.0 ± 3.9 nM, corresponding to a 5-fold increase in intracellular cGMP vs. baseline ($p < 0.005$) (**Figure 3.26**). The addition of $100 \mu\text{M}$ 8-Br-cGMP resulted in significant elevation of cGMP levels compared to doses of 10 or $25 \mu\text{M}$ 8-Br-cGMP ($p < 0.005$). To compare, the addition of 100 or 1000 ng/ml ANP to cell culture, in separate experiments, resulted in elevations in cGMP levels to 34.5 ± 0.7 nM and 37.9 ± 0.1 nM, respectively, vs. baseline ($p < 0.05$). Collectively, these results suggest that intracellular cGMP levels can be elevated by 3-5-fold when large doses of 8-Br-cGMPs are added to E11.5 ventricular cell cultures compared to untreated cells.

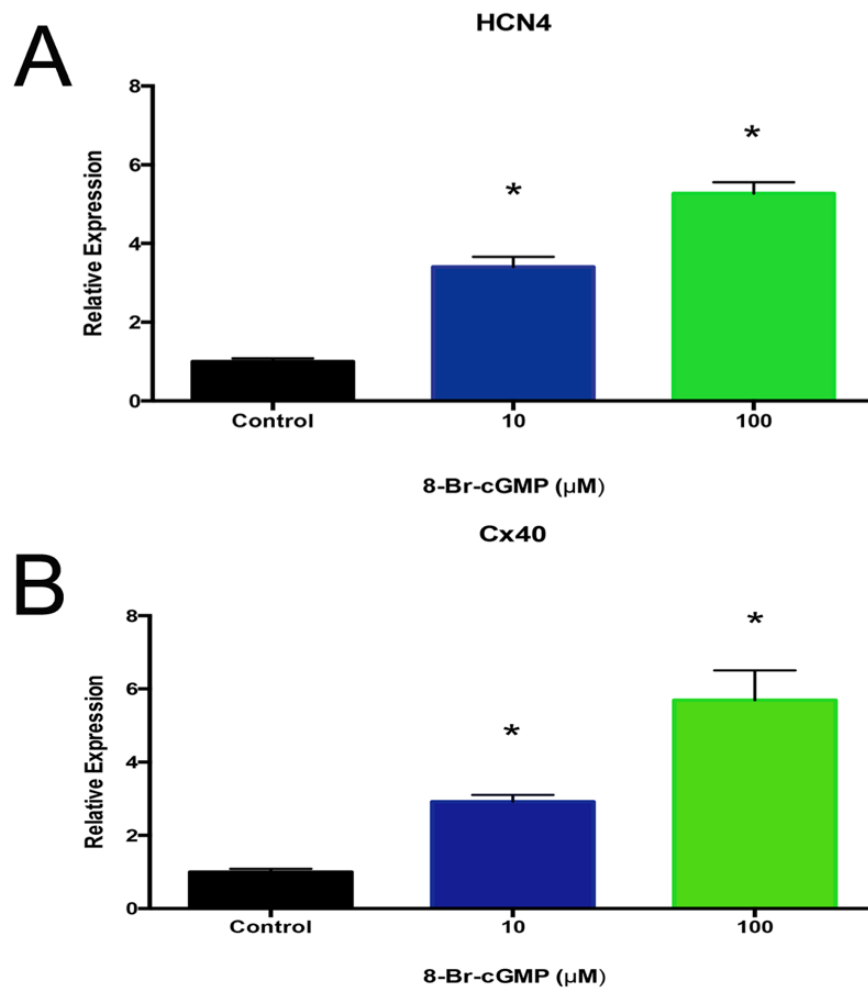
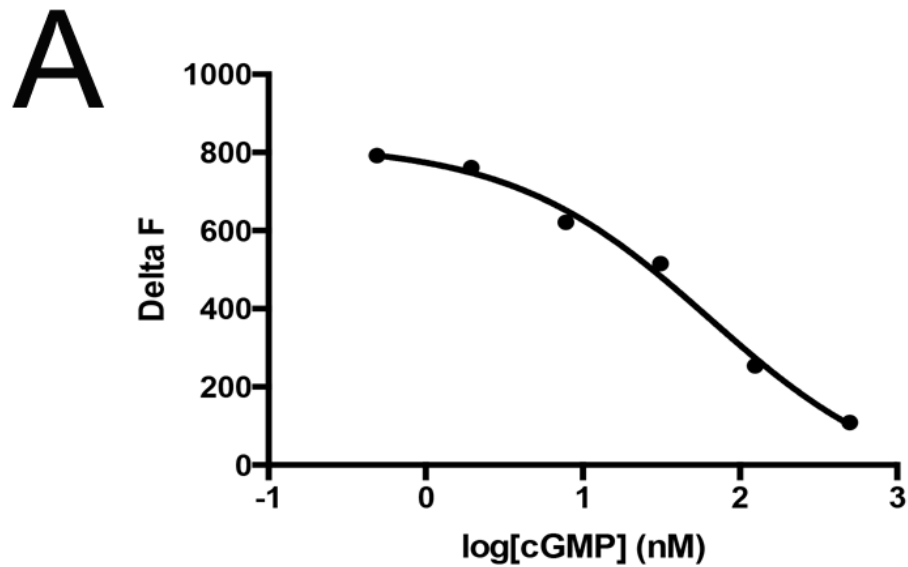


Figure 3.24. Effects of exogenous addition of 8-Br-cGMP on gene expression of Cx40 and HCN4 in E11.5 ventricular cells. Addition of the exogenous compound 8-Br-cGMP at concentrations of 10 μM and 100 μM significantly increased gene expression of both HCN4 and Cx40 in a dose-dependent manner. N=9 independent experiments. GAPDH was used as the housekeeping gene. Each bar represents mean \pm SEM. * $p < 0.05$ vs. control, One-way ANOVA with Tukey post hoc test.



B

Final [8-Br-cGMP] (nM)	Delta F
500	109
125	254
31.25	515
7.81	621
1.95	761
0.49	792

Figure 3.25. Generation of standard curve using 8-Br-cGMP. A) The standard curve for 8-Br-cGMP was generated by plotting Delta F values obtained from known concentrations of 8-Br-cGMP. These concentrations covered an average range between 0-100 μ M (concentration of added 8-Br-cGMP per well). The experimentally determined Delta F values were obtained utilizing known concentrations of 8-Br-cGMP and the competitive immunoassay kit. **B)** Table displaying the concentrations of 8-Br-cGMP tested, which were equivalent to the standard concentrations provided in the kit, along with their experimentally determined Delta F values. Single point in standard curve represents the mean of three independent experiments.

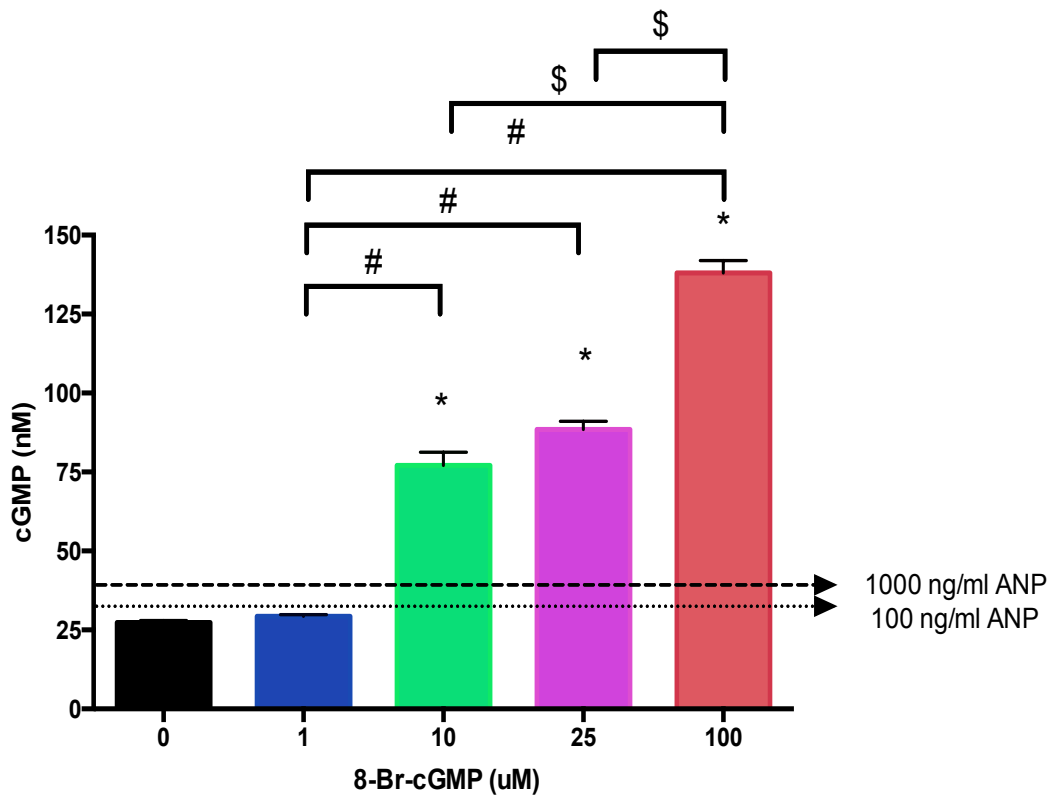


Figure 3.26. Intracellular permeability of 8-Br-cGMP in E11.5 ventricular cells. To determine the intracellular permeability of 8-Br-cGMP in E11.5 ventricular cells, exogenous 8-Br-cGMP (1, 10, 25, or 100 μM) was added to cell culture and intracellular cGMP (nM) was measured. Compared to control, addition of 10 μM and 25 μM 8-Br-cGMP doses resulted in a 3-fold increase in intracellular cGMP; addition of 100 μM 8-Br-cGMP resulted in a 5-fold increase in intracellular cGMP. Dashed arrows are used for a comparison of intracellular cGMP levels between exogenous addition of 8-Br-cGMP vs. ANP. To compare, addition of 100 or 1000 ng/ml ANP (over 48 hours) in separate experiments resulted in cGMP levels of 34.5 ± 0.7 nM and 37.9 ± 0.1 nM, respectively. $N=3$ independent experiments, performed in duplicate wells. Each bar represents mean \pm SEM. * $p < 0.05$ vs. control, # $p < 0.05$ vs. 1 μM 8-Br-cGMP, \$ $p < 0.05$ vs. 100 μM 8-Br-cGMP, One-way ANOVA with Tukey post hoc test.

3.3.10 Cardiomyogenic Differentiation is Enhanced in Embryonic Ventricular Cells Treated with 8-Br-cGMP

To examine the effects on ventricular cell differentiation, 8-Br-cGMP was added to E11.5 ventricular cells generated by crossing two knock-in mouse strains (Nkx2.5-Cre and Rosa-LacZ) as described in our previous studies (Zhang and Pasumarthi, 2007; Feridooni et al., 2017). The crossing of Nkx2.5-Cre homozygotes with Rosa-LacZ homozygotes resulted in the generation of double knock-in Nkx2.5 Cre-Rosa LacZ embryos in which the Cre-protein excised a floxed stop cassette (transcriptional terminator) with an activated LacZ gene in cells of Nkx2.5+ cell lineage (**Figure 3.27**). The Nkx2.5 lineage was tracked through expression of β -gal protein identified in immunofluorescence staining. Using this approach, embryonic CPCs can be identified as cells positive for β -Gal but not MF20 (β -Gal⁺/MF20⁻) since Nkx2.5⁺/MF20⁻ cells were shown to differentiate into CMs (McMullen et al., 2009; Zhang and Pasumarthi, 2007). Additionally, cells positive for both β -Gal and MF20 represent the CM population (β -Gal⁺/MF20⁺). With the addition of 8-Br-cGMP to E11.5 cell culture, the percentage of CPCs (expressed as a percent of the total number of cells viewed per field) significantly decreased with 10 μ M and 100 μ M doses compared to that of control cultures (28 ± 0.5 % and 14 ± 0.7 % respectively vs. 38 ± 2.2 %, $p < 0.005$, **Figure 3.28**). In contrast, addition of 8-Br-cGMP at 10 μ M and 100 μ M doses resulted in a significant increase in the percentage of CMs, vs. control (28 ± 0.6 % and 38 ± 0.7 % respectively, vs. 20 ± 0.9 %, $p < 0.005$, **Figure 3.29**).

It is possible that cGMP may play a role in promoting differentiation of CPCs into VCS cells, as evidenced by the decrease in percentage of CPCs upon addition of 8-Br-

cGMP coupled to the results from Section 3.3.9 where gene expression of the VCS markers increased significantly upon addition of the same compound. The second messenger molecule cGMP may also play a role in promoting differentiation of CMs, as evidenced by the increase in the percentage of CMs upon addition of 8-Br-cGMP.

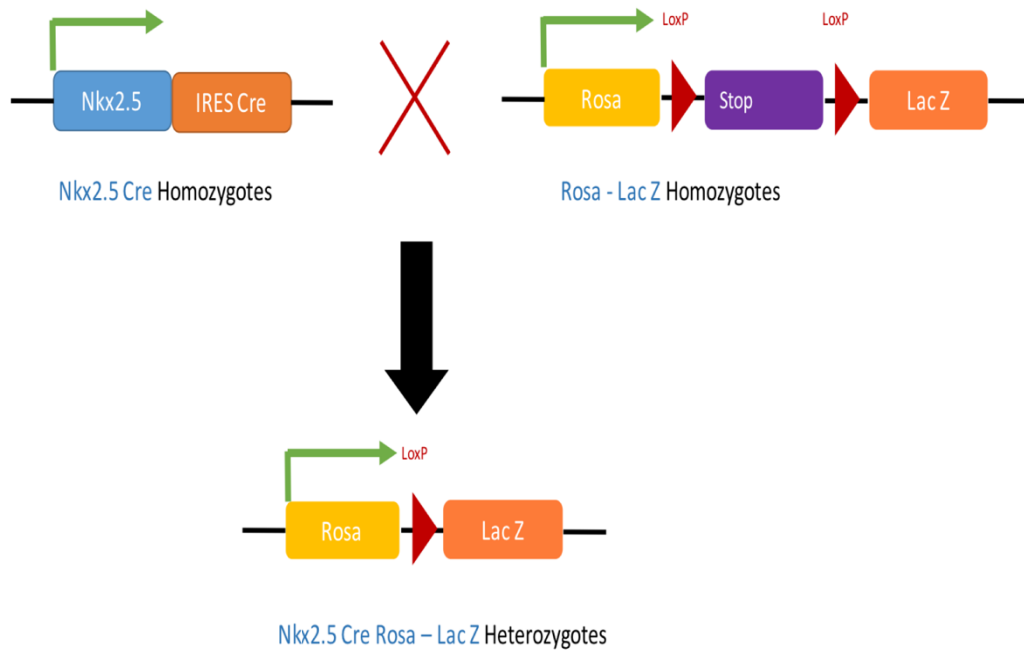


Figure 3.27. Conditional activation of the *LacZ* reporter gene allowing for cells of the Nkx2.5 cell lineage to be genetically labelled. (A) Schematic diagram showing the cross between Nkx2.5-Cre (NC) mice with an internal ribosomal entry sequence (IRES) and Cre-recombinase (Cre) coding sequence inserted into the 3' untranslated region of the Nkx2.5 gene, and Rosa-LacZ (RL) mice with a transcriptional terminator stop cassette proximal to the β -galactosidase (*LacZ*) gene flanked LoxP sites. The genetic crossing of NC and RL mice results in the generation of double knock-in NCRL embryos with a Cre-protein excised a floxed stop cassette with an activated *LacZ* gene in cells of Nkx2.5⁺ cell lineage.

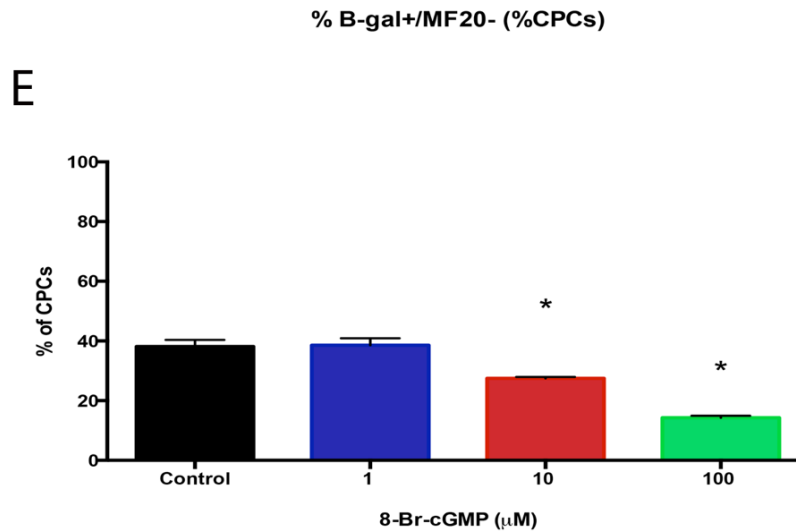
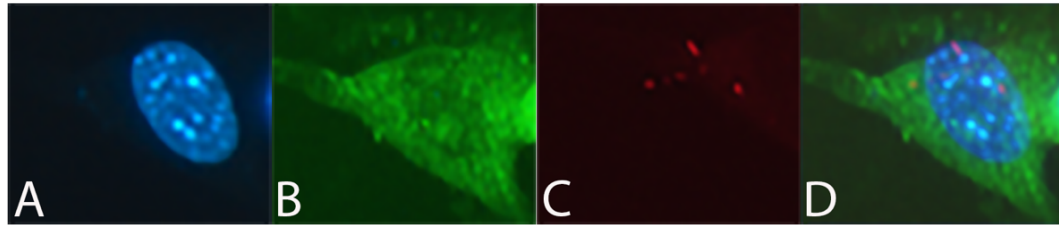


Figure 3.28. Cellular differentiation of cardiac progenitor cells (CPCs) is influenced by addition of exogenous cGMP (8-Br-cGMP) in E11.5 Nkx2.5 Cre-Rosa LacZ (NCRL) mouse ventricular cells, as denoted by changes in protein expression obtained via immunofluorescence. Representation of a single CPC from E11.5 NCRL ventricular cell culture with staining for **A)** Hoechst (nuclei) **B)** β -gal protein **C)** sarcomeric myosin (MF20) and **D)** an image overlay. **E)** The percentage of CPCs (expressed as a percent of the total number of cells counted per field), identified by NKX+/MF20- staining, decreased following addition of 8-Br-cGMP to cell culture (10, 100 μM). CPCs do not express β -gal. N=6 independent experiments. Each bar represents mean \pm SEM. * $p < 0.05$ vs Control, One-way ANOVA with Tukey post hoc test.

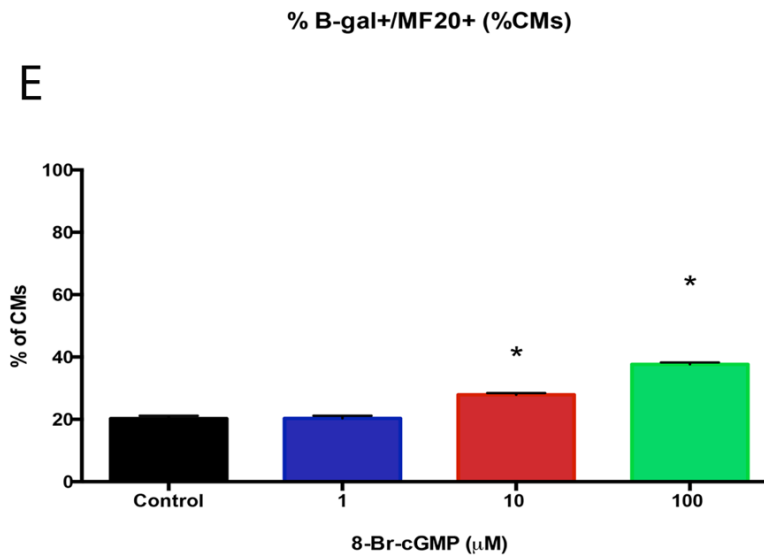
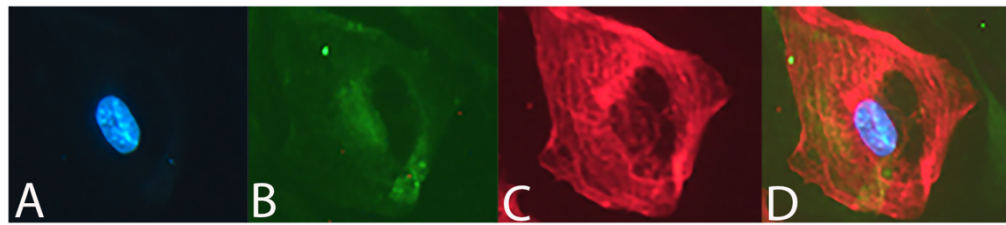


Figure 3.29. Cellular differentiation of cardiomyocytes is influenced by addition of exogenous cGMP (8-Br-cGMP) in E11.5 *Nkx2.5 Cre-Rosa LacZ* (NCRL) mouse ventricular cells, as denoted by changes in protein expression obtained via immunofluorescence. Representation of a single CM from E11.5 NCRL ventricular cell culture with staining for **A)** Hoechst (nuclei) **B)** β -gal protein **C)** sarcomeric myosin (MF20) and **D)** an image overlay. **E)** The percentage of CMs (expressed as a percent of the total number of cells counted per field), identified by NKX+/MF20+ staining, increased following addition of 8-Br-cGMP to cell culture (10, 100 μ M). CMs express β -gal. N=6 independent experiments. Each bar represents mean \pm SEM. * p <0.05 vs. control, One-way ANOVA with Tukey post hoc test.

3.3.11 Effects of Rp-8-pCPT-cGMPS, a Protein Kinase G Inhibitor, on Gene Expression of HCN4 and Cx40 in E11.5 Ventricular Cells in The Presence and Absence of ANP

To determine if ANP/NPR-A signaling-mediated changes in VCS marker gene expression involved the stimulation of protein kinase G (PKG), we tested the effects of a PKG inhibitor in E11.5 ventricular cells. A 100 μ M dose of Rp-8-pCPT-cGMPS was added to E11.5 ventricular cell culture every 12 hours for a period of 24 hours in the presence or absence of ANP (1000 ng/ml) (**Figure 3.30**). HCN4 expression was significantly reduced upon addition of this compound alone by \sim 4.2-fold (0.24 ± 0.02 , $p < 0.00005$) vs. control (**Figure 3.30 A**). This reduction in HCN4 gene expression by Rp-8-pCPT-cGMPS alone was significantly less than the combination of ANP plus Rp-8-pCPT-cGMPS by \sim 1.4-fold (0.73 ± 0.09 , $p < 0.00005$). To test whether there could be synergistic effects on downregulated HCN4 expression by the combined blockade of NPR-A receptor with blockade of PKG, the combination of A71915 + Rp-8-pCPT-cGMPS was tested. This combination resulted in a significant reduction in the gene expression of HCN4 by \sim 10-fold (0.10 ± 0.03 , $p < 0.00005$) vs. control.

The addition of Rp-8-pCPT-cGMPS significantly reduced Cx40 gene expression by \sim 3.8-fold (0.26 ± 0.005) vs. control and was significantly less than the combination of ANP plus Rp-8-pCPT-cGMPS which was reduced by \sim 1.3-fold (0.79 ± 0.03) ($p < 0.00005$, **Figure 3.30 B**). The combination of A71915 + Rp-8-pCPT-cGMPS resulted in a significant reduction in gene expression of Cx40 by \sim 11-fold (0.09 ± 0.02 , $p < 0.00005$). Overall, this seems to imply that 1) ANP may be rescuing the decline in gene expression caused by Rp-8-pCPT-cGMPS, and 2) cGMP signalling may be linked to ANP/NPR-A activation, and

PKG may be a downstream target of this signalling, resulting in induction of Cx40 and HCN4, in order to promote formation of the Purkinje fiber network of the developing embryonic mouse heart.

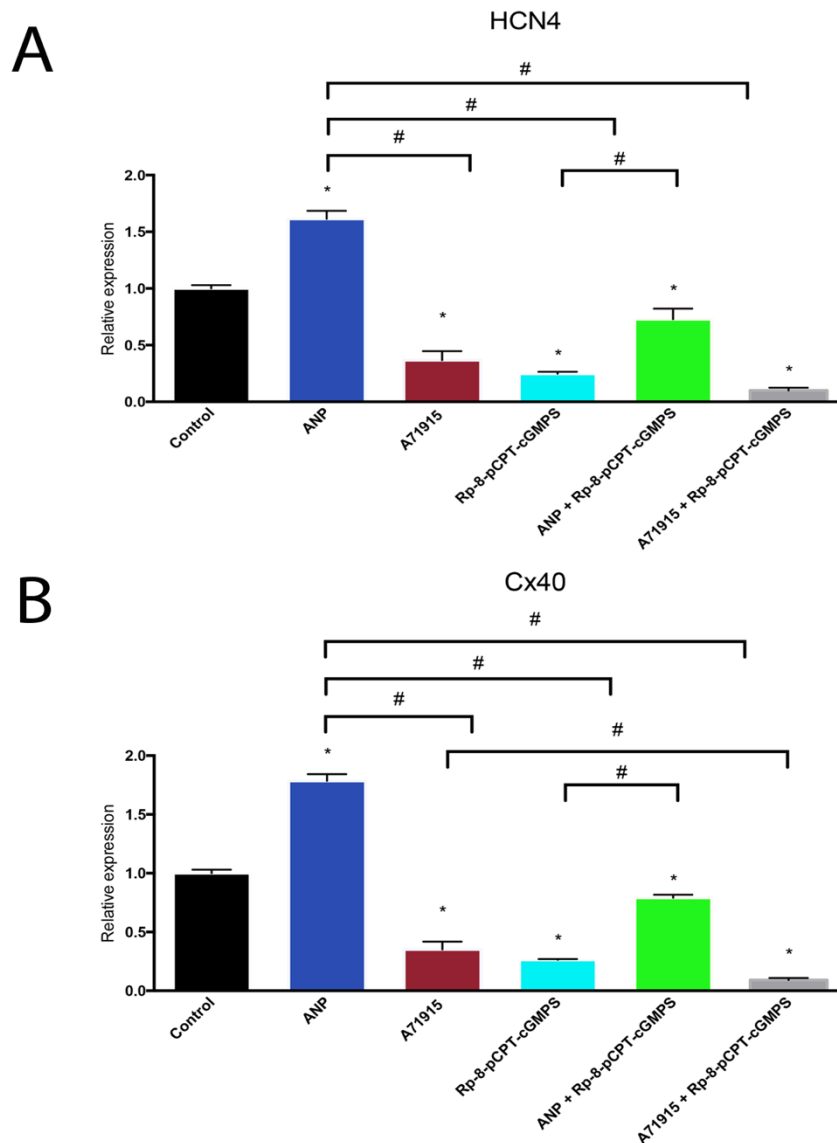


Figure 3.30. Effects of protein kinase G inhibitor – Rp-8-pCPT-cGMPS on gene expression of HCN4 and Cx40 in the presence or absence of ANP, in E11.5 ventricular cells. E11.5 ventricular cells were incubated with Rp-8-pCPT-cGMPS (100 μ M) in the presence and absence of ANP, for 24 hours, with dosing every 12 hours. The addition of Rp-8-pCPT-cGMPS alone significantly reduced HCN4 and Cx40 gene expression. In combination with ANP, it appears that ANP may be rescuing the decline in gene expression provided by Rp-8-pCPT-cGMPS. N=8 independent experiments. Each bar represents mean \pm SEM. * p <0.05 vs. control, # p <0.05 between groups as indicated, One-way ANOVA with Tukey post hoc test.

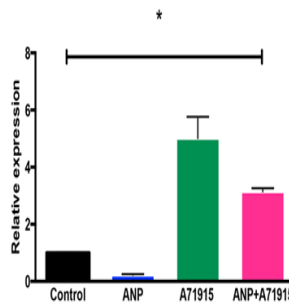
3.3.12 Effects of ANP on MicroRNA Regulation of HCN4 and Cx40 in E11.5 and E14.5 Mouse Ventricular Cells

Gene expression is regulated by transcriptional, post-transcriptional, translational and post-translational mechanisms. MicroRNAs (miRNA) are short non-coding RNAs which can bind to 3' UTR sequences in one or more target mRNAs and subsequently decrease protein levels by destabilizing mRNAs and/or suppressing translation (Cannell et al., 2008). ANP has been shown to regulate the expression of a number miRNAs in human vascular smooth muscle cells via the cGMP/PKG pathway (Kotlo et al., 2011). Recent studies have identified regulatory roles for miRNAs in controlling the levels of HCN4 (miRNA 1a and miRNA 133, Fu et al., 2011; D'Souza et al., 2014; Li et al., 2015) and Cx40 (miRNA 27b, Takahashi et al., 2016) in cardiac tissue. However, it is not known whether ANP plays any role in the regulation of HCN4 and Cx40 gene expression via miRNA regulation in embryonic ventricular cells. Thus, expression analysis of the miRNA 1a, 133 and 27b was performed by qPCR upon administration of ANP (1000 ng/ml), or A71915 (1 μ M), or combination of both, to E11.5 cell cultures (**Figure 3.31**). The addition of ANP significantly reduced the expression of 1a, 133, and 27b vs. control by ~5-fold, ~3.3-fold, and ~1.6-fold, respectively (0.2 ± 0.02 , 0.3 ± 0.03 , 0.6 ± 0.03 , respectively, $p < 0.05$). In contrast, the addition of A71915 significantly increased expression of all three miRNAs tested (5.0-fold \pm 0.7, 4.3-fold \pm 0.7, 3.1-fold \pm 0.3, respectively, $p < 0.05$). The combination of ANP and A71915 treatment significantly increased miRNA expression of 1a, 133 and 27b vs. control (3.2-fold \pm 0.1, 3.8-fold \pm 0.4 and 2.2-fold \pm 0.2 respectively, $p < 0.05$); this was significantly greater than vs. ANP alone, but not different compared to A71915 alone (**Figure 3.31**). Similar

regulation of all three miRNAs was observed in E14.5 ventricular cultures treated with or without ANP and/or A71915 (**Figure 3.32**). Collectively, these results suggest that increases in HCN4 and Cx40 mRNAs levels in ANP treated embryonic ventricular cells could be mediated in part via significant decreases in miRNA species that are known to destabilize the respective target mRNAs (Fu et al., 2011; D'Souza et al., 2014; Takahashi et al., 2016).

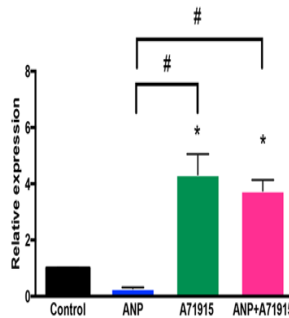
E11.5

A



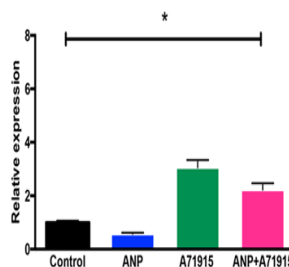
miRNA 1a

B



miRNA 133

C



miRNA 27b

Figure 3.31. Effects of exogenous ANP (1000 ng/ml) and/or A71915 (1 μ M) on microRNA levels in E11.5 mouse ventricular cells. Analysis of the miRNA expression of **A)** miRNA 1a and **B)** miRNA 133, which have been shown to regulate HCN4 mRNA expression, and **C)** miRNA 27b, which has been shown to regulate Cx40 mRNA expression, was performed by RT-qPCR upon administration of ANP and/or A71915 to E11.5 cell culture. MiRNA expression was normalized using U6 levels via $\Delta\Delta C_T$ method. For all three miRNAs analyzed, addition of ANP significantly reduced expression of miRNAs, whereas addition of A71915 increased expression of miRNAs. N=7 independent experiments. Each bar represents mean \pm SEM. * $p < 0.05$ vs control, # $p < 0.05$ between groups as indicated, One-way ANOVA with Tukey post hoc test.

E14.5

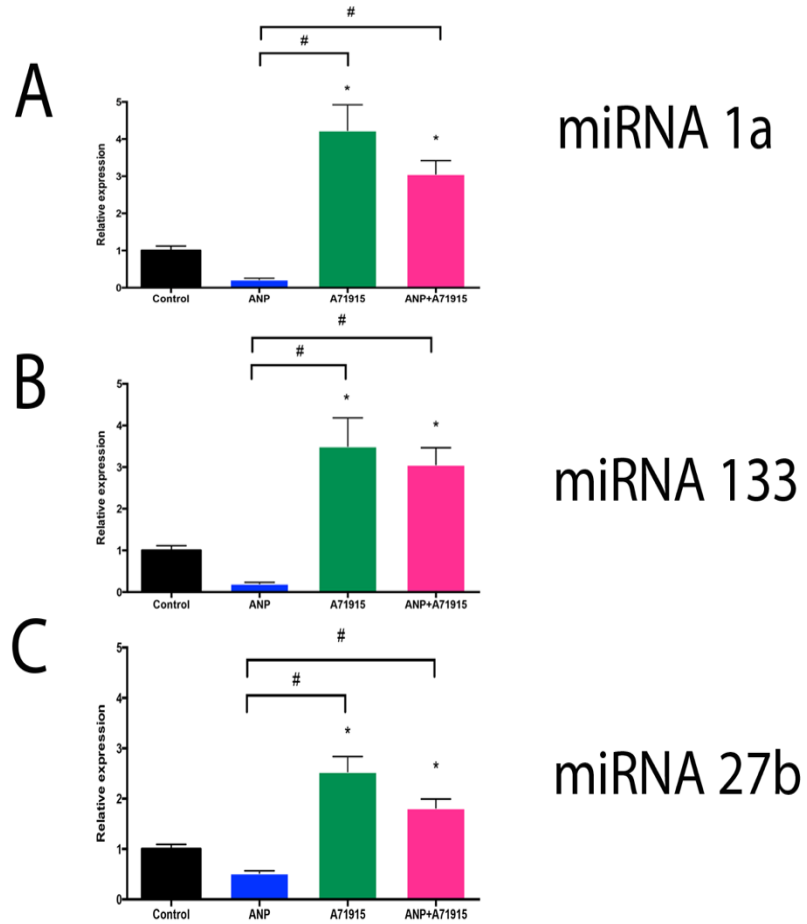


Figure 3.32. Effects of exogenous ANP (1000 ng/ml) and/or A71915 (1 μ M) on microRNA levels in E14.5 mouse ventricular cells. Analysis of the miRNA expression of **A)** miRNA 1a and **B)** miRNA 133, which have been shown to regulate HCN4 mRNA expression, and **C)** miRNA 27b, which has been shown to regulate Cx40 mRNA expression, was performed by RT-qPCR upon administration of ANP and/or A71915 to E14.5 cell culture. MiRNA expression was normalized using U6 levels via $\Delta\Delta C_T$ method. For all three miRNAs analyzed, addition of ANP significantly reduced expression of miRNAs, whereas addition of A71915 increased expression of miRNAs. N=7 independent experiments. Each bar represents mean \pm SEM. * $p < 0.05$, # $p < 0.05$ between groups as indicated, One-way ANOVA with Tukey post hoc test.

3.3.13 Effects of the NPRA-KO Genotype on MicroRNA Regulation of HCN4 and Cx40 in E14.5 and Neonatal Mouse Heart Tissue

We next wanted to determine whether ablation of the NPR-A receptor could have an effect on miRNA expression of 1a, 133, and 27b in E14.5 heart tissue (**Figure 3.33 A-C**). Compared to WT ventricles, homozygous NPRA-KO ventricles demonstrated upregulation of miRNAs 1a and 133 (4.8-fold \pm 0.7 and 11.2-fold \pm 3.8, $p < 0.05$) vs. control. For both miRNAs 1a and 133, heterozygotes expressed miRNAs at a similar level vs. control ($p = \text{NS}$). For 27b miRNA expression, there were no statistical differences between any of the three genotypes ($p = \text{NS}$). Expression of miRNA 208a was also analyzed, as it has been found to be required for Cx40 expression by another group (Callis et al., 2009). Mice with the miRNA 208a $-/-$ phenotype were shown to demonstrate insufficient Cx40 expression leading to the development of cardiac conduction abnormalities (Callis et al., 2009). At E14.5, we found that in NPRA-KO mice, homozygotes had significant downregulation of miRNA 208a by \sim 4-fold (0.25 ± 0.05 , $p < 0.0005$, **Figure 3.33 D**).

The effect of genetic ablation of NPR-A on miRNA expression of 1a, 133, and 27b was also examined in ND1 heart tissue. In ND1s, compared to WT, miRNA 1a expression was significantly upregulated in heterozygotes and homozygotes vs. WT mice (4.6-fold \pm 0.9 and 12.6-fold \pm 0.8, $p < 0.05$); miRNA 1a expression was significantly upregulated in homozygotes vs. heterozygotes ($p < 0.05$, **Figure 3.34 A**). MiRNA 133 expression was significantly upregulated in homozygotes vs. WT mice (12.6-fold \pm 0.8, $p < 0.0005$); miRNA 133 expression was significantly upregulated in homozygotes vs. heterozygotes (12.6-fold \pm 0.8 vs. 2.8-fold \pm 0.6, $p < 0.005$, **Figure 3.34 B**). Expression of miRNA 133 was

similar between heterozygotes and WT mice ($p=NS$). The expression of miRNA 27b was similar across all three genotypes ($p=NS$, **Figure 3.34 C**).

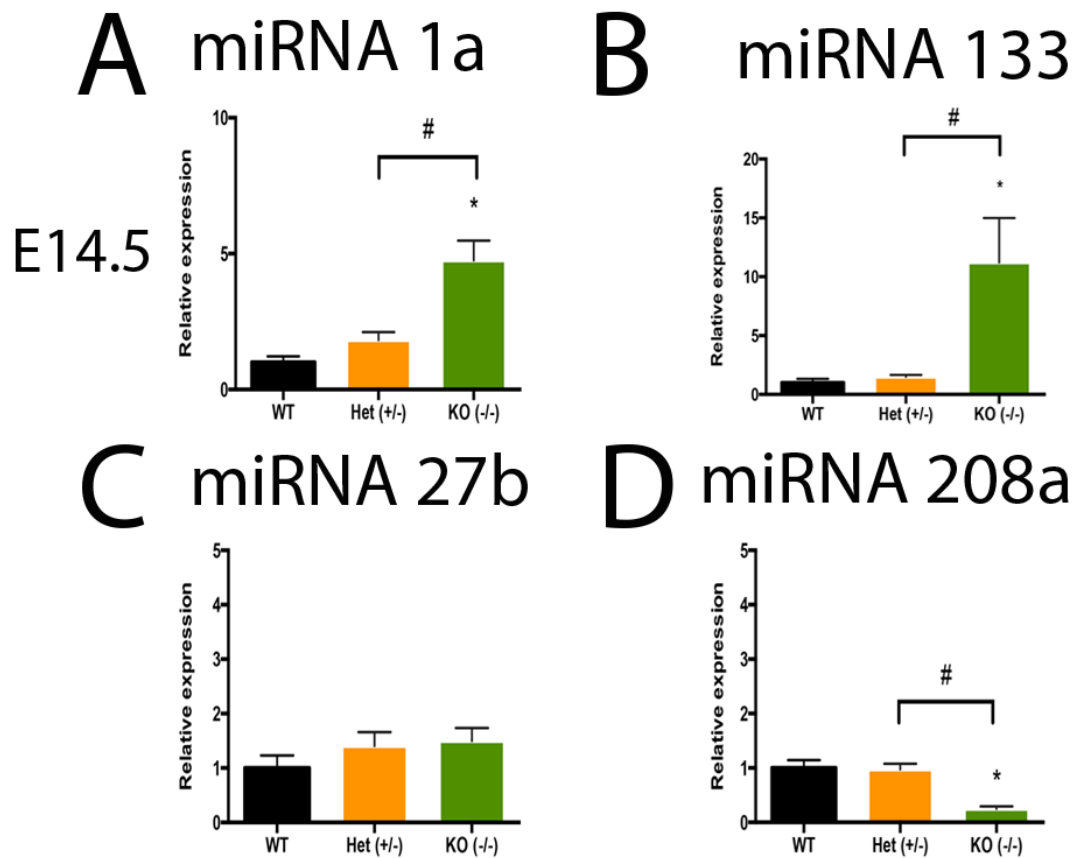


Figure 3.33. Effects of the NPRA-KO genotype on microRNA levels in E14.5 ventricles of NPRA-KO mice. At E14.5, analysis of miRNAs reveals that in NPRA-KO mice, compared to WT mice, homozygous NPRA-KO mice demonstrated upregulation of miRNAs **A)** 1a and **B)** 133. **C)** There were no significant differences in miRNA 27b expression between genotypes. **D)** Homozygous NPRA-KO mice demonstrated significant downregulation of miRNA 208a vs. WT. MiRNA expression was normalized using U6 levels via $\Delta\Delta C_T$ method. N=4 independent experiments. Each bar represents mean \pm SEM. * $p < 0.05$ vs. control, # $p < 0.05$ between other groups as indicated, One-way ANOVA with Tukey post hoc test.

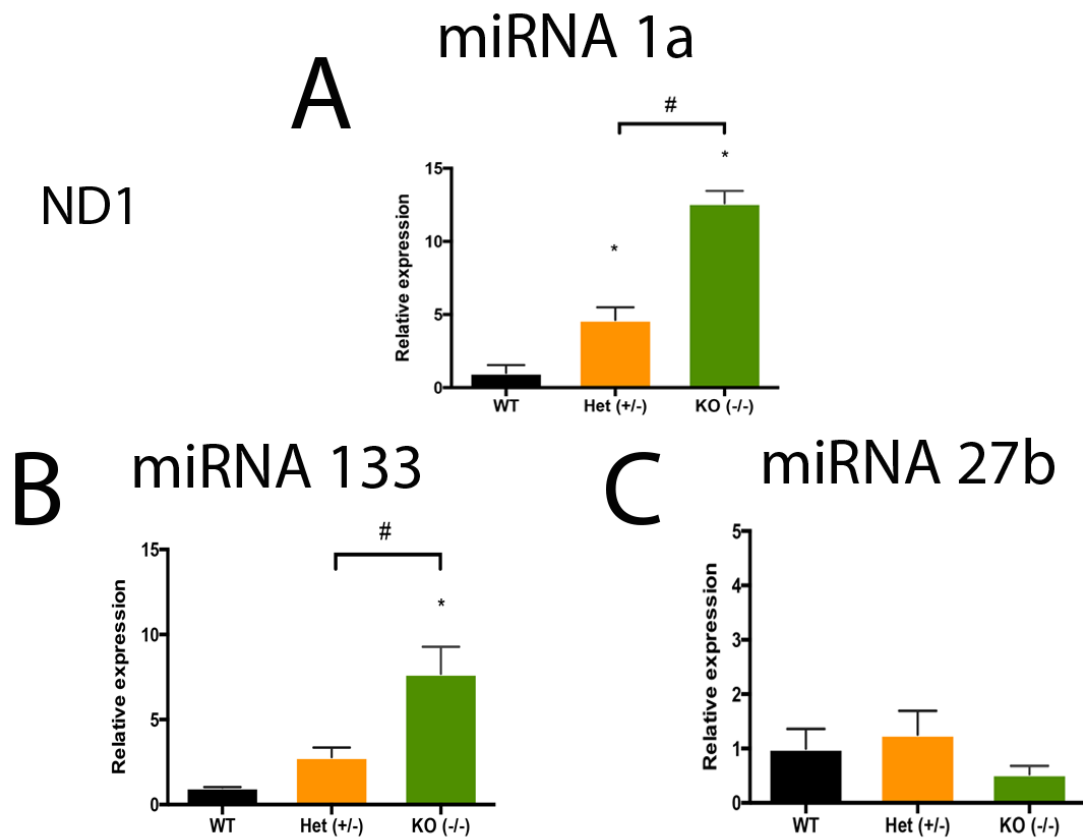


Figure 3.34. Effects of the NPRA-KO genotype on microRNA levels in neonate (ND1) hearts of NPRA-KO mice. A) Heterozygous and homozygous NPRA-KO mice demonstrated significant upregulation of miRNA 1a vs. WT. **B)** Homozygous NPRA-KO mice demonstrated significant upregulation of miRNA 133 vs. WT. **C)** There were no significant differences in miRNA 27b expression between genotypes. MiRNA expression was normalized using U6 levels via $\Delta\Delta C_T$ method. N=4 independent experiments. Each bar represents mean \pm SEM. * $p < 0.05$ vs. control, # $p < 0.05$ between groups as indicated, One-way ANOVA with Tukey post hoc test.

CHAPTER 4: CHARACTERIZATION OF PHARMACOLOGICAL PROPERTIES OF THE NPR-A ANTAGONIST A71915 IN EMBRYONIC MOUSE VENTRICULAR CELLS

4.1 Background and Hypothesis

The NPR-A antagonist A71915 (see **Figure 1.8**), was initially discovered in a study comparing several ANP receptor antagonists with one another in cultured bovine transformed aortic endothelial cells (BTAEC) which contain 90% NPR-C and 10% NPR-A/NPR-B receptors (Von Geldern et al., 1990). This study showed for the first time that A71915 was a potent inhibitor of ANP-induced cGMP production in BTAEC cells. Subsequently, this inhibitor was shown to block ANP induced cellular effects in human neuroblastoma NB-OK-1 cells expressing NPR-A but not NPR-C receptors and thus it was designated as an NPR-A specific inhibitor (Delporte et al., 1992). Their study determined the capacity of A71915 to limit ANP binding, and to suppress ANP-stimulated cGMP elevation (Delporte et al., 1992). A71915 was shown to displace [¹²⁵I] ANP with an inhibition constant (K_i) value of 0.65 nM, the lowest K_i of the seven compounds tested. Thus, A71915 was deemed the most potent antagonist of the NPR-A receptor (Delporte et al., 1992). ANP dose-response curves measuring cGMP production in NB-OK-1 cells showed that A71915 shifted the dose-response curve to the right for all doses tested (Delporte et al., 1992). However, there is scant information in the literature about the ability of A71915 to exert any pharmacological effects via NPR-C.

Previous experiments conducted with A71915 in E11.5 ventricular cell cultures (see Chapter 3) have uncovered some unique features for this inhibitor such as: A) the

inhibitor alone at a concentration of 1 μ M decreased gene expression below the baseline (see Section 3.3.2) and B) when combined with 1000ng/ml of ANP, ANP did not rescue the inhibitory effects of A71915. Based on these results, it is not clear whether A71915 acts as a competitive or non-competitive inhibitor in E11.5 ventricular cells. It is also not clear if A71915 could act on NPR-C receptors since we have shown that E11.5 ventricular cells express both NPR-A and NPR-C receptors (Hotchkiss et al., 2015). We were particularly curious about the antagonistic nature of A71915 in embryonic ventricular cells, since this compound was tested in numerous experiments in this thesis. Hence, we pursued further characterization of pharmacological properties of A71915 using E11.5 ventricular cells. **We hypothesized that binding of A71915 to NPR-A receptors prevents endogenous ANP from binding to its cognate receptors, thus behaving as a competitive antagonist in embryonic mouse ventricular cells.**

4.2 Specific Aims

1. To generate dose-response curves for ANP, using a fixed concentration of ANP (1000 ng/ml) and varying concentrations of A71915. This was done by measuring endogenous cGMP in E11.5 ventricular mouse cells post-treatment.
2. To generate dose-response curves for A71915, using a fixed concentration of A71915 (1 μ M) and varying concentrations of ANP. This was done by measuring endogenous cGMP in E11.5 ventricular mouse cells post-treatment.
3. To determine the type of antagonistic behaviour of A71915 in E11.5 ventricular mouse cells.

4.3 Results

4.3.1 Generation of Dose-Response Plots for ANP in E11.5 Ventricular Cells

In Section 3.3.3, we demonstrated that the binding of ANP to NPR-A receptors led to a significant increase in cGMP signalling, and that this cGMP signalling was correlated with significant induction in the gene expression of HCN4 and Cx40. We wanted to generate dose-response plots for ANP, by testing the effects of adding 1, 10, 100 or 1000 ng/ml ANP to E11.5 ventricular cell cultures and acutely measuring the changes in intracellular cGMP production. This would allow us to see the effects of exogenous ANP at lower concentrations, on cGMP production. The competitive immunoassay for measurement of cGMP was performed, as previously described in Section 3.3.3. The baseline level of cGMP in untreated cultures was measured as 29.7 ± 0.1 nM per 100,000 cells. Compared to control, only doses of 100 ng/ml and 1000 ng/ml ANP resulted in a significant increase in intracellular cGMP production (100 ng/ml ANP: 34.5 ± 0.7 nM; 1000 ng/ml ANP: 37.9 ± 0.09 nM, $p < 0.05$) (**Figure 4.1**).

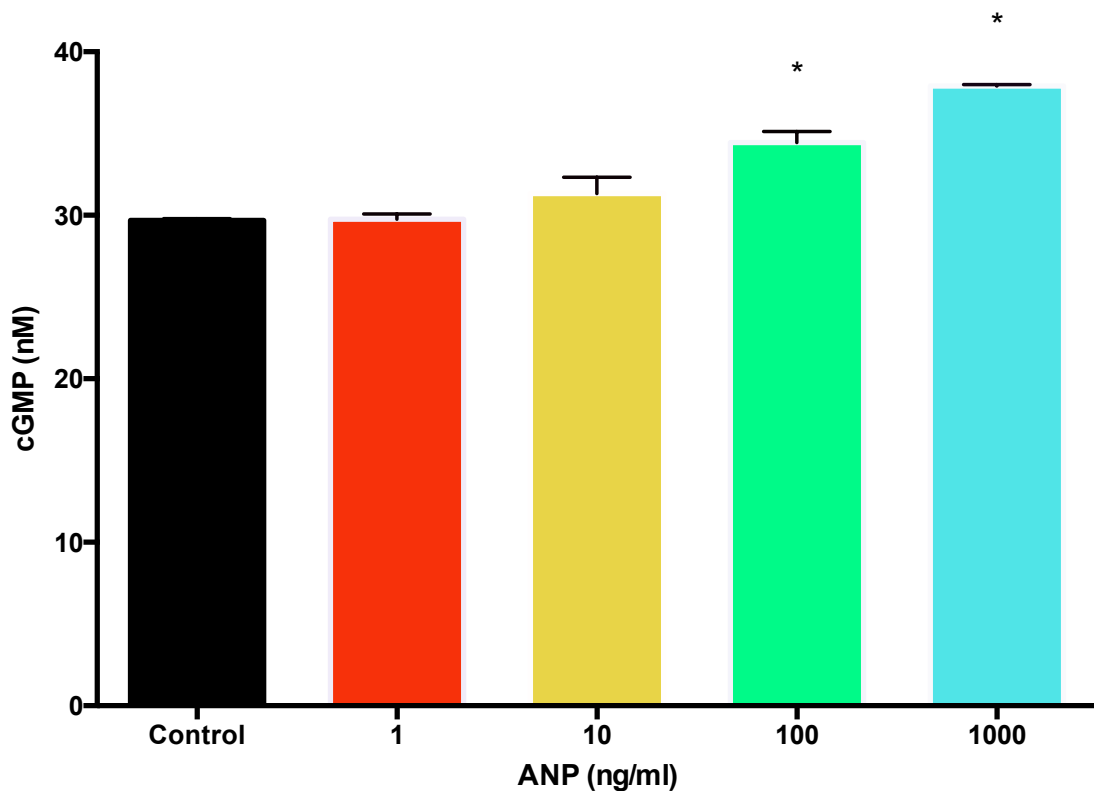


Figure 4.1. Dose-response for ANP on cGMP production in E11.5 ventricular cells. The effects of exogenous ANP on intracellular cGMP production was determined by stimulating isolated E11.5 cells with ANP, then measuring cGMP using a competitive immunoassay. This was done at varying concentrations (1, 10, 100, and 1000 ng/ml) to establish a dose-response for ANP. The baseline level of cGMP in control cultures was measured to be 29.7 ± 0.1 nM per 100,000 cells. Addition of exogenous ANP resulted in a significant increase in cGMP at concentrations of 100 and 1000 ng/ml. N=6 independent experiments, performed in duplicate wells. Each bar represents mean \pm SEM. * $p < 0.05$, One-way ANOVA with Tukey post hoc test.

4.3.2 Generation of Dose-Response Plots for A71915 in E11.5 Ventricular Cells in the Absence of Exogenous ANP

We previously demonstrated in Section 3.3.3 that the addition of A71915 (1 μM) alone to cell culture resulted in a significant decrease in cGMP production vs. control, and that a decrease in cGMP (8-Br-cGMP) was correlated with a decrease in gene expression of Cx40 and HCN4 (Section 3.3.9). Next, we wanted to generate dose-response plots for A71915, determining the effect of this antagonist at varying concentrations (0.1, 0.25, 0.5, 1, 2, 5, or 10 μM) on intracellular cGMP production in E11.5 ventricular cells. The baseline level of cGMP measured was 29.3 ± 0.1 nM, per 100,000 cells. Compared to control, there was a dose-dependent decline in intracellular cGMP production using concentrations from 0.25 to 10 μM A71915, with a 0.25 μM dose of A71915 producing 25.3 ± 0.6 nM cGMP, and with a 10 μM dose of A71915 producing 9.9 ± 0.09 nM cGMP ($p < 0.05$, **Figure 4.2**). These results suggest that A71915 acts as an inverse agonist in the absence of exogenous ANP in E11.5 ventricular cells.

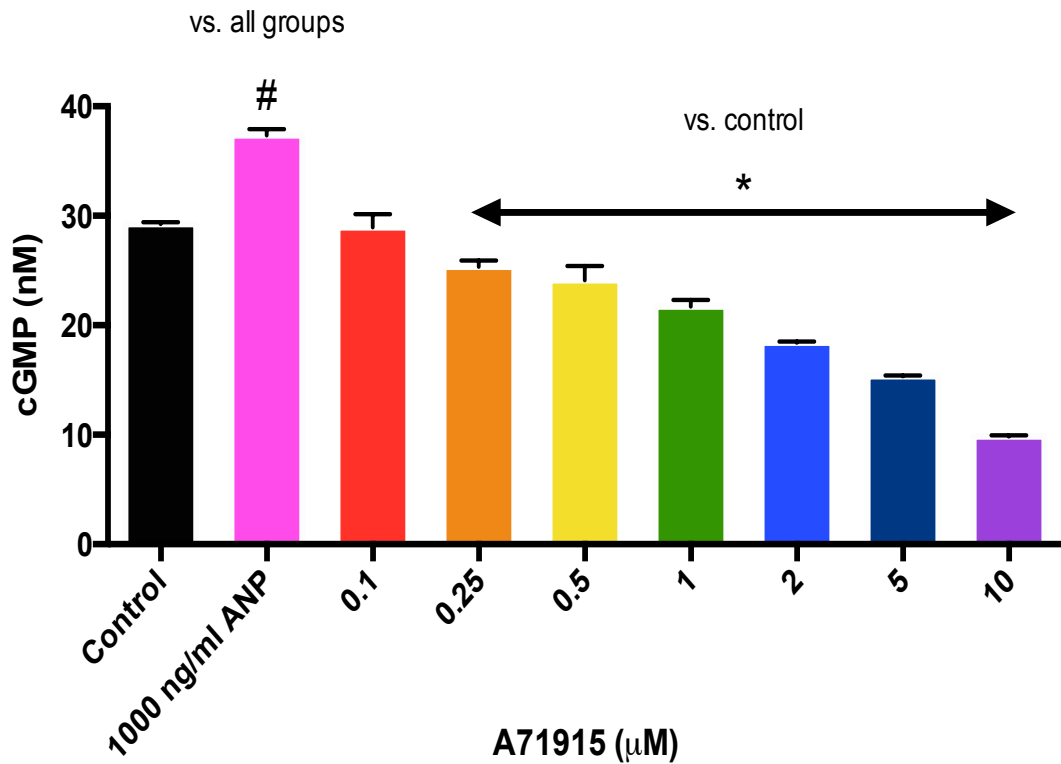


Figure 4.2. Dose-response for A71915 on cGMP production in E11.5 ventricular cells. The effects of exogenous A71915 on intracellular cGMP production was determined by incubating isolated E11.5 cells with A71915, then measuring cGMP using a competitive immunoassay. This was done at varying concentrations (0.1 to 10 μM) to establish a dose-response for A71915. The baseline level of cGMP was measured to be 29.3 ± 0.1 nM per 100,000 cells. Addition of A71915 resulted in a significant decrease in cGMP at concentrations between 0.25 and 10 μM . N=6 independent experiments, performed in duplicate wells. Each bar represents mean \pm SEM. * $p < 0.05$ vs. Control; # $p < 0.05$ vs. all groups, One-way ANOVA with Tukey post hoc test.

4.3.3 Effects of A71915 on ANP-Induced cGMP Production in E11.5 Ventricular Cells

We wanted to determine the potential effects of A71915 on the ability of ANP to induce cGMP production in E11.5 ventricular cells at varying inhibitor concentrations (0.5, 1, 2 and 5 μ M). In **Figure 4.3**, values that were significantly different from control are noted ($p < 0.05$). Cells treated with A71915 alone at all concentrations, revealed significant reductions in cGMP levels compared to control values and these data are consistent with the data shown in **Figure 4.2**. Among each treatment group consisting of a fixed concentration of A71915 (0.5, 1, 2 μ M) combined with variable concentrations of ANP (1-1000 ng/ml), there appears to be an upward trend of gradually increasing cGMP production with increasing concentrations of ANP. At 5 μ M A71915, it appears that even with the addition of increasing concentrations of ANP, cGMP levels remained similar to one another ($p = \text{NS}$). These results suggest that higher concentrations of ANP (1000 ng/ml) can partially overcome inhibitory effects of A71915 to a certain extent under the experimental conditions described here.

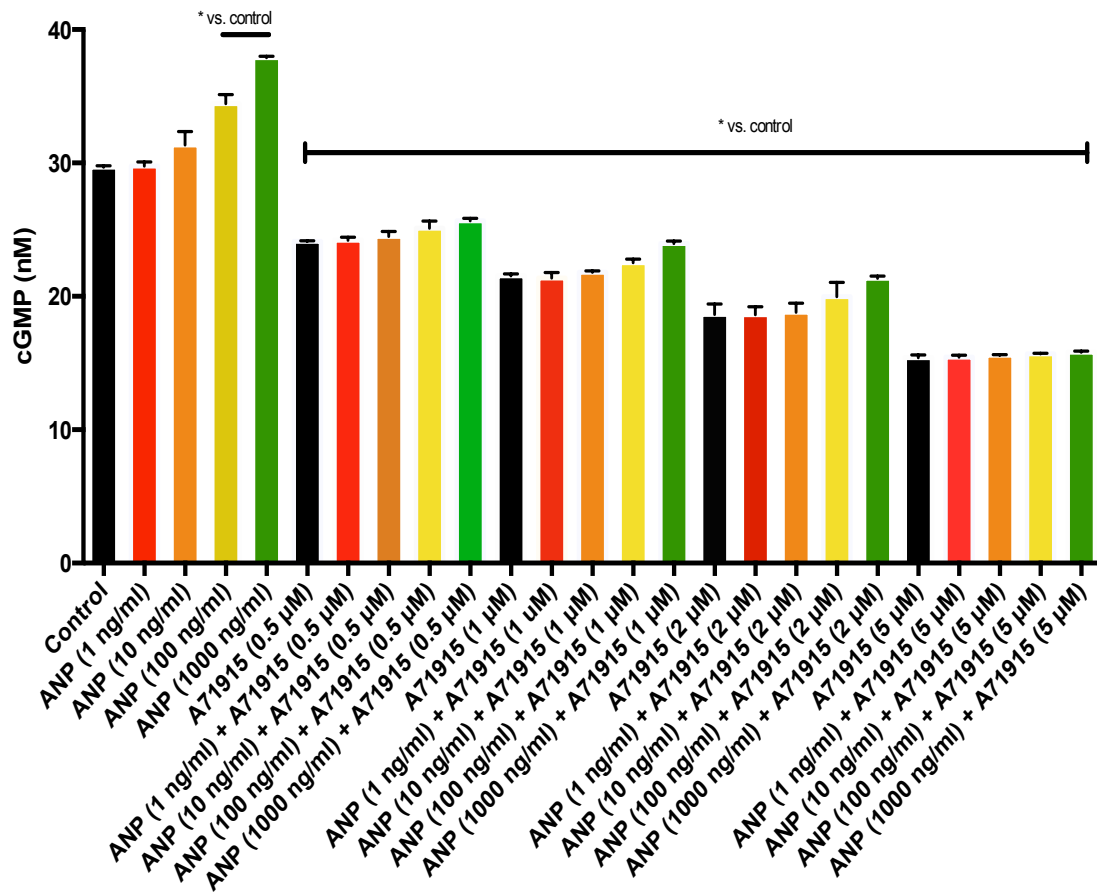


Figure 4.3. Dose-response for ANP on cGMP production in E11.5 ventricular cells, using fixed concentrations of A71915 (0.1, 0.5, 1, 2, 5 μM). The effects of exogenous ANP on intracellular cGMP production was determined by stimulating isolated E11.5 cells with ANP, then measuring cGMP using a competitive immunoassay, in combination with fixed concentrations of A71915 (0.5, 1, 2, or 5 μM). This was done at varying concentrations (1, 10, 100, and 1000 ng/ml) to establish a dose-response for ANP. The baseline level of cGMP was measured to be 29.7 ± 0.1 nM per 100,000 cells. Addition of exogenous ANP resulted in a significant increase in cGMP at vs. control as noted. N=6 independent experiments, performed in duplicate wells. Each bar represents mean \pm SEM. *p<0.05, One-way ANOVA with Tukey post hoc test.

4.3.4 Determining the Type of Antagonism of A71915

We next wanted to determine whether the NPR-A inhibitor, A71915 when used at a concentration of 1 μ M, was acting in a competitive or non-competitive manner in the presence of exogenous ANP. Specifically, we wanted to determine whether the ANP dose-response curve for cGMP production could be shifted to the right in the presence of 1 μ M A71915. From the results presented in Sections 4.3.1 and 4.3.3, we first compared dose-response curves generated using second messenger responses to varying concentrations of ANP (1, 10, 100 and 1000 ng/ml) in the presence or absence of 1 μ M A71915 (**Figure 4.4**). Comparison with ANP + 1 μ M A71915 was done since this combination was used extensively for studies conducted in Chapter 3. The X-axis consists of the range of concentrations of ANP whereas the Y-axis consists of the percent maximum response of cGMP levels. Although the maximal responses and shapes of the curves were similar, the presence of the inhibitor caused a shift in the ANP dose response curve to the right. These results indicate that A71915 at 1 μ M concentration can act as a competitive inhibitor for ANP concentrations ranging from 10-100 ng/ml, but not at 1000 ng/ml. Subsequently, we compared the LogEC₅₀ of the ANP + 1 μ M A71915 curve to that of the ANP curve (-7.541 vs. -7.861) using a four-parameter logistic sigmoidal dose response analysis and found that these values were significantly different from each other ($p < 0.05$, **Figure 4.4**). In addition, the Hill slopes for both curves were found to be close to 1 (0.91 for ANP vs. 1.34 for ANP + 1 μ M A71915) which indicates the presence of a single binding site for these agents in E11.5 ventricular

cells. Therefore, these results suggest that A71915 acts as a competitive inhibitor for ANP binding (10-100 ng/ml) in E11.5 ventricular cells.

Although A71915-mediated decreases in cGMP levels at other fixed antagonist concentrations (e.g. 0.5, 2 and 5 μ M) were overcome by increasing concentrations of ANP, there were no significant differences between the logEC50 values of the dose response curves for ANP and ANP+A71915 at those other concentrations (data not shown). Based on these results, A71915 may not be acting as a competitive antagonist at those other concentrations in E11.5 ventricular cells. Taking into account the results from Section 4.3.2, A71915 can behave as an inverse agonist in the absence of ANP.

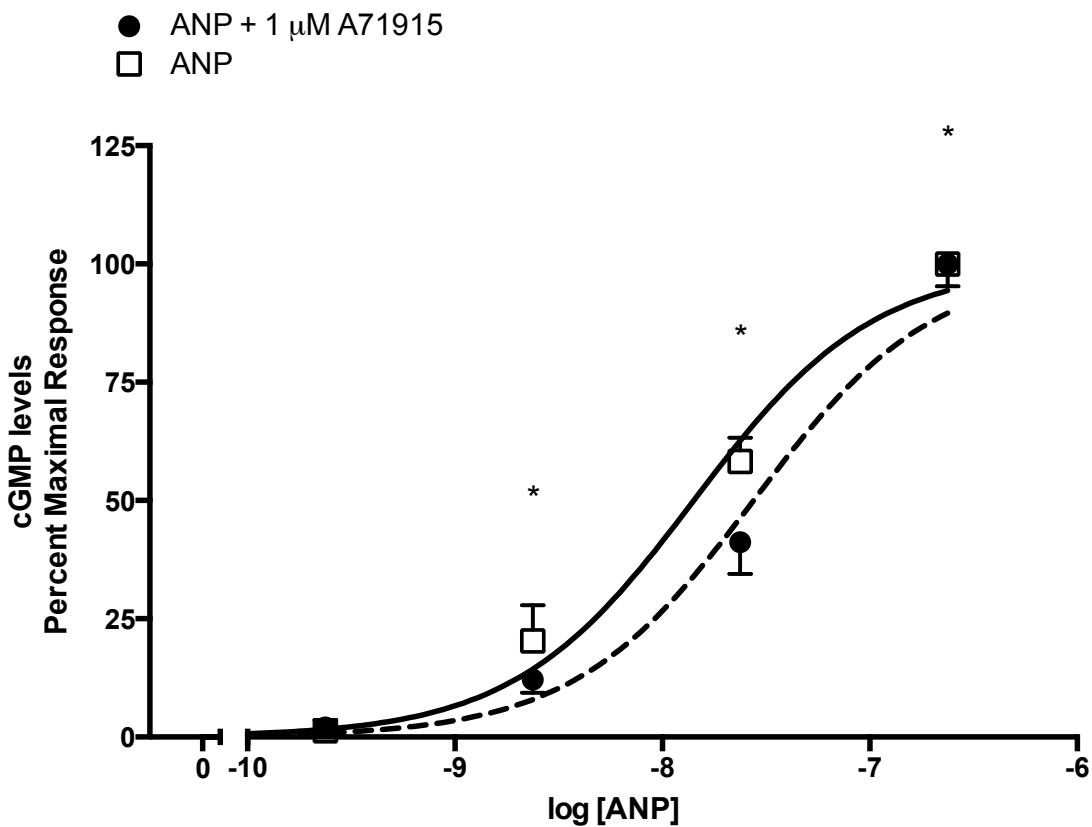


Figure 4.4. Determining the type of antagonism of A71915 through dose-response curves with varying concentrations of ANP (1, 10, 100, 1000 ng/ml) in the absence or presence of A71915 (1 μ M). In order to determine whether A71915 was a competitive antagonist or not, dose response curves were generated plotting ANP alone (0, 1, 10, 100, 1000 ng/ml, white squares) vs. ANP (0, 1, 10, 100, 1000 ng/ml) + A71915 (1 μ M, black circles). N=6 independent experiments. Each bar represents mean \pm SEM. *p<0.05, Four-parameter logistic sigmoidal dose response analysis.

4.3.5 Effects of A71915 Dosage on ANP-Induced Changes in Ventricular Conduction System Gene Expression

We wanted to determine how various doses of A71915 (0.1 to 5 μ M) in the presence or absence of ANP treatment affected Cx40 and HCN4 gene expression in E11.5 ventricular cells. Compared to ANP treatment (1000 ng/ml), the combination of ANP (1000 ng/ml) + A71915 (0.1 μ M) resulted in similar levels of HCN4 and Cx40 gene expression (p =NS) (**Figure 4.5 A, 4.6 A**). However, compared to ANP treatment, the combination of ANP + A71915 (0.5 μ M) resulted in a significantly lower level of both HCN4 and Cx40 gene expression (**Figures 4.5 B and 4.6 B**; 1.2-fold \pm 0.007 and 1.1-fold \pm 0.003 respectively, p <0.00005). This result was similar for the subsequent doses of ANP + 1 μ M A71915, ANP + 2 μ M A71915, and ANP + 5 μ M A71915 (p <0.05, **Figures 4.5 and 4.6, panels C-E**). Therefore, when A71915 was used at 0.5 μ M or higher concentrations in combination with 1000 ng/ml ANP, this significantly lowers gene expression of both genes vs. ANP treatment alone.

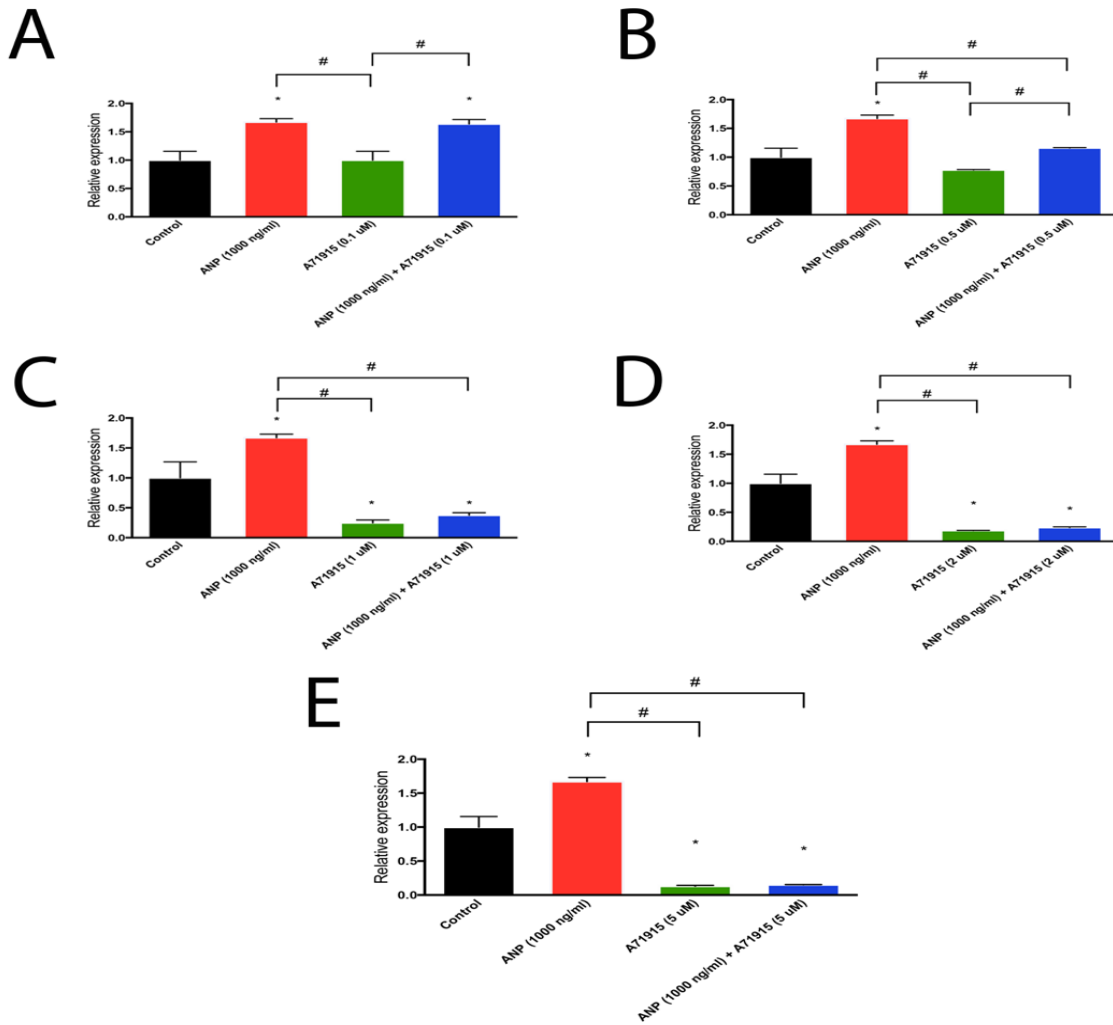


Figure 4.5. RT-qPCR analysis of HCN4 gene expression in E11.5 mouse ventricular cells following addition of exogenous ANP (1000 ng/ml) in combination with varying concentrations of A71915 (0.1, 0.5, 1, 2 and 5 μ M) over 48 hours. Cells were incubated with ANP + various doses of A71915 to determine changes in gene expression vs. ANP alone. **A)** ANP + 0.1 μ M A71915; **B)** ANP + 0.5 μ M A71915; **C)** ANP + 1 μ M A71915; **D)** ANP + 2 μ M A71915; **E)** ANP + 5 μ M A71915. Compared to ANP alone, the combinations of ANP + 0.5 μ M, ANP + 1 μ M, ANP + 2 μ M and ANP + 5 μ M resulted in significant reductions in HCN4 gene expression, whereas combinations with A71915 doses less than 0.5 μ M were similar to ANP alone. As the dose of A71915 increased in combination with ANP, there was a trend toward decreased HCN4 expression. GAPDH was used as the housekeeping gene. N=3 experiments per group. Each bar represents mean \pm SEM. * p <0.05 control, # p <0.05 between groups as indicated, One-way ANOVA with Tukey's multiple comparisons post hoc test.

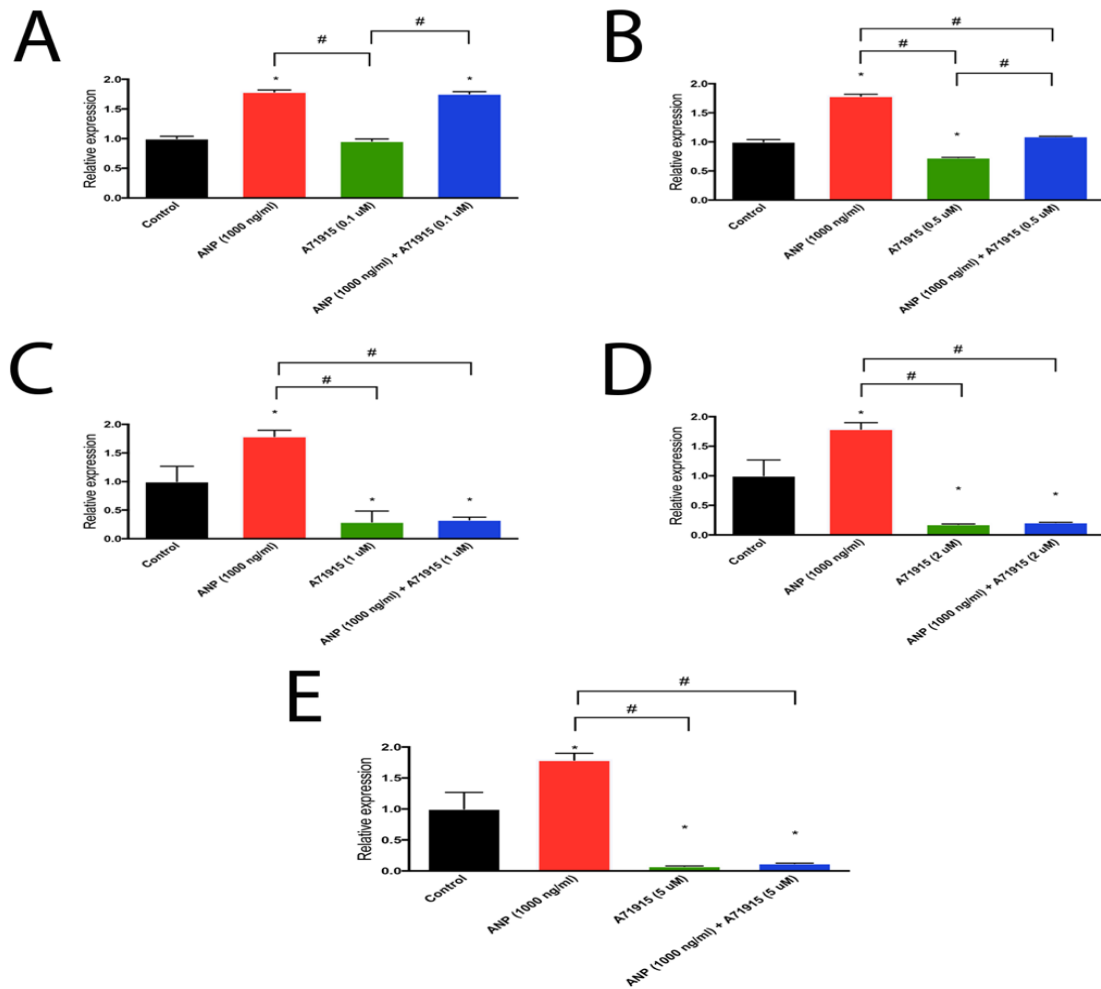


Figure 4.6. RT-qPCR analysis of Cx40 gene expression in E11.5 mouse ventricular cells following addition of exogenous ANP (1000 ng/ml) in combination with varying concentrations of A71915 (0.1, 0.5, 1, 2 and 5 μ M) over 48 hours. Cells were incubated with ANP + various doses of A71915 to determine changes in gene expression vs. ANP alone. **A)** ANP + 0.1 μ M A71915; **B)** ANP + 0.5 μ M A71915; **C)** ANP + 1 μ M A71915; **D)** ANP + 2 μ M A71915; **E)** ANP + 5 μ M A71915. Compared to ANP alone, the combinations of ANP + 0.5 μ M, ANP + 1 μ M, ANP + 2 μ M and ANP + 5 μ M resulted in significant reductions in Cx40 gene expression, whereas combinations with A71915 doses less than 0.5 μ M were similar to ANP alone. As the dose of A71915 increased in combination with ANP, there was a trend toward decreased Cx40 expression. GAPDH was used as the housekeeping gene. N=3 experiments per group. Each bar represents mean \pm SEM. *p<0.05 vs. Control, #p<0.05 between groups as indicated, One-way ANOVA with Tukey's multiple comparisons post hoc test.

4.3.6 Determining the Natriuretic Peptide Receptor Selectivity for A71915

ANP is known to bind to not only NPR-A, but also NPR-B, and NPR-C receptors. Since A71915 shares some structural similarities with ANP, we wanted to determine if A71915 was selective for NPR-A blockade, or non-selective. It has been shown that stimulation of NPR-C leads to decreases in cAMP signalling, (Pagano and Anand-Srivastava, 2001). We also questioned whether A71915-mediated reduction of cGMP levels in embryonic ventricular cells relies solely on its actions on the NPR-A receptor (Section 4.3.2) or could be via its actions on NPR-C triggering a potential crosstalk with the NPR-A/cGMP signalling system.

First, we designed an experiment to test the selectivity of A71915 for NPR-A. We generated timed pregnancies crossing NPRA-KO homozygous (-/-) male mice with BL6 female mice to generate E11.5 embryos that were heterozygous for NPRA-KO (+/-). E11.5 NPR-A^{+/-} ventricular cells were cultured and dose-response plots for varying concentrations of A71915 (0 to 10 μ M) were generated (**Figure 4.7**). Partial ablation of the receptor (50% blockade) removed the inhibitory effects of A71915 on cGMP as seen in Section 4.3.2. At all concentrations of A71915 tested, there were no longer any reductions in cGMP levels vs. control (p=NS). Therefore, with this experiment, we were able to rule out any off-target effects of A71915. Interestingly, baseline cGMP was measured at 21.7 ± 0.6 nM in E11.5 NPR-A^{+/-} ventricular cells. This appears to be much lower than the baseline cGMP we have recorded for experiments done with fully functional NPR-A receptors (~28-30 nM range). These differences in baseline cGMP

could be due to strain variance (BL6/NPRA-KO transgenic line vs. CD1 mice) or may also be due to the loss of a single copy of the *Npr1* gene.

To test if A71915 could be also acting via NPR-C, we performed a competitive immunoassay to measure changes in cAMP with increasing concentrations of A71915. Since, it was shown that NPR-C signalling leads to a downregulation of cAMP (Pagano and Anand-Srivastava, 2001), we wanted to determine if A71915 treatment could modulate the intracellular levels of cAMP in embryonic ventricular cells. We used a competitive immunoassay for cAMP and followed a similar protocol as with measurement of cGMP. However, one major change using this immunoassay is that we plated 4,000 E11.5 ventricular cells per well, as opposed to 100,000 cells per well, as this had previously been determined to be the optimal cell density for measurement of cAMP in E11.5 cells (Hotchkiss 2013, unpublished). E11.5 ventricular cells were incubated with either control, ANP (1000 ng/ml), A71915 (range of concentrations from 0.1 to 10 μ M), and to serve as a positive control, we added isoproterenol (ISO) (100 nM) alone, or in combination with either 1000 ng/ml ANP or 1 μ M A71915 (**Figure 4.8**). Under basal conditions, baseline cAMP was measured at 7.0 ± 0.3 nM, per 4,000 cells. ANP alone (1000 ng/ml) and various concentrations of A71915 (0.1 to 5 μ M) did not have a significant effect on levels of cAMP production ($p=NS$). Treatment with ISO (100 nM) alone significantly elevated cAMP levels which were measured at 28.9 ± 0.1 nM, vs. control ($p<0.05$). ISO in combination with ANP (1000 ng/ml) and with A71915 (1 μ M) also resulted in significant increases in cAMP levels ($p<0.05$), however there were no significant differences between all three groups containing ISO ($p=NS$). Since A71915

does not appear to affect cAMP levels, it is unlikely that A71915 is selective for NPR-C. In conclusion, A71915 is an antagonist that is highly selective for NPR-A, but not NPR-C in embryonic ventricular cells.

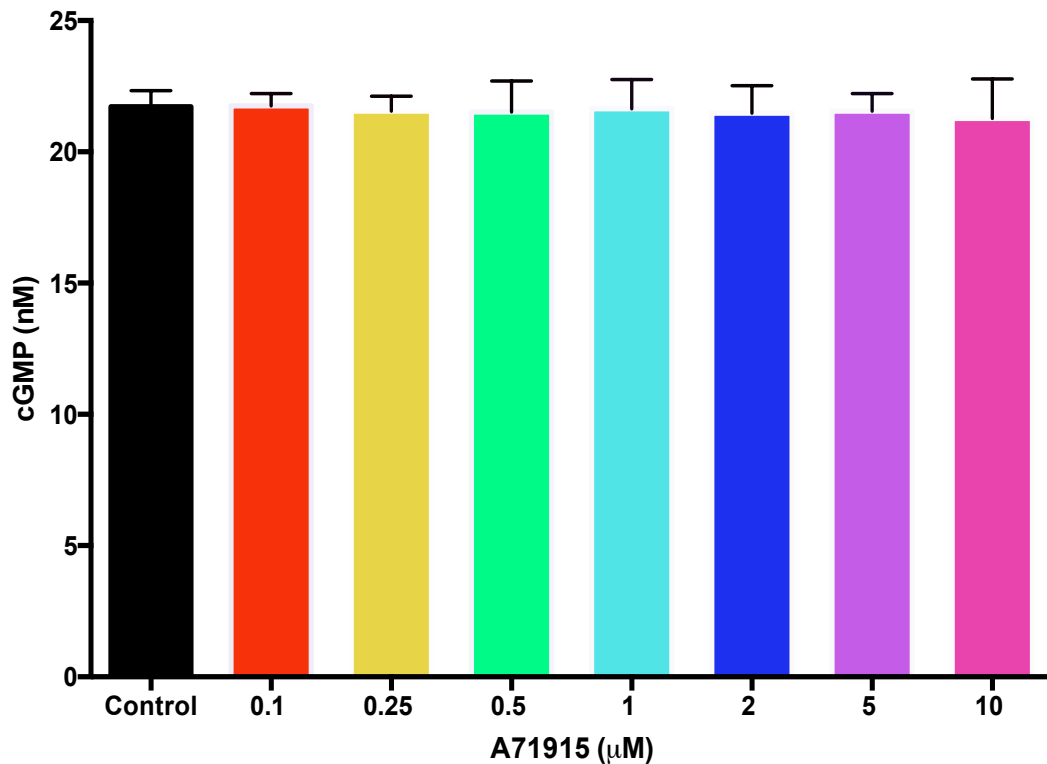


Figure 4.7. Determining selectivity of A71915 for NPR-A by measuring changes in cGMP production that occur with partial genetic ablation of the NPR-A receptor (NPR-A^{+/-}). To determine whether A71915 was a selective inhibitor for NPR-A, E11.5 ventricular cells from NPR-A^{+/-} hearts were cultured and incubated with various concentrations of A71915 (ranging from 0.1 to 10 μM) and cGMP production was measured. Partial ablation of the NPR-A receptor prevented changes in cGMP levels from occurring with increasing doses of A71915, vs. control. Therefore, A71915 may be highly selective for NPR-A. Baseline cGMP was measured at 21.7 ± 0.6 nM per 100,000 cells, which was much lower than baseline cGMP recorded in other experiments with fully functional NPR-A receptors (~28-30 nM range). N=6 independent experiments, performed in duplicate wells. Each bar represents mean ± SEM. *p<0.05, One-way ANOVA with Tukey post hoc test.

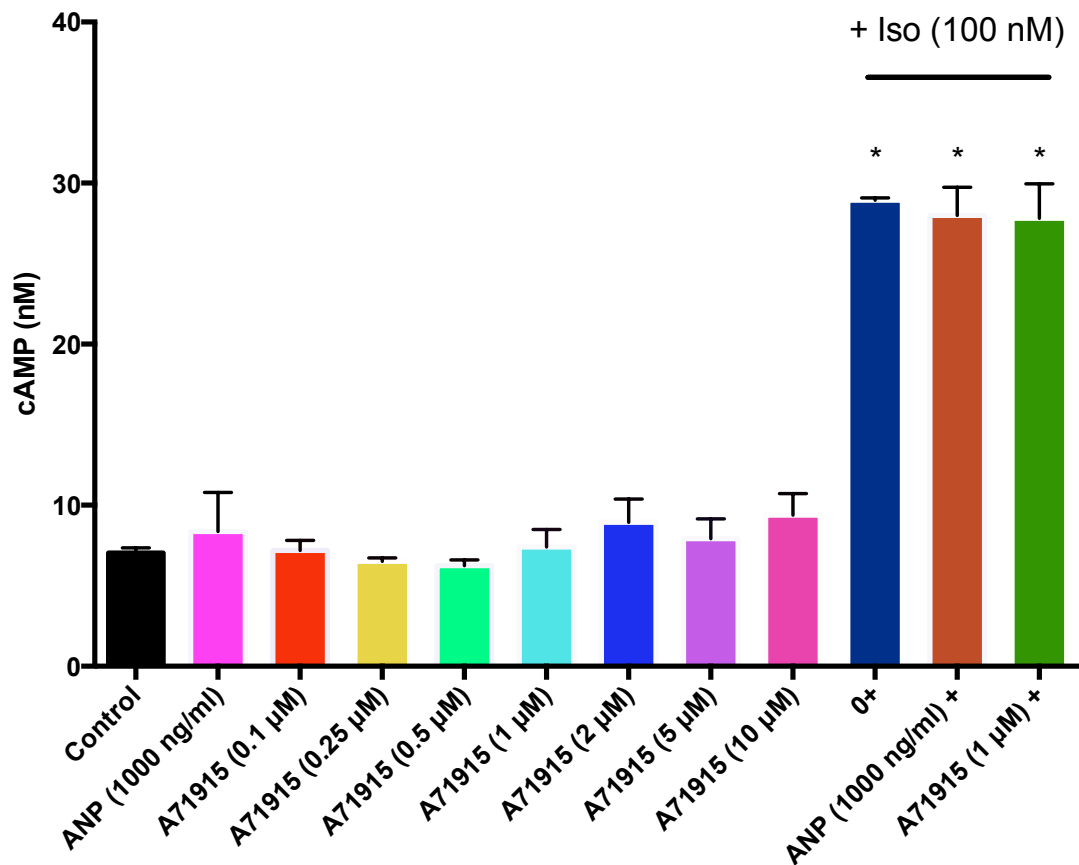


Figure 4.8. Determining selectivity of A71915 for NPR-C by measuring changes in cAMP signalling. To determine if A71915 was non-selective (i.e. could bind to NPR-C receptors and affect cAMP signalling), E11.5 ventricular cells were incubated with varying concentrations of A71915 and cAMP production was measured. Increasing doses of A71915 had no effect on cAMP levels vs. control. Isoproterenol (ISO) was added alone as a positive control, significantly increasing cAMP levels vs. control. ISO in combination with either ANP (1000 ng/ml) or A71915 (1 μM) also increased cAMP levels vs. control. However, there were no significant differences between all 3 groups containing ISO. Therefore, it is unlikely that A71915 is acting via NPR-C receptor in E11.5 ventricular cells. Baseline cAMP was measured at 7.0 ± 0.3 nM per 4,000 cells. N=6 independent experiments, performed in duplicate wells. Each bar represents mean \pm SEM. * $p < 0.05$, One-way ANOVA with Tukey post hoc test.

CHAPTER 5: CHARACTERIZING THE POTENTIAL FOR SIGNALLING INTERACTIONS BETWEEN ATRIAL NATRIURETIC PEPTIDE, ENDOTHELIN-1, AND NEUREGULIN-1 SIGNALLING PATHWAYS IN THE DEVELOPMENT OF THE VENTRICULAR CONDUCTION SYSTEM

5.1 Background and Hypothesis

The results seen in Chapter 3 convey that the ANP/NPR-A/cGMP signalling pathway is biologically active in the mouse embryonic heart and through this pathway gene expression of important VCS markers, Cx40 and HCN4, is regulated. In addition, these results provide a framework to suggest that ANP may be involved in the formation of the VCS in the embryonic heart. NRG-1 may play an important role in the formation of the CCS. It has been shown that overexpression of NRG-1 and its cognate receptors in the heart, ErbB4 and ErbB2, results in hyper-trabeculation (Parodi & Kuhn, 2014). This has been shown to lead to ventricular non-compaction and could potentially lead to the development of CHDs (Parodi & Kuhn, 2014). Using a CCS-*lacZ* reporter mouse line, Rentschler et al. (2002) studied the effects of exogenous NRG-1 on cultured embryonic hearts. NRG-1 was capable of increasing β -gal expression, providing evidence that NRG-1 is capable of stimulating the differentiation of CMs into CCS cells (Rentschler et al., 2002). ET-1 has also been studied in the context of the development of the CCS, and ET-1 may also play a role in its formation. Gourdie et al. (1998) showed that exogenous ET-1 added to chick ventricular CMs was capable of converting them into Purkinje fiber cells. Despite a progressive maturation of the CCS in embryonic mouse ventricles from E8.5 to E17.5 stages, the inductive effects of ET-1 and NRG-1 appear to be limited beyond E10.5-11.5 stages (Gourdie et al., 1998; Rentschler et al., 2002; Patel and Kos,

2005; Meyer and Birchmeier, 1995; Gassmann et al., 1995; Takebayashi-Suzuki et al., 2000; Mikawa and Hurtado, 2007). Given the effects of ANP on induction of VCS marker gene expression beyond the E11.5 stage of ventricular development (**Figures 3.12 and 3.13**), it is possible that ANP may act as a stage-specific paracrine factor in VCS development. Since ANP, ET-1 and NRG-1 have all been shown to be present in the developing ventricular trabeculae of the embryonic heart (Hotchkiss et al., 2015; Rentschler et al., 2002; Gourdie et al., 1998), it is possible that there may be signalling interactions occurring between ANP, NRG-1, ET-1 and their respective cognate receptors to guide development of the VCS. **We hypothesize that the three distinct signalling systems of ANP, NRG-1 and ET-1, interact in a cooperative manner, to form a cellular signalling network that guides development of the VCS in the embryonic mouse heart.**

5.2 Specific Aims

1. To determine the potential role of ET-1 and NRG-1 in inducing VCS marker gene expression in E11.5 ventricular cell cultures.
2. To determine if ET-1 and/or NRG-1 signalling systems modulate the levels of second messenger molecule cGMP in embryonic ventricular cells.
3. To determine if exogenous addition of ANP, ET-1 and/or NRG-1 induce activity of a Cx40-promoter construct.

5.3 Results

5.3.1 Effects of ET-1 and NRG-1 on Percent Distribution of Cells Expressing HCN4 and Cx40 in E11.5 Ventricular Cultures

Since ET-1 and NRG-1 have been shown to induce differentiation of CMs into CCS cells in chick and mouse models (Gourdie et al., 1998; Rentschler et al., 2002), we

wanted to determine the effects of ET-1 or NRG-1 alone on protein expression of Cx40 and HCN4 in embryonic ventricular cells (therefore, in the VCS), by adding exogenous forms of the peptides, and then comparing the effects of ET-1 and NRG-1 with ANP. We chose to use concentrations of 1.5 nM for ET-1 and 2.5 nM for NRG-1, based on the results of Patel & Kos' study (2005), which demonstrated that at E9.5, the addition of these paracrine factors alone at these concentrations resulted in increases in gene expression of Cx40 in the mouse embryonic heart. Either ANP (1000 ng/ml), ET-1 (1.5 nM) or NRG-1 (2.5 nM) was added to E11.5 cell cultures every 12 hours over a period of 48 hours, after which cells were immunolabelled with MF20 for detection of CMs and with anti-HCN4 antibody to identify HCN4 (**Figure 5.1**). The percentage of cells that stained positively for MF20+ and HCN4+ were counted per field at 40x magnification (of the total number of cells counted per field), denoted as HCN4+/MF20+ cells. These cells are characterized as VCS cells since they are CMs that stain positive for these VCS markers. The percent of HCN4+/MF20+ cells upon addition of either ET-1 or NRG-1 increased significantly vs. control (ET-1: $87 \pm 3\%$; NRG-1: $87 \pm 4\%$; Control: $63 \pm 5\%$, $p < 0.005$, **Figure 5.2 A**). It is important to note from these results that each of the paracrine factors increased the percent of HCN4+/MF20+ cells to the same degree vs. control and there were no significant differences between paracrine factor treatment groups ($p = \text{NS}$).

The effects of these paracrine factors on the percentage of HCN4+/MF20- cells was also determined. HCN4+/MF20- cells are non-CMs/VCS progenitors present in the embryonic ventricles that stain positively for HCN4 but are negative for MF20.

Compared to control, the addition of ET-1 or NRG-1 resulted in a significant decrease in the percent of HCN4+/MF20- cells (ET-1: $43 \pm 4\%$; NRG-1: $44 \pm 3\%$, Control: $63 \pm 4\%$, $p < 0.005$, **Figure 5.2 B**). There were no significant differences in the percent of HCN4+/MF20- cells between ANP, ET-1, or NRG-1 treatment groups ($p = \text{NS}$). We calculated the ratio of HCN4+/MF20+ to HCN4+/MF20- cells per treatment group, which would determine how each of the paracrine factors impacted the conversion of non-CMs to VCS cells (**Figure 5.3**). The ratio of cells for the control group was 0.98 ± 0.08 cells. Compared to control, the addition of ET-1 (1.5 nM) to E11.5 cell culture resulted in a cell ratio of 2.2 ± 0.3 . The addition of NRG-1 (2.5 nM) resulted in a cell ratio of 2.0 ± 0.18 . The cell ratios for ET-1 and NRG-1 treated groups were each significantly higher vs. control ($p < 0.005$), suggesting that ET-1 and NRG-1 may be capable of promoting non-CM cells in the embryonic mouse heart to VCS cells, along with ANP.

The effects of ANP, ET-1, and NRG-1 on protein expression of Cx40 at E11.5 was determined in mouse ventricular cells, using the same concentrations and dose timing as with HCN4 protein expression (**Figure 5.4**). Compared to control, although it appears that the percentage of Cx40+/MF20+ cells increased with treatment of each of the paracrine factors, this increase was not statistically significant ($p = \text{NS}$, **Figure 5.5 A**). The effect of ET-1 and NRG-1 on protein expression of Cx40 mirrors the immunofluorescence results of the effects of ANP on Cx40 expression at 1000 ng/ml in Section 3.3.1. There were no significant differences in the percentages of Cx40+/MF20+ cells between ANP, ET-1, or NRG-1 treatment groups ($p = \text{NS}$).

The percentage of Cx40+/MF20- cells (non-CM cells) significantly decreased vs. control with ET-1 or NRG-1 treatment (ET-1: $31 \pm 4\%$; NRG-1: $28 \pm 3\%$; Control: $63 \pm 5\%$, $p < 0.005$, **Figure 5.5 B**). The ratio of Cx40+/MF20+ to Cx40+/MF20- cells was calculated to determine the proportion of non-CM cells that were converted to VCS cells upon addition of either ET-1 or NRG-1 (**Figure 5.6**). The cell ratio in the control group was 1.2 ± 0.1 . The cell ratio of the ET-1 treated group was 3.2 ± 0.6 . The cell ratio of the NRG-1 treated group was 3.4 ± 0.7 . Therefore, the addition of ET-1 or NRG-1 resulted in a significant increase in this cell ratio vs. control ($p < 0.05$), suggesting that these paracrine factors could also be involved, as with ANP, in inducing differentiation of non-CM cells into VCS cells.

The total number of nuclei counted per field was determined among all treatment groups immunostained for anti-HCN4 or anti-Cx40 antibody and there were no significant differences among groups ($p = \text{NS}$, **Figure 5.7 A**). To determine the potential impact of ET-1 or NRG-1 on the proliferation of CMs in cells immunolabelled with anti-Cx40 antibody, we counted the number of MF20+ cells for both treatment groups. Compared to control, there was a statistically significant increase in the number of MF20+ cells with ET-1 treatment (51 ± 7 cells) and with NRG-1 treatment (56 ± 6 cells) vs. control (25 ± 2 cells, $p < 0.005$, **Figure 5.7 B**). There were no statistically significant differences among ANP, ET-1, or NRG-1 groups for the number of MF20+ cells counted ($p = \text{NS}$). These immunostaining experiments suggest that ET-1 and NRG-1 increase HCN4 protein expression in E11.5 ventricular cells, but not Cx40 protein expression. Also, both treatments reduced the percentages of non-CMs with HCN4/Cx40 protein

(HCN4+/MF20-, Cx40+/MF20- cells) and favoured differentiation of VCS cells vs. non-CMs cells as seen in the increased cell ratios vs. control.

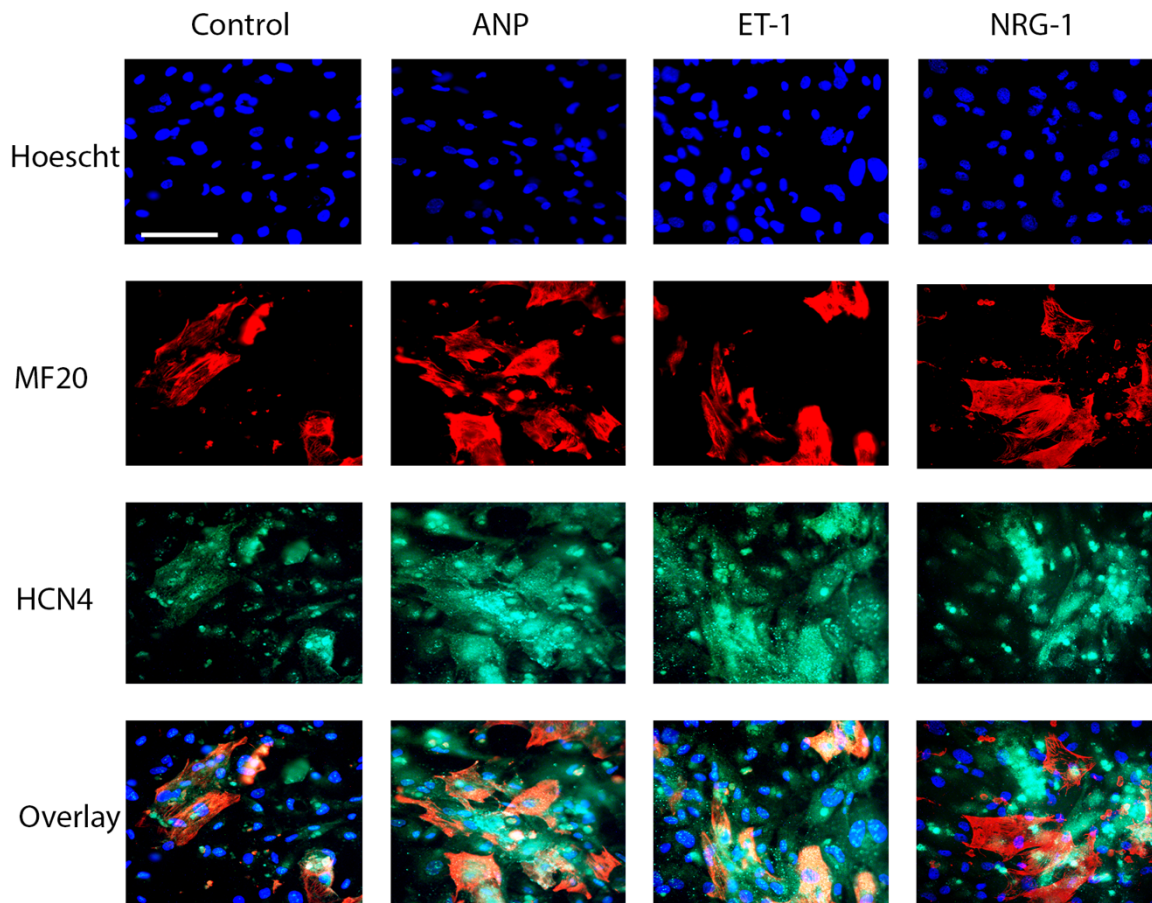


Figure 5.1. Expression of HCN4 protein in E11.5 mouse ventricular cells following addition of ET-1 or NRG-1 over 48 hours. E11.5 ventricular cells were cultured, and ANP (1000 ng/ml), ET-1 (1.5 nM) or NRG-1 (2.5 nM) treatment was given every 12 hours over a 48-hour period. Cells were immunolabelled for detection of HCN4 protein. The same field of cells are labelled with Hoechst nuclear stain, sarcomeric myosin antibodies (MF20), HCN4 protein and an image overlay. CMs were identified as MF20+. Ventricular conduction system (VCS) cells were counted as those that identified as both HCN4+ and MF20+ (HCN4+/MF20+). N=10 experiments per group. Scale bar = 100 μ M.

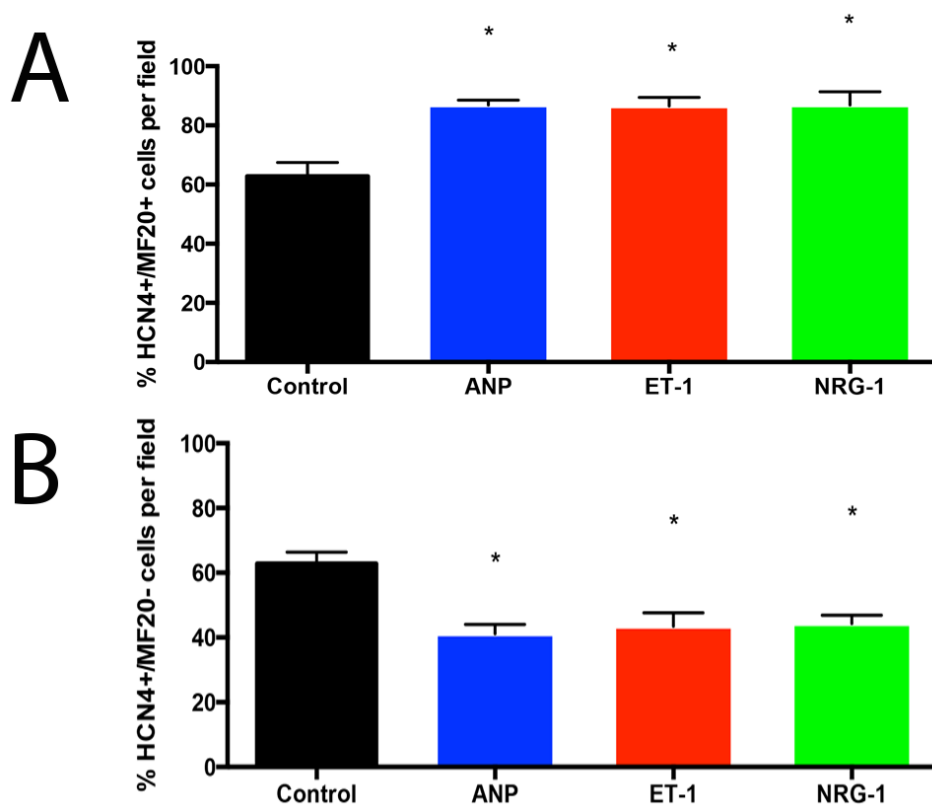


Figure 5.2. Percentage (%) of HCN4+/MF20+ and HCN4+/MF20- cells in E11.5 mouse ventricular cells following addition of ET-1 or NRG-1 over 48 hours. E11.5 ventricular cells were cultured and ANP (1000 ng/ml), ET-1 (1.5 nM), or NRG-1 (2.5 nM) was added every 12 hours over a 48-hour period. Cells were immunolabelled for detection of HCN4 protein. CMs were identified as MF20+. **A)** Bar graph represents the percentage (%) of HCN4+/MF20+ cells per field (quantified through immunolabelling) upon exposure to each of the 3 paracrine factors over 48 hours. HCN4+/MF20+ cells were identified as ventricular conduction system (VCS) cells. ANP (1000 ng/ml), ET-1 (1.5 nM) and NRG-1 (2.5 nM) significantly increased the % of HCN4+/MF20+ cells per field vs. control. There were no significant differences among the three paracrine factors. **B)** Bar graph represents the percentage (%) of HCN4+/MF20- cells per field (quantified through immunolabelling) upon exposure to each of the 3 paracrine factors over 48 hours. HCN4+/MF20- cells were identified as non-CMs expressing HCN4 protein. ANP (1000 ng/ml), ET-1 (1.5 nM) and NRG-1 (2.5 nM) significantly decreased the % of HCN4+/MF20- cells per field vs. control. There were no significant differences among the three paracrine factors. N=10 experiments per group, ~800-950 cells were counted from 10 fields for each group. Each bar represents mean \pm SEM. * $p < 0.05$ vs. control, One-way ANOVA with Tukey's multiple comparisons post hoc test.

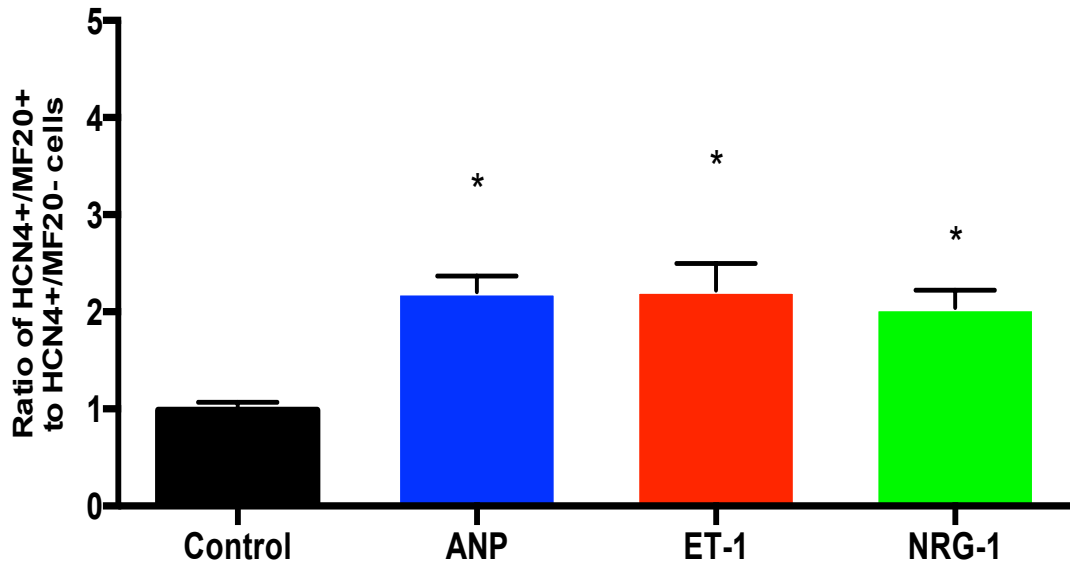


Figure 5.3. Calculated ratio of HCN4+/MF20+ cells to HCN4+/MF20- cells in E11.5 mouse ventricular cells following addition of ET-1 or NRG-1 over 48 hours. E11.5 ventricular cells were cultured and ANP (1000 ng/ml), ET-1 (1.5 nM) or NRG-1 (2.5 nM) was added every 12 hours over a 48-hour period. Cells were immunolabelled for detection of HCN4 protein. CMs were identified as MF20+. Bar graph represents the ratio of VCS cells (HCN4+/MF20+) to non-CMs that stained positively for HCN4 (HCN4+/MF20-) cells upon exposure to each of the three paracrine factors over 48 hours. ANP, ET-1, and NRG-1 significantly increased the cell ratio, favouring differentiation of VCS cells. There were no significant differences between paracrine factor groups. N=10 experiments per group, ~800-950 cells were counted from 10 fields for each group. Each bar represents mean \pm SEM. * $p < 0.05$ vs. control (no treatment), One-way ANOVA with Tukey's multiple comparisons post hoc test.

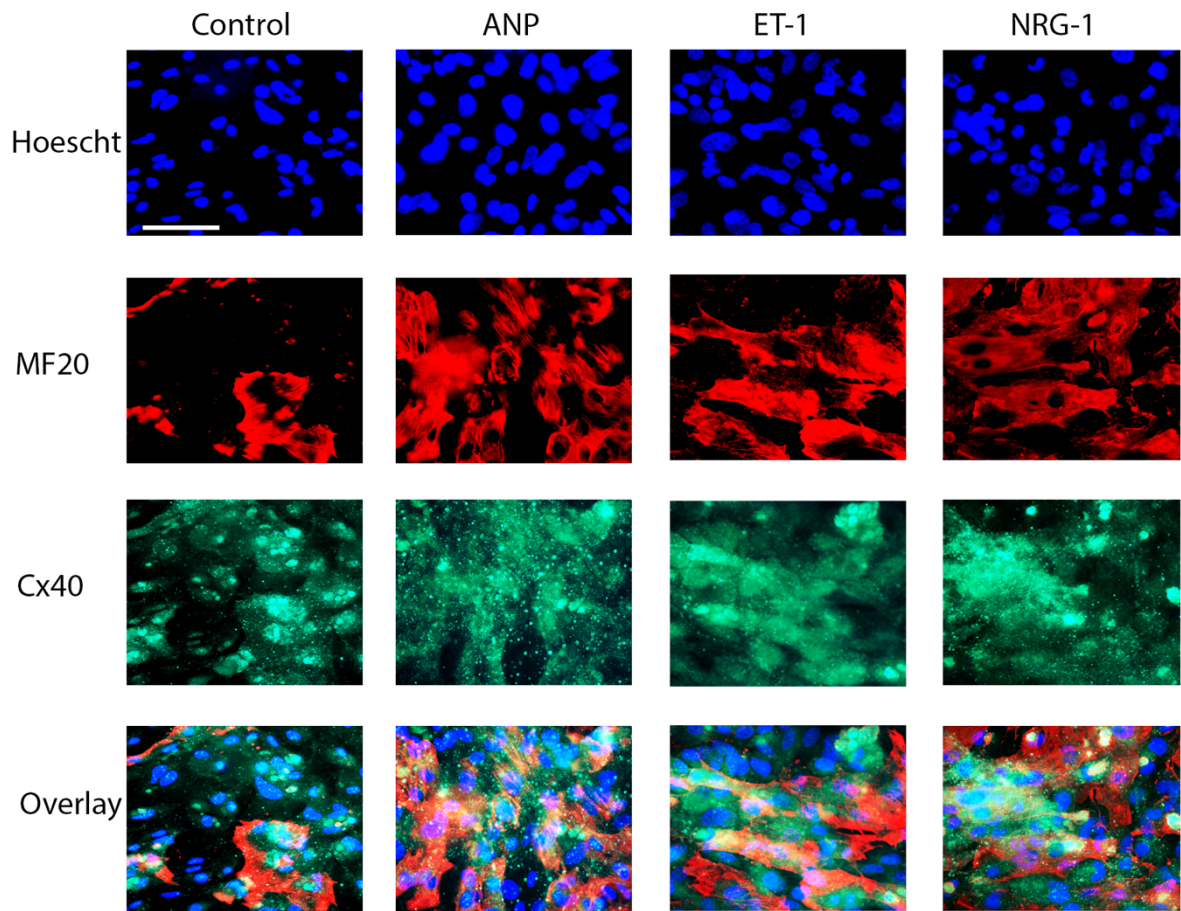


Figure 5.4. Expression of Cx40 protein in E11.5 mouse ventricular cells following addition of ET-1 or NRG-1 over 48 hours. E11.5 ventricular cells were cultured, and ANP (1000 ng/ml), ET-1 (1.5 nM) or NRG-1 (2.5 nM) treatment was given every 12 hours over a 48-hour period. Cells were immunolabelled for detection of Cx40 protein. The same field of cells are labelled with Hoechst nuclear stain, sarcomeric myosin antibodies (MF20), Cx40 protein and an image overlay. CMs were identified as MF20+. Ventricular conduction system (VCS) cells were counted as those that identified as both Cx40+ and MF20+ (Cx40+/MF20+). N=10 experiments per group. Scale bar = 100 μ M.

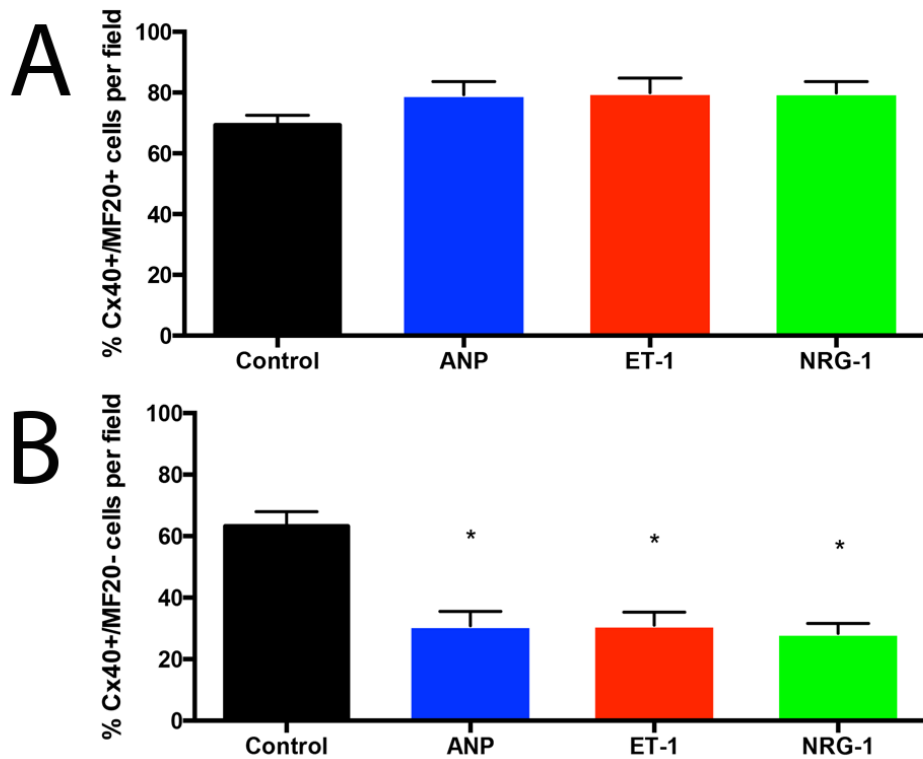


Figure 5.5. Percentage (%) of Cx40+/MF20+ and Cx40+/MF20- cells in E11.5 mouse ventricular cells following addition of ET-1 or NRG-1 over 48 hours. E11.5 ventricular cells were cultured and ANP (1000 ng/ml), ET-1 (1.5 nM), or NRG-1 (2.5 nM) was added every 12 hours over a 48-hour period. Cells were immunolabelled for detection of Cx40 protein. CMs were identified as MF20+. **A)** Bar graph represents the percentage (%) of Cx40+/MF20+ cells per field (quantified through immunolabelling) upon exposure to each of the 3 paracrine factors over 48 hours. Cx40+/MF20+ cells were identified as ventricular conduction system (VCS) cells. None of the paracrine factors had an effect on % Cx40+/MF20+ cells vs. control. **B)** Bar graph represents the percentage (%) of Cx40+/MF20- cells per field (quantified through immunolabelling) upon exposure to each of the 3 paracrine factors over 48 hours. Cx40+/MF20- cells were identified as non-CMs expressing HCN4 protein. ANP (1000 ng/ml), ET-1 (1.5 nM) and NRG-1 (2.5 nM) significantly decreased the % of Cx40+/MF20- cells per field vs. control. There were no significant differences among the three paracrine factors. N=10 experiments per group, ~800-950 cells were counted from 10 fields for each group. Each bar represents mean \pm SEM. * $p < 0.05$ vs. control, One-way ANOVA with Tukey's multiple comparisons post hoc test.

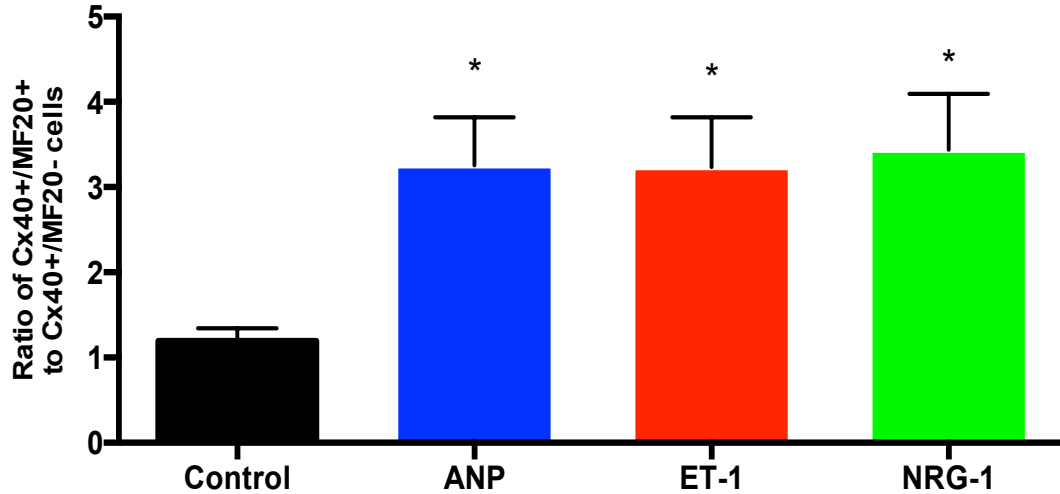


Figure 5.6. Calculated ratio of Cx40+/MF20+ cells to Cx40+/MF20- cells in E11.5 mouse ventricular cells following addition of ET-1 or NRG-1 over 48 hours. E11.5 ventricular cells were cultured and ANP (1000 ng/ml), ET-1 (1.5 nM) or NRG-1 (2.5 nM) was added every 12 hours over a 48-hour period. Cells were immunolabelled for detection of Cx40 protein. CMs were identified as MF20+. Bar graph represents the ratio of VCS cells (Cx40+/MF20+) to non-CMs that stained positively for Cx40 (Cx40+/MF20-) cells upon exposure to each of the three paracrine factors over 48 hours. ANP, ET-1, and NRG-1 significantly increased the cell ratio, favouring differentiation of VCS cells. There were no significant differences between paracrine factor groups. N=10 experiments per group, ~800-950 cells were counted from 10 fields for each group. Each bar represents mean \pm SEM. * $p < 0.05$ vs. control (no treatment), One-way ANOVA with Tukey's multiple comparisons post hoc test.

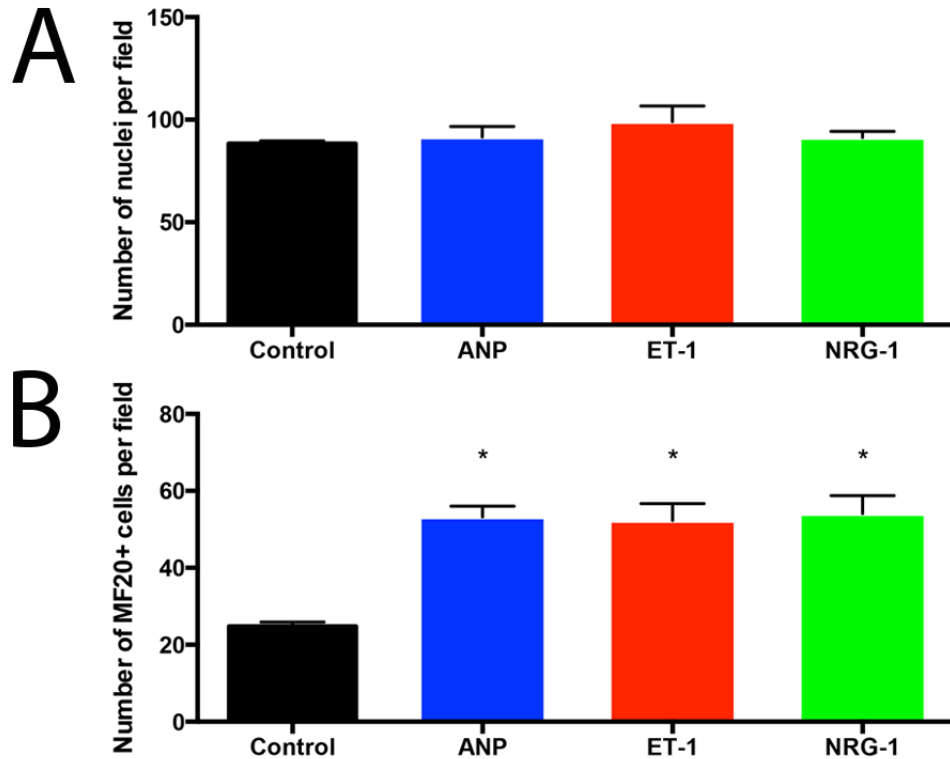


Figure 5.7. Number of nuclei per field (A) and number of MF20+ cells (B) per field in E11.5 cells immunolabelled with anti-HCN4 or anti-Cx40 antibody following addition of ANP, ET-1 or NRG-1 over 48 hours. E11.5 ventricular cells were cultured and ANP (1000 ng/ml), ET-1 (1.5 nM), or NRG-1 (2.5 nM) was added every 12 hours over a 48-hour period. Cells were immunolabelled for detection of HCN4 or Cx40 protein. CMs were identified as MF20+. **A)** The number of nuclei per field were counted per treatment group; there were no significant differences between groups. **B)** The number of MF20+ cells (CMs) per field were counted. ANP, ET-1 and NRG-1 each significantly increased the number of MF20+ cells vs. control. N=20 experiments per group, ~800-950 cells were counted from 10 fields for each group. Each bar represents mean \pm SEM. * $p < 0.05$ vs. control (no treatment), One-way ANOVA with Tukey's multiple comparisons post hoc test.

5.3.2 Effects of ET-1 and NRG-1 on Gene Expression of HCN4 and Cx40 in E11.5 Ventricular Cells

We wanted to determine the effects of exogenous ET-1 and NRG-1 on HCN4 and Cx40 gene expression in E11.5 ventricular cells using RT-qPCR as previously described. GAPDH was used as the housekeeping gene in all experiments. Briefly, E11.5 ventricular cell cultures were treated with either ET-1 (1.5 nM) or NRG-1 (2.5 nM) for 12 hours over a period of 48 hours. A control group was used as a negative control, and ANP (1000 ng/ml) treatment was used as a positive control. Cells were then processed for RNA extraction, followed by synthesis of cDNA and analysis of the genes of interest through RT-qPCR. The control group was assigned a relative expression value of 1.0. For HCN4 expression analysis, compared to control, the addition of ET-1 was not statistically significant ($p=NS$, **Figure 5.8**). As a positive control group, ANP treatment resulted in a significant increase in gene expression of HCN4 vs. control (1.7-fold \pm 0.06), yielding a similar result as seen in Section 3.3.2 ($p<0.005$). NRG-1 treatment also increased gene expression of HCN4 vs. control by 2.4-fold \pm 0.08 ($p<0.005$).

Interestingly, the induction of HCN4 gene expression by ANP was significantly greater than that of ET-1, and the induction of HCN4 gene expression by NRG-1 was significantly greater than that of ANP ($p<0.005$). Thus, of the 3 paracrine factors, NRG-1 treatment seemed to induce the greatest amount of gene expression of HCN4. Lastly, there was a statistically significant difference between gene expression of HCN4 with ET-1 vs. NRG-1 treatment ($p<0.005$). Taken together with results from Section 5.3.1, while the percentage of CMs positive for HCN4 was significantly increased with ET-1

treatment, gene expression was not; whereas both gene expression levels and percentage of CMs expressing HCN4 were significantly increased with ANP or NRG-1.

We subsequently tested paired combinations of the 3 paracrine factors and measured their effects on gene expression of HCN4 in E11.5 ventricular cell culture in order to determine if there were any additive effects by combining paracrine factors. The combination of ET-1 + ANP resulted in a statistically significant increase in HCN4 gene expression vs. control by 1.3-fold \pm 0.05 ($p < 0.005$, **Figure 5.9 A**). This combination resulted in significantly greater induction of HCN4 gene expression than ET-1 alone, was significantly less than the induction that resulted from ANP treatment alone ($p < 0.05$). The combination of ET-1 + NRG-1 was tested next, also resulting in a significant increase in gene expression of HCN4 vs. control (1.8-fold \pm 0.1, $p < 0.005$, **Figure 5.9 B**). This combination resulted an increase in gene expression of HCN4 that was significantly greater than ET-1 alone, but was significantly less than with NRG-1 alone ($p < 0.005$). The last combination to be tested was NRG-1 + ANP. Interestingly, this combination resulted in an additive effect, which may perhaps even be synergistic, in significantly inducing gene expression of HCN4 by 3.3-fold \pm 0.3 ($p < 0.005$, **Figure 5.9 C**). The induction yielded by this combination was significantly greater than the induction provided by either ANP or NRG-1 alone ($p < 0.005$). Therefore, while the combinations of ET-1/ANP and ET-1/NRG-1 resulted in inductive effects on gene expression of HCN4, they were not additive, whereas the combination of NRG-1 + ANP resulted in an induction that was additive, and may even be synergistic.

We wanted to determine if all three paracrine factors together: ANP + ET-1 + NRG-1, could have an impact on the gene expression of HCN4 vs. control, in order to determine if there were possible inductive or additive effects. Compared to control, the 3 paracrine factors together significantly increased HCN4 gene expression by 2.7-fold \pm 0.2 ($p < 0.005$, **Figure 5.9 D**). This combination was significantly greater in inducing gene expression vs. ANP or ET-1 alone, but was similar to NRG-1 alone.

To determine if blockade of the NPR-A receptor had an effect on HCN4 gene expression of ET-1-treated cells at E11.5, ET-1 was combined with A71915 (1 μ M) and gene expression of HCN4 was determined. The combination of ET-1 + A71915 resulted in a significant reduction in gene expression of HCN4 by \sim 1.5-fold (0.67 ± 0.02) vs. control and vs. ET-1 alone ($p < 0.005$, **Figure 5.10 A**). Interestingly, A71915 alone resulted in a greater reduction in gene expression of HCN4 vs. this combination, raising the possibility that the presence of ET-1 in combination with A71915 may be preventing the reduction of gene expression to some degree. To determine whether blockade of NPR-A with A71915 had an impact on the induction in gene expression of HCN4 provided by NRG-1 treatment alone, the combination of NRG-1 + A71915 was tested. Compared to control, the combination of NRG-1 + A71915 treatment resulted in a significant decrease in gene expression of HCN4 by \sim 3.6-fold (0.3 ± 0.04 , $p < 0.005$, **Figure 5.10 B**). What is interesting to note here is that, unlike the combination of ET-1/A71915, the combination of NRG-1/A71915 reduced gene expression of HCN4 to a similar degree as that of A71915 alone, suggesting that at these concentrations, NRG-1 may not be

capable of rescuing the decline in gene expression of HCN4 caused by addition of A71915.

Changes to the gene expression of Cx40 in E11.5 ventricular cell culture was also determined by testing each of the three paracrine factors (**Figure 5.11**). A control group was utilized as a negative control and ANP treatment was utilized as a positive control again. Addition of ET-1 did not result in a significant change in gene expression of Cx40 ($p=NS$). The addition of ANP resulted in an induction in Cx40 gene expression by 1.8-fold ± 0.07 ($p<0.005$), similar to what was seen in the results of Section 3.3.2. This was statistically different vs. control and ET-1 groups ($p<0.005$). The addition of NRG-1 to cell culture resulted in significant induction by 2.1-fold ± 0.1 ($p<0.005$) vs. control and ET-1 groups. There were no statistically significant differences between gene expression of Cx40 provided by ANP treatment vs. NRG-1 treatment alone ($p=NS$). Of the three paracrine factors, NRG-1 seemed to provide the greatest induction in Cx40 gene expression, similar to the results seen with HCN4 gene expression. Taken together, percent distribution of Cx40+/MF20+ cells and gene expression of Cx40 were not significantly changed with the addition of ET-1 alone. While the percent distribution of Cx40+/MF20+ cells was unaffected by ANP or NRG-1, gene expression of Cx40 was significantly induced by both of these paracrine factors.

Paired combinations of the three paracrine factors was tested to determine their effects on gene expression of Cx40 in E11.5 cell culture. The combination of ET-1 + ANP significantly induced gene expression of Cx40 by 1.4-fold ± 0.02 ($p<0.005$, **Figure 5.12 A**). As with HCN4 gene expression, this combination resulted in higher induction than ET-1

alone, but was less than the induction caused by ANP alone ($p < 0.005$). The combination of ET-1 + NRG-1 resulted in induction of Cx40 gene expression by 1.8-fold \pm 0.1, and this was statistically significant vs. control and vs. ET-1 alone ($p < 0.005$, **Figure 5.12 B**).

However, the induction provided by this combination was similar to expression resulting from NRG-1 alone ($p = \text{NS}$). The combination of NRG-1 + ANP resulted in an induction that was additive and may perhaps also be synergistic, similar to what was seen with HCN4 gene expression analysis (**Figure 5.12 C**). Gene expression of Cx40 was increased by 2.8 \pm 0.1 ($p < 0.005$); this was significantly greater than control, NRG-1 and ANP treatment groups ($p < 0.005$). Therefore, as seen with the effect of the combination of paracrine factors on HCN4 gene expression analysis, with Cx40 gene expression, ET-1/ANP and ET-1/NRG-1 resulted in induction but was not additive, but NRG-1/ANP resulted in induction that was also additive and may also be synergistic.

We wanted to determine if all three paracrine factors together: ANP + ET-1 + NRG-1, could have an impact on the gene expression of Cx40 vs. control. Compared to control, the 3 paracrine factors together significantly increased Cx40 gene expression by 2.7-fold \pm 0.1 ($p < 0.005$, **Figure 5.12 D**). This combination was significantly greater in inducing gene expression vs. ANP, ET-1 or NRG-1 alone. It is possible that adding all three paracrine factors may have resulted in induction that was additive or synergistic.

We also tested if blockade of the NPR-A receptor with A71915 had an effect on Cx40 gene expression of ET-1 treated cells. ET-1 was combined with A71915 and Cx40 gene expression was determined. This combination resulted in a significant decrease in gene expression of Cx40 by \sim 1.8-fold (0.5 ± 0.03 , $p < 0.005$, **Figure 5.13 A**). Similar to

results seen with HCN4 gene expression, A71915 alone resulted in a greater reduction in gene expression of Cx40 vs. this combination, suggesting that ET-1 in the presence of A71915 may be playing a role in prevent the reduction of gene expression of not only HCN4, but also Cx40, to some degree. The combination of NRG-1 + A71915 was also tested to determine its effect on Cx40 gene expression. This combination resulted also in a significant reduction in gene expression by ~3.3-fold (0.3 ± 0.06 , $p < 0.005$, **Figure 5.13 B**). However, this reduction was similar to that of A71915 alone ($p = \text{NS}$). Similar to HCN4 gene expression analysis, it appears that the presence of NRG-1 with A71915 at these concentrations was not sufficient enough to revert the reduction in gene expression of Cx40 that occurred.

A. Use of ErbB Antagonist AG1478

We studied the effects of the ErbB antagonist (receptor for NRG-1) AG1478 on gene expression of HCN4 and Cx40. Neuregulins are members of the family of epidermal growth factors, and signal through receptor tyrosine kinases ErbB2, ErbB3, and ErbB4 in order to regulate proliferation, differentiation and survival of several cell types that includes CMs (Zhu et al., 2010). We chose to specifically use AG1478 based on the results of Zhu et al.'s (2010) study, where it was shown that blockade of NRG-1/ErbB signalling with AG1478 at a concentration of 10 nM, in human embryonic stem cell-derived cardiomyocytes (hESC-CMs) resulted in preferential differentiation of cells toward the working CM cell type while simultaneously reducing the proportion of nodal cells. This provides evidence that this signalling system is required for proliferation and differentiation of CMs in the developing heart. However, the use of AG1478 to study

NRG-1/ErbB signalling in the context of the developing VCS has not yet been studied, thus we decided to test the effects of this inhibitor compound on gene expression of the important VCS markers Cx40 and HCN4.

B. Use of Non-Selective ET-1 Receptor Antagonist PD145065

The effects of the ET-1 receptor non-selective antagonist PD145065 on gene expression of HCN4 and Cx40 was examined to see whether inhibition of the ET-1 receptors in the heart, ET-A and ET-B, could lead to changes in VCS gene expression. ET-1 is known to play an important role in regulating the cell cycle, and can also act on CMs to induce a premature CM transition toward terminal differentiation in the fetal heart (Paradis et al., 2014). This paper suggested that hypoxia-induced ET-1 expression can act as a stressor during fetal development to prematurely guide CMs to terminally differentiate from a mononucleate to a binucleate phenotype, which can have long-term consequences on heart development and function (Paradis et al., 2014). The use of the compound PD145065, at a concentration of 10 nM, was capable of blocking the changes in binucleation caused by ET-1, as well as attenuating the ET-1 mediated inhibitory effects on proliferation of fetal CMs (Paradis et al., 2014). However, the use of this compound in the context of studying the role of ET-1 in the formation of the VCS in the embryonic mouse heart has not yet been studied, so we chose to examine the effects of PD145065 on gene expression of HCN4 and Cx40.

E11.5 ventricular cell cultures were treated with either no treatment (negative control), ANP (1000 ng/ml; positive control), ET-1 (1.5 nM), NRG-1 (2.5 nM), PD145065 (10 nM), or AG1478 (10 μ M) and gene expression of HCN4 was determined. Since the

AG1478 compound was prepared using DMSO (while all other compounds were prepared with water), we added DMSO positive controls (Control with DMSO, ET-1 with DMSO, ANP with DMSO, and NRG-1 with DMSO) as experimental groups. There were no significant differences in gene expression of HCN4 within each treatment group prepared with or without DMSO (Control vs. Control DMSO, ANP vs. ANP DMSO, NRG-1 vs. NRG-1 DMSO, $p=NS$, **Figure 5.14**). To simplify analysis for the remainder of this section, we chose to use the paracrine factor treated with DMSO as the positive control for comparison vs. AG1478, and the paracrine factor without DMSO (water) as the positive control for comparison vs. PD145065. Compared to control, the addition of AG1478 (10 μ M) to E11.5 ventricular cell culture resulted in a significant reduction in gene expression of HCN4 by ~ 3.7 -fold (0.27 ± 0.03), and this was also significantly reduced vs. NRG-1 treatment alone ($p < 0.005$). We also tested the effects of combining ANP + AG1478 on gene expression of HCN4, and found that this combination resulted in a significant decrease vs. control by ~ 1.3 -fold (0.76 ± 0.03); this was also significantly lower than vs. ANP treatment alone ($p < 0.005$). Interestingly, although the combination of ANP + AG1478 still resulted in reduced HCN4 gene expression, the gene expression resulting from this combination was significantly greater than vs. AG1478 alone ($p < 0.005$). This raises the possibility that the presence of ANP in combination with this ErbB antagonist may rescue the decline in HCN4 gene expression, opening up the possibility for potential ANP and ErbB receptor signalling interactions in the context of the developing VCS. The last combination to be tested was ET-1 + AG1478. This also resulted in a reduction in gene expression vs. control by ~ 2.1 -fold (0.48 ± 0.06 ,

$p < 0.00005$). An interesting note is that there was a statistically significant difference between AG1478 alone vs. ET-1 + AG1478 ($p < 0.005$), indicating that ET-1 may be capable of rescuing the decline in gene expression, a similar effect to what was observed with the ANP + AG1478 combination.

We tested the same experimental groups for changes in Cx40 gene expression as well. Again, there were no significant differences in Cx40 gene expression within groups comparing DMSO to non-DMSO treated groups ($p = \text{NS}$, **Figure 5.15**). Compared to control, the use of AG1478 (10 μM) resulted in a significant decrease in Cx40 gene expression by ~ 5.9 -fold (0.17 ± 0.007) and this was also significantly lower vs. NRG-1 treatment alone ($p < 0.00005$). The combination of ANP + AG1478 significantly decreased Cx40 gene expression vs. control, by ~ 1.6 -fold (0.63 ± 0.05 , $p < 0.00005$). This combination led to a lesser decrease in gene expression vs. ANP alone, suggesting as in the case with HCN4 expression, that the presence of ANP may be rescuing the effects of this ErbB antagonist in reducing gene expression of Cx40 ($p < 0.005$). The final combination of ET-1 + AG1478 resulted in a significant decrease in Cx40 gene expression by ~ 3.4 -fold (0.29 ± 0.06 , $p < 0.005$) vs control. For Cx40 gene expression, there was no statistically significant difference between AG1478 alone vs. ET-1 + AG1478, indicating that ET-1 may not be rescuing the effects of AG1478 on reducing Cx40 gene expression, unlike the role of ANP ($p = \text{NS}$). In contrast, as noted above for HCN4 gene expression analysis, ET-1 may play a role in rescuing the effects of AG1478 in inhibiting HCN4 gene expression.

To study the effects of the non-selective ET-1 receptor antagonist PD145065 on gene expression of HCN4 and Cx40, the same experimental groups were utilized as previously mentioned. For HCN4 gene expression, again there were statistically no significant differences between groups when comparing the presence or absence of DMSO ($p=NS$, **Figure 5.16**). The addition of PD145065 (10 nM) to E11.5 ventricular cell culture resulted in a significant decrease in HCN4 gene expression vs. control ~ 2.8 -fold (0.36 ± 0.03 , $p < 0.005$). This was also significantly lower vs. ET-1 alone ($p < 0.005$). The combination of ANP + PD145065 resulted in a decrease in gene expression of HCN4 as well, by ~ 1.7 -fold (0.60 ± 0.04 , $p < 0.005$), and this was significantly lower vs. ANP treatment alone as well ($p < 0.0005$). Although the combination of ANP + PD145065 resulted in a decrease in HCN4 gene expression, this was still greater than vs. PD145065 alone ($p < 0.005$). Thus, it is possible that the presence of ANP, in combination with this non-selective ET-1 receptor antagonist, ANP may rescue the decrease in HCN4 gene expression, suggesting the potential for ANP and ET-1 receptor signalling interactions in helping to form the VCS via induction of HCN4 gene expression. The last combination that was tested was NRG-1 + PD145065, and this combination resulted in only a modest decrease in HCN4 expression vs. control by ~ 1.2 -fold (0.85 ± 0.06), however, this was not significantly different vs. control ($p=NS$). Thus, due to the presence of NRG-1, it seems that HCN4 gene expression levels were rescued almost to the level of control expression, which suggests the possibility that NRG-1/ET-1 pathway signalling interactions could be important in promoting development of the VCS via HCN4 expression. The NRG-1 + PD145065 combination resulted in gene expression that was

significantly greater vs. PD145065 alone, which further lends credibility to the possibility for signalling interactions between NRG-1/ET-1 receptor signal transduction pathways ($p < 0.005$).

The effects of PD145065 on Cx40 gene expression was also determined. Again, there were no statistically significant differences between groups treated in the presence or absence of DMSO ($p = \text{NS}$, **Figure 5.17**). Compared to control, the addition of PD145065 (10 nM) resulted in a significant decrease in Cx40 gene expression by ~ 4.6 -fold (0.22 ± 0.01 , $p < 0.005$). This was also significantly lower than the gene expression of Cx40 resulting from the addition of ET-1 alone ($p < 0.0005$). The combination of ANP + PD145065 decreased Cx40 gene expression vs. control, by ~ 2.1 -fold (0.48 ± 0.03 , $p < 0.005$); this was also significantly lower than vs. ANP treatment alone ($p < 0.005$). Again, it seems that ANP may be playing a role in rescuing the decline in gene expression of Cx40 caused by the addition of PD145065, since gene expression of Cx40 was significantly lowered with PD145065 alone vs. the combination with ANP ($p < 0.005$). The combination of NRG-1 + PD145065 resulted in a significant decrease in gene expression of Cx40 vs. control, by ~ 1.4 -fold (0.72 ± 0.07 , $p < 0.005$), unlike what was seen with HCN4 gene expression, where expression levels were similar. Thus, perhaps in the context of HCN4 gene expression, NRG-1 could be interacting with ET-1 receptors to rescue the decrease in gene expression, while it does not appear to be the case with Cx40 gene expression. The NRG-1 + PD145065 combination resulted in a greater level (although still reduced) of Cx40 gene expression vs. PD145065 alone, suggesting that

NRG-1, to some degree, could be interacting with ET-1 receptors to rescue Cx40 expression, although perhaps not to the same degree as with HCN4 gene expression.

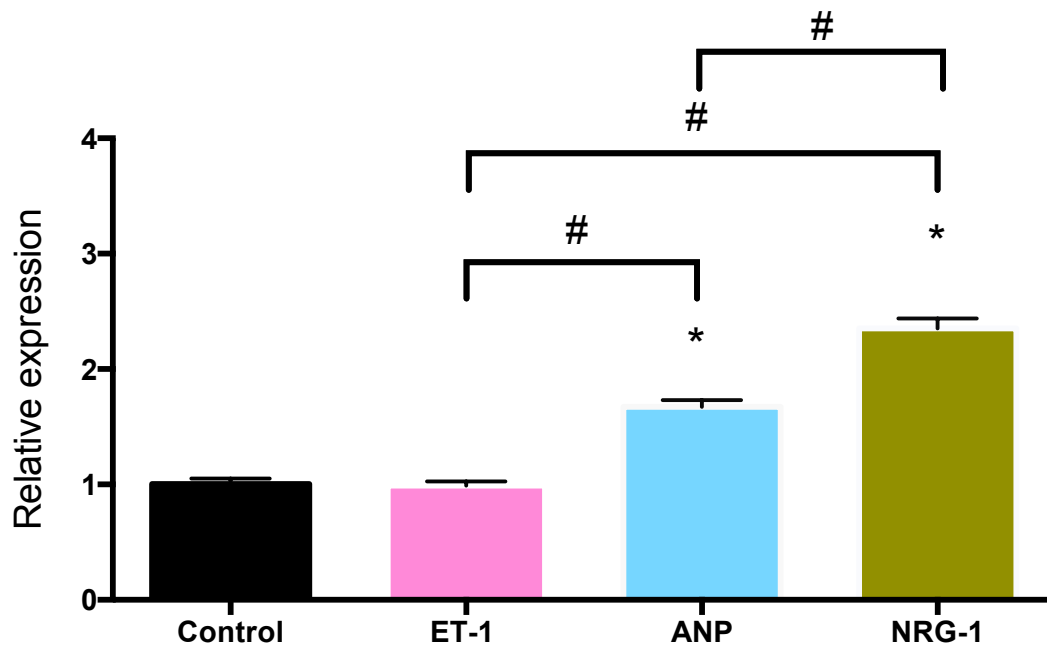


Figure 5.8. RT-qPCR analysis of HCN4 gene expression in E11.5 mouse ventricular cells following addition of ET-1 or NRG-1 over 48 hours. Compared to control, addition of ET-1 to cell culture had no significant effect on HCN4 gene expression. NRG-1 significantly increased gene expression of HCN4, and this was significantly greater than vs. ET-1 or vs. ANP alone. GAPDH was used as the housekeeping gene. N=6 experiments per group. Each bar represents mean ± SEM. *p<0.05 vs. control, #p<0.05 between groups as indicated, One-way ANOVA with Tukey's multiple comparisons post hoc test.

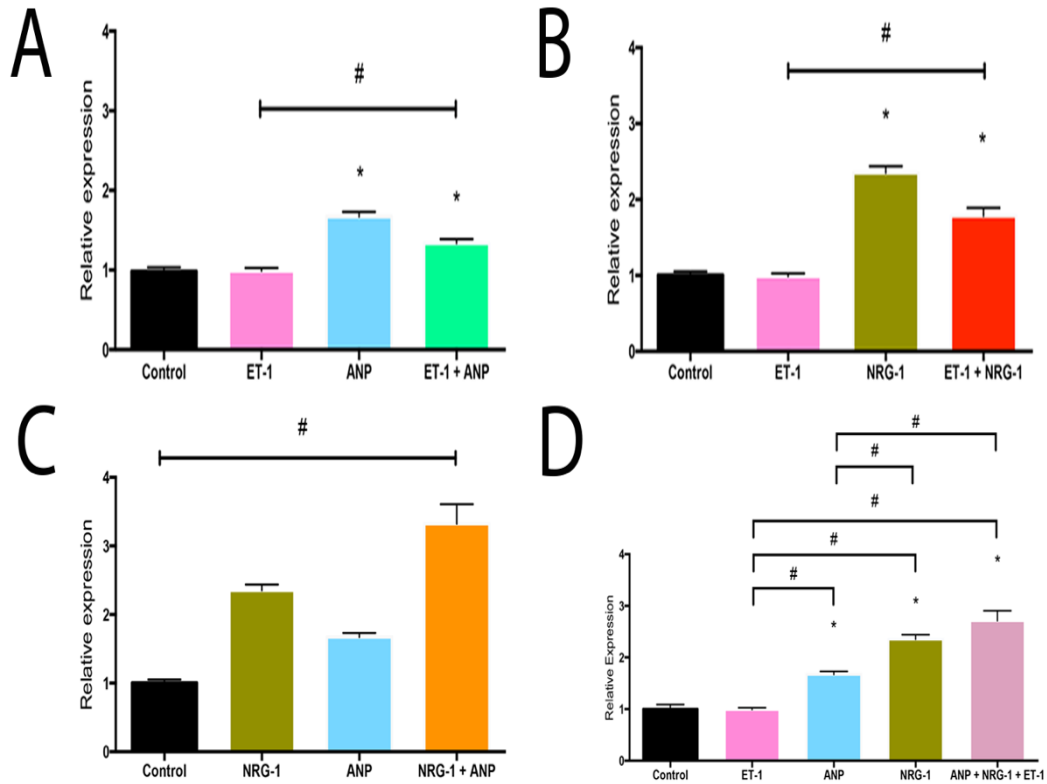


Figure 5.9. RT-qPCR analysis of HCN4 gene expression in E11.5 mouse ventricular cells following addition of combination treatments of ANP, NRG-1 and/or ET-1 over 48 hours. Cells were incubated with combinations of paracrine factors to determine if induction or additive/synergistic effects in HCN4 gene expression could occur. Cells were treated with **A)** ET-1 + ANP combination, **B)** ET-1 + NRG-1 combination, **C)** NRG-1 + ANP combination, and **D)** ANP + NRG-1 + ET-1 combination. The combinations of ET-1 + ANP and ET-1 + NRG-1 resulted in induction that was significant vs. control. The combination of NRG-1 + ANP significantly induced HCN4 gene expression and may also be additive/synergistic. The combination of ANP + NRG-1 + ET-1 significantly induced HCN4 gene expression which may be additive/synergistic. GAPDH was used as the housekeeping gene. N=6 experiments per group. Each bar represents mean \pm SEM. * $p < 0.05$ vs. control, # $p < 0.05$ between groups as indicated, One-way ANOVA with Tukey's multiple comparisons post hoc test.

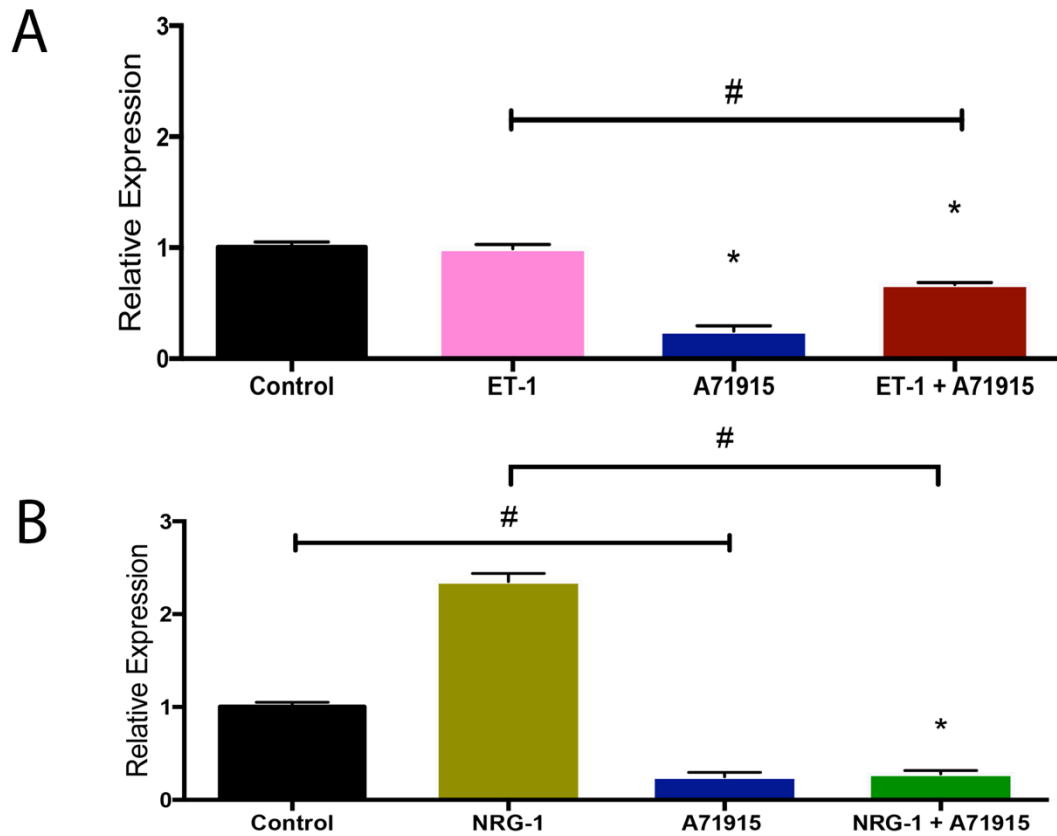


Figure 5.10. RT-qPCR analysis of HCN4 gene expression in E11.5 mouse ventricular cells following addition of ET-1 or NRG-1 in combination with A71915 over 48 hours. Cells were incubated with either ET-1 or NRG-1, in combination with A71915, to determine the effects of these paracrine factors on HCN4 gene expression upon blockade of NPR-A receptors. The combination of ET-1 + A71915 and NRG-1 + A71915 significantly reduced gene expression; in both cases the combinations were significantly lower than vs. the paracrine factors alone. Despite the presence of these paracrine factors, the decline in gene expression was not able to be reversed in combination with A71915. GAPDH was used as the housekeeping gene. N=6 experiments per group. Each bar represents mean \pm SEM. * $p < 0.05$ vs. control, # $p < 0.05$ between groups as indicated, One-way ANOVA with Tukey's multiple comparisons post hoc test.

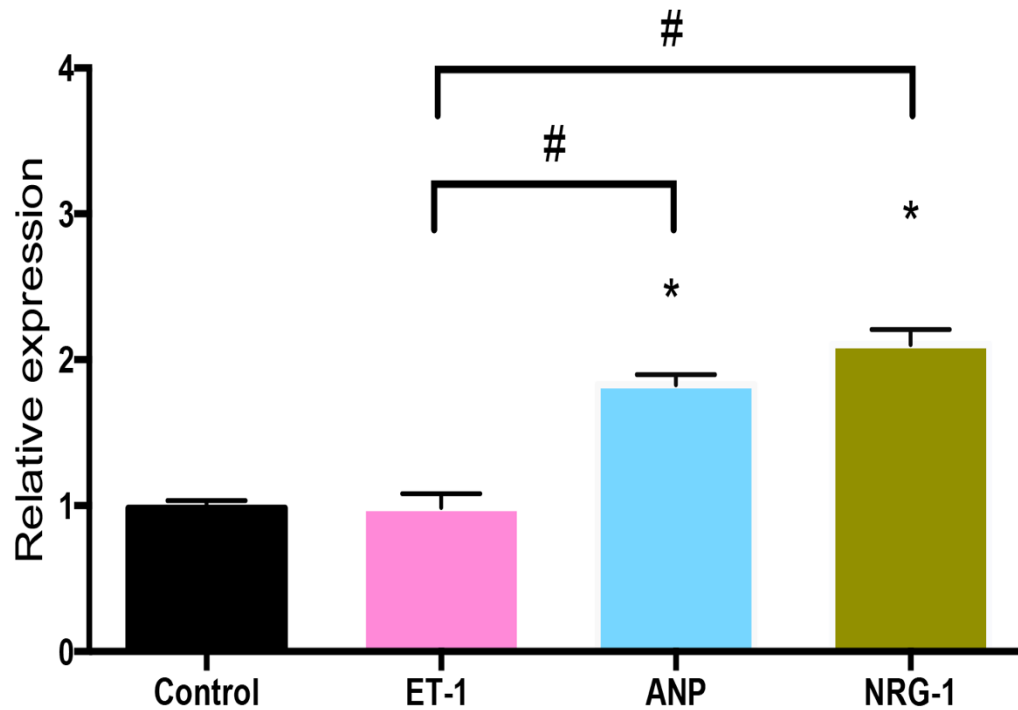


Figure 5.11. RT-qPCR analysis of Cx40 gene expression in E11.5 mouse ventricular cells following addition of ET-1 or NRG-1 over 48 hours. Compared to control, addition of ET-1 to cell culture had no significant effect on Cx40 gene expression. NRG-1 significantly increased gene expression of Cx40, and this was significantly greater than vs. ET-1 alone. GAPDH was used as the housekeeping gene. N=6 experiments per group. Each bar represents mean \pm SEM. * $p < 0.05$ vs. control, # $p < 0.05$ between groups as indicated, One-way ANOVA with Tukey's multiple comparisons post hoc test.

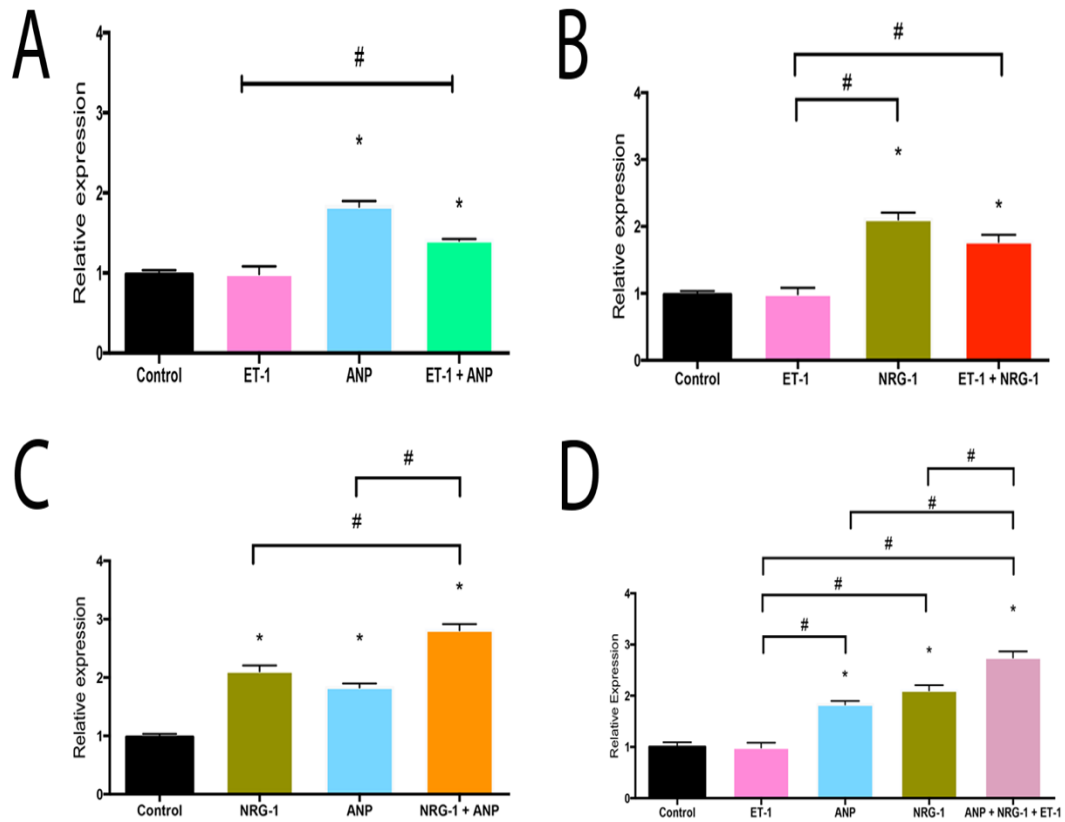


Figure 5.12. RT-qPCR analysis of Cx40 gene expression in E11.5 mouse ventricular cells following addition of combination treatments of ANP, NRG-1 and/or ET-1 over 48 hours. Cells were incubated with combinations of paracrine factors to determine if induction or additive/synergistic effects in Cx40 gene expression could occur. Cells were treated with **A)** ET-1 + ANP combination, **B)** ET-1 + NRG-1 combination, **C)** NRG-1 + ANP combination, and **D)** ANP + NRG-1 + ET-1 combination. The combinations of ET-1 + ANP and ET-1 + NRG-1 resulted in induction that was significant vs. control. The combination of NRG-1 + ANP significantly induced Cx40 gene expression and may also be additive/synergistic. The combination of ANP + NRG-1 + ET-1 significantly induced Cx40 gene expression which may be additive/synergistic. GAPDH was used as the housekeeping gene. N=6 experiments per group. Each bar represents mean \pm SEM. * $p < 0.05$ vs. control, # $p < 0.05$ between groups as indicated, One-way ANOVA with Tukey's multiple comparisons post hoc test.

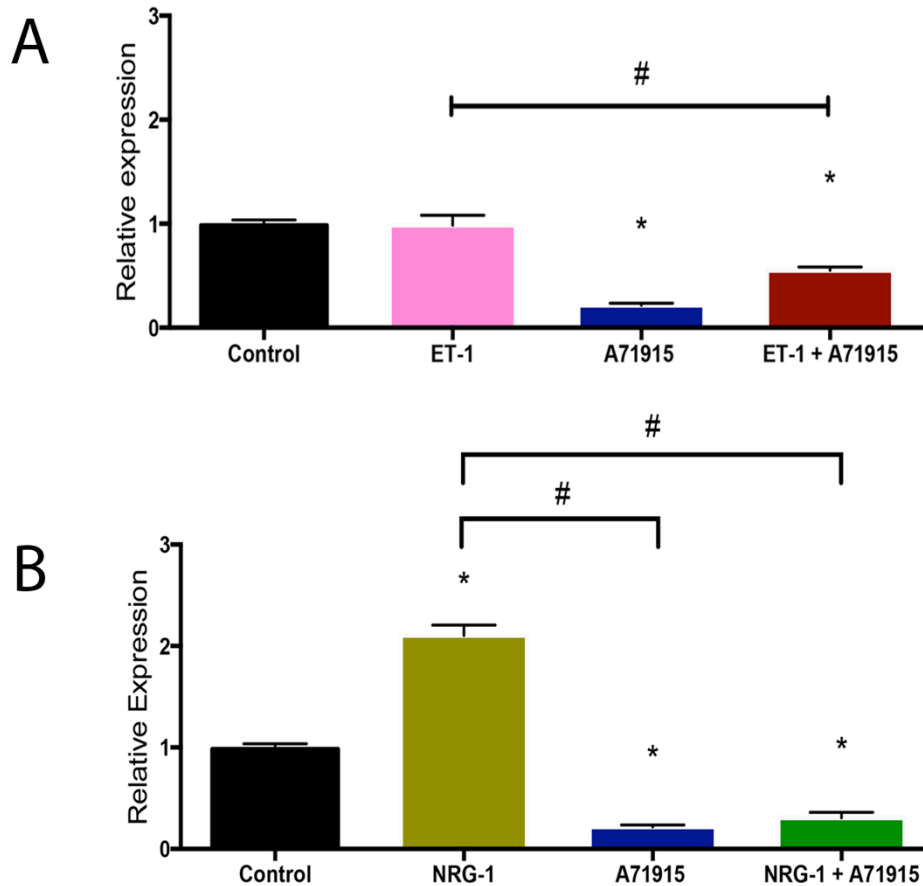


Figure 5.13. RT-qPCR analysis of Cx40 gene expression in E11.5 mouse ventricular cells following addition of ET-1 or NRG-1 in combination with A71915 over 48 hours. Cells were incubated with either ET-1 or NRG-1, in combination with A71915, to determine the effects of these paracrine factors on Cx40 gene expression upon blockade of NPR-A receptors. The combination of ET-1 + A71915 and NRG-1 + A71915 significantly reduced gene expression; in both cases the combinations were significantly lower than vs. the paracrine factors alone. Despite the presence of these paracrine factors, the decline in gene expression was not able to be reversed in combination with A71915. GAPDH was used as the housekeeping gene. N=6 experiments per group. Each bar represents mean \pm SEM. * $p < 0.05$ vs. control, # $p < 0.05$ between groups as indicated, One-way ANOVA with Tukey's multiple comparisons post hoc test.

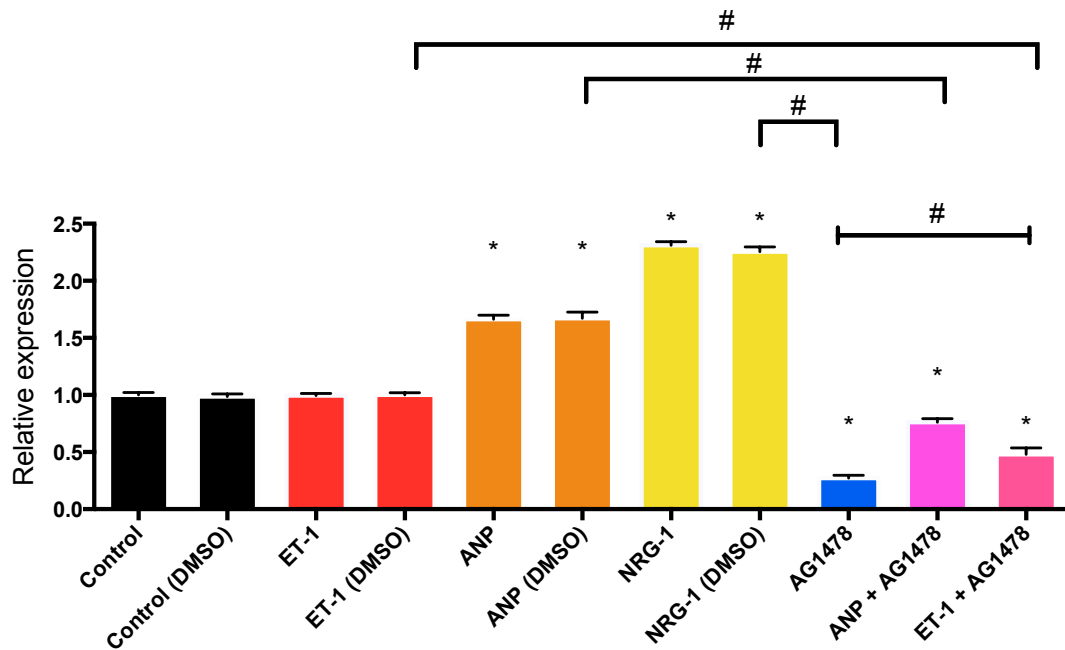


Figure 5.14. RT-qPCR analysis of HCN4 gene expression in E11.5 mouse ventricular cells following addition of ErbB receptor antagonist AG1478, and ANP or ET-1 in combination with AG1478, over 48 hours. Cells were incubated with AG1478 (10 nM) alone, or in combination with ET-1 or ANP, to determine the effects of ErbB receptor blockade on HCN4 gene expression. AG1478 significantly reduced HCN4 gene expression. When combined with ANP or with ET-1, gene expression was significantly increased vs. AG1478 alone. GAPDH was used as the housekeeping gene. Since AG1478 was prepared in DMSO, DMSO controls were tested for all experiments. N=6 experiments per group. Each bar represents mean \pm SEM. * p <0.05 vs. control, # p <0.05 between groups as indicated, One-way ANOVA with Tukey's multiple comparisons post hoc test.

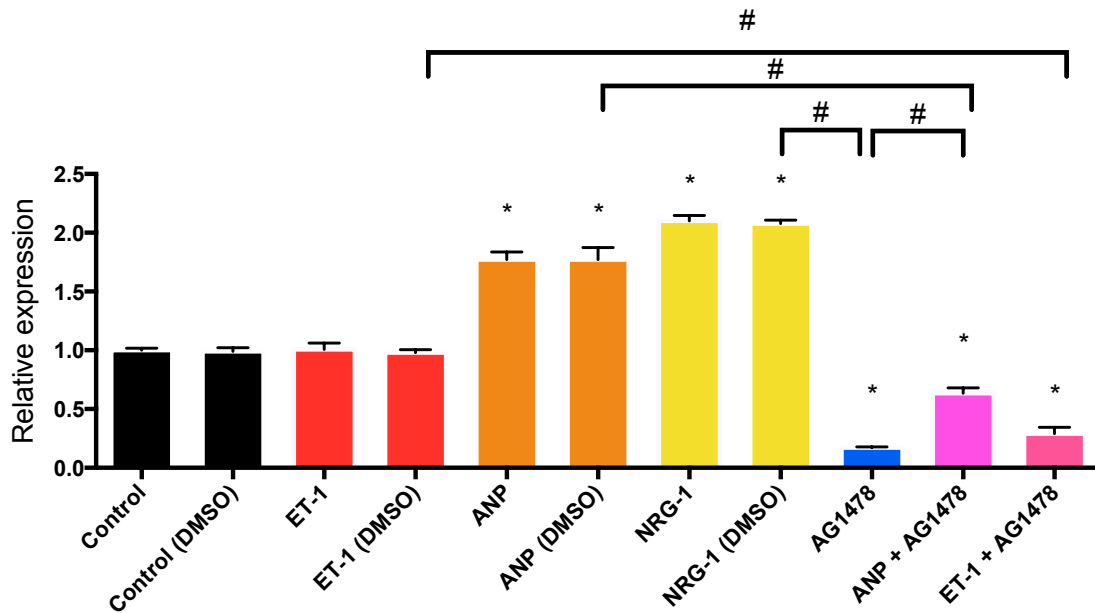


Figure 5.15. RT-qPCR analysis of Cx40 gene expression in E11.5 mouse ventricular cells following addition of ErbB receptor antagonist AG1478, and ANP or ET-1 in combination with AG1478, over 48 hours. Cells were incubated with AG1478 (10 nM) alone, or in combination with ET-1 or ANP, to determine the effects of ErbB receptor blockade on Cx40 gene expression. AG1478 significantly reduced Cx40 gene expression. When combined with ANP, gene expression was significantly increased vs. AG1478 alone. However, when combined with ET-1, gene expression remained reduced. GAPDH was used as the housekeeping gene. Since AG1478 was prepared in DMSO, DMSO controls were tested for all experiments. N=6 experiments per group. Each bar represents mean \pm SEM. * $p < 0.05$ vs. control, # $p < 0.05$ between groups as indicated, One-way ANOVA with Tukey's multiple comparisons post hoc test.

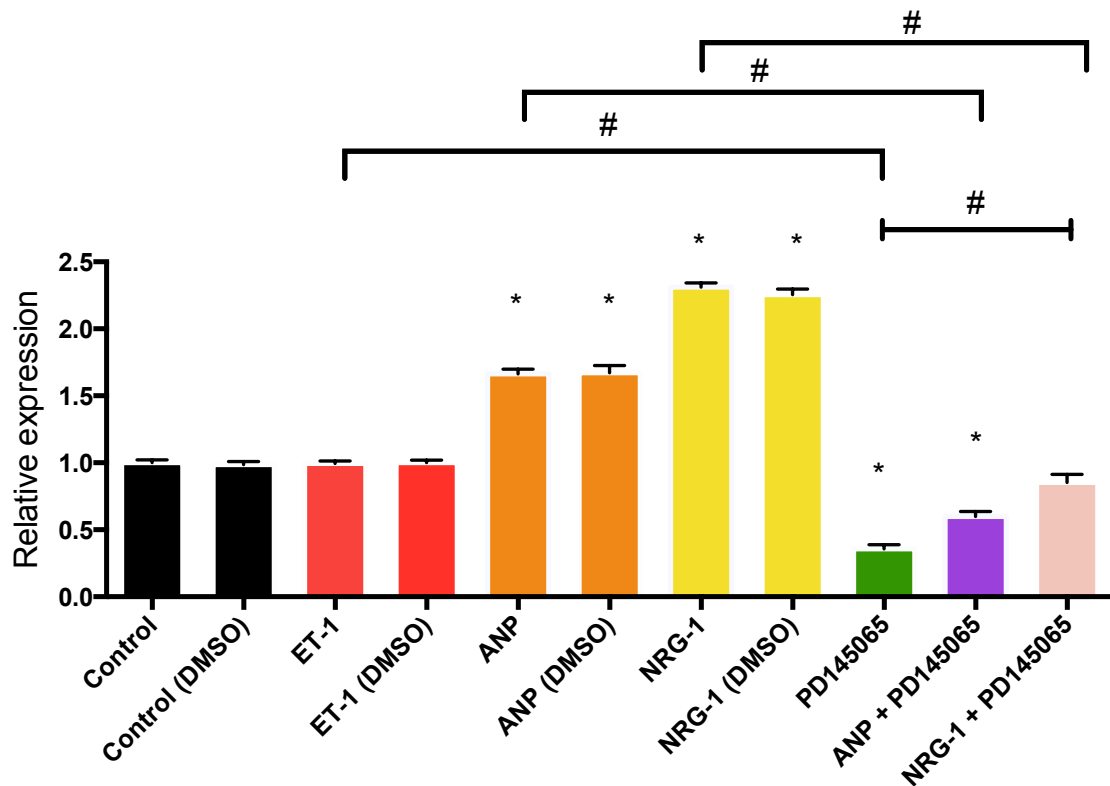


Figure 5.16. RT-qPCR analysis of HCN4 gene expression in E11.5 mouse ventricular cells following addition of non-selective ET-1 receptor antagonist PD145065, and ANP or NRG-1 in combination with PD145065, over 48 hours. Cells were incubated with PD145065 (10 μ M) alone, or in combination with NRG-1 or ANP, to determine the effects of ET-1 receptor blockade on HCN4 gene expression. PD145065 significantly reduced HCN4 gene expression. When combined with ANP or with NRG-1, gene expression was significantly increased vs. PD145065 alone. The combination of NRG-1 + PD145065 brought gene expression almost to control levels. GAPDH was used as the housekeeping gene. Since PD145065 was prepared in water, controls (with water) were tested for all experiments. N=6 experiments per group. Each bar represents mean \pm SEM. * p <0.05 vs. control, # p <0.05 between groups as indicated, One-way ANOVA with Tukey's multiple comparisons post hoc test.

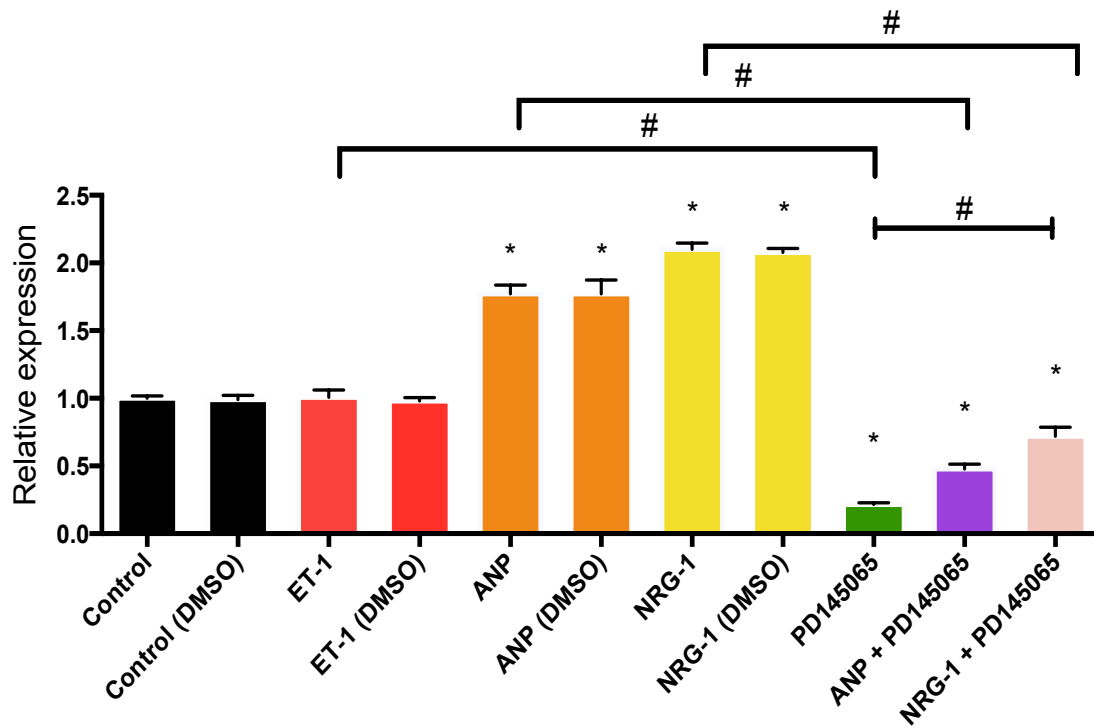


Figure 5.17. RT-qPCR analysis of Cx40 gene expression in E11.5 mouse ventricular cells following addition of non-selective ET-1 receptor antagonist PD145065, and ANP or NRG-1 in combination with PD145065, over 48 hours. Cells were incubated with PD145065 (10 μ M) alone, or in combination with NRG-1 or ANP, to determine the effects of ET-1 receptor blockade on Cx40 gene expression. PD145065 significantly reduced Cx40 gene expression. When combined with ANP or with NRG-1, gene expression was significantly increased vs. PD145065 alone. GAPDH was used as the housekeeping gene. Since PD145065 was prepared in water, controls (with water) were tested for all experiments. N=6 experiments per group. Each bar represents mean \pm SEM. * p <0.05 vs. control, # p <0.05 between groups as indicated, One-way ANOVA with Tukey's multiple comparisons post hoc test.

5.3.3 Effects of ET-1 and NRG-1 on Intracellular Production of cGMP in E11.5 Mouse Ventricular Cells

To determine whether there is a potential for signalling interactions between NPR-A and ET-1 or NRG-1 signalling pathways with respect to HCN4 and Cx40 gene expression, we chose to measure intracellular cGMP levels in E11.5 ventricular cells upon addition of either ET-1 or NRG-1, and their respective inhibitors in the presence or absence of ANP. This was performed using the competitive immunoassay as previously described (**Figure 2.3**).

First, we designed a set of experiments to determine if each of the paracrine factors alone could alter cGMP levels within E11.5 ventricular cells. In this experiment, we also investigated the impact of adding ANP in combination with either ET-1 or NRG-1 and if that could impact cGMP signalling, and also the combinations of the NPR-A antagonist A71915 with either ET-1 or NRG-1. To determine the potential impact of ET-1 on cGMP signalling, cells were stimulated with either no treatment, ET-1 (1.5 nM) alone, ANP (1000 ng/ml) + ET-1 (1.5 nM), A71915 (1 μ M) alone, or ET-1 (1.5 nM) + A71915 (1 μ M). The basal level of cGMP was measured to be 28.5 ± 0.6 nM per 100,000 cells (**Figure 5.18**). Compared to control, the addition of ET-1 did not significantly alter cGMP production ($p=NS$). The combination of ANP + ET-1 resulted in a significant increase in cGMP production (35.8 ± 0.2 nM, $p<0.005$). The addition of A71915 alone, which served as a control, significantly decreased cGMP production (22.7 ± 0.4 nM, $p<0.005$). The combination of ET-1 + A71915 also resulted in a significant decrease in cGMP production that was significantly less vs. control and vs. ET-1 treatment alone (26.7 ± 0.1 nM,

$p < 0.05$). This suggests that ET-1 may not be playing a role in rescuing the decline in cGMP production provided by the presence of A71915.

To determine the potential impact of NRG-1 on cGMP signalling, cells were stimulated with either no treatment, NRG-1 (2.5 nM) alone, ANP (1000 ng/ml) + NRG-1 (2.5 nM), A71915 (1 μ M) alone, or NRG-1 (2.5 nM) + A71915 (1 μ M). The basal level of cGMP was measured to be 28.5 ± 0.6 nM per 100,000 cells (**Figure 5.19**). The addition of NRG-1 significantly increased cGMP production vs. control (40.2 ± 1.1 nM, $p < 0.005$). The combination of ANP + NRG-1 also increased cGMP production vs. control (41.9 ± 0.8 nM, $p < 0.005$) although this was not different vs. NRG-1 treatment alone. The addition of A71915 alone, which served as a control, significantly decreased cGMP production vs. control (21.9 ± 1.4 nM, $p < 0.005$). The combination of NRG-1 + A71915 resulted in a similar level of cGMP production as control ($p = \text{NS}$). This suggests the possibility that the presence of NRG-1 in combination with the NPR-A antagonist A71915 may be rescuing the decline in cGMP production provided by the antagonist. This combination (26.5 ± 0.7 nM) was significantly lower in cGMP production vs. NRG-1 alone ($p < 0.05$).

We also sought to determine if the NRG-1/ErbB receptor antagonist AG1478 could have an impact on cGMP production in E11.5 ventricular cells. Cells were treated with either no treatment (negative control), ANP (1000 ng/ml; positive control), ET-1 (1.5 nM), or NRG-1 (2.5 nM), with and without DMSO. Cells were also treated with AG1478 (10 μ M), and the combinations of ANP + AG1478, and ET-1 + AG1478. To simplify analysis for the remainder of this section, we chose to use the paracrine factor treated with DMSO as the positive control for comparison vs. AG1478, and the paracrine

factor without DMSO (water) as the positive control for comparison vs. PD145065.

There were no significant differences in cGMP production within groups treated with or without DMSO ($p=NS$, **Figure 5.20**). The baseline level of cGMP measured was 29.9 ± 0.4 nM per 100,000 cells. Compared to control, the addition of AG1478 (10 μ M) to cells resulted in a significant decrease in cGMP production (20.0 ± 0.1 nM, $p<0.005$) and this was also significantly less than NRG-1 treatment alone ($p<0.005$). Interestingly, the combination of ANP + AG1478 resulted in merely a modest decrease in cGMP production vs. control (29.4 ± 0.6 nM) that was not significantly different ($p=NS$).

Therefore, due to the presence of ANP, it appears that when added in combination with AG1478, cGMP production seems to be rescued almost to the control level of cGMP production, thus it is possible that ANP/ErbB signalling may converge on cGMP signalling to potentially alter development of the VCS. The ANP + AG1478 combination resulted in cGMP production that was significantly greater than AG1478 alone, further indicating that ANP may play an important role in interacting with ErbB receptors to promote formation of the VCS ($p<0.005$). The combination of ET-1 + AG1478 was also tested on production of cGMP. This led to a decrease in cGMP that was significantly less than control (20.4 ± 0.4 nM, $p<0.005$). However, compared to AG1478 alone, this combination was similar in cGMP levels ($p=NS$), indicating that the presence of ET-1 may not be sufficient enough to rescue the decrease in cGMP levels due to AG1478.

Lastly, we wanted to determine the potential impact of the ET-1 non-selective receptor antagonist PD145065 on cGMP production in E11.5 ventricular cells, using the same experimental groups as above, which could provide some insight into potential

signalling interactions between ANP, ET-1, NRG-1 and their receptors. Again, there were no significant differences within groups comparing treatment with DMSO to treatment without ($p=NS$). The baseline level of cGMP measured was 30.0 ± 0.4 nM. Compared to control, PD145065 (10 nM) significantly decreased cGMP levels (21.0 ± 0.4 nM, $p<0.005$, **Figure 5.21**); this was also significantly less than ET-1 treatment alone ($p<0.005$). The combination of ANP + PD145065 resulted in a significant decrease in cGMP vs. control (22.4 ± 0.4 nM, $p<0.005$), meaning that ANP may not have been able to rescue the decline in cGMP by PD145065. Indeed, when comparing the cGMP levels measured with PD145065 alone vs. ANP + PD145065, there were no significant differences ($p=NS$). NRG-1 + PD145065 was also tested; this combination led to modest decrease in cGMP (28.7 ± 0.8 nM) which was similar to control levels of cGMP ($p=NS$), suggesting the possibility that the presence of NRG-1 with PD145065 may be rescuing the decline in cGMP, bringing it almost to the level of control. To support this, this combination of NRG-1 + PD145065 resulted in significantly greater in cGMP production vs. PD145065 alone ($p<0.005$); thus it is possible that NRG-1/ET-1 receptor signalling may converge upon cGMP signalling as a means to promote development of the VCS in the embryonic mouse heart.

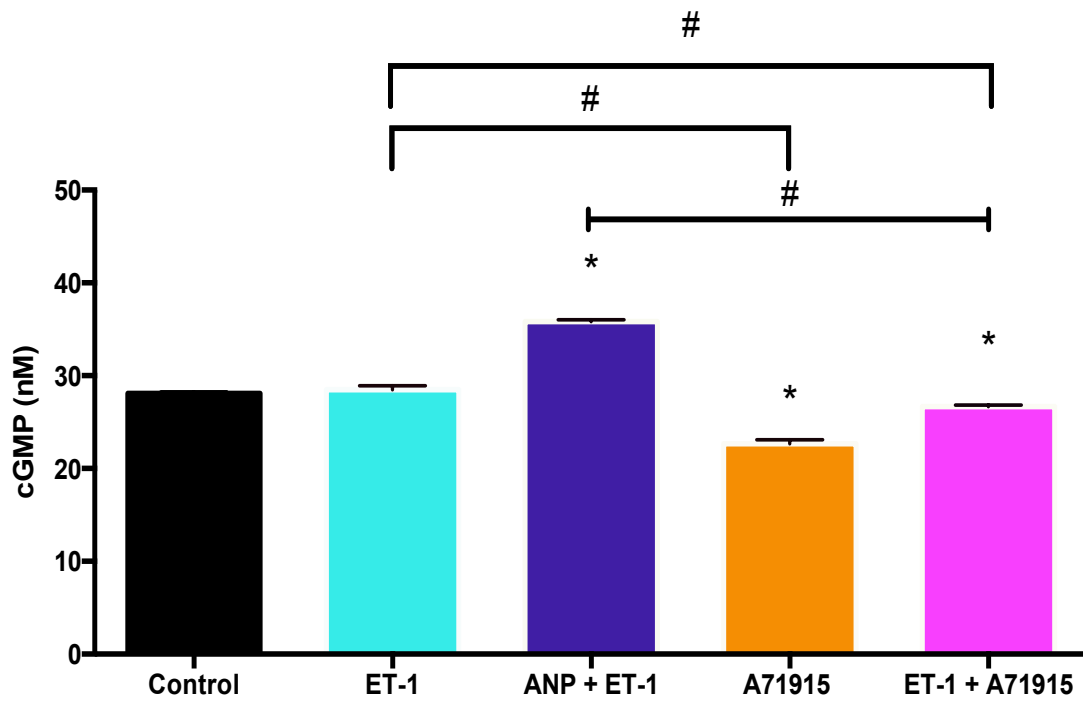


Figure 5.18. The effects of ET-1 on cGMP production in E11.5 ventricular cells. The effects of ET-1 on intracellular cGMP production were determined by stimulating isolated E11.5 cells with ET-1 (1.5 nM), then measuring cGMP using a competitive immunoassay. The baseline level of cGMP was measured to be 28.5 ± 0.6 nM per 100,000 cells. Addition of ET-1 did not significantly change cGMP vs. control. However, the combination of ET-1 + A71915 resulted in a significant reduction in cGMP levels vs. control and vs. ET-1 alone. N=6 independent experiments, performed in duplicate wells. Each bar represents mean \pm SEM. * $p < 0.05$ vs. control, # $p < 0.05$ between groups as indicated, One-way ANOVA with Tukey post hoc test.

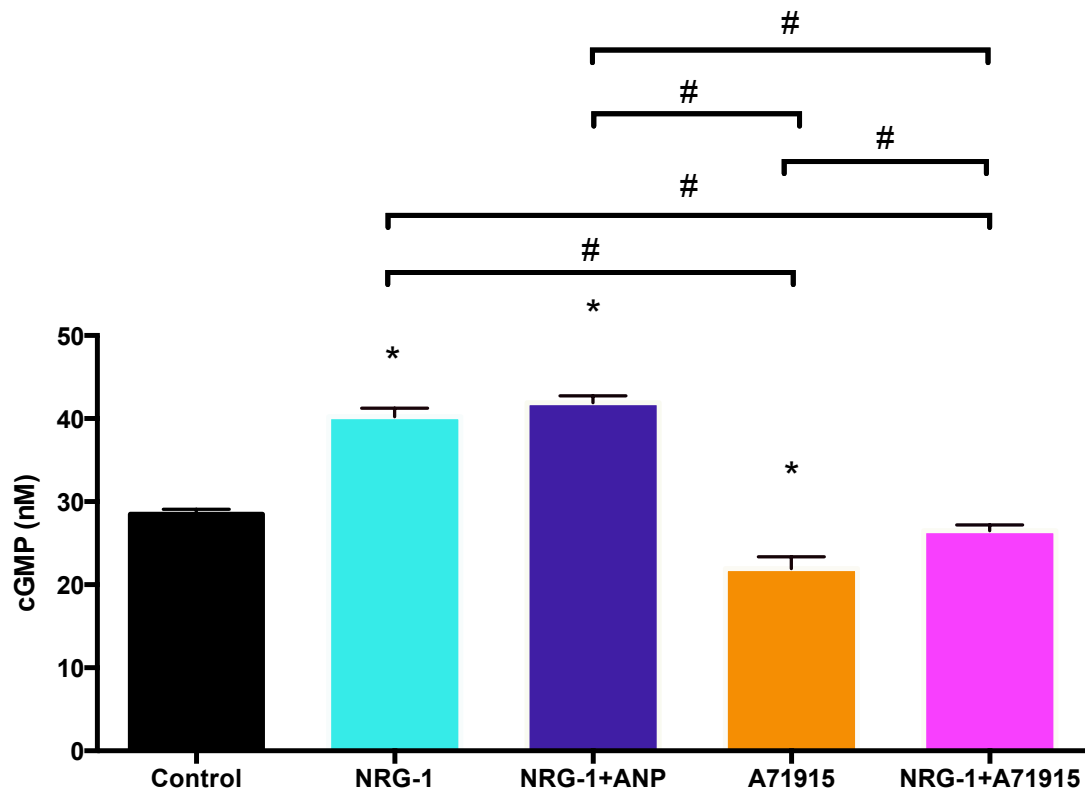


Figure 5.19. The effects of NRG-1 on cGMP production in E11.5 ventricular cells. The effects of NRG-1 on intracellular cGMP production were determined by stimulating isolated E11.5 cells with NRG-1 (2.5 nM), then measuring cGMP using a competitive immunoassay. The baseline level of cGMP was measured to be 28.5 ± 0.6 nM per 100,000 cells. Addition of ET-1 did not significantly change cGMP vs. control. However, the combination of ET-1 + A71915 resulted in a significant reduction in cGMP levels vs. control and vs. ET-1 alone. N=6 independent experiments, performed in duplicate wells. Each bar represents mean \pm SEM. * $p < 0.05$ vs. control, # $p < 0.05$ between groups as indicated, One-way ANOVA with Tukey post hoc test.

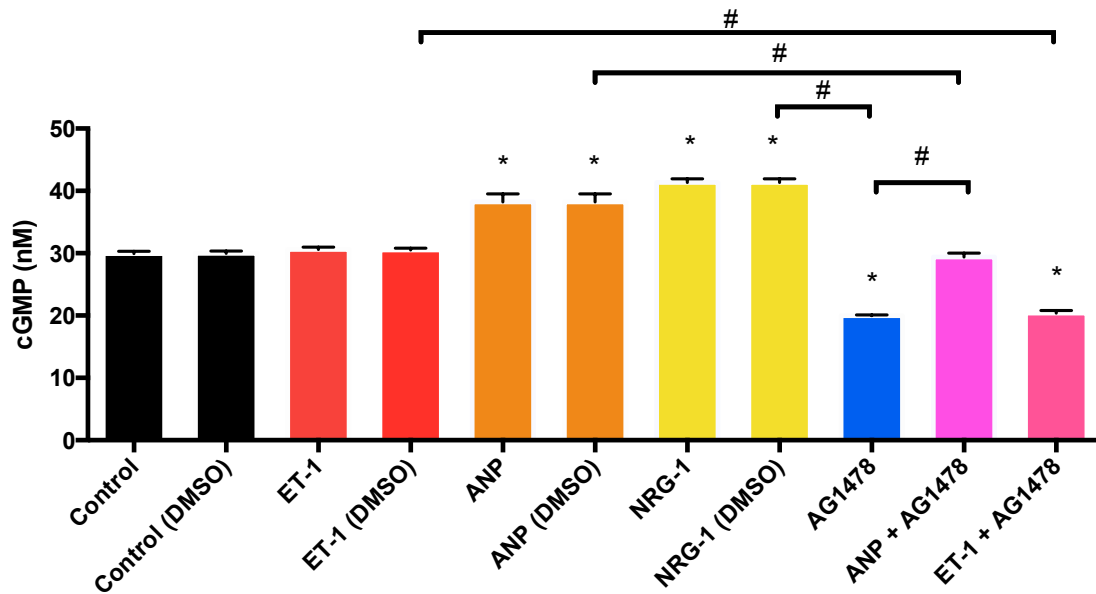


Figure 5.20. The effects of AG1478 on cGMP production in E11.5 ventricular cells. The effects of AG1478 (10 nM) on intracellular cGMP production were determined by stimulating isolated E11.5 cells with AG1478 alone, and also in combination with either ANP or ET-1, then measuring cGMP using a competitive immunoassay. The baseline level of cGMP was measured to be 29.9 ± 0.4 nM per 100,000 cells. AG1478 significantly reduced cGMP levels. ANP was able to significantly elevate this reduction in cGMP when added in combination with AG1478. When ET-1 was added with AG1478, cGMP levels were similar to that of AG1478 alone, suggesting that ET-1 may not have an effect in rescuing the decrease in cGMP. N=6 independent experiments, performed in duplicate wells. Each bar represents mean \pm SEM. * $p < 0.05$ vs. control, # $p < 0.05$ between groups as indicated, One-way ANOVA with Tukey post hoc test.

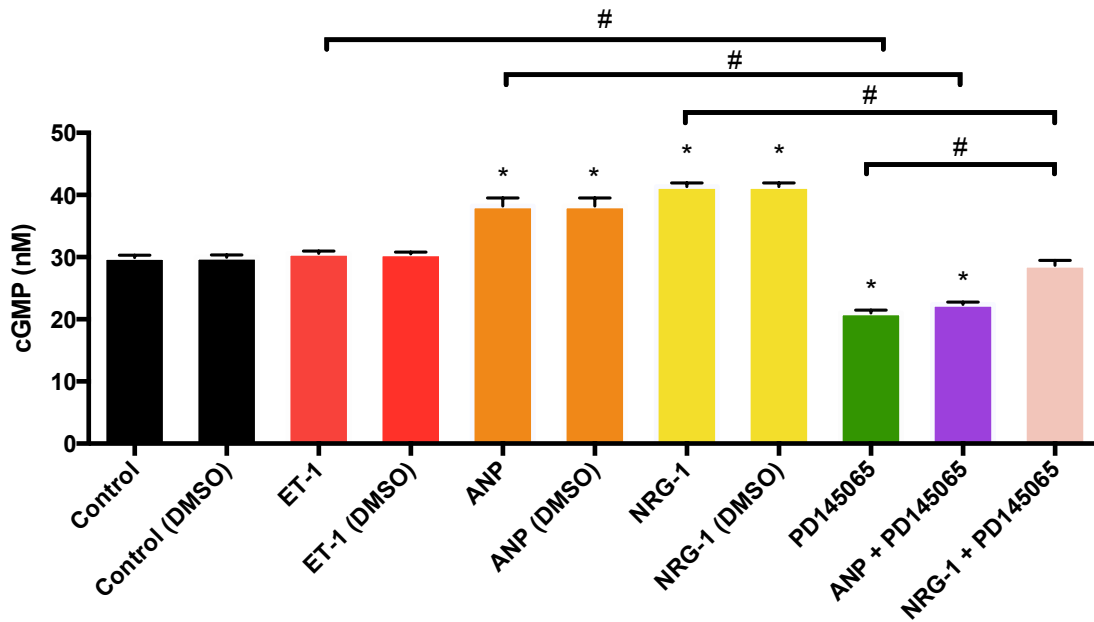


Figure 5.21. The effects of PD145065 on cGMP production in E11.5 ventricular cells. The effects of PD145065 (10 μ M) on intracellular cGMP production were determined by stimulating isolated E11.5 cells with PD145065 alone, and also in combination with either ANP or NRG-1, then measuring cGMP using a competitive immunoassay. The baseline level of cGMP was measured to be 30.0 ± 0.4 nM per 100,000 cells. PD145065 significantly reduced cGMP levels. ANP was able to significantly elevate this reduction in cGMP when added in combination with AG1478. When NRG-1 was added with AG1478, cGMP levels increased almost to the level of control. Therefore, ANP and NRG-1 may have rescued the decline in cGMP from AG1478. N=6 independent experiments, performed in duplicate wells. Each bar represents mean \pm SEM. * $p < 0.05$ vs. control, # $p < 0.05$ between groups as indicated, One-way ANOVA with Tukey post hoc test.

5.3.4 Comparative Effects of ANP, ET-1 and NRG-1 on Cardiomyocyte Hypertrophy in E11.5 Mouse Ventricular Cells

Several studies have indicated that ANP may play an important role in limiting hypertrophy in the heart, since mice that lacked NPR-A had enlarged hypertrophic hearts, whereas mice that overexpressed ANP had smaller hearts (Steinhilper et al., 1990). In contrast, ET-1 has been shown to induce hypertrophic growth in CMs (Zhao et al., 1998, Nishida et al., 1993, Shubeita et al., 1990, Fischer et al., 1997). NRG-1 has been shown to be essential for development of the myocardial trabeculae and cardiac morphogenesis by promoting the proliferation, survival, and maturation of CMs, and was capable of inducing hypertrophic growth in both neonatal and adult ventricular myocytes (Zhao et al., 1998). However, despite the evidence that these three paracrine factors play regulatory roles in cardiac hypertrophy in the neonatal and adult heart, there is little evidence to describe a potential role for ANP, ET-1, or NRG-1 to influence hypertrophy of embryonic CMs.

Briefly, E11.5 ventricular cells were cultured from pregnant CD1 mice for 20 hours, followed by incubation with either ANP (1000 ng/ml), ET-1 (1.5 nM), or NRG-1 (2.5 nM), their respective inhibitors alone: A71915 (1 μ M), PD145065 (10 nM) or AG1478 (10 μ M), and lastly, combinations of paracrine factors with their respective receptor inhibitors, every 12 hours for a period of 48 hours (similar dosing protocol as with previous immunofluorescence and RT-qPCR experiments). Then, cells were immunolabelled with MF20 to identify CMs in culture. Lastly, cell area was determined for each treatment group. (**Figure 5.22**). Treatment of cells with ANP or A71915 did not significantly alter cell area vs. control (p =NS, **Figure 5.22 A**). However, treatment with

A71915 resulted in increased cell area vs. ANP ($63004 \pm 2016 \mu\text{m}^2$ vs. $42664 \pm 6179 \mu\text{m}^2$, $p < 0.05$). The combination of ANP + A71915 did not significantly alter cell area vs. control ($p = \text{NS}$). There were no significant differences in cell area with A71915 treatment alone vs. the combination treatment of ANP + A71915 ($p = \text{NS}$). In contrast, ET-1 treatment significantly increased cell area vs. control ($98653 \pm 7685 \mu\text{m}^2$, $p < 0.005$, **Figure 5.22 B**). The non-selective ET-1 receptor inhibitor, PD145065 did not significantly alter cell area vs. control ($p = \text{NS}$); however, PD145065 treatment significantly decreased cell area vs. ET-1 alone (43547 ± 1203 vs. $98653 \pm 7685 \mu\text{m}^2$, $p < 0.005$). The combination of ET-1 + PD145065 did not significantly alter cell area vs. control ($p = \text{NS}$); however, the cell area resulting from this combination was significantly reduced vs. ET-1 alone ($p < 0.005$). There were no significant differences in cell area with PD145065 treatment alone vs. the combination treatment of ET-1 + PD145065 ($p = \text{NS}$). The addition of NRG-1 to cells significantly increased cell area vs. control ($80255 \pm 6620 \mu\text{m}^2$, $p < 0.005$, **Figure 5.22 C**). Treatment with the ErbB receptor antagonist AG1478 did not significantly alter cell area vs. control ($p = \text{NS}$); however, AG1478 treatment significantly decreased cell area vs. NRG-1 alone (40680 ± 1051 vs. $80255 \pm 6620 \mu\text{m}^2$, $p < 0.005$). The combination of NRG-1 + AG1478 did not significantly alter cell area vs. control ($p = \text{NS}$); however, the cell area resulting from this combination was significantly reduced vs. NRG-1 alone ($p < 0.00005$). There were no significant differences in cell area with AG1478 treatment alone vs. the combination treatment of NRG-1 + AG1478 ($p = \text{NS}$).

Overall, it appears that ANP may not have a significant impact on cell size of E11.5 CMs, whereas ET-1 and NRG-1 may induce hypertrophy in CMs. Blockade of the

NPR-A receptor may promote hypertrophy in these E11.5 CMs, since cell area significantly increased vs. ANP, however this was still similar to control cell area. Blockade of PD145065 or AG1478 may be anti-hypertrophic; and when used in combination with their respective paracrine factors, it appears that the overall net effect, at these concentrations, may be anti-hypertrophic.

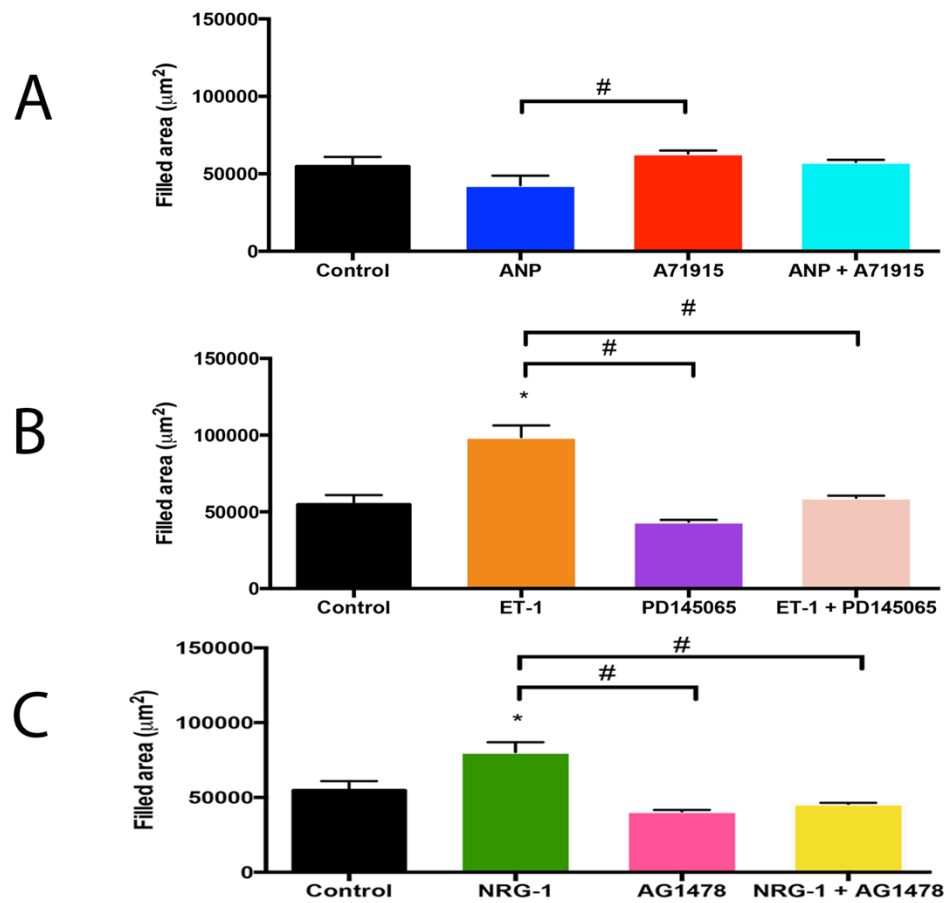


Figure 5.22. Effects of ANP, ET-1, and NRG-1 on cardiac hypertrophy of CMs of E11.5 ventricular cells. E11.5 ventricular cells were treated with ANP (1000 ng/ml), ET-1 (1.5 nM), or NRG-1 (2.5 nM) for 48 hours and were then immunolabelled with sarcomeric myosin (MF20) for detection of CMs. The cell size/area of CMs were determined per treatment group. **A)** ANP had no effect on cell area of CMs; **B)** ET-1 significantly increased cell area of CMs; **C)** NRG-1 significantly increased cell area CMs. Inhibition of NPR-A receptors with A71915, ET-1 receptors with PD145065, and ErbB receptors with AG1478 did not significantly alter cell area vs. control. N=40 cells per group. Each bar represents mean \pm SEM. * $p < 0.05$ vs. control, # $p < 0.05$ between groups as indicated, One-way ANOVA with Tukey post hoc test.

5.3.5 Effects of Rp-8-pCPT-cGMPS on Gene Expression of HCN4 and Cx40 in E11.5 Ventricular Cells in Combination with ET-1 or NRG-1

We previously determined that the ANP/NPR-A/cGMP pathway was biologically active at E11.5 in the embryonic mouse heart (Section 3.3.3), and that increased production of intracellular cGMP due to the binding of ANP to NPR-A led to significant induction of the gene expression of VCS markers Cx40 and HCN4, indicating that development of the VCS may proceed through this pathway. In Section 5.3.3, we investigated the possible role of cGMP signalling in the ET-1/ET receptor and NRG-1/ErbB receptor signal transduction pathways, and also whether cGMP signalling could play a role in potential signalling interactions between ANP, ET-1, NRG-1 and their cognate receptors. Next, we wanted to determine if a downstream target of cGMP signalling, protein kinase G (PKG) could affect Cx40 and/or HCN4 gene expression, when E11.5 ventricular cells were incubated with ET-1 or NRG-1. To do this, we blocked PKG with a PKG inhibitor (Rp-8-pCPT-cGMPS), which is a competitive, reversible cGMP-dependent PKG inhibitor compound that behaves as a cGMP analogue. If cGMP signalling is involved with these other paracrine factors, by inhibiting PKG, this should reduce gene expression of Cx40 and HCN4. If cGMP signalling was not involved with these two paracrine factors, then blockade of PKG should either have little or no effect on Cx40/HCN4 gene expression. Rp-8-pCPT-cGMPS (100 μ M) was added to E11.5 ventricular cell culture every 12 hours for a period of 24 hours, in the presence or absence of ET-1 or NRG-1, and gene expression of HCN4 and Cx40 were measured with RT-qPCR. We also tested the effects of the non-selective ET receptor antagonist PD145065 (10 μ M) or the ErbB receptor antagonist AG1478 (10 nM), in combination

with Rp-8-pCPT-cGMPS on gene expression of these genes. For all experiments below, cells were treated with Rp-8-pCPT-cGMPS alone (positive control), and HCN4 and Cx40 gene expression were found to be reduced to similar levels as seen previously in Section 3.3.11.

To determine whether PKG could be involved in potential ET-1/ET-1 receptor-mediated changes to HCN4 gene expression, we tested the effects of the combination of ET-1 + Rp-8-pCPT-cGMPS on gene expression, resulting in a similar level of gene expression vs. control and vs. ET-1 alone ($p=NS$, **Figure 5.23 A**). However, this combination induced higher HCN4 expression vs. Rp-8-pCPT-cGMPS alone (0.69 ± 0.32 vs. 0.25 ± 0.02 , $p<0.05$). This seems to suggest that the presence of ET-1, in combination with Rp-8-pCPT-cGMPS, may have been able to rescue the decline in gene expression provided by the PKG inhibitor alone. To determine whether simultaneous blockade of PKG and blockade of ET-1 receptors could synergistically alter HCN4 gene expression, we tested the effects of the combination of PD145065 + Rp-8-pCPT-cGMPS on gene expression, resulting in a significant reduction in HCN4 gene expression by ~ 4.6 -fold (0.22 ± 0.005 , $p<0.05$). However, this was similar to the level of gene expression provided by either PD145065 treatment or Rp-8-pCPT-cGMPS treatment alone ($p=NS$). Therefore, there does not appear to be any additive/synergistic effects offered by combining blockade of ET receptors + blockade of PKG with respect to changes in gene expression of HCN4.

To determine whether PKG could be involved in potential NRG-1/ErbB receptor-mediated changes to HCN4 gene expression, we tested the effects of the combination of

NRG-1 + Rp-8-pCPT-cGMPS on HCN4 gene expression, which resulted in a similar gene expression level of HCN4 as control ($p=NS$, **Figure 5.23 B**). However, this combination significantly reduced HCN4 gene expression vs. NRG-1 alone (0.98 ± 0.04 vs. 2.18 ± 0.14 , $p<0.00005$). Also, this combination significantly increased HCN4 gene expression vs. Rp-8-pCPT-cGMPS alone (0.98 ± 0.04 vs. 0.25 ± 0.02 , $p<0.00005$). This suggests that the presence of NRG-1, in combination with the PKG inhibitor, may have been able to alleviate the decrease in gene expression caused by the inhibitor alone. To determine whether simultaneous blockade of PKG and blockade of ErbB receptors could synergistically alter HCN4 gene expression, we tested the effects of the combination of AG1478 + Rp-8-pCPT-cGMPS on HCN4 gene expression, resulting in a significant reduction in gene expression, by ~ 9.6 -fold (0.10 ± 0.004 , $p<0.00005$). However, this was similar to the level of gene expression provided by either AG1478 treatment or Rp-8-pCPT-cGMPS treatment alone ($p=NS$). Therefore, there does not seem to be any additive/synergistic effects provided by combining blockade of ErbB receptors + blockade of PKG with respect to changes in the gene expression of HCN4.

To determine whether PKG could be involved in potential ET-1/ET-1 receptor-mediated changes to Cx40 gene expression, we tested the effects of the combination of ET-1 + Rp-8-pCPT-cGMPS, resulting in a significant decrease in gene expression by ~ 7.8 -fold (0.13 ± 0.006 , $p<0.00005$) vs. control; this was also significantly lower than vs. ET-1 treatment alone (**Figure 5.24 A**). However, this combination did not significantly alter Cx40 gene expression vs. Rp-8-pCPT-cGMPS alone ($p=NS$). This seems to suggest that in terms of Cx40 gene expression, the presence of ET-1 in combination with the PKG

inhibitor was insufficient to alter the already reduced gene expression provided by the PKG inhibitor itself. To test whether simultaneous blockade of PKG and ET-1 receptors could synergistically alter Cx40 gene expression, the effects of the combination of PD145065 + Rp-8-pCPT-cGMPS on Cx40 gene expression was tested, resulting in significant reduction of Cx40 gene expression by ~8.6-fold (0.12 ± 0.003 , $p < 0.005$) vs. control. However, this was similar to the reduction in gene expression provided by either PD145065 alone or Rp-8-pCPT-cGMPS alone ($p = \text{NS}$), thus there does not seem to be any additive/synergistic effects in combining blockade of ET-1 receptors + blockade of PKG with regards to the gene expression of Cx40.

To determine whether PKG could be involved in potential NRG-1/ErbB receptor-mediated changes to Cx40 gene expression, we tested the effects of the combination of NRG-1 + Rp-8-pCPT-cGMPS on Cx40 gene expression (**Figure 5.24 B**). Compared to control, this combination resulted in a similar level of gene expression ($p = \text{NS}$), but this combination greatly reduced Cx40 gene expression vs. NRG-1 treatment alone (0.97 ± 0.09 vs. 2.07 ± 0.08 , $p < 0.00005$). This combination increased Cx40 gene expression vs. Rp-8-pCPT-cGMPS treatment alone (0.97 ± 0.09 vs. 0.26 ± 0.006 , $p < 0.00005$). The presence of NRG-1 may have been able to alleviate the decrease in gene expression of Cx40 caused by the PKG inhibitor alone. Next, we wanted to test the effects of combined blockade of PKG and blockade of ErbB receptors using the combination of AG1478 + Rp-8-pCPT-cGMPS, on Cx40 gene expression. Compared to control, this combination resulted in a significant reduction in gene expression by ~7.1-fold (0.14 ± 0.006 , $p < 0.00005$). However, this combination was similar to the expression level

provided by either AG1478 or Rp-8-pCPT-cGMPS alone ($p=NS$). Thus, it does not appear that there was an additive/synergistic effect in suppressing Cx40 gene expression by combining both blockade of ErbB receptors + blockade of PKG.

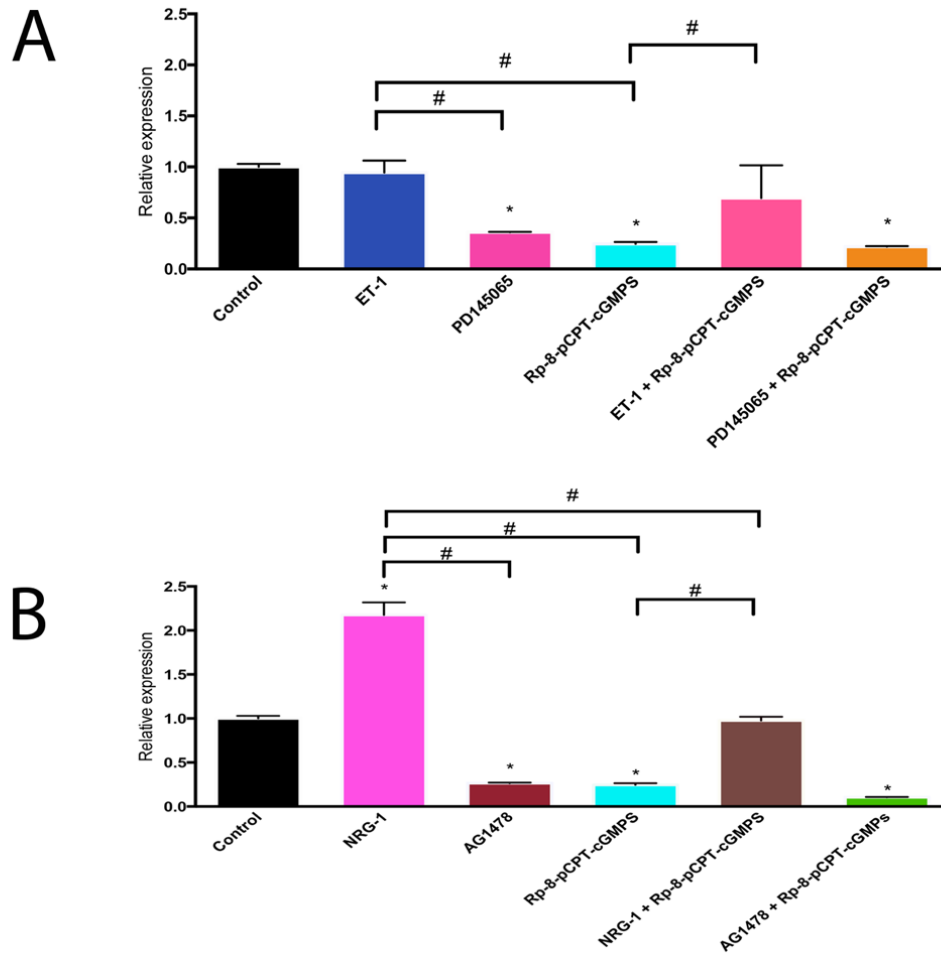


Figure 5.23. RT-qPCR analysis of HCN4 gene expression in E11.5 mouse ventricular cells following addition of Rp-8-pCPT-cGMPS in combination with ET-1 or NRG-1 over 48 hours. Cells were incubated with Rp-8-pCPT-cGMPS (100 μ M) in combination with either ET-1 (1.5 nM) or NRG-1 (2.5 nM) to determine if changes in gene expression of HCN4 could occur. **A)** There was no significant difference in HCN4 gene expression provided by the combination of ET-1 + Rp-8-pCPT-cGMPS vs. control. However, the combination of ET-1 + Rp-8-pCPT-cGMPS resulted in significantly higher gene expression vs. Rp-8-pCPT-cGMPS alone, bringing it similar to control levels of expression. **B)** There was no significant difference in gene expression provided by the combination of NRG-1 + Rp-8-pCPT-cGMPS vs. control. However, the combination of NRG-1 + Rp-8-pCPT-cGMPS resulted in significantly higher gene expression vs. Rp-8-pCPT-cGMPS alone, bringing it similar to control levels of expression. Therefore, ET-1 and NRG-1 may have been able to rescue the decline in gene expression caused by Rp-8-pCPT-cGMPS alone. GAPDH was used as the housekeeping gene. N=5 experiments per group. Each bar represents mean \pm SEM. * $p < 0.05$ vs. control, # $p < 0.05$ between groups as indicated, One-way ANOVA with Tukey's multiple comparisons post hoc test.

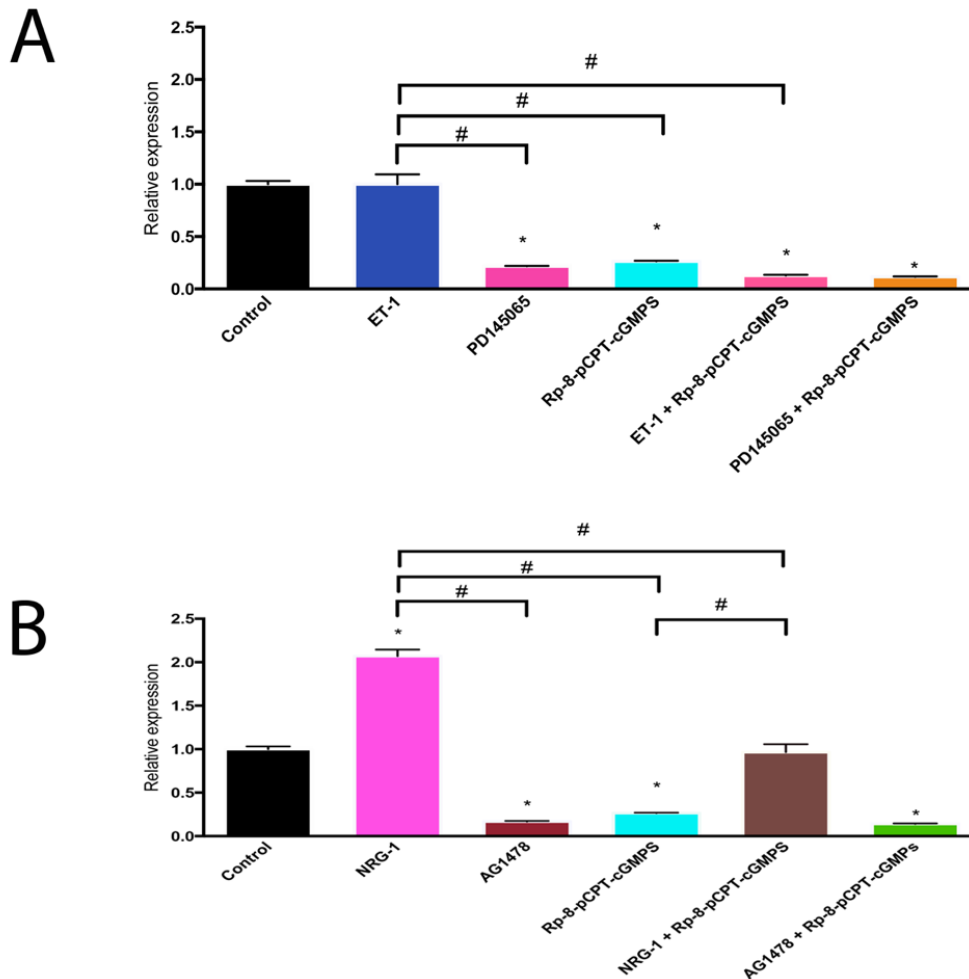


Figure 5.24. RT-qPCR analysis of Cx40 gene expression in E11.5 mouse ventricular cells following addition of Rp-8-pCPT-cGMPS in combination with ET-1 or NRG-1 over 48 hours. Cells were incubated with Rp-8-pCPT-cGMPS (100 μ M) in combination with either ET-1 (1.5 nM) or NRG-1 (2.5 nM) to determine if changes in gene expression of Cx40 could occur. **A)** The combination of ET-1 + Rp-8-pCPT-cGMPS resulted in a significant reduction in gene expression vs. control, and was similar to the effects of Rp-8-pCPT-cGMPS alone, suggesting that ET-1 may have been unable to rescue the decline in Cx40 gene expression caused by Rp-8-pCPT-cGMPS. **B)** The combination of NRG-1 + Rp-8-pCPT-cGMPS did not significantly alter Cx40 gene expression vs. control. This combination resulted in significantly higher gene expression vs. Rp-8-pCPT-cGMPS alone, bringing it similar to control levels of expression. NRG-1 may have been able to rescue the decline in gene expression caused by Rp-8-pCPT-cGMPS. GAPDH was used as the housekeeping gene. N=5 experiments per group. Each bar represents mean \pm SEM. * p <0.05 vs. control, # p <0.05 between groups as indicated, One-way ANOVA with Tukey's multiple comparisons post hoc test.

5.3.6 Determining the Luciferase Activity of a Cx40-Promoter Construct Upon Addition of ANP, ET-1, or NRG-1

We wanted to investigate whether each of the three paracrine factors, ANP, ET-1, or NRG-1, could have an effect on inducing the activity of the mouse Cx40 promoter to further expand our mechanistic approach to understanding if these paracrine factors interact with a VCS marker like Cx40 in order to potentially induce development of the VCS, as the embryonic mouse heart matures. To do this, our goal was to test the luciferase activity of a Cx40-promoter construct upon addition of either exogenous ANP (1000 ng/ml), ET-1 (1.5 nM), or NRG-1 (2.5 nM). We utilized a Cx40 promoter clone construct containing a 1.2kb mouse Cx40 promoter sequence insert. The promoter sequence was cloned in Bgl II and Hind III sites of the pEGX-PG04 vector (**Figure 2.4**). This promoter construct utilized a dual-reporter system consisting of GLuc as the promoter reporter and SEAP as the internal control for signal normalization. Briefly, we transfected the Cx40 promoter clone vector DNA E11.5 ventricular cells and allowed cell cultures to incubate for 24 hours. Then, ANP, ET-1 or NRG-1 was added to cells. After 24 hours of incubation with these compounds, media was collected, and luciferase assays were performed to test the activity of the Cx40 promoter. A subsequent luciferase assay was performed after another 24 hours (48 hours following initial incubation with paracrine factors). The Luc/SEAP ratio (RLU) was determined for each treatment group.

In E11.5 ventricular cells, after 24 hours, the Luc/SEAP ratios of ANP, ET-1, and NRG-1 were all significantly greater vs. control (Control: 0.65 ± 0.03 RLU; ANP: 0.90 ± 0.06 RLU; ET-1: 0.88 ± 0.04 RLU; NRG-1: 0.94 ± 0.05 RLU, $p < 0.005$, **Figure 5.25 A**). There were no significant differences between any of the three paracrine factors ($p = \text{NS}$).

Following 48 hours, similar trends existed, whereby the Luc/SEAP ratios of ANP, ET-1 and NRG-1 were all significantly greater vs. control ($p < 0.05$) but were not significantly different compared to each other (Control: 0.65 ± 0.04 RLU; ANP: 0.86 ± 0.06 RLU; ET-1: 0.86 ± 0.04 RLU; NRG-1: 0.89 ± 0.05 RLU, **Figure 5.25 B**). Taken together, these results suggest that in E11.5 ventricular cells, Cx40 promoter activity is stimulated by ANP (1000 ng/ml), ET-1 (1.5 nM), and NRG-1 (2.5 nM), providing further evidence that each of these three paracrine factors may play a role in inducing Cx40 gene expression to help to promote formation of the VCS in the developing embryonic mouse heart.

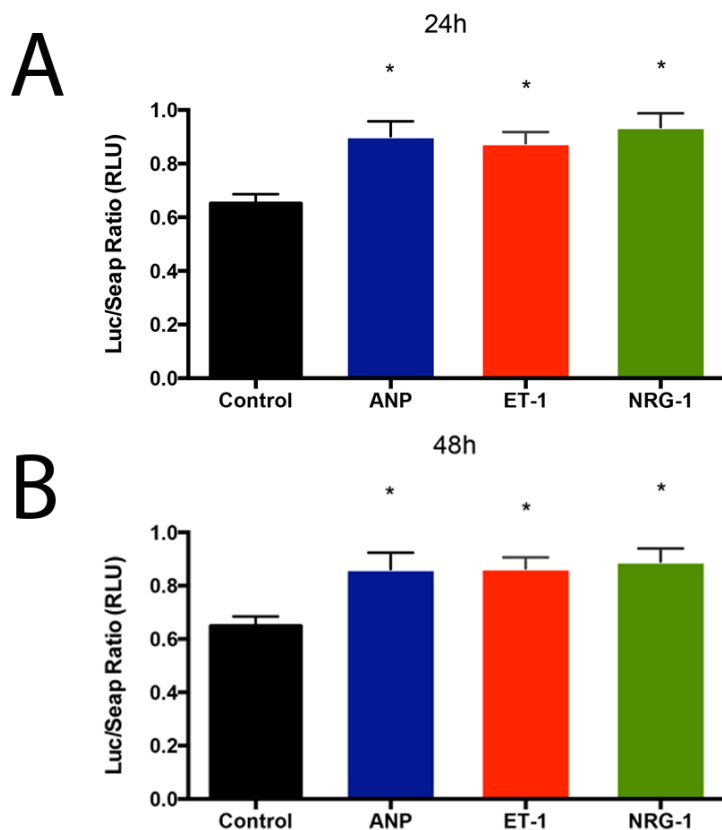


Figure 5.25. Effects of ANP, ET-1 and NRG-1 on luciferase activity of mouse Cx40-promoter clone in E11.5 ventricular cells. E11.5 cells were transfected with the mouse Cx40-promoter clone, and then after 24 hours, ANP (1000 ng/ml), ET-1 (1.5 nM), or NRG-1 (2.5 nM) was added to cells. After 24 hours or 48 hours following paracrine factor treatment, media was collected and assayed for detection of luciferase. The Luc/SEAP ratio (RLU) was determined for each group. **A)** After 24 hours, the Luc/SEAP ratio was significantly greater for all three paracrine factors vs. control. There were no significant differences between the paracrine factors. **B)** After 48 hours, there the Luc/SEAP ratio was still significantly greater for all three paracrine factors vs. control. There were no significant differences between the paracrine factors. N=8 independent experiments, performed in triplicate wells. *p<0.05 vs. control, One-way ANOVA with Tukey's multiple comparisons post hoc test.

CHAPTER 6: DISCUSSION

6.1 Summary of Results

The overall aim of my doctoral thesis work was to determine the potential role of ANP signalling in the development of the embryonic VCS. Numerous congenital heart diseases (CHDs) result from the impairment of the components of the CCS, including dysregulation of cardiac transcription factors that are known to regulate expression of ANP. Therefore, our interest in studying the function of ANP in the development of the VCS could provide some insight into the molecular mechanisms governing its development.

In the literature, there is not much known about the molecular mechanisms that guide development of the CCS, particularly the VCS, and a role for ANP has not been well established. It is known that ANP is transiently expressed in the embryonic ventricles and atria during cardiac development, which raises the possibility that this paracrine factor may be interacting with NPR-A receptors present in the trabecular myocardium to promote differentiation of various cardiac cell types to VCS cells. In this thesis, we have provided evidence that exogenous addition of ANP increased percent distribution of HCN4- and Cx40-positive cells and gene expression of the VCS markers, Cx40 and HCN4, through the NPR-A/cGMP signalling transduction pathway, in the embryonic mouse heart as well as in primary ventricular cell cultures. We have characterized the pharmacological properties of the NPR-A antagonist A71915, which has not been described well in the literature. Furthermore, we have explored the potential for signalling interactions between ANP and other paracrine factors known to

have a role in the formation of the VCS: NRG-1 and ET-1. These signalling experiments provided further insight into the notion that a complex signalling network may exist in the ventricular trabeculae that can guide differentiation of cell types like CPCs and CMs into becoming VCS cells, which will eventually form Purkinje fibers of the mature VCS.

Taken together, results from this thesis provide evidence that ANP has an important role to play in the development of the VCS, which may provide some insight into the molecular mechanisms of various CHDs involving dysregulation of the VCS and ANP. Furthermore, we hope that these results will facilitate the development of therapeutic strategies in the clinic to help children and patients born with CHDs.

6.2 Characterizing the Role of Atrial Natriuretic Peptide Signalling in the Development of the Embryonic Ventricular Conduction System

6.2.1 Context

Genetic mutations in key transcription factors such as Tbx5, MEF2C, GATA4, which are known to be regulators of ANP gene expression, cause impairments in cardiogenesis, not only in animal models, but also in human patients with CHDs (Bruneau et al., 2001; Bruneau et al., 2008; Lin et al., 1997; Schott et al., 1998; Garg et al., 2003). The CHD known as Holt-Oram Syndrome is caused by single-gene mutations in Tbx5 and is correlated with atrial and ventricular septal defects and conduction system deficits (Mori and Bruneau, 2004). In a mouse model of Holt-Oram Syndrome, it has been shown that a dysregulation in the spatial expression pattern of ANP occurred (Bruneau et al., 2001). In this study, Tbx5 haploinsufficient mice displayed marked

reduction in ANP and Cx40 transcription (Bruneau et al., 2001). Due to the unique temporal and spatial expression pattern of ANP in the embryonic ventricles, ANP may play an important role in VCS development.

Although ET-1 has been shown to play a critical role in the development of the CCS in chick heart development (Gourdie et al., 1998), mice lacking ET-1 receptors (*Ednra* and *Ednrb*) were viable and they did not reveal any CCS related abnormalities (Hua et al., 2014). Moreover, treatment of *CCS-lacZ* mouse embryos with ET-1 did not change reporter gene expression pattern (Rentschler et al. 2002). Using the same *CCS-lacZ* reporter readout, Rentschler et al. (2002) found that NRG-1 can act as a paracrine factor to induce embryonic mouse CMs to differentiate into CCS cells, but that this paracrine effect may be declining as development of the embryo proceeds. This was because the group found that as the embryo matured past E11.5, they did not detect differences in expression levels of *lacZ* between control and NRG-1 treated embryonic hearts. Therefore, this raises the possibility that the inductive effects of a paracrine factor like NRG-1 could be restricted to a specific developmental period during heart development. Given the partial development of primordia for the AV node, Bundle of His and bundle branches and absence of Purkinje fibers at the E11/12 stages in mouse hearts (Viragh and Challice, 1977), we hypothesized that additional factors such as ANP may be involved in Purkinje cell formation and maturation and development of the VCS.

6.2.2 Effects of ANP on Protein and Gene Expression of HCN4, Cx40 and Cardiac Transcription Factors

Evidence in the literature has described a role for NPR-A signalling systems in cardiac development. Genetic ablation of the NPR-A receptor in mice (*Npr1*^{-/-}) led to reduced survival (Knowles et al., 2001). Additionally, at mid to late gestation, *Npr1*^{-/-} mice developed cardiac hypertrophy, and experienced morphological abnormalities such as dextrocardia and mesocardia (Scott et al., 2009; Cameron and Ellmers, 2003; Lopez et al., 1995; Ellmers et al., 2002). Recently, it has been suggested that ANP may play a local paracrine role in regulating the balance between CPC proliferation and differentiation through NPR-A/cGMP signalling throughout cardiogenesis (Hotchkiss et al., 2015). However, the molecular mechanisms underlying the importance of NPR-A signalling systems in cardiac development has been poorly understood. We hypothesized that ANP-mediated NPR-A signalling plays a role in the formation and development of the VCS, and that the decreased survivability and abnormal cardiac morphogenesis present in *NPR-A*^{-/-} mice may be attributed to impairments in component(s) of the VCS.

To study the potential impact of ANP/NPR-A signalling on development of the Purkinje fiber network and VCS, we tested whether the addition of exogenous ANP could impact protein and/or gene expression of two important VCS markers, HCN4 and Cx40 at various developmental stages: E11.5, E14.5, E17.5 and neonatal stages using techniques such as immunostaining, QPCR and reporter gene expression assays. HCN4 channels generate the I_f current in the heart, providing pacemaker activity in the SA node (Ludwig et al., 1998; DiFrancesco, 1993; Accili et al., 2002). All components of the

CCS express HCN4 by E14.5. Also, HCN4 is highly expressed in first heart field (FHF) precursor cells that will eventually become CCS cells (Liang et al., 2013). We chose to study HCN4 as one of our VCS markers of choice because it is expressed prenatally in the ventricular trabeculae, which houses cellular precursors which will eventually form the bundle branches and Purkinje fibers of the mature VCS, and because its postnatal expression becomes confined to the Purkinje fibers in the ventricular myocardium (Han et al., 2002). Cx40 is a gap junction protein necessary for allowing direct exchange of small molecules between adjacent cells (Dbouk et al., 2009). In the embryonic heart, by E14.5, all components of the CCS express Cx40 excluding the SA node and the outer portion of the AV node. After birth, its expression becomes restricted to the Purkinje fibers (Delorme et al., 1995; Sankova et al., 2012). Thus, Cx40 is also an excellent VCS marker to study Purkinje fiber formation because it is also expressed prenatally in ventricular trabeculae and postnatally in Purkinje fibers.

It is technically challenging to obtain a sufficient number of cells from E11.5 ventricles to perform western blot analyses. Thus, we employed immunostaining techniques to monitor the effects of ANP on HCN4 and Cx40 protein expression in both CM and non-CM populations. The addition of exogenous ANP (1000 ng/ml) increased the number of cells expressing HCN4 but not Cx40 in E11.5 mouse ventricular cells. All other concentrations less than 1000 ng/ml did not provide any significant changes in immunoreactive cell number for either marker. ANP was delivered every 12 hours over a 48-hour time period. We chose this particular time period because previous results from our lab demonstrated that the addition of a single dose of ANP (100 ng/ml) over a

24-hour time period did not yield significant changes in Cx40 or HCN4 gene expression (Hotchkiss, 2013; unpublished). Notably, in this thesis, we found that the bioactivity of exogenous ANP present in the conditioned medium of E11.5 ventricular cells even after 12 hours of incubation was very similar to that of freshly prepared ANP, when used at a 1000 ng/ml concentration. The absence of significant changes in the expression profiles of HCN4 and Cx40 in earlier studies conducted by our laboratory (Hotchkiss, 2013; unpublished) could be attributed to the loss of bioactivity or degradation combined with insufficient dosage of ANP (single treatment of 100 ng/ml over a 24-hour period) in those experiments.

Natriuretic peptides are known to be degraded by neutral endopeptidases or neprilysins (NEPs) and insulin degrading enzymes as well as the NPR-C clearance pathway (Potter, 2011). Very little is known about the expression pattern of enzymes degrading natriuretic peptides during heart development. Earlier work from our laboratory detected NPR-C protein in E11.5 ventricular lysates but this receptor was ineffective in coupling to the G_i pathway (Hotchkiss et al., 2015) which was an established event during NPR-C signalling (Anand-Srivastava et al., 1996). The addition of the NPR-A antagonist A71915 (1 μ M) reduced the number of immunoreactive cells for both HCN4 and Cx40, suggesting that blockade of the NPR-A receptor could negatively impact formation of the VCS. We also tested a combination of ANP (1000 ng/ml) and A71915 (1 μ M) on the number of immunoreactive HCN4 and Cx40 cells and found that the inhibitory effect of A71915 persisted despite the presence of ANP.

We also determined if ANP could impact differentiation kinetics of a population of non-CMs that were also positive for VCS markers (HCN4 or Cx40). At all concentrations tested, ANP reduced the percentage of these cells, whereas A71915 alone and in combination with ANP increased the percentage of these cells. Furthermore, ANP increased the ratio of VCS marker positive CMs to non-CMs in E11.5 ventricular cell cultures whereas A71915 reduced this ratio. This seems to indicate that exogenous ANP may have converted HCN4+ or Cx40+ non-CM cells into VCS marker positive CMs, and that blockade of the NPR-A receptor may have reversed this effect. To further lend credence to the hypothesis that ANP could be causing differentiation of various cell types to VCS cells, we found that at E11.5, exogenous ANP increased the number of CMs present per field through MF20 staining for sarcomeric myosin. Thus, ANP may play a role in causing differentiation of non-CM cells to VCS cells. Although ANP-mediated increases in the number of HCN4 or Cx40 positive CMs could be attributed to changes in cell proliferation rates, this is unlikely due to the fact that ANP treatment led to a significant decrease in cell cycle activity of embryonic CPCs with no changes in CM cell cycle activity in E11.5 cultures (Hotchkiss et al., 2015).

The addition of exogenous ANP (1000 ng/ml) induced mRNA levels of both HCN4 and Cx40 and the addition of A71915 alone or in combination with ANP resulted in reduction in gene expression of both genes, at E11.5. Additionally, we found that in E14.5 ventricular tissue, homozygous NPR-A-KO (NPR-A)^{-/-} mice display significant reductions in gene expression of both HCN4 and Cx40. Therefore, taken together, these

results suggest the possibility that ANP-mediated NPR-A signalling may be involved in formation of the VCS through induction of HCN4 and Cx40.

We also examined potential changes in protein and gene expression of HCN4 and Cx40 upon addition of exogenous ANP and/or A71915 across several developmental stages: at E11.5, when the Purkinje fiber network/VCS begins to form, at E14.5 which represents when the Purkinje fiber network/VCS has approximately half-formed, and at E17.5, which represents when Purkinje fiber network/VCS specification has neared completion. Within each embryonic stage, treatment with ANP increased HCN4 and Cx40 positive cell numbers and gene expression, suggesting that the inductive effects of ANP may not be as highly restricted to specific developmental periods. However, there were differences in the effects of the treatment groups across the developmental periods. When comparing differences in treatments across embryonic stages, the greatest induction in Cx40 positive (but not HCN4) cell number, and HCN4/Cx40 gene expression, caused by addition of exogenous ANP, occurred at E14.5.

Although it has been shown in various cell types that genetic mutations in key transcription factors such as Tbx5, MEF2C, GATA4, lead to dysregulation in gene expression of ANP, cause impairments in cardiogenesis, and contribute toward the incidence of CHD in humans (Bruneau et al., 2001; Bruneau et al., 2008; Lin et al., 1997; Schott et al., 1998; Garg et al., 2003), we found that exogenous ANP did not significantly modulate gene expression of GATA4, HAND2, Tbx5, or MEF2C in E11.5 ventricular cells. It is possible that modulation of the gene expression of these cardiac transcription factors by ANP may be cell type specific or stage specific. Furthermore, it is possible that

downstream targets of these transcription factors or changes in the activity of these transcription factors could be modulated after ANP treatment, although this remains to be determined.

6.2.3 Determination of Natriuretic Peptide Receptor Signalling Mediators Involved in the Regulation of Ventricular Conduction System Specific Marker Gene Expression and Formation of the Ventricular Conduction System

While a role for the ANP/NPR-A/cGMP signalling pathway has been described in cellular growth and proliferation of various cell types (see **Tables 1.1 and 1.3**), little is known about its potential role in embryonic heart development. Second messenger analysis experiments in E11.5 ventricular cells using various doses of ANP confirmed that ANP (100 and 1000 ng/ml) can significantly increase endogenous cGMP levels in acutely isolated ventricular cells. This result is consistent with previous studies which documented similar increases in cGMP levels in embryonic ventricular cells (Hotchkiss et al., 2015) and adult Purkinje CMs (Anand-Srivastava et al., 1989) after treatment with ANP. Furthermore, stimulatory effects of ANP on HCN4 and Cx40 gene expression and the inhibitory effects of A71915 as well as genetic ablation of NPR-A on HCN4 and Cx40 gene expression strongly suggest that NPR-A signalling is critical for VCS development. While these results suggest that ANP/NPR-A/cGMP signalling pathway is biologically active in E11.5 ventricular cells, stimulatory effects of ANP on VCS marker gene expression may also be attributed to the actions of ANP on other natriuretic peptide receptors such as NPR-B and NPR-C as well as to the cGMP-independent pathways.

It is unlikely that ANP increases VCS gene expression through NPR-B receptor stimulation in E11.5 ventricular cells since the concentrations used for ANP in this study (100 and 1000 ng/ml, approximately 30 and 300 nM) were far below the half-maximal concentration (25 μ M) that was required for ANP/NPR-B mediated cGMP production in cell culture studies (Schulz et al., 1989). Although NPR-C receptors are capable of inhibiting the adenylyl cyclase (AC) pathway (Anand-Srivastava et al., 1996; Pagano and Anand-Srivastava, 2001), and are present in E11.5 ventricles (Hotchkiss et al., 2015), our cAMP analysis indicates that the NPR-C/ G_i pathway may not be active in these cells. We found that ANP treatment alone did not alter the endogenous levels of cAMP in E11.5 ventricular cells. Further, ANP treatment in combination with ISO was unable to significantly alter the increased cAMP production resulting from ISO treatment alone. Thus, these results suggest that NPR-C/ G_i signalling pathway may not be responsible for ANP-mediated effects on VCS gene expression in our experiments.

In chronic cardiac hypertrophy, elevated plasma levels of ANP are associated with NPR-A desensitization and it has been shown that ANP binding to NPR-A can stimulate a unique cGMP-independent signalling pathway in CMs (Kinoshita, 2010; Klaiber et al., 2011). Activation of NPR-A leads to subsequent activation of Ca^{2+} -permeable transient receptor potential canonical 3/6 (TRPC3/TRPC6) cation channels, which form a stable complex with NPR-A. Activation of TRPC3/TRPC6 channels leads to sodium and calcium influx, and this increased calcium influx triggers further calcium influx through L-type Ca^{2+} channels (LTCCs) to further increase intracellular Ca^{2+} to pathological levels (Kinoshita et al., 2010; Klaiber et al., 2011). As stated earlier, such a

cGMP-independent pathway may also account for ANP-mediated effects on VCS gene expression. However, additional experiments using cell permeable compound 8-Br-cGMP or a PKG inhibitor (Rp-8-pCPT-cGMPS) firmly confirmed the role of NPR-A/cGMP/PKG pathway in the regulation of HCN4 and Cx40 gene expression in ANP treated embryonic ventricular cells. Therefore, we did not pursue the role of a cGMP-independent pathway in our ANP treated cultures, however, such a possibility could be further examined in future studies.

We utilized high concentrations of ANP (1000 ng/ml) to study protein and gene expression of HCN4/Cx40 and endogenous cGMP production which was consistent with numerous studies that also utilized a range of high concentrations of exogenous ANP in both cardiovascular and non-cardiovascular cell types (Koide et al., 1996; DiCicco-Bloom et al., 2004; O'Tierney et al., 2010; Glenn et al., 2009; Stastna et al., 2010). In the adult rat, circulating concentrations of ANP have been measured at ranges between 100 and 400 pg/ml (Ortola et al., 1987; Jankowski et al., 2001; Wei et al., 1987). However, at E20 in fetal rats, a high plasma concentration of ANP was found (2.7 ng/ml) (Wei et al., 1987). The plasma concentration of ANP has been shown to be more than 5 times greater in fetal circulation compared to maternal circulation in sheep and rats (Cheung et al., 1987; Wei et al., 1987). In tissue, the concentration of ANP in fetal rat ventricles was found to be more than 20 times higher compared to the concentration of ANP present in postnatal ventricles (Wei et al., 1987). Therefore, since ANP concentrations were higher in tissue of fetal ventricles, it is possible that the ventricular trabeculae of the embryonic heart contain zones that are rich with ANP, creating a microenvironment

where “pockets” of ANP are highly concentrated in the interstitial fluid. The high concentration of ANP present in the interstitial fluid surrounding the trabeculae may be several orders greater in magnitude compared to the concentration of ANP found in plasma or circulation. Therefore, despite the fact that extra-physiological concentrations of ANP were utilized in this study, this may well represent the ANP-rich regions of trabeculae that would be difficult to measure in an animal model or in humans, given the autocrine/paracrine nature of ANP and its ability to interact with nearby NPR-A receptors of surrounding CMs.

6.2.4 Effects of Exogenous ANP on Cell Survival and Growth, Proliferation and Differentiation of Cardiac Progenitor Cells and Cardiomyocytes

ANP has been shown to regulate proliferation and growth of various cardiovascular and non-cardiovascular cell types through an autocrine/paracrine manner (see **Tables 1.1 and 1.3**). ANP was shown to stimulate apoptosis in various cell types, including in neonatal rat CMs, and in pulmonary vascular smooth muscle cells, while also inhibiting apoptosis in cell types including serum-deprived PC12 cells (D’Souza et al., 2004; Wu et al., 1997; Deprez et al., 2001; Fiscus et al., 2001). The pro-apoptotic effects of ANP on neonatal rat CMs were found to be mediated by cGMP, and stimulation of cells with catecholamines increased cAMP levels, which reversed this effect (anti-apoptosis) (Wu et al., 1997). It was suggested that cGMP activity inhibited apoptosis in PC12 cells (Fiscus et al., 2001). Therefore, these results suggest that the cell survival and proliferation effects elicited by ANP may be cell type specific. In embryonic

CM cultures, there is no clear consensus on a defined role for ANP/NPR-A signalling on regulating cell growth and proliferation. One study demonstrated that exogenous addition of human ANP induced proliferation in embryonic chick CMs through NPR-A mediated signalling (Koide et al., 1996). In contrast, another study demonstrated that the addition of human or porcine exogenous ANP to fetal sheep CMs inhibited proliferation induced by Ang II through NPR-A mediated signalling (O'Tierney et al., 2010). The discrepancy in reported outcomes may be explained by the fact that numerous studies that examined the role of ANP in cellular proliferation employed heterologous systems, that is, that cells were treated with ANP originating from a different species (Hotchkiss et al., 2015). In this thesis, we utilized a homologous system to study the effects of ANP on formation of the VCS, using mouse ANP on mouse primary cultures. Previous studies from our laboratory demonstrated that ANP can inhibit cell cycle activity in CPCs but not in CMs in E11.5 ventricular cell cultures (Hotchkiss et al., 2015). It is important to note that ANP treatment (1-1000 ng/ml) in the present study did not lead to any significant changes in the total cell number (measured as nuclei per field) compared to untreated controls in E11.5 ventricular cells. Although this observation does not rule out the possibility of changes in cell cycle activity in individual cell types as reported in our earlier studies (Hotchkiss et al., 2015), it eliminates the possibility of a pro-apoptotic role for ANP in our cell culture system.

Many of the studies described above attribute the capability of ANP to modulate cell growth and proliferation to occur via NPR-A/cGMP signalling or NPR-C/cAMP signalling, specifically either through an increase in cGMP or decrease in cAMP (Abell et

al., 1989; Tripathi and Pandey, 2012; Horio et al., 2000; Tsuruda et al., 2002; Koide et al., 1996; Pandey et al., 2000; Woodard and Rosado, 2008; O'Tierney et al., 2010). We decided to investigate the potential for ANP/NPR-A/cGMP signalling to modulate proliferation and/or differentiation of CPCs and CMs at E11.5. The addition of ANP significantly increased cGMP production both in CPCs (100, 1000 ng/ml) and in CMs (1000 ng/ml). Interestingly, the production of cGMP was greater in the CPC population vs. in CMs, suggesting that CPCs may be more sensitive to ANP-induced stimulation of NPR-A. In addition, exogenous addition of 8-Br-cGMP to E11.5 ventricular cell cultures significantly decreased the number of CPCs and the number of CMs increased in a dose dependent manner. It is possible that through ANP/NPR-A stimulation, cGMP could be promoting differentiation of CPCs (thus reducing their numbers) while increasing differentiation of CMs into a VCS phenotype. This notion is consistent with the earlier report that showed that ANP can decrease DNA synthesis in CPCs but not in CM populations in E11.5 mouse ventricular cell cultures (Hotchkiss et al., 2015).

ANP may play an important role in protecting the heart against cardiac hypertrophy, since NPRA-KO mice display enlarged hearts whereas mice overexpressing ANP display smaller hearts (Steinhilber et al., 1990). Several studies have demonstrated that exogenous ANP can inhibit cardiac hypertrophy both *in vitro* and *in vivo* (Horio et al., 2000; Rosenkranz et al., 2003; Laskowski et al., 2006; Kilic et al., 2007; Knowles et al., 2001, Lopez et al., 1995; Oliver et al., 1997). At E11.5, although there was a trend toward decreased cell area of CMs upon addition of exogenous ANP, this was not statistically significant versus control. Blockade of the NPR-A receptor with A71915 also

resulted in similar cell area of CMs as with control. Therefore, in our study, neither ANP or A71915 had an effect on cardiac hypertrophy at E11.5. However, it is important to consider that we examined the effects of ANP on cardiac hypertrophy *in vitro*, in E11.5 ventricular cells, rather than *in vivo* in a whole animal model. Additionally, we provided ANP treatment every 12 hours over a 48-hour period, thus not only did we study cardiac hypertrophy in acutely isolated cells, but also with a potentially short time period. It is challenging to correlate our findings at the cellular level with the pathophysiology that could be occurring in whole, intact animals or humans, and it is highly likely that cardiac hypertrophy develops over a much longer, and extended period of time.

6.2.5 Characterization of the Effects of ANP/NPR-A Signalling on Embryonic Ventricular Conduction System Development using the Cx40^{egfp} Mouse Model

Several studies have highlighted the importance of Cx40 to promote formation and development of the CCS. Cx40^{-/-} mice have been shown to develop severe CCS deficits including, decreased atrial and atrioventricular conduction, increased QRS complex duration, bundle branch block, slow conduction in the right bundle branch, increased incidence of inducible atrial fibrillation and ventricular tachycardia, and the occurrence of spontaneous arrhythmias (Simon et al., 1998; Tamaddon et al., 2000; Hagendorff et al., 1999; Bevilacqua et al., 2000). While several models exist to study the impact of genetic manipulations on conduction system development (Myers and Fishman, 2003; Di Lisi et al., 2000; Nguyen-Tran et al., 2000; Kondo et al., 2003; Rentschler et al., 2002) we chose to use the Cx40^{egfp} knock-in reporter mouse model because: 1) Cx40 appears to be the best marker for the His-Purkinje system, and 2) Cx40

is expressed strongly in atrial CMs, the AV node, Bundle of His and bundle branches, and the Purkinje fibers, of the CCS (Miquerol et al., 2004). Cx40 is expressed in the CCS, both prenatally, and postnatally, allowing one to visualize development of the CCS throughout numerous developmental periods. It is likely that EGFP does not significantly interfere with physiological functioning of the heart of Cx40^{egfp+/-} mice, since the ECGs, bundle branch velocities, and profiles of action potentials recorded from both WT and Cx40^{egfp+/-} mice were similar (Tamaddon et al., 2000; Van Rijen et al., 2001). Several studies have employed this model for this purpose, demonstrating that heterozygous knockout of the Nkx2.5 gene (Nkx2.5^{+/-}) lead to hypoplasia of the Purkinje fiber network and conduction system deficits (Jay et al., 2004; Meysen et al., 2007).

To confirm the effects of ANP treatment on Cx40 expression, Cx40^{egfp+/-} whole embryos at E10.5 were incubated with ANP and/or A71915 for 24 hours, and at E11.5, hearts were removed and visualized for EGFP expression patterns. ANP-treated hearts revealed strong EGFP signals in both atrial chambers, in the coronary vasculature, and in both ventricles, with the left ventricle having the strongest signal overall. In contrast, A71915 alone, or in combination with ANP, was correlated with hearts having weak EGFP signals. While these results suggest that ANP/NPRA signalling is important for Cx40 gene expression, it is important to note that EGFP signal is visualized from the epicardial surface in these early stage embryos and thus may represent a combined signal derived from developing coronary vasculature (albeit at a very low level at E11.5) as well as ventricular trabeculae.

To ensure that ANP/NPR-A signalling is important for VCS formation, we next focused on the imaging of Purkinje fiber arborisation in the endocardial surface of neonatal ventricles derived from compound crosses between double heterozygous mice (Cx40^{egfp+/-} and NPR-A^{+/-}). This approach has been widely used to study the development and maturation of Purkinje fibers in earlier studies (Miquerol et al., 2004; Jay et al., 2004; Meysen et al., 2007). Although homozygous Cx40^{egfp+/+} mice are viable and do not reveal any morphological abnormalities in CCS development (Miquerol et al., 2004), we were unable to generate Cx40^{egfp+/-}/NPR-A^{-/-} pups from these compound crosses possibility due to early embryonic lethality that could arise from the loss of three functional alleles (1 Cx40 and 2 NPR-A) important for VCS formation. However, comparative analysis of neonatal mice born with Cx40^{egfp+/-}/NPR-A^{+/+} or Cx40^{egfp+/-}/NPR-A^{+/-} genotypes revealed that most of the hearts (5 out of 7) from NPR-A^{+/-} displayed significantly less arborisation of the Purkinje fiber network, abnormal Purkinje fiber structure, and severe hypoplasia. These results are in agreement with the effects of exogenous addition of ANP or NPR-A inhibitor A71915 on VCS marker gene expression in E11.5 ventricular cell or whole embryo cultures.

6.2.6 Post-Transcriptional and Transcriptional Mechanisms Responsible for Changes in HCN4 and Cx40 Gene Expression in Response to Modulation of the ANP/NPR-A Signalling Pathway

Changes in VCS marker gene expression in response to ANP treatment or genetic ablation of NPR-A could be attributed to multiple mechanisms including transcriptional, post-transcriptional and translational mechanisms. A recent study revealed that ANP

treatment can alter the expression levels of a number of miRNAs in human aortic smooth muscle cells and some of these changes have been mechanistically linked to vascular smooth muscle cell relaxation (Kotlo et al., 2011). Interestingly, this study has identified unique sets of miRNAs that are regulated in response to ANP (particulate guanylyl cyclase activator) but not in response to S-nitroso-N-acetylpencillamine (SNAP; a NO donor and soluble guanylyl cyclase activator). One of such unique miRNAs identified by Kotlo et al. (2011), miRNA 27b, has recently been linked to the downregulation of Cx40 expression in the atria of obese mice possibly by targeting the 3' UTR of Cx40 transcripts (Takahashi et al., 2016). Moreover, miRNA 27b levels were shown to be significantly upregulated from E12.5 to E18.5 stages of ventricular development (Chinchilla et al., 2011) and Cx40-positive Purkinje fiber arborisation is known to be increased by the E16.5 stage. Based on these findings, we reasoned that miRNA-mediated regulation of VCS marker gene expression (Cx40 and HCN4) may serve as an underlying mechanism in the context of the effects of ANP on VCS formation.

Further survey of the literature indicated that miRNA 208 can also regulate Cx40 gene expression in the heart (Callis et al., 2009). Similarly, several studies linked miRNA 1a and 133 to cardiac development and regulation of HCN4 gene expression (D'Souza et al., 2014; Li et al., 2015; Ivey et al., 2008; Zhao et al., 2007). Notably, homozygous miRNA 1 KO mice exhibited 50% lethality by weaning age due to CCS deficits and ventricular septal defects (Zhao et al., 2007). Thus, in this study, we have focused on miRNAs that are known to target Cx40 (27b and 208a) and HCN4 (1a and 133) transcripts in ANP treated embryonic ventricular cell cultures or NPRA-KO hearts. We

found that in E11.5 and E14.5 ventricular cells, exogenous ANP significantly downregulated miRNAs 1a, 133, and 27b, and A71915 reversed these effects. These changes in miRNA levels are inversely related to the mRNAs levels of HCN4 and Cx40 in ANP or A71915 treated primary cultures and further suggest that ANP increases VCS marker gene expression by decreasing the levels of miRNAs 1a, 133, and 27b.

In contrast to exogenous ANP treatment results, genetic ablation of NPR-A displayed significant upregulation of miRNA 1a and 133, whereas miRNA 27b was not significantly different vs. WT in E14.5 as well as neonatal NPR-A^{-/-} ventricles. Both pharmacological inhibition of NPR-A, and genetic ablation of the NPR-A receptor, resulted in upregulation of miRNA 1a and 133. Interestingly, while pharmacological inhibition of NPR-A led to upregulation of 27b in E11.5/E14.5 primary cultures, there were no significant differences between NPR-A^{-/-} and NPR-A^{+/+} (WT) ventricles, at E14.5 and neonatal stages. Lastly, our finding that the genetic ablation of NPR-A led to downregulation of miRNA 208a is consistent with the results of Callis et al.'s (2009) study, which found that miRNA 208a KO mice displayed reduced Cx40 gene expression, leading to conduction system deficits. Taken together, this provides evidence that ANP/NPR-A signalling may induce Cx40 gene expression through upregulation of miRNA 208a. However, due to lack of tissue samples from NPR-A-KO mice as well as time constraints, we were unable to determine the effects of the NPR-A genotype on miRNA 208a levels in other developmental stages (like neonatal) aside from E14.5. In addition, we did not test the effects of ANP and/or A71915 on miRNA 208a expression in embryonic ventricular cell cultures. Therefore, further experiments are warranted to

tease out the potential role miRNAs could play in the development of the CCS, through regulation of Cx40 and HCN4 gene expression.

Increased gene expression of VCS markers after ANP treatment could also be explained by increased transcriptional activity of Cx40 and HCN4 genes. The promoter regions for both genes were cloned and sequenced (Grapin-Botton et al., 1997; Kuratomi et al., 2007), however, these sequences were not available in our lab to perform transcriptional regulation studies. We recently obtained a 1.2 kb mouse Cx40 promoter driven secreted Gaussia luciferase reporter construct (Cx40p-GLuc-CMV-SeAP) and tested the ability of ANP, ET-1 and NRG-1 to promote the secretion of GLuc in transfected E11.5 ventricular cell cultures compared to that in transfected cultures that were not treated with any exogenous paracrine factors. We found that the ratio of GLuc to secreted alkaline phosphatase (SEAP; transfection normalization control) was significantly increased in response to all three treatments. These results suggest that all three paracrine factors can regulate Cx40 gene expression via transcriptional regulatory mechanisms. A quick examination of the 5' flanking sequence of the mouse Cx40 gene (Grapin-Botton et al., 1997) revealed a few known transcription factor binding sites such as SP1, AP2, C/EBP, MRE and Y-Box. Further deletion analysis is required to map the response elements or transcription factors involved in the Cx40 promoter regulation by ANP, ET-1 and NRG-1. It should be noted that due to time constraints, we were unable to test the effects of ANP, ET-1 and NRG-1 treatments on a blank vector or control plasmid devoid of Cx40 promoter region to ensure that these results are not due to the presence of any cryptic transcription start sites in GLuc/SEAP construct. Therefore,

further work needs to be done in this area to ascertain the role of these three paracrine factors on Cx40-promoter activity in the embryonic mouse heart.

6.3 Characterizing the Pharmacological Properties of the NPR-A Antagonist A71915

6.3.1 Context

Throughout this thesis, we have treated cells and tissues with a combination of A71915 and ANP together, often resulting in similar observations as with A71915 treatment alone. This led us to hypothesize that A71915 may be acting as a competitive antagonist to outcompete endogenous ANP in cells. Compounds like A71915 can help us to further understand the role of ANP in physiology and cell biology. A71915 is a truncated form of ANP. Certain ANP analogues were shown to antagonize the increased intracellular cGMP levels produced by ANP stimulation of NPR-A *in vitro* in vascular smooth muscle cells and also *in vivo* (Kitajima et al., 1989; Von Geldern et al., 1990). Delporte et al. (1992) tested the potency of several NPR-A antagonists on cultured human neuroblastoma NB-OK-1 cells and found that A71915 had the greatest potency. This group also tested the effect of these various antagonists in combination with ANP, on cGMP production and found that A71915 shifted the ANP dose-response curve the furthest to the right. It was also recognized that the presence of a disulfide bridge in the structure of an NPR-A antagonist like A71915 is essential to cause changes to cGMP levels through NPR-A, since antagonists lacking this structure were unable to decrease ANP-induced cytosolic cGMP levels (Delporte et al., 1992).

6.3.2 Determining the Antagonistic Nature of A71915

While treatment of E11.5 ventricular cells with ANP demonstrated increased intracellular cGMP production in a dose-dependent manner, these second messenger responses were blocked by the NPR-A specific inhibitor A71915 when used at the 0.5 to 5 μ M concentration range. Notably, cGMP levels in cells treated with all ANP + A71915 combination treatments were significantly lower than those observed with untreated cells. Additional dose response experiments with the NPR-A specific inhibitor A71915 alone (0.5 to 10 μ M) revealed significant decreases in intracellular cGMP levels compared to the levels in untreated cultures. Although these results suggest that A71915 can effectively block ANP-mediated effects in E11.5 ventricular cells (e.g. cGMP levels, HCN4 and Cx40 gene expression levels), it is possible that A71915 may be acting as an inverse agonist at the NPR-A receptor. A71915-mediated reduction of cGMP levels in embryonic ventricular cells may also be attributed to possible actions of the inhibitor on NPR-C receptors, triggering a potential crosstalk with the NPR-A/cGMP signalling pathway. However, the inability of A71915 to lower cGMP levels in heterozygous NPR-A knockout E11.5 ventricular cells as well as the absence of any effects of A71915 on intracellular levels of cAMP in the presence or absence of ANP and/or ISO in WT E11.5 ventricular cultures suggest that the inhibitory effects of A71915 on cGMP are not mediated through the NPR-C/ G_i signalling system. Alternatively, such an inhibition may also be explained by the fact that high concentrations of A71915 may be either outcompeting the endogenous ANP for receptor binding and/or stabilizing the NPR-A receptor in an inactive state. Although previous studies from our laboratory have

identified both proANP and a mature form of ANP in the conditioned media of E11.5 ventricular cells (Hotchkiss et al., 2015), further studies are needed to confirm whether the baseline levels of cGMP can be reduced in the presence of neutralizing antibodies for ANP.

Recent studies suggest that there are unique differences between binding abilities of ANP and A71915 to NPR-A receptors. NPR-A receptors exist as preformed dimers and the extracellular domains of the dimers bind to natriuretic peptides in a 2:1 stoichiometric ratio (Parat et al., 2008, Rondeau et al., 1995; He et al., 2001; Ogawa et al., 2004). When ANP binds to the NPR-A, the extracellular domain monomers undergo a twisting motion, causing the two juxtamembrane domains in the dimer to rotate in opposite directions (Ogawa et al., 2004; Ogawa et al., 2009). Rotation of the juxtamembrane domains in the dimerized receptor is thought to re-orient the two intracellular domains into an active conformation, thereby enabling GC activity (Ogawa et al., 2004; Misono et al., 2005; Qiu et al., 2004).

In contrast, A71915 has been shown to stabilize the extracellular domain dimer in a distinct, inactive conformation (Parat et al., 2008). Despite the fact that A71915 is nearly half the size of ANP (13 residues versus 28 residues), a single molecule of A71915 was capable of fitting into the binding cleft using molecular modeling studies (Parat et al., 2008). The disulfide-linked ring is conserved in A71915. It was found that the residue D-Tic¹⁶ resulted in suboptimal binding of A71915 with hydrophobic pocket 2 in the extracellular domain of NPR-A (Parat et al., 2008). In subsequent studies, it was shown that the orientation of the two juxtamembrane domains is differentially altered when

NPR-A is bound to A71915 when compared to the binding of NPR-A with ANP (Parat et al., 2010). Indeed, such binding differences may explain the inhibitory effects of A71915 on cGMP levels in E11.5 ventricular cells and also offer a basis for inverse agonism.

A71915 has been frequently used as an NPR-A selective blocker at concentrations ranging from 1-10 μ M by several investigators (Delporte et al., 1992; Von Geldern et al., 1990; Misono et al., 2005). It is also worth noting that A71915 was used at a dose of 1 μ M for the majority of experiments in this thesis and this dose was initially chosen based on previous work published in our laboratory (Hotchkiss et al., 2015). In order to determine whether A71915 acts a competitive or non-competitive antagonist, we generated ANP dose-response curves in the presence or absence of at 1 μ M concentration of the antagonist. The ANP + A71915 dose response curve right-shifted compared to the ANP curve and further statistical analysis confirmed that A71915 behaves as a competitive antagonist vs. ANP concentrations ranging from 10-100 ng/ml, but not at an ANP concentration of 1000 ng/ml. Furthermore, in the absence of ANP, A71915 behaves as an inverse agonist. We observed similar results with the combination treatment of ANP (1000 ng/ml) + A71915 (1 μ M) compared to A71915 treatment alone and a better response for combination treatments could have been achieved using higher concentrations of ANP to outcompete A71915, although this remains to be tested.

6.4 Characterizing the Potential for Signalling Interactions Between ANP, ET-1 and NRG-1 Signalling Systems in the Development of the Ventricular Conduction System

6.4.1 Context

It has been hypothesized that paracrine interactions between embryonic CMs and cardiac endothelial/endocardial cells may play an important role in driving the local recruitment of conduction system cells from beating CMs (Mikawa and Hurtado, 2007) or from bipotential progenitor cells derived from first and second heart fields (Miquerol et al., 2013; Liang et al., 2015). Since endothelial cells are the only cell type present in both the endocardium and in arterial endothelium, and they are both adjacent to CMs that are capable of differentiating into Purkinje fibers, it was hypothesized that an endothelial cell-derived signal may play a role in the recruitment of conduction system cells (Mikawa and Hurtado, 2007). ET-1 was found to convert CMs into CCS cells in the embryonic chick heart (Gourdie et al., 1998). ET-1 is a paracrine factor released from endothelial cells. In the chick heart, Purkinje fibers develop close to the developing coronary vasculature. Therefore, it is highly possible that secreted factors from endothelial/endocardial cells could provide instructive cues to guide undifferentiated CPCs, or even CMs, to become CCS cells, converting the primitive myocardium into trabecular myocardium. In addition to ET-1, another paracrine factor known as NRG-1 is also secreted from endothelial/endocardial cells, and was also shown to induce formation of the CCS in the mouse embryonic heart (Rentschler et al., 2002). We know that ANP is not released from endothelial/endocardial cells, but is released from CMs in the myocardium. ANP was found to be expressed transiently in the embryonic atria and ventricles in the mouse, and becomes confined in its expression to the ventricular trabeculae by E11 (Christoffels et al., 2000). Therefore, the ventricular trabeculae, which

is destined to become the bundle branches and Purkinje fibers of the mature VCS, may house ANP, NRG-1 and ET-1, which could be capable of interacting with their own cognate receptors, or perhaps even engage in signalling crosstalk with one another, setting the stage for a potentially complex cellular signalling network that may guide the spatial and temporal development of the VCS in the embryonic heart.

There appears to be a complex cellular network at play in the formation and development of the VCS. In this thesis, we have provided evidence that the ANP/NPR-A/cGMP pathway is biologically active at E11.5 in the mouse embryonic heart, and contributes toward development of the VCS through induction of the important VCS markers, HCN4 and Cx40. Work done to demonstrate induction of the CCS by NRG-1 using the CCS-*lacZ* model used whole embryo cultures and it is possible that exogenous factors may not be reaching adequately in those systems (Rentschler et al., 2002). The effects of NRG-1 and ET-1 on primary cultured E11.5 cells needed to be tested to determine if they were capable of promoting formation of the VCS on their own; this was determined in this thesis (Chapter 5). Trabeculae at E11.5 and beyond have been shown to express both NRG-1 and ET-1 (de la Pompa and Epstein, 2012; Meyer and Birchmeier, 1995; Gassmann et al., 1995; Lee et al., 1995; Kramer et al., 1996, Marchionni, 1995; Mikawa and Hurtado, 2007; Takebayashi-Suzuki et al., 2000). Hypothetically, if ET-1 or NRG-1 were unable to alter VCS gene expression on their own at E11.5, there also exists the possibility that these paracrine factors may display positive (synergistic) or negative (antagonistic) interactions with each other and we explored these possibilities as well, in Chapter 5.

The possibility of crosstalk signalling between ANP, ET-1 and NRG-1 and their respective receptors in embryonic heart development has yet to be examined. However, there are some studies that have revealed the potential for crosstalk signalling between some of these paracrine factors outside of the heart. For example, ET-1 induced stimulation of MAPK/Erk2 activity was shown to be inhibited by the addition of exogenous ANP in kidney mesangial cells, an effect that was reversed when the NPR-A antagonist A71915 was added (Pandey et al., 2000). A downstream target of ANP/NPR-A signalling is activation of PKG (Woodard and Rosado, 2008). In adult CMs, it was shown that ET-1 induced stimulation of Erk was attenuated by regulator of G-protein signalling 2 (RGS2), which is a downstream target of activated PKG (Xie and Palmer, 2007). Thus, it is possible that ANP- induced activation of PKG may have led to activation of RGS2, reversing the effects of ET-1 induced stimulation of Erk in adult CMs. This raises the possibility that the ANP/NPR-A signalling system may interact with the ET-1/ and ET-A/ET-B receptor signalling system to regulate the activity of Erk in the embryonic heart.

There is evidence in the literature to support the potential for crosstalk signalling between NRG-1 and ET-1 signalling. Patel and Kos (2005) determined that ET-1 and NRG-1 were both capable of independently upregulating the same set of CCS markers in the mouse embryonic heart: Cx40, Cx45, Nkx2.5, GATA4, Irx4, HF-1b and MinK. Expression of NRG-1 has been detected in the developing mouse endocardial endothelium by *in situ* hybridization (Zhao et al., 1998), which led a study to examine if NRG-1 expression could be detected in endothelial cells obtained from adult hearts. In adult rat hearts, coronary microvascular endothelial cells were isolated from ventricles,

and were cultured for analysis of NRG-1 expression. NRG-1 mRNA was detected in confluent primary cultures of these cells using a NRG-1 specific cDNA probe (Zhao et al., 1998). Additionally, when exogenous ET-1 (100 nM) was added to the cell culture, this led to a significant increase in NRG-1 mRNA expression approximately 16 hours after addition of the drug (Zhao et al., 1998). This led to the hypothesis that expression of NRG-1 may be regulated by ET-1 signalling (Zhao et al., 1998). This same study utilized a soluble recombinant form of human NRG-1, known as glial growth factor 2 (rhGGF2), and added this to neonatal rat ventricular myocyte primary cell culture (20 ng/ml), and measured the level of prepro-ANP mRNA expression. Addition of NRG-1 led to a significant increase in prepro-ANP mRNA within 60 minutes of incubation, and mRNA expression doubled at 16 hours post-treatment. (Zhao et al., 1998). Although these mentioned studies have only examined the relationships between these three paracrine factors in the context of cardiac hypertrophy, these results still lead to the possibility that ANP, NRG-1, and/or ET-1 signalling may converge to guide development of the embryonic heart. Therefore, we sought to determine potential interactions between ANP, ET-1, NRG-1 and their respective receptors with respect to changes in protein and gene expression of HCN4/Cx40 and cGMP signalling.

6.4.2 Characterizing the Potential for Signalling Interactions Between ANP, ET-1 and NRG-1 Signalling Systems by Examining Changes to HCN4/Cx40 Protein and Gene Expression and Intracellular cGMP Production

The effects of NRG-1 or ET-1 alone on protein expression of HCN4 and Cx40 in E11.5 ventricular cells were examined, and it was found that similar to ANP, both ET-1 and NRG-1 were able to increase the percentage of E11.5 ventricular CMs positive for

HCN4 but not Cx40 and promote the conversion of VCS marker positive non-CMs to VCS marker positive CMs. When we examined the effects of ET-1 or NRG-1 alone on gene expression we found that gene expression levels of HCN4 and Cx40 after addition of exogenous ET-1 were similar to control, whereas NRG-1 significantly induced gene expression of both genes. We tested the effects of adding the non-selective ET receptor antagonist PD145065 and the ErbB receptor antagonist AG1478, on gene expression of HCN4 and Cx40, to determine if blockade of these receptors could alter gene expression. PD145065 was utilized in a study to show that the compound was capable of inhibiting binucleation and proliferation of fetal CMs caused by ET-1 (Paradis et al., 2014). AG1478 was utilized in a study to show that blockade of ErbB receptors in human embryonic stem cell-derived CMs (hESC-CMs) resulted in preferential differentiation of cells toward the working myocyte cell type, while simultaneously reducing the proportion of nodal cells (Zhu et al., 2010). However, in both cases, neither of these compounds have been studied in the context of the developing VCS and Purkinje fiber network. The addition of PD145065 or AG1478 significantly decreased gene expression of both genes, further providing evidence that the ET-1 and NRG-1 signalling systems may be involved in VCS formation. Based on the published literature, there seems to be specific developmental windows for ET-1 (E9.5-E11.5) and NRG-1 (E8.5-E10.5) to regulate CCS development (Gourdie et al., 1998; Rentschler et al., 2002). Here, we have demonstrated that in ventricular cells in the mouse at E11.5, the ET-1 receptor and ErbB receptor signalling pathways may be active to promote formation of the embryonic VCS. Although not tested, it is possible that ET-1 may continue to promote VCS development

past the E11.5 stage, however, this has not been tested by studies in the literature or in this thesis and remains to be determined. Rentschler et al.'s (2002) study demonstrated that the inductive effects of NRG-1 on the CCS could be restricted to a specific developmental period during heart development, since it appeared that NRG-1 had a less of an effect on CCS development past the E10.5 stage. The results from this thesis have shown that ANP provides induction of the VCS from at least the E11.5-E17.5 period. Taken together, we speculate that as the effect of NRG-1 induction on CCS development declines past E11.5, ANP and ET-1 signalling systems dominate to promote further development of the VCS in the embryonic mouse heart. While Rentschler et al.'s (2002) study demonstrated that past E10.5, NRG-1 did not significantly induce development of the CCS vs. control treated whole embryos and that ET-1 did not induce any changes to the development of the CCS at E9.5, compared to the findings in this thesis which demonstrate that the ET-1 and NRG-1 signalling systems were active at E11.5 to promote development of the VCS, the differences in study designs/models between their study and this thesis should be taken into consideration. Their study employed a CCS-*lacZ* mouse model where they qualitatively visualized development of the CCS through expression of *lacZ* in whole embryos/whole hearts. In contrast, in this thesis, we utilized isolated ventricular cells. Drug delivery may have been more effective in isolated cells than in whole hearts.

We also tested the potential for ET-1 or NRG-1 to affect cGMP levels in E11.5 ventricular cells. At E11.5, ET-1 was unable to alter cGMP levels whereas NRG-1 significantly increased cGMP levels, vs. control. We tested the effects of blockade of ET-

1 receptors and ErbB receptors with PD145065 and AG1478 respectively, and found that addition of each inhibitor alone significantly reduced cGMP levels. This provides evidence that ET-1 receptor signalling and NRG-1 receptor signalling may alter cGMP levels in E11.5 ventricular cells, and may be coupled to changes seen in HCN4/Cx40 gene expression to induce formation of the VCS. NRG-1 has been shown to increase NO production in rat CMs (Brero et al., 2010). Given that NO can increase soluble GC activity and promote production of cGMP, this may explain why cGMP levels increased after cells were treated with NRG-1. However, additional work is needed to define precise mechanisms underlying the reduction of cGMP in response to PD145065 and AG1478 treatments.

We tested the effects of combining ANP or NRG-1 with PD145065, to determine if these paracrine factors could potentially rescue the decline in gene expression of HCN4/Cx40 provided by PD145065 alone. In the presence of ANP or NRG-1, in combination with the non-selective ET-1 receptor antagonist PD145065, ANP appears to rescue the decrease in HCN4 and Cx40 gene expression, and NRG-1 may rescue the decrease in HCN4 gene expression only, suggesting the potential for ANP/ET-1 receptor and NRG-1/ET-1 receptor interactions in helping to form the VCS via induction of VCS gene(s).

We also tested the effects of combining ANP or ET-1 with AG1478 to determine if these paracrine factors could rescue the decline in HCN4/Cx40 gene expression provided by AG1478 alone. The presence of ANP in combination with AG1478 appears to rescue the decline in HCN4 and Cx40 gene expression, and ET-1 may be capable of

rescuing the decline in HCN4 gene expression only, potentially raising the possibility that interactions could exist between ANP/ErbB receptors and ET-1/ErbB receptors to guide development of the VCS.

Next, we conducted a series of RT-qPCR experiments to determine the potential for synergistic activity with all three paracrine factors together, or combinations of 2 paracrine factors, on gene expression of HCN4 and Cx40. The combination of ANP, ET-1, and NRG-1 all together, significantly induced HCN4 and Cx40 gene expression vs. control; it appeared that out of all tested pair combinations, only the combination of ANP and NRG-1 may synergistically induce HCN4 and Cx40 expression. When combining NRG-1 or ET-1 with the NPR-A inhibitor A71915, we found that this combination reduced gene expression of Cx40 and HCN4, suggesting that it may be possible for interactions between NPR-A receptors and ET-1 or NRG-1.

There may be compensatory responses to promote development of the CCS when one paracrine factor and/or its respective receptors are lacking. It was demonstrated that in ET-1 receptor KO mice, there were no CCS deficits reported (Hua et al., 2014). In this scenario, it is possible that ANP and/or NRG-1 signalling pathways could have compensated for the lack of ET-1/ET-1 receptor signalling to help promote development of the CCS in the mouse embryonic heart. Furthermore, it has been demonstrated that NPRA-KO mice display reduced survival and develop cardiac hypertrophy and morphological abnormalities during development (Cameron and Ellmers, 2003; Lopez et al., 1995; Ellmers et al., 2002; Scott et al., 2009). Results from this thesis have demonstrated that VCS development may be impaired in NPRA-KO mice

due to decreased HCN4/Cx40 gene expression at E14.5. In NPRA-KO mice that do survive, it is possible that compensatory pathways may exist from ET-1 and/or NRG-1 signalling to rescue CCS defects. NRG-1/ErbB2/ErbB4 signalling has been shown to be essential for cardiac development since NRG-1/ErbB2/ErbB4 KO mice do not survive past mid-gestation due to aborted development of the ventricular trabeculae and potentially due to impaired VCS development (Meyer and Birchmeier, 1995; Gassmann et al., 1995; Lee et al., 1995; Kramer et al., 1996, Marchionni, 1995). Therefore, this suggests that the loss of NRG-1 cannot be compensated by either ANP and/or ET-1 signalling pathways during embryonic heart development, whereas the ANP/NPR-A and ET-1/ET-1 receptor signalling pathways may be partially or fully dispensable during VCS development.

We tested the effects of combination treatments of the three paracrine factors and receptor inhibitor drugs on cGMP levels to determine if these levels could be altered. When we combined the NPR-A inhibitor A71915 with ET-1 or NRG-1, cGMP levels were reduced in both cases, suggesting the possibility that NPR-A receptor signalling may interact with ET-1 or NRG-1 to alter cGMP signalling, which may in turn alter gene expression of HCN4 or Cx40. The combinations of ANP/ET-1 and ANP/NGR-1 did not synergistically affect cGMP levels.

When ANP was combined with PD145065, ANP did not appear to rescue the decline in cGMP caused by PD145065 alone, since there were no differences in cGMP levels between the two groups. The combination of NRG-1 and PD145065 led to a modest decrease in cGMP, which was similar to control levels of cGMP, suggesting that

the presence of NRG-1 may rescue the decline in cGMP caused by PD145065. Thus, it is possible that NRG-1/ET-1 receptor signalling may converge upon cGMP signalling to guide development of the VCS.

When ANP was combined with AG1478, this resulted in a modest decrease in cGMP production vs. control, rescuing cGMP levels to that of control. This suggests the possibility for ANP/ErbB signalling converging on cGMP to further induce development of the VCS. The combination of ET-1 and AG1478 led to a decrease in cGMP production that was significantly less than control, but was similar to that of AG1478 alone, indicating that despite the presence of ET-1, it may not have been sufficient to rescue the decline in cGMP levels caused by AG1478 alone.

Since ANP in combination with PD145065 did not appear to rescue the decline in cGMP caused by PD145065 alone, it is possible that ANP may have an inhibitory role in ET-1/ET-1 receptor signalling in VCS development at E11.5, like in Pandey et al.'s (2000) study, where exogenous ANP inhibited ET-1 induced stimulation of MAPK/Erk2 in kidney mesangial cells. This negative interaction at E11.5 or potentially at later developmental stages between ANP/NPR-A and ET-1/ET-1 receptors may be necessary to prevent VCS development in unwanted regions of the heart. For example, subendocardial localization of the VCS, particularly to a few cell layers, may be achieved by the negative interactions in zones distal to VCS areas so that those zones may remain as working CMs.

We wanted to determine the effects of blocking PKG on HCN4 and Cx40 gene expression, in combination with ET-1 or NRG-1, in order to determine the potential for

ANP/NPR-A/cGMP/PKG signalling system to interact with ET-1 or NRG-1 signalling systems. The combination of ET-1 + Rp-8-pCPT-cGMPS rescued the decline in gene expression of HCN4 vs. Rp-8-pCPT-cGMPS alone but was insufficient to rescue the decline in gene expression of Cx40. The combination of NRG-1 + Rp-8-pCPT-cGMPS seemed to rescue the decline in HCN4 and Cx40 gene expression. To determine if combined blockade of ET-1 receptors and PKG could synergistically reduce HCN4/Cx40 gene expression, we combined PD145065 and Rp-8-pCPT-cGMPS resulting in a reduction in HCN4 and Cx40 gene expression vs. control, which was similar to the level of expression provided by PD145065 alone or Rp-8-pCPT-cGMPS treatment alone. Thus, there did not appear to be any additive/synergistic effects offered by combining blockade of ET receptors and blockade of PKG with respect to changes in HCN4 and Cx40 gene expression. Similarly, to test whether combined blockade of ErbB receptors and PKG could synergistically reduce HCN4 and/or Cx40 gene expression, we combined AG1478 and Rp-8-pCPT-cGMPS which reduced HCN4 and Cx40 gene expression vs. control, but levels of expression were similar with AG1478 or Rp-8-pCPT-cGMPS treatment alone. Thus, there did not appear to be any additive/synergistic effects gained by combining blockade of ErbB receptors and blockade of PKG with respect to changes in HCN4 and Cx40 gene expression. Taken together, these results provide evidence that NRG-1 may be involved in PKG-induced induction of HCN4 and Cx40 gene expression, either by converging on PKG signalling or interacting with NPR-A (and the downstream effector PKG). In contrast, it is unclear whether ET-1 interacts with PKG (either alone or through downstream NPR-A signalling) to affect HCN4 or Cx40 gene

expression. Since NRG-1 increases NO production in CMs and NO increases the production of cGMP (Brero et al., 2010), it is likely that NRG-1 treatment may lead to downstream activation of PKG to induce HCN4/Cx40 gene expression. On the other hand, there does not appear to be an association between ET-1 receptor signalling and PKG activation in cardiac or non-cardiac cell types described in the literature, and the results presented in this thesis do not provide a definitive role for PKG involvement in ET-1 receptor signalling in the modulation of VCS development. Further work needs to be done to tease out whether PKG activity is involved in ET-1 mediated development of the VCS.

It is important to note that from these experiments, we cannot definitely provide deeper mechanistic insights into interactions between ANP/ET-1/NG-1 and their receptors with respect to the development of the VCS. However, we have presented evidence that induction of HCN4/Cx40 genes and changes to cGMP signalling upon exposure to combinations of paracrine factors and their inhibitors points to the possibility that signalling interactions may exist in the embryonic mouse heart. A continued investigation into the interplay between the paracrine factors ANP, ET-1 and NRG-1 and their signalling pathways and transcriptional regulatory networks will help to facilitate our understanding of the molecular mechanisms involved in the proliferation, differentiation, and patterning of conduction system cells (Mikawa & Hurtado, 2007).

6.4.3 Effects of ET-1 and NRG-1 on Cardiomyocyte Cell Growth/Hypertrophy in the Embryonic Heart

Both ET-1 and NRG-1 have been shown to induce hypertrophic growth of adult CMs *in vivo* (Zhao et al., 1998; Nishida et al., 1993; Shubeita et al., 1990; Fischer et al., 1997). In rabbit ventricular trabeculae exposed to ET-1 treatment, ET-1 induced a gradual increase in developed force of contractions over 24 hours of culture (Bupha-Intr et al., 2012). NRG-1 was shown to induce hypertrophic growth of both neonatal and adult ventricular CMs (Zhao et al., 1998). In their study, NRG-1 was added to cell cultures of rat neonatal and adult ventricular CMs, increasing both cell size and myofibrillar development (Zhao et al., 1998). There is currently a lack of evidence to describe a potential role for ET-1 and NRG-1 to affect cell growth in embryonic CMs. After culturing E11.5 ventricular cells with either NRG-1 or ET-1 for 20 hours, we found that ET-1 or NRG-1 significantly increased cell area of CMs vs. control. When we added the receptor inhibitors PD145065 or AG1478 to cells, there were no statistically significant differences in cell area vs. control. Thus, at concentrations of 1.5 nM and 2.5 nM of ET-1 and NRG-1 respectively, they may promote cell growth/hypertrophy in ventricular CMs at E11.5 in the embryonic mouse heart. It is possible that the concentrations of the inhibitor drugs used were insufficient to provide a significant difference in cell area of CMs vs. control. Therefore, the cell area of CMs may alter with use of higher concentrations of the inhibitor drugs, although this remains to be tested.

6.5 Clinical Significance

CHD can often be a debilitating disease, affecting 12 to 14 per 1,000 newborns and also adults who may not display symptoms at an early age (Bruneau et al., 2008;

Subramanyan et al., 2000; Hoffman and Kaplan, 2012). Often, children or adults with CHD must undergo strenuous rounds of surgery, which may drastically reduce their quality of life. Birth defects in the heart lead to the development of CHD, many of which often result in the development of severe conduction system deficits. If patients develop arrhythmias from CHDs, pharmacological interventions are often not sufficient enough to provide a cure. Although progress has been made to elucidate the electrophysiological mechanisms governing development of the CCS and the incidence of CHDs, less is understood about the molecular mechanisms. ANP, a paracrine factor involved in natriuresis and diuresis in the human body, may also play a significant role in the development of the VCS. ANP has been shown to be transiently expressed in the ventricular trabeculae of the embryonic heart, which will eventually give rise to the bundle branches and Purkinje fibers of the mature VCS, raising the possibility that ANP/NPR-A/cGMP signalling could be involved in the development of the cardiac Purkinje fiber network and the VCS (Christoffels et al., 2000). Additionally, ET-1 and NRG-1, both of which are paracrine factors described in the literature to be secreted by endothelial/endocardial cells, have been shown to promote differentiation of CMs to CCS cells in chick and mouse embryonic hearts respectively (Gourdie et al., 1998; Rentschler et al., 2002). Additionally, ET-1 and NRG-1 were also found to be highly expressed in the ventricular trabeculae (Takebayashi-Suzuki et al., 2000; de la Pompa and Epstein, 2012). Therefore, it is possible that a complex cellular signalling network may exist in the ventricular trabeculae of the mouse embryonic heart whereby ANP, ET-1, and NRG-1 may interact with each other and their signalling systems to guide

differentiation of various cardiac cell types to conduction system cells, in order to promote formation and development of the cardiac Purkinje fiber network of the VCS. Work in this thesis has provided evidence that the ANP/NPR-A/cGMP signalling system is biologically active in the embryonic mouse heart, and may promote development of the VCS through downstream PKG signalling and induction of HCN4 and/or Cx40 genes. Furthermore, we have characterized the pharmacological properties of the NPR-A antagonist A71915, of which scant information is available in the literature, which provides an avenue for exploration with regards to effects of blockade of the NPR-A receptor on correcting potential ectopic pacemaker formation and increased conduction system rhythmic abnormalities experienced by patients with various cardiac diseases including CHDs. Lastly, we have explored the potential for interactions between ANP/NG-1/ET-1 signalling systems in the development of the VCS, revealing a significant layer of complexity that needs to be teased out further in detail. A summary of the potential for signalling interactions as devised from the experiments performed in this thesis is shown in **Figure 6.1**.

Nepilysin (NEP), a zinc-containing, membrane-bound, neutral endopeptidase can bind to and degrade natriuretic peptides, and its inhibition presents a therapeutic approach to treating congestive heart failure (CHF) (Potter, 2011). CHF is a condition where the heart is unable to pump enough blood to the organs, leading to tissue congestion, and affecting the ability of the kidney to dispose of sodium and water, thereby increasing edema (Woodard and Rosado, 2008). Oral NEP inhibitors have been administered to elevate plasma natriuretic peptide concentrations, including ANP, in

both human and animal models. By inhibiting NEP, this increases plasma ANP levels in the body to promote sodium excretion during heart failure, attenuating blood pressure and blood volume in this diseased state (Potter, 2011). Taking into the account the findings presented in this thesis, that ANP may play a role in the induction of the VCS, it is possible that NEP inhibitors may also be beneficial to patients with conduction system deficits by increasing ANP levels, which may provide additional development of the VCS for patients that are lacking functionality in component(s) of the VCS.

The clinical significance of work performed in this thesis also extends to addressing the current problem in regenerative medicine of pharmacological therapies and surgical interventions being unable to efficiently replace lost myocardium in disease states or injury. Transplanted fetal CMs and cardiac stem cells have been shown to significantly improve cardiac performance with minimal complications to the host myocardium (Rubart et al., 2003; Roell et al., 2007; Bolli et al., 2011; Makkar et al., 2012). In this thesis, we have demonstrated that exogenous cGMP was capable of reducing proliferation of CPCs *in vitro* at E11.5. Thus, it is possible that when transplanting CPCs into damaged myocardium, these cells could be exposed to high concentrations of “pockets” of ANP released as an autocrine/paracrine factor throughout the heart, which could potentially convert these CPCs into VCS cells. This may provide a potential avenue for transplantation to facilitate the enrichment of pacemaker or conduction system cells *in vitro* in order to treat patients presenting with severe conduction system deficits or blockade.

Conversely, blockade of the NPR-A receptor with A71915 could regulate the occurrence of arrhythmias in patients with conduction system defects, presenting an area of opportunity to explore in pharmacological therapeutics. ANP synthesis in the ventricles is significantly enhanced in various diseased states including CHD and ischemic heart disease (Chien et al., 1991). Due to the development of arrhythmias post-transplantation in patients it is possible that transplanted CPCs and/or CMs could activate NPR-A signalling pathways to induce ectopic pacemaker formation and therefore, lead to the generation of more arrhythmias in the patient. Thus, another potential application for A71915 could be to reduce ectopic pacemaker activity through blockade of NPR-A receptors in the heart.

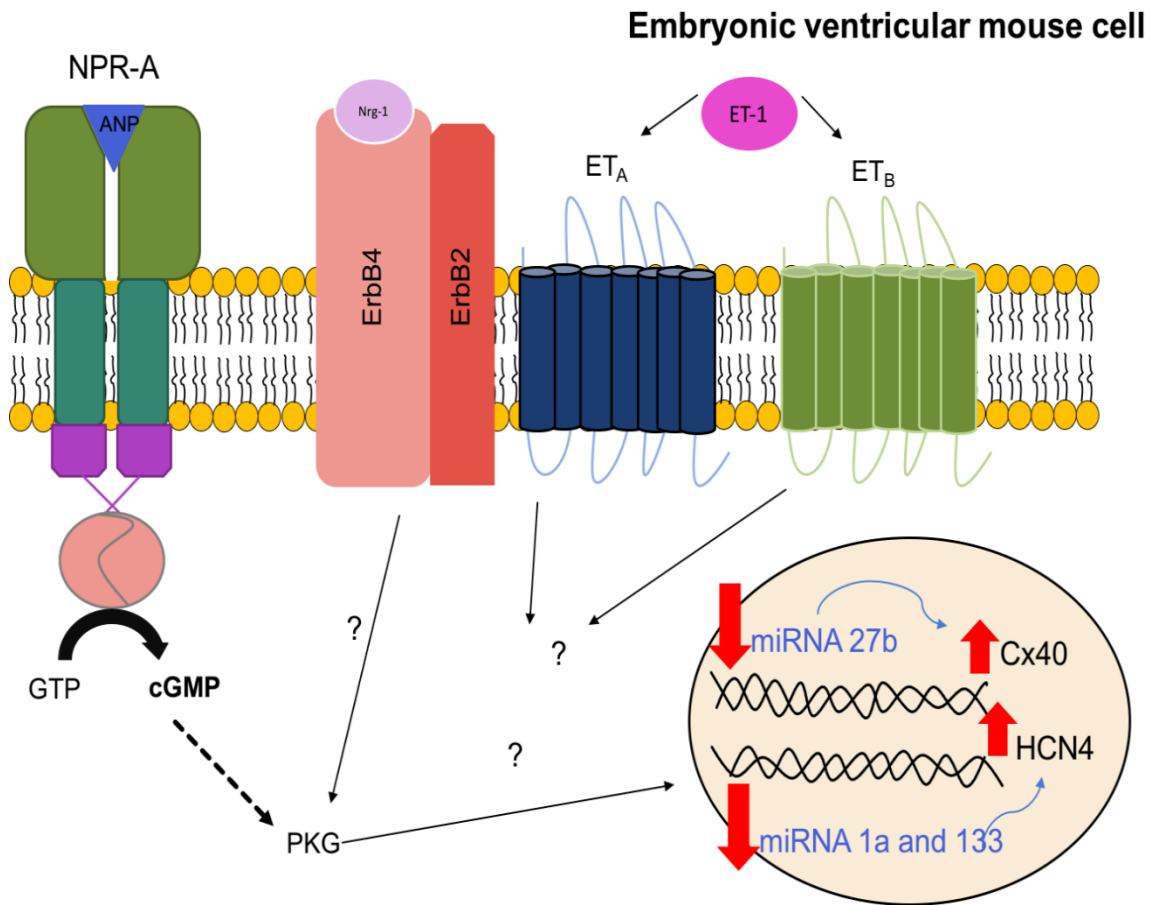


Figure 6.1. Complex cellular network involving ANP, ET-1 and NRG-1 signalling pathways may be involved in signalling interactions to promote formation and development of the ventricular conduction system in the embryonic mouse heart.

6.6 Limitations and Future Directions

The findings in this thesis indicate that the ANP/NPR-A/cGMP signalling pathway is biologically active in the embryonic mouse heart, and may contribute toward development of the VCS through stimulation of PKG leading to induction of HCN4 and Cx40 genes. Additionally, ANP/NPR-A signalling may affect regulation of important miRNAs which in turn, regulate HCN4/Cx40 gene expression. In our study, we have been unable to identify a potential link between stimulation of PKG and the changes to miRNA expression we observed, which both independently led to induction of HCN4 and Cx40, and so there is certainly an opportunity for further exploration to continue to elucidate the mechanism(s) by which ANP stimulates development of the Purkinje fiber network and VCS. In addition, although we used immunofluorescence to determine changes to protein expression of HCN4 and Cx40 as well as a Cx40^{egfp} reporter model, this needs to be validated with Western blot experiments. Although a cGMP-independent pathway exists following NPR-A stimulation by ANP in the context of chronic hypertrophy, the existence of such a pathway in the development of the VCS has not yet been examined in the literature, or in this thesis. It is possible that this pathway could play a role in the development of the VCS, and therefore, future work needs to be done to test if NPR-A stimulation could lead to TRPC3/6 activation and subsequent Ca²⁺ influx through LTCCs, in the development of the VCS. Our investigation into the potential interactions between ANP, ET-1 and NRG-1 signalling pathways shed some insight into the complexity of this cellular network, and although efforts have been made to elucidate the potential for interplay, further work needs to be done.

Lastly, although luciferase assays indicated that all three paracrine factors induced Cx40-promoter activity, there was a lack of control plasmid in our experiments, and so this group will need to be added in future studies. Furthermore, it remains to be determined which specific regions of the Cx40 promoter could be induced by ANP, ET-1, or NRG-1.

6.7 Conclusions

A considerable body of literature has described the detailed development of the CCS in the embryonic heart, including the involvement of important paracrine factors such as ET-1 and NRG-1. Work in this thesis has demonstrated the possibility that a paracrine factor known as ANP may also play a role in the development of the VCS, and that this may occur through an independent signalling pathway (ANP/NPR-A/cGMP/PKG) or potentially via interactions with ET-1 and/or NRG-1 and their respective signalling systems.

REFERENCES

- Aanhaanen WTJ, Brons JF, Dominguez JN, Rana MS, Norden J, Airik R, Wakker V, de Gier-de Vries C, Brown NA, Kispert A, et al. (2009). The Tbx2+ primary myocardium of the atrioventricular canal forms the atrioventricular node and the base of the left ventricle. *Circ. Res.* 104, 1267.
- Abell TJ, Richards AM, Ikram H, Espiner EA, Yandle T. (1989). Atrial natriuretic factor inhibits proliferation of vascular smooth muscle cells stimulated by platelet-derived growth factor. *Biochem Biophys Res Commun* 160, 1392-1396.
- Accili EA, Proenza C, Baruscotti M, DiFrancesco D. (2002). From funny current to HCN channels: 20 years of excitation. *News Physiol Sci* 17, 32-37.
- Airhart N, Yang YF, Roberts CT, Silberbach M. (2003). Atrial natriuretic peptide induces natriuretic peptide receptor-cGMP-dependent protein kinase interaction. *The Journal of Biological Chemistry* 278, 38693-38698.
- Alev C, Urschel S, Sonntag S, Zoidl G, Fort AG, Hoher T, Matsubara M, et al. (2008). The neuronal connexin36 interacts with and is phosphorylated by CAMKII in a way similar to CAMKII interaction with glutamate receptors. *Proc Natl Acad Sci USA* 105, 20964-20969.
- Alsan BH, Schultheiss TM. (2002). Regulation of avian cardiogenesis by Fgf8 signalling. *Development* 129, 1935-1943.
- Anand RJ, Hackham DJ. (2005). The role of gap junctions in health and disease. *Crit Care Med* 33, S535-S538.
- Anand-Srivastava MB, Srivastava AK, Cantin M. (1987). Pertussis toxin attenuates atrial natriuretic factor-mediated inhibition of adenylate cyclase. Involvement of inhibitory guanine nucleotide regulatory protein. *J Biol Chem* 262, 4931-4934.
- Argentin S, Ardati A, Tremblay S, Lihmann I, Robitaille L, Drouin J, Nemer M. (1994). Developmental stage-specific regulation of atrial natriuretic factor gene transcription in cardiac cells. *Mol Cell Biol* 14, 777-790.
- Bartel DP. (2004). MicroRNAs: genomics, biogenesis, mechanism, and function. *Cell* 116, 281-297.
- Basson CT, Bachinsky DR, Lin RC, Levi T, Elkins JA, Soultis J, Grayzel D, et al. (1997). Mutations in human TBX5 cause limb and cardiac malformation in Holt-Oram syndrome. *Nat Genet* 15, 30-35.

- Beblo DA, Veenstra RD. (1997). Monovalent cation permeation through the connexin40 gap junction channel. Cs, Rb, K, Na, Li, TEA, TMA, TBA, and effects of anions Br, Cl, F, acetate, aspartate, glutamate, and NO₃. *J Gen Physiol* 109, 509-522.
- Becker JR, Chatterjee S, Robinson TY, Bennett JS, Panakova D, Galindo CL, Zhong L, et al. (2014). Differential activation of natriuretic peptide receptors modulates cardiomyocyte proliferation during development. *Development* 141, 335-345.
- Belaguli NS, Sepulveda JL, Nigam V, Charron F, Nemer M, Schwartz RJ. (2000). Cardiac tissue enriched factors serum response factor and GATA-4 are mutual coregulators. *Mol Cell Biol* 20, 7550-7558.
- Benson DW, Silberbach GM, Kavanaugh-McHugh A, Cottrill C, Zhang Y, Riggs S, Smalls O. (1999). Mutations in the cardiac transcription factor Nkx2.5 affect diverse cardiac developmental pathways. *J Clin Invest* 104, 1567-1573.
- Bevilacqua LM, Simon AM, Maguire CT, Gehrman J, Wakimoto H, Paul DL, Berul CI. (2000). A targeted disruption in connexin40 leads to distinct atrioventricular conduction defects. *J Interv Card Electrophysiol* 4, 459-467.
- Bolli R, Chugh AR, D'Amario D, Loughran JH, Stouddard MF, Ikram S, Beache GM, et al. (2011). Cardiac stem cells in patients with ischemic cardiomyopathy (SCIPIO): initial results of a randomized phase 1 trial. *Lancet* 378: 1847-1857.
- Boron WF, Boulpaep EL. (2009). *Medical physiology*. Philadelphia, PA: Elsevier.
- Boyett MR. (1994). 'And the beat goes on'. The cardiac conduction system: the wiring system of the heart. *Exp Physiol* 10, 1035-1049.
- Brero A, Ramella R, Fitou A, Dati C, Alloatti G, Gallo MP, Levi R. (2010). Neuregulin-1beta1 rapidly modulates nitric oxide synthesis and calcium handling in rat cardiomyocytes. *Cardiovasc Res* 88, 443-452.
- Bruneau BG, Nemer G, Schmitt JP, Charron F, Robitaille L, Caron S, Conner DA, et al. (2001). A murine model of Holt-Oram syndrome defines roles of the T-box transcription factor Tbx5 in cardiogenesis and disease. *Cell* 106, 709-721.
- Bruneau BG. (2008). The developmental genetics of congenital heart disease. *Nature* 451, 943-948.
- Bruneau BG. (2011). Atrial natriuretic factor in the developing heart: a signpost for cardiac morphogenesis. *Can J Physiol Pharmacol* 89, 533-537.
- Buckingham M, Meilhac S, Zaffran S. (2005). Building the mammalian heart from two sources of myocardial cells. *Nature reviews Genetics* 6, 826-835.

- Bupha-Intr T, Haizlip KM, Janssen P. (2012). Role of endothelin in the induction of cardiac hypertrophy in vitro. *PLoS ONE* 7, e43179.
- Burgess TL, Kelly RB. (1987). Constitutive and regulated secretion of proteins. *Annu Rev Cell Biol* 3, 243-293.
- Cai CL, Liang X, Shi Y, Chu PH, Pfaff SL, Chen J, Evans S. (2003). *Isl1* identifies a cardiac progenitor population that proliferates prior to differentiation and contributes a majority of cells to the heart. *Dev Cell* 5, 877-889.
- Cai X, Hagedorn CH, Cullen BR. (2004). Human microRNAs are processed from capped, polyadenylated transcripts that can also function as mRNAs, *RNA-Publ. RNA Soc* 10, 1957-1966.
- Callis TE, Pandya K, Seok HY, Tang R, Tatsuguchi M, Huang Z, Chen J, et al. (2009). MicroRNA-208a is a regulator of cardiac hypertrophy and conduction in mice. *J Clin Invest* 119, 2772-2786.
- Cameron VA, Ellmers LJ. (2003). Minireview: natriuretic peptides during development of the fetal heart and circulation. *Endocrinology* 144, 2191-2194.
- Cannell IG, Kong YW, Bushell M. (2008). How do microRNAs regulate gene expression? *Biochem Soc Trans* 36, 1224-1231.
- Cao L, Gardner DG. (1995). Natriuretic peptides inhibit DNA synthesis in cardiac fibroblasts. *Hypertension* 25, 227-234.
- Chang MS, Lowe DG, Lewis M, Hellmiss R, Chen E, Goeddel DV. (1989). Differential activation by atrial and brain natriuretic peptides of two different receptor guanylate cyclases. *Nature* 341, 68-72.
- Chapman SC, Schubert FR, Schoenwolf GC, Lumsden A. (2003). Anterior identity is established in chick epiblast by hypoblast and anterior definitive endoderm. *Development* 130, 5091-5101.
- Chen H, Shi S, Acosta L, Li W, Lu J, Bao S, Chen Z, Yang Z, Schneider MD, Chien KR, et al. (2004). BMP10 is essential for maintaining cardiac growth during murine cardiogenesis. *Development* 131, 2219-2231.
- Cheung CY, Gibbs DM, Brace RA. (1987). Atrial natriuretic factor in maternal and fetal sheep. *Am J Physiol* 252, E279-282.
- Chien KR, Knowlton KU, Zhu H, Chien S. (1991). Regulation of cardiac gene expression during myocardial growth and hypertrophy: molecular studies of an adaptive physiologic response. *Faseb J* 5, 3037-3046.

Chinchilla A, Lozano E, Daimi H, Esteban FJ, Crist C, Aranega AE, Franco D. (2011). MicroRNA profiling during mouse ventricular maturation: a role for miR-27 modulating Mef2c expression. *Cardiovasc Res* 89, 98-108.

Christoffels VM, Habets PE, Franco D, Campione M, de Jong F, Lamers WH, Bao ZZ, Palmer S, et al. (2000). Chamber formation and morphogenesis in the developing mammalian heart. *Dev Biol* 223, 266-278.

Christoffels VM, Mommersteeg MTM, Trowe MO, Prall OWJ, deGierde VC, Soufan AT, Bussen M, Schuster-Gossler K, Harvey RP, Moorman AFM, et al. (2006). Formation of the venous pole of the heart from an Nkx2-5-negative precursor population requires Tbx18. *Circ. Res.* 98, 1555-1563.

Christoffels VM, Moorman AF. (2009). Development of the cardiac conduction system: why are some regions of the heart more arrhythmogenic than others? *Circ Arrhythm Electrophysiol* 2, 195-207.

Condorelli DF, Parenti R, Spinella F, Salinaro TA, Belluardo N, Cardile V, Circata F. (1998). Cloning of a new gap junction gene (Cx36) highly expressed in mammalian brain neurons. *Eur J Neurosci* 10, 1202-1208.

D'Souza A, Bucchi A, Johnsen AB, Logantha SJ, Monfredi O, Yanni J, Prehar S, et al. (2014). Exercise training reduces resting heart rate via downregulation of the funny channel HCN4. *Nature Communications* 5, 3775.

D'Souza SP, Davis M, Baxter GF. (2004). Autocrine and paracrine actions of natriuretic peptides in the heart. *Pharmacol Ther* 101, 113-129.

Dai YS, Cserjesi P, Markham BE, Molkentin JD. (2002). The transcription factors GATA4 and dHAND physically interact to synergistically activate cardiac gene expression through a p300-dependent mechanism. *J Biol Chem* 277, 24390-24398.

Davenport AP, Hyndmann KA, Dhaun N, Southan C, Kohan DE, Pollock JS, Pollock DM, Webb DJ, et al. (2016). Endothelin. *Pharmacol Rev* 68, 357-418.

Dbouk HA, Mroue RM, El-Sabban ME, Talhouk RS. (2009). Connexins: a myriad of functions extending beyond assembly of gap junction channels. *Cell Communication and Signalling* 7, 1-17.

de la Pompa JL, Epstein JA. (2012). Coordinating tissue interactions: Notch signalling in cardiac development and disease. *Dev. Cell* 22, 244-254.

Delorme B, Dahl E, Jarry-Guichard T, Marics I, Briand JP, Willecke K, Gros D, et al. (1995). Developmental regulation of connexin 40 gene expression in mouse heart correlates with the differentiation of the conduction system. *Dev Dyn* 204, 358-371.

- Delporte C, Winand J, Poloczek P, Geldern TV, Christophe J. (1992). Discovery of a potent atrial natriuretic peptide antagonist for ANP_A receptors in the human neuroblastoma NB-OK-1 cell line. *European Journal of Pharmacology* 224, 183-188.
- Deprez I, Darmon ME, Hira M, Adam M, Sanquer S, Teiger E, Chetboul V, et al. (2001). Adenovirus mediated transfer of the atrial natriuretic peptide gene in rat pulmonary vascular smooth muscle cells leads to apoptosis. *J Lab Clin Med* 137, 155-164.
- Dhaunsi GS, Hassid A. (1996). Atrial and C-type natriuretic peptides amplify growth factor activity in primary aortic smooth muscle cells. *Cardiovasc Res* 31, 37-47.
- Di Lisi R, Sandri C, Franco D. (2000). An atrioventricular canal domain defined by cardiac troponin I transgene expression in the embryonic myocardium. *Anat Embryol (Berl)* 202, 95-101.
- DiCicco-Bloom E, Lelievre V, Zhou X, Rodriguez W, Tam J, Waschek JA. (2004). Embryonic expression and multifunctional actions of the natriuretic peptides and receptors in the developing nervous system. *Dev Biol* 271, 161-175.
- DiFrancesco D. (1993). Pacemaker mechanisms in cardiac tissue. *Annu Rev Physiol* 58, 299-327.
- Dobrzynski H, Boyett MR, Anderson RH. (2007). New insights into pacemaker activity promoting understanding of sick sinus syndrome. *Circulation* 115, 1921-1932.
- Dora KA, Garland CJ, Kwan HY, Yao X. Endothelial cell protein kinase G inhibits release of EDHF through a PKG-sensitive cation channel. (2001). *Am J Physiol Heart Circ Physiol* 280, 1272-1277.
- Dun W, Boyden PA. (2008). The Purkinje cell: 2008 style. *J Mol Cell Cardiol*, 617-624.
- Durocher D, Nemer M. (1998). Combinatorial interactions regulating cardiac transcription. *Dev Genet* 22, 250-262.
- Elfgang C, Eckert R, Lichtenberg-Frate H, Butterweck A, Traub O, Klein RA, Hulser DF, et al. (1995). Specific permeability and selective formation of gap junction channels in connexin-transfected HeLa cells. *J Cell Biol* 129, 805-817.
- Ellmers LJ, Knowles JW, Kim HS, Smithies O, Maeda N, Cameron VA. (2002). Ventricular expression of natriuretic peptides in Npr1(-/-) mice with cardiac hypertrophy and fibrosis. *Am J Physiol Heart Circ Physiol* 283, H707-714.
- Evans SM, Yelon D, Conlon FL, Kirby ML. (2010). Myocardial lineage development. *Circ Res* 107, 1428-1444.

Evans WH, Martin PE. (2002). Lighting up gap junction channels in a flash. *Bioessays* 24, 876-880.

Feridooni T, Hotchkiss A, Baguma-Nibasheka M, Zhang F, Allen B, Chinni S, Pasumarthi KBS. (2017). Effects of B-adrenergic receptor drugs on embryonic ventricular cell proliferation and differentiation and their impact on donor cell transplantation. *Am J Physiol Heart Circ Physiol* 312, H919-H931.

Feridooni T. (2014). The effects of beta-adrenergic drugs on proliferation and differentiation of mid-gestation ventricular cells and their impact on donor cell transplantation (Doctoral dissertation), Dalhousie University.

Fischer TA, Ungureanu-Longrois D, Singh K, de Zengotita J, DeUgarte D, Alali A, Gadbut AP, et al. (1997). Regulation of bFGF expression and ANG II secretion in cardiac myocytes and microvascular endothelial cells. *Am J Physiol* 272, H958-968.

Fiscus RR, Tu AW, Chew SB. (2001). Natriuretic peptides inhibit apoptosis and prolong the survival of serum-deprived PC12 cells. *NeuroReport* 12, 185-189.

Fishman MC, Chien KR. (1997). Fashioning the vertebrate heart: earliest embryonic decisions. *Development* 124, 2099-2117.

Fu JD, Rushing SN, Lieu DK, Chan CW, Kong CW, Geng L, Wilson KD, et al. (2011). Distinct roles of microRNA-1 and -499 in ventricular specification and functional maturation of human embryonic stem cell-derived cardiomyocytes. *PLoS ONE* 6, e27417.

Fujisaki H, Ito H, Hirata Y, Tanaka M, Hata M, Lin M, Adachi S, et al. (1995). Natriuretic peptides inhibit angiotensin-II induced proliferation of rat cardiac fibroblasts by blocking endothelin-1 gene expression. *J Clin Invest* 96, 1059-1065.

Fuller F, Porter JG, Arfsten AE, Miller J, Schilling JW, Scarborough RM, Lewicki JA, et al. (1988). Atrial natriuretic peptide clearance receptor. Complete sequence and functional expression of cDNA clones. *J Biol Chem* 263, 9395-9401.

Garcia-Frigola C, Shi Y, Evans SM. (2003). Expression of the hyperpolarization-activated cyclic nucleotide-gated cation channel HCN4 during mouse heart development. *Gene Expr. Patterns* 3, 777-783.

Garg V, Kathiriya IS, Barnes R, Schluterman MK, King IN, Butler CA, Rothrock CR, et al. (2003). GATA4 mutations cause human congenital heart defects and reveal an interaction with TBX5. *Nature* 424, 443-447.

Gaspard GJ, Pasumarthi KB. (2008). Quantification of cardiac fibrosis by colour-substractive computer-assisted image analysis. *Clin Exp Pharmacol Physiol* 35, 679-686.

- Gassmann M, Casagrande F, Orioli D, Simon H, Lai C, Klein R, Lemke G. (1995). Aberrant neural and cardiac development in mice lacking the ErbB4 neuregulin receptor. *Nature* 378, 390–394.
- Gessert S, Kuhl M. (2010). The multiple phases and faces of wnt signalling during cardiac differentiation and development. *Circulation Research* 107, 186-199.
- Glenn DJ, Rahmutula D, Nishimoto M, Liang F, Gardner DG. (2009). Atrial natriuretic peptide suppresses endothelin gene expression and proliferation in cardiac fibroblasts through a GATA4-dependent mechanism. *Cardiovasc Res* 84, 209-217.
- Goldstein DS, Zimlichman R, Stull R, Keiser HR, Kopin IJ. (1986). Estimation of intrasynaptic norepinephrine concentrations in humans. *Hypertension* 8, 471-475.
- Gourdie RG, Wei Y, Kim D, Klatt SC, Mikawa T. (1998). Endothelin-induced conversion of embryonic heart muscle cells into impulse-conducting Purkinje fibers. *Proc. Natl. Acad. Sci. USA* 95, 6815-6818.
- Grapin-Botton A, Bonnin MA, Le Douarin NM. (1997). Hox gene induction in the neural tube depends on three parameters: competence, signal supply and paralogue group. *Development* 124, 849-859.
- Grego-Bessa J, Luna-Zurita L, del Monte G, Bolos V, Melgar P, Arandilla A, Garratt AN, Zang H, Mukoyama Y, et al. (2007). Notch signalling is essential for ventricular chamber development. *Developmental Cell* 12, 415-429.
- Gros D, Dupays L, Alcolea S, Meysen S, Miquerol L, Theveniau-Ruissy M. (2004). Genetically modified mice: tools to decode the functions of connexins in the heart – new models for cardiovascular research. *Cardiovascular Research* 62, 299-308.
- Gros D, Theveniau-Ruissy M, Bernard M, Calmels T, Kober F, Sohl G, Willecke K, et al. (2010). Connexin 30 is expressed in the mouse sinoatrial node and modulates heart rate. *Cardiovasc Res* 85, 45-55.
- Hagendorff A, Schumacher B, Kirchhoff S, Luderitz B, Willecke K. (1999). Conduction disturbances and increased atrial vulnerability in connexin40-deficient mice analyzed by transesophageal stimulation. *Circulation* 99, 1508-1515.
- Han W, Bao W, Wang Z, Nattel S. (2002). Comparison of ion-channel subunit expression in canine cardiac Purkinje fibers and ventricular muscle. *Circ Res* 91, 790-797.
- Harvey RP. (2002). Patterning the vertebrate heart. *Nat Rev Genet* 3, 544-556.
- Harzheim D, Pfeiffer KH, Fabritz L, Kremmer E, Buch T, Waishman A, Kirchhof P, et al. (2008). Cardiac pacemaker function of HCN4 channels in mice is confined to embryonic development and requires cyclic AMP. *Embo J* 27, 692-703.

- Hattori F, Chen H, Yamashita H, Tohyama S, Satoh Y, Yuasa S, Li W, et al. (2010). Nongenetic method for purifying stem cell-derived cardiomyocytes. *Nature* 7, 61-66.
- Hawkrigde AM, Heublein DM, Bergen HR, Cataliotti A, Burnett JC, Muddiman DC. (2005). Quantitative mass spectral evidence for the absence of circulating brain natriuretic peptide in severe human heart failure. *Proc Natl Acad Sci USA* 102, 17442-17447.
- He XI, Chow Dc, Martick MM, Garcia KC. (2001). Allosteric activation of a spring-loaded natriuretic peptide receptor dimer by hormone. *Science* 293, 1657-1662.
- Herrman S, Stieber J, Stockl G, Hofmann F, Ludwig A. (2007). HCN4 provides a 'depolarization reserve' and is not required for heart rate acceleration in mice. *Embo J* 26, 4423-4432.
- Hertig CM, Kubalak SW, Wang Y, Chien KR. (1999). Synergistic roles of neuregulin-1 and insulin-like growth factor-1 in activation of the phosphatidylinositol 3-kinase pathway and cardiac chamber morphogenesis. *J Biol Chem* 274, 37362-37369.
- Hiroi Y, Kudoh S, Monzen K, Ikeda Y, Yazaki Y, Nagai R, Komuro I. (2001). Tbx5 associates with Nkx2-5 and synergistically promotes cardiomyocyte differentiation. *Nat Genet* 28, 276-280.
- Hirst-Jensen BJ, Sahoo P, Kieken F, Delmar M, Sorgen PL. (2007). Characterization of the pH-dependent interaction between the gap junction protein connexin43 carboxyl terminus and cytoplasmic loop domains. *J Biol Chem* 282, 5801-5813.
- Hoffman JI, Kaplan S. (2002). The incidence of congenital heart disease. *J Am Coll Cardiol* 39, 1890-1900.
- Horio T, Nishikimi T, Yoshihara F, Matsuo H, Takishita S, Kanagawa K. (2000). Inhibitory regulation of hypertrophy by endogenous atrial natriuretic peptide in cultured cardiac myocytes. *Hypertension* 35, 19-24.
- Horsthuis T, Buermans HP, Brons JF, Verkerk AO, Bakker ML, Wakker V, Clout DE, et al. (2009). Gene expression profiling of the forming atrioventricular node using a novel tbx3-based node-specific transgenic reporter. *Circ Res* 105, 61-69.
- Hotchkiss A. (2013). The effects of calcium channel blockade and atrial natriuretic peptide signalling on proliferation and differentiation of cardiac progenitor cells (Doctoral dissertation), Dalhousie University.
- Hotchkiss A, Feridooni T, Baguma-Nibasheka M, McNeil K, Chinni S, Pasumarthi KB. (2015). Atrial natriuretic peptide inhibits cell cycle activity of embryonic cardiac progenitor cells via its NPR-A receptor signalling axis. *Am J Physiol Cell Physiol* 308, C557-C569.

- Hotchkiss A, Feridooni T, Zhang F, Pasumarthi KB. (2014). The effects of calcium channel blockade on proliferation and differentiation of cardiac progenitor cells. *Cell Calcium* 55, 238-251.
- Hua LJ, Vedantham V, Barnes RM, Hu J, Robinson AS, Bressan M, Srivastava D, Black BL. (2014). Specification of the mouse cardiac conduction system in the absence of endothelial signalling. *Dev Biol.* 392, 245-254.
- Hyer J, Johansen M, Prasad A, Wessels A, Kirby ML, Gourdie RG, et al. (1999). Induction of Purkinje fiber differentiation by coronary arterialisation. *Proc Natl Acad Sci USA* 96, 13214–13218.
- Inagami T, Misono KS, Fukumi H, Maki M, Tanaka I, Takayanagi R, Imada T, et al. (1987). Structure and physiological actions of rat atrial natriuretic factor. *Hypertension* 10, 113-117.
- Irons CE, Sei CA, Glembotski CC. (1993). Regulated secretion of atrial natriuretic factor from cultured ventricular myocytes. *Am J Physiol* 264, H282-285.
- Itoh H, Pratt RE, Ohno M, Dzau VJ. (1992). Atrial natriuretic polypeptide as a novel antigrowth factor of endothelial cells. *Hypertension* 19, 758-761.
- Ivey KN, Muth A, Arnold J, King FW, Yeh RF, Fish JE, Hsiao EC, et al. (2008). MicroRNA regulation of cell lineages in mouse and human embryonic stem cells. *Cell Stem Cell* 2, 219-229.
- Jankowski M, Rachelska G, Donghao W, McCann SM, Gutkowska J. (2001). Estrogen receptors activate atrial natriuretic peptide in the rat heart. *Proc Natl Acad Sci USA* 98, 11765-11770.
- Jaubert J, Martin N, Washburn LL, Lee BK. (1999). Three new allelic mouse mutations cause skeletal overgrowth involve the natriuretic peptide receptor C gene. *Proc Natl Acad Sci USA* 96, 10278-10283.
- Jay PY, Harris BS, Maguire CT, Buerger A, Wakimoto H, Tanaka M, Kupersmidt S, et al. (2004). Nkx2-5 mutation causes anatomic hypoplasia of the cardiac conduction system. *J Clin Invest* 113, 1130-1137.
- Jewett JR, Koller KJ, Goeddel DV, Lowe DG. (1993). Hormonal induction of low affinity receptor guanylyl cyclase. *Embo J* 12, 769-777.
- John SW, Krege JH, Oliver PM, Hagaman JR, Hodgkin JB, Pang SC, Flynn TG, et al. (1995). Genetic decreases in atrial natriuretic peptide and salt-sensitive hypertension. *Science* 267, 679-681.

- John SW, Veress AT, Honrath U, Chong CK, Peng L, Smithies O, Sonnenberg H. (1996). Blood pressure and fluid-electrolyte balance in mice with reduced or absent ANP. *Am J Physiol* 271, R109-114.
- Kasahara H, Wakimoto H, Liu M, Maguire CT, Converso KL, Shioi T, Huang WY, Manning WJ, et al. (2001). Progressive atrioventricular conduction defects and heart failure in mice expressing a mutant Nkx2.5 homeoprotein. *J Clin Invest* 108, 189–201.
- Kedzierski R, Yanagisawa M. (2001). Endothelin system: The double-edged sword in health and disease. *Annu Rev Pharmacol Toxicol* 41, 851-876.
- Khairy P, Balaji S. (2009). Cardiac Arrhythmias in Congenital Heart Diseases. *Indian Pacing and Electrophysiology Journal* 9, 299-317.
- Kilic A, Bubikat A, Gassner B, Baba HA, Kuhn M. (2007). Local actions of atrial natriuretic peptide counteract angiotensin II stimulated cardiac remodeling. *Endocrinology* 148, 4162-4169.
- Kinnunen P, Taskinen T, Jarvinen M, Ruskoaho H. (1991). Effect of phorbol ester on the release of atrial natriuretic peptide from the hypertrophied rat myocardium. *Br J Pharmacol* 102, 453-461.
- Kinoshita H, Kuwahara K, Nishida M, Jian Z, Rong X, Kiyonaka S, Kuwabara Y, et al. (2010). Inhibition of TRPC6 channel activity contributes to the antihypertrophic effects of natriuretic peptides-guanylyl cyclase-A signalling in the heart. *Circ Res* 106, 1849-1860.
- Kirby ML. *Cardiac Development*. New York: Oxford University Press; 2007, p. 5-272.
- Kirk EP, Sunde M, Costa MW, Rankin SA, Wolstein O, Castro ML, Butler TL, et al. (2007). Mutations in cardiac T-box factor gene *Tbx20* are associated with diverse cardiac pathologies, including defects of septation and valvulogenesis and cardiomyopathy. *Am J Hum Genet* 81, 280-291.
- Kishimoto I, Dubois SK, Garbers DL. (1996). The heart communicates with the kidney exclusively through guanylyl cyclase A receptor: acute handling of sodium and water in response to volume expansion. *Proc Natl Acad Sci USA* 93, 6215-6219.
- Kitajima Y, Minamitake Y, Furuya M, Takehisa M, Katayama T, Tanake S. (1989). Linear alpha-human atrial natriuretic peptide analogs display receptor binding activity and inhibit alpha-hANP-induced cGMP accumulation. *Biochem Biophys Res Commun* 164, 1295-1301.

Klaiber M, Dankworth B, Kruse M, Hartmann M, Nikolaev VO, Yang RB, Volker K, et al. (2011). A cardiac pathway of cyclic GMP-independent signalling of guanylyl cyclase A, the receptor for atrial natriuretic peptide. *PNAS* 108, 18500-18505.

Knowles JW, Esposito G, Mao L, Hagaman JR, Fox JE, Smithies O, Rockman HA et al. (2001). Pressure-independent enhancement of cardiac hypertrophy in natriuretic peptide receptor A-deficient mice. *J Clin Invest* 107, 975-984.

Koide M, Akins RE, Harayama H, Yasui K, Yokota M, Tuan RS. (1996). Atrial natriuretic peptide accelerates proliferation of chick embryonic cardiomyocytes in vitro. *Differentiation* 61, 1-11.

Koller KJ, Lowe DG, Bennett GL, Minamino N. (1991). Selective activation of the B natriuretic peptide receptor by CNP. *Science* 252, 120-123.

Komuro I, Izumo S. (1993). *Csx*: a murine homeobox-containing gene specifically expressed in the developing heart. *Proc Natl Acad Sci.* 90, 8145-8149.

Kondo RP, Anderson RH, Kuperschmidt S, Roden DM, Evans SM. (2003). Development of the cardiac conduction system as delineated by *minK-lacZ*. *J Cardiovasc Electrophysiol* 14:383- 391.

Kook H, Itoh H, Choi BS, Sawada N, Doi K, Hwang TJ, Kim KK, et al. (2003). Physiological concentration of atrial natriuretic peptide induces endothelial regeneration in vitro. *Am J Physiol Heart Circ Physiol* 284, H1388-1397.

Kotlo KU, Hesabi B, Danziger RS. (2011). Implication of microRNAs in atrial natriuretic peptide and nitric oxide signalling in vascular smooth muscle cells. *Am J Physiol Cell Physiol* 301, C929-C937.

Kramer R, Bucay N, Kane DJ, Martin LE, Tarpley JE, Theill LE. (1996). Neuregulins with an Ig-like domain are essential for mouse myocardial and neuronal development. *Proc. Natl. Acad. Sci. USA* 93, 4833- 4838.

Kuratomi S, Kuratomi A, Ishii TM, Nakao K, Saito Y, Takano M. (2007). NRSF regulates the developmental and hypertrophic changes of HCN4 transcription in rat cardiac myocytes. *Biochem Biophys Res Commun* 353, 67-73.

Kwak BR, Jongsma HJ. (1996). Regulation of cardiac gap junction channel permeability and conductance by several phosphorylating conditions. *Mol Cell Biochem* 157, 93-99.

Kwon C, Arnold J, Hsiao EC, Taketo MM, Conklin BR, Srivastava D. (2007). Canonical Wnt signalling is a positive regulator of mammalian cardiac progenitors. *Proc Natl Acad Sci USA* 104, 10894-10899.

- Lagos-Quintana M, Rauhut R, Lendeckel W, Tuschl T. (2001). Identification of novel genes encoding for small expressed RNAs. *Science* 294, 853-858.
- Laskowski A, Woodman OL, Cao AH, Drummond GR, Marshall T, Kaye DM, Ritchie RH. (2006). Antioxidant actions contribute to the antihypertrophic effects of atrial natriuretic peptide in neonatal rat cardiomyocytes. *Cardiovasc Res* 72, 112-123.
- Lau NC, Lim LP, Weinstein EG, Bartel DP. (2001). An abundant class of tiny RNAs with probable regulatory roles in *C. elegans*. *Science* 294, 858-862.
- Lee KF, Simon H, Chen H, Bates B, Hung MC, Hauser C. (1995). Requirement for neuregulin receptor erbB2 in neural and cardiac development. *Nature* 378, 394-398.
- Lee RC, Ambros V. (2001). An extensive class of small RNAs in *C. elegans*. *Science* 294, 862-864.
- Levin ER, Frank HJ. (1991). Natriuretic peptides inhibit rat astroglial proliferation: mediation by C receptor. *Am J Physiol* 261, R453-R457.
- Li Y, Madiraju P, Anand-Srivastava MB. (2012). Knockdown of natriuretic peptide receptor-A enhances receptor C expression and signalling in vascular smooth muscle cells. *Cardiovascular Research* 93, 350-359.
- Li YD, Hong YF, Yusufuaji Y, Tang BP, Zhou HX, Xu GJ, Li JX, et al. (2015). Altered expression of hyperpolarization-activated cyclic nucleotide-gated channels and microRNA-1 and -133 in patients with age-associated atrial fibrillation. *Mol Med Rep* 12, 3243-3248.
- Liang X, Evans SM, Sun Y. (2015). Insights into cardiac conduction system formation provided by HCN4 expression. *Trends Cardiovasc Med* 25, 1-9.
- Liang X, Wang G, Lin L, Lowe J, Zhang Q, Bu L, Chen YH et al. (2013). HCN4 dynamically marks the first heart field and conduction system precursors. *Circ Res* 113, 399-407.
- Lin Q, Schwarz J, Bucana C, Olson EN. (1997). Control of mouse cardiac morphogenesis and myogenesis by transcription factor MEF2C. *Science* 276, 1404-1407.
- Lincoln TM, Cornwell TL. (1993). Intracellular cyclic GMP receptor proteins. *Faseb J* 7, 328-338.
- Lindsay EA, Vitelli F, Su H, Morishima M, Huynh T, Pramparo T, Jurecic V, et al. (2001). *Tbx1* haploinsufficiency in the DiGeorge syndrome region causes aortic arch defects in mice. *Nature* 410, 97-101.
- Livak KJ, Schmittgen TD. (2001). Analysis of relative gene expression data using real-time quantitative PCR and the 2^{-ΔΔC(T)} Method. *Methods* 25, 402-408.

- Lopez MJ, Wong SK, Kishimoto I, Dubois S, Mach V, Friesen J, Garbers DL, Beuve A. (1995). Salt-resistant hypertension in mice lacking the guanylyl cyclase-A receptor for atrial natriuretic peptide. *Nature* 378, 65-68.
- Ludwig A, Zong X, Jeglitsch M, Hofmann F, Biel M. (1998). A family of hyperpolarization-activated mammalian cation channels. *Nature* 393, 587-591.
- Ma L, Lu MF, Schwartz RJ, Martin JF. (2005). Bmp2 is essential for cardiac cushion epithelial-mesenchymal transition and myocardial patterning. *Development* 132, 5601-5611.
- Makkar RR, Smith RR, Cheng K, Malliaras K, Thomson LE, Berman D, Czer LS, et al. (2012). Intracoronary cardiosphere-derived cells for heart regeneration after myocardial infarction (CADUCEUS): a prospective, randomized phase 1 trial. *Lancet* 379, 895-904.
- Mangoni ME, Nargeot JL. (2008). Genesis and regulation of the heart automaticity. *Physiol Rev* 88, 919-982.
- Marchionni MA. (1995). Cell-cell signaling. Neu tack on neuregulin. *Nature* 378, 334-335.
- McGrath MF, de Bold ML, de Bold AJ. (2005). The endocrine function of the heart. *Trends Endocrinol Metab* 16, 469-477.
- McMullen NM, Zhang F, Hotchkiss A, Bretzner F, Wilson JM, Ma H, Wafa K et al. (2009). Functional characterization of cardiac progenitor cells and their derivatives in the embryonic heart post-chamber formation. *Developmental Dynamics: an official publication of the American Association of Anatomists* 238, 2787-99.
- McMullen NM, Zhang F, Pasumarthi KBS. (2009). Assessment of embryonic myocardial cell differentiation using a dual fluorescent reporter system. *Journal of Cellular and Molecular Medicine* 13, 2834-2842.
- Meganathan K, Sotiriadou I, Natarajan K, Hescheler J, Sachinidis A. (2015). Signalling molecules, transcription growth factors, and other regulators revealed from in-vivo and in-vitro models for the regulation of cardiac development. *International Journal of Cardiology* 183, 117-128.
- Meyer D, Birchmeier C. (1995). Multiple essential functions of neuregulin in development. *Nature* 378, 386-390.
- Meysen S, Marger L, Hewett KW, Jarry-Guichard T, Agarkova I, Chauvin JP, Perriard JC, et al. (2007). Nkx2.5 cell-autonomous gene function is required for the postnatal formation of the peripheral ventricular conduction system. *Dev Biol* 303, 740-753.

- Mikawa T, Fischman DA. (1996). The polyclonal origin of myocyte lineages. *Annu Rev Physiol* 58, 509–21.
- Mikawa T, Hurtado R. (2007). Development of the cardiac conduction system. *Seminars in Cell and Developmental Biology* 18, 90-100.
- Mikawa T. Cardiac lineages. (1999). In: Harvey RP, Rosenthal N, editors. *Heart development*. San Diego: Academic Press; p. 19–33.
- Milanesi R, Baruscotti M, Gneccchi-Ruscione T, DiFrancesco D. (2006). Familial sinus bradycardia associated with a mutation in the cardiac pacemaker channel. *N Engl J Med* 354, 151-157.
- Miquerol L, Bellon A, Moreno N, Beyer S, Meilhac SM, Buckingham M, Franco D, et al. (2013). Resolving cell lineage contributions to the ventricular conduction system with a Cx40-GFP allele: a dual contribution of the first and second heart fields. *Developmental Dynamics* 242, 665-677.
- Miquerol L, Meysen S, Mangoni M, Patrick B, Harold VMR, Abran P, Jongsm H, et al. (2004). Architectural and functional asymmetry of the His-Purkinje system of the murine heart. *Cardiovascular Research* 63, 77-86.
- Misono KS, Ogawa H, Qiu Y, Ogata CM. (2005). Structural studies of the natriuretic peptide receptor: a novel hormone-induced rotation mechanism for transmembrane signal transduction. *Peptides* 26, 957-968.
- Molkentin JD, Lin Q, Duncan SA, Olson EN. (1997). Requirement of the transcription factor GATA4 for heart tube formation and ventral morphogenesis. *Genes Dev* 11, 1061-1072.
- Montrezor LH, Piccinato CA, Collares CV, Vireque AA, Silva AA. (2015). Effects of angiotensin II, atrial natriuretic peptide and endothelin-1 on proliferation and steroidogenic output of bovine granulosa cells cultured in a chemically defined system. *Anim Reprod Sci* 152, 8-16.
- Moretti A, Caron L, Nakano A, Lam JT, Bernshausen A, Chen Y, Qyang Y et al. (2006). Multipotent embryonic isl1+ progenitor cells lead to cardiac, smooth muscle, and endothelial cell diversification. *Cell* 127, 1151–65.
- Mori AD, Bruneau BG. (2004). TBX5 mutations and congenital heart disease: Holt-Oram syndrome revealed. *Curr Opin Cardiol* 19, 211-215.
- Mori AD, Zhu Y, Vahora I, Nieman B, Koshiba-Takeuchi K, Davidson L, Pizard A, Seidman JG, et al. (2006). Tbx5-dependent rheostatic control of cardiac gene expression and morphogenesis. *Dev. Biol.* 297, 566-586.

- Morii N, Nakao K, Kihara M, Sugawara A, Sakamoto M, Yamori Y, Imura H. (1986). Decreased content in left atrium and increased plasma concentration of atrial natriuretic polypeptide in spontaneously hypertensive rats (SHR) and SHR stroke-prone. *Biochem Biophys Res Commun* 135, 74-81.
- Morin S, Charron F, Robitaille L, Nemer M. (2000). GATA-dependent recruitment of MEF2 proteins to target promoters. *Embo J* 19, 2046-2055.
- Morin S, Pozzulo G, Robitaille L, Cross J, Nemer M. (2005). MEF2-dependent recruitment of the HAND1 transcription factor results in synergistic activation of target promoters. *J Biol Chem* 280, 32272-32278.
- Morita E, Yasue H, Yoshimura M, Ogawa H, Jougasaki M, Matsumura T, Mukoyama M, et al. (1993). Increased plasma levels of brain natriuretic peptide in patients with acute myocardial infarction. *Circulation* 88, 82-91.
- Moubarak M, Magaud C, Saliba Y, Chatelier A, Bois P, Faivre JF, Fares N. (2015). Effects of atrial natriuretic peptide on rat ventricular fibroblasts during differentiation into myofibroblasts. *Physiol Res* 64, 495-503.
- Musso E, Vassalle M. (1982). The role of calcium in overdrive suppression of canine cardiac Purkinje fibres. *Circ Res*, 167-180.
- Myers DC, Fishman GI. (2003). Molecular and functional maturation of the murine cardiac conduction system. *Trends Cardiovasc Med* 13, 289-295.
- Nemer M, Lavigne JP, Drouin J, Thibault G, Gannon M, Antakly T. (1986). Expression of atrial natriuretic factor gene in heart ventricular tissue. *Peptides* 7:1147-1152.
- Nguyen-Tran VT, Kubalak SW, Minamisawa S, Fiset C, Wollert KC, Brown AB, Ruiz-Lozano P, et al. (2000). A novel genetic pathway for sudden cardiac death via defects in the transition between ventricular and conduction system cell lineages. *Cell* 102, 671– 682.
- Nishida M, Carley W, Gerritsen ME, Ellingsen O, Kelly RA, Smith TW. (1993). Isolation and characterization of human and rat cardiac microvascular endothelial cells. *Am J Physiol* 264, H639-H652.
- Nof E, Luria D, Brass D, Marek D, Lahat H, Reznik-Wolf H, Pras E, et al. (2007). Point mutation in the HCN4 cardiac ion channel pore affecting synthesis, trafficking, and functional expression is associated with familial asymptomatic sinus bradycardia. *Circulation* 116, 463-470.
- O'Tierney PF, Chattergoon NN, Louey S, Giraud GD, Thornburg KL. (2010). Atrial natriuretic peptide inhibits angiotensin II-stimulated proliferation in fetal cardiomyocytes. *J Physiol* 588, 2879–2889.

- Ogawa H, Qiu Y, Huang L, Tam-Chang SW, Young HS, Misono KS. (2009). Structure of the atrial natriuretic peptide receptor extracellular domain in the unbound and hormone-bound states by single-particle electron microscopy. *FEBS J* 276, 1347-1355.
- Ogawa H, Qiu Y, Ogata CM. (2004). Crystal structure of hormone-bound atrial natriuretic peptide receptor extracellular domain: rotation mechanism for transmembrane signal transduction. *J Biol Chem* 279, 28625-28631.
- Oliver PM, Fox JE, Kim R, Rockman HA, Kim HS, Reddick RL, Pandey KN, Milgram SL, et al. (1997). Hypertension, cardiac hypertrophy, and sudden death in mice lacking natriuretic peptide receptor A. *Proc Natl Acad Sci USA* 94, 14730-14735.
- Olson EN, Srivastava D. (1996). Molecular pathways controlling heart development. *Science* 272, 671-676.
- Omland T, Aakvaag A, Bonarjee VV, Caidahl K, Lie RT, Nilsen DW, Sundsfjord JA, et al. (1996). Plasma brain natriuretic peptide as an indicator of left ventricular systolic function and long-term survival after acute myocardial infarction. Comparison with plasma atrial natriuretic peptide and N-terminal proatrial natriuretic peptide. *Circulation* 93, 1963-1969.
- Ortola FV, Ballermann BJ, Anderson S, Mendez RE, Brenner BM. (1987). Elevated plasma atrial natriuretic peptide levels in diabetic rats. Potential mediator of hyperfiltration. *J Clin Invest* 80, 670-674.
- Pagano M, Anand-Srivastava MB. (2001). Cytoplasmic domain of natriuretic peptide receptor C constitutes Gi activator sequences that inhibit adenylyl cyclase activity. *The Journal of Biological Chemistry* 276, 22064-22070.
- Pandey KN, Nguyen HT, Li M, Boyle JW. (2000). Natriuretic peptide receptor-A negatively regulates mitogen-activated protein kinase and proliferation of mesangial cells: role of cGMP-dependent protein kinase. *Biochem Biophys Res Commun* 271, 374-379.
- Paradis A, Xiao D, Zhou J, Zhang L. (2014). Endothelin-1 promotes cardiomyocyte terminal differentiation in the developing heart via heightened DNA methylation. *11*, 373-380.
- Parat M, Blanchet J, De Lean A. (2010). Role of juxtramembrane and transmembrane domains in the mechanism of natriuretic peptide receptor A activation. *Biochemistry* 49, 4601-4610.
- Parat M, McNicoll N, Wilkes B, Fournier A, De Lean A. (2008). Role of extracellular domain dimerization in agonist-induced activation of natriuretic peptide receptor A. *Mol Pharmacol* 73, 431-440.

- Parodi EM, Kuhn B. (2014). Signalling between microvascular endothelium and cardiomyocytes through neuregulin. *Cardiovascular Research* 102, 194-204.
- Patel R, Kos L. (2005). Endothelin-1 and neuregulin-1 convert embryonic cardiomyocytes into cells of the conduction system in the mouse. *Developmental Dynamics* 233, 20-28.
- Peracchia C, Wang XG, Peracchia LL. (2000). Slow gating of gap junction channels and calmodulin. *J Membr Biol* 178, 55-70.
- Peracchia C. (2004). Chemical gating of gap junction channels; roles of calcium; pH and calmodulin. *Biochem Biophys* 1662, 61-80.
- Pero SC, Shukla GS, Cookson MM, Flemer S, Krag DN. (2007). Combination treatment with Grb7 peptide and Doxorubicin or Trastuzumab (Herceptin) results in cooperative cell growth inhibition in breast cancer cells. *Br J Cancer* 96, 1520-1525.
- Pfeifer A, Klatt P, Massberg S, Ny L. (1998). Defective smooth muscle regulation in cGMP kinase I-deficient mice. *Embo J* 17, 3045-3051.
- Pierpont ME, Basson CT, Benson DW, Gelb BD, Giglia TM, Goldmuntz E, McGee G, et al. (2007). Genetic basis for congenital heart defects: current knowledge: a scientific statement from the American Heart Association Congenital Cardiac Defects Committee, Council on Cardiovascular Disease in the Young: endorsed by the American Academy of Pediatrics. *Circulation* 115, 3015-3038.
- Potter LR, Abbey-Hosch S, Dickey DM. (2006). Natriuretic peptides, their receptors, and cyclic guanosine monophosphate-dependent signalling functions. *Endocrine Review* 27, 47-72.
- Potter LR. (2011). Natriuretic peptide metabolism, clearance and degradation. *FEBS J* 278, 1808-1817.
- Qiu Y, Ogawa H, Miyagi M, Misono KS. (2004). Constitutive activation and uncoupling of the atrial natriuretic peptide receptor by mutations at the dimer interface. Role of the dimer structure in signalling. *J Biol Chem* 279, 6115-6123.
- Remme CA, Verkerk AO, Hoogaars WMH, Aanhaanen WTJ, Scicluna BP, Annink C, van den Hoff MJB, Wilde AAM, van Veen TAB, Veldkamp MW, et al. (2009). The cardiac sodium channel displays differential distribution in the conduction system and transmural heterogeneity in the murine ventricular myocardium. *Basic Res. Cardiol.* 104, 511-522.
- Rentschler S, Harris BS, Kuznekoff L, Jain R, Manderfield L, Lu MM, Morley GE, Patel VV, Epstein JA. (2011). Notch signalling regulates murine atrioventricular conduction and the formation of accessory pathways. *J. Clin. Invest.* 121, 525-533.

- Rentschler S, Yen AH, Lu J, Petrenko NB, Lu MM, Manderfield LJ, Patel VV, Fishman GI, Epstein JA. (2012). Myocardial Notch signalling reprograms cardiomyocytes to a conduction-like phenotype. *Circulation* 126, 1058-1066.
- Rentschler S, Zander J, Meyers K, France D, Levine R, Porter G, Rivkees SA, Morley GE, Fishman, GI. (2002). Neuregulin-1 promotes formation of the murine cardiac conduction system. *Proc. Natl. Acad. Sci. USA* 99, 10464-10469.
- Roell W, Lewalter T, Sasse P, Tallini YN, Choi BR, Breitbach M, Doran R, et al. (2007). Engraftment of connexin 43-expressing cells prevents post-infarct arrhythmia. *Nature* 450, 819-824.
- Rondeau JJ, McNicoll N, Gagnon J, Bouchard N, Ong H, De Lean A. (1995). Stoichiometry of the atrial natriuretic factor-R1 receptor complex in the bovine zona glomerulosa. *Biochemistry* 34, 2130-2136.
- Rosenkranz AC, Woods RL, Dusting GJ, Ritchie RH. (2003). Antihypertrophic actions of the natriuretic peptides in adult rat cardiomyocytes: importance of cyclic GMP. *Cardiovasc Res* 57, 515-522.
- Rubart M, Pasumarthi KB, Nakajima H, Soonpaa MH, Nakajima HO, Field LJ. (2003). Physiological coupling of donor and host cardiomyocytes after cellular transplantation. *Circ Res* 92, 1217-1224.
- Ruskoaho H, Kinnunen P, Taskinen T, Vuolteenaho O, Leppaluoto J, Takala TE. (1989). Regulation of ventricular atrial natriuretic peptide release in hypertrophied rat myocardium. Effects of exercise. *Circulation* 80, 390-400.
- Rutenberg JB, Fischer A, Jia H, Gessler M, Zhong TP, Mercola M. (2006). Developmental patterning of the cardiac atrioventricular canal by Notch and Hairy-related transcription factors. *Development* 133, 4381-4390.
- Sankova B, Benes J, Jr., Krejci E, Dupays L, Theveniau-Ruissy M, Miquerol L, Sedmera D. (2012). The effect of connexin40 deficiency on ventricular conduction system function during development. *Cardiovasc Res* 95, 469-479.
- Schlossmann J, Ammendola A, Ashman K, Zong X, Huber A, Neubauer G, Wang GX, et al. (2000). Regulation of intracellular calcium by a signalling complex of IRAG, IP3 receptor and cGMP kinase IB. *Nature* 404, 197-201.
- Schorlemmer A, Matter ML, Shohet RV. (2008). Cardioprotective signalling by endothelin. *Trends Cardiovasc Med* 18, 233-239.

- Schott JJ, Benson DW, Basson CT, Pease W, Silberbach GM, Moak JP, Maron BJ, et al. (1998). Congenital heart disease caused by mutations in the transcription factor NKX2-5. *Science* 281, 108-111.
- Schulz S, Singh S, Bellet RA, Singh G, Tubb DJ, Chin H, Garbers DL. The primary structure of a plasma membrane guanylyl cyclase demonstrates diversity within this new receptor family. *Cell* 58, 1155-1162.
- Schulze-Bahr E, Neu A, Friederich P, Kaupp UB, Breithardt G, Pongs O, Isbrandt D. (2003). Pacemaker channel dysfunction in a patient with sinus node disease. *J Clin Invest* 111, 1537-1545.
- Schweizer PA, Yampolsky P, Malik R, Thomas D, Zehelein J, Katus HA, Koenen M. (2009). Transcriptional profiling of HCN-channel isoforms throughout mouse cardiac development. *Basic Res Cardiol* 104,621-629.
- Scott NJ, Ellmers LJ, Lainchbury JG, Maeda N, Smithies O, Richards AM, Cameron VA. (2009). Influence of natriuretic peptide receptor-1 on survival and cardiac hypertrophy during development. *Biochim Biophys Acta* 1792, 1175-1184.
- Sedmera D, Harris BS, Grant E, Zhang N, Jourdan J, Kurkova D, Gourdie RG. (2008). Cardiac expression patterns of endothelin-converting enzyme (ECE): implications for conduction system development. *Dev Dyn* 237, 1746-1753.
- Sedmera D, Pexieder T, Vuillemin M, Thompson RP, Anderson RH. (2000). Developmental patterning of the myocardium. *Anat. Rec.* 258, 319–337.
- Sedmera D, Reckova M, DeAlmeida A, Coppin SR, Kubalak SW, Gourdie RG, Thompson RP. (2003). Spatiotemporal pattern of commitment to slowed proliferation in the embryonic mouse heart indicates progressive differentiation of the cardiac conduction system. *Anat Rec A Discov Mol Cell Evol Biol* 274, 773-777.
- Serafino A, Moroni N, Psaila R, Zonfrillo M, Andreola F, Wannenes F, Mercuri L, et al. (2012). Anti-proliferative effect of atrial natriuretic peptide on colorectal cancer cells: evidence for an Akt-mediated cross-talk between NHE-1 activity and Wnt/B-catenin signalling. *Biochim Biophys Acta* 1822, 1004-1018.
- Seul KH, Tadros PN, Beyer EC. (1997). Mouse connexin40: gene structure and promoter analysis. *Genomics* 46, 120-126.
- Sharma GD, Nguyen HT, Antonov AS, Gerrity RG, von Geldern T, Pandey KN. (2002). Expression of atrial natriuretic peptide receptor-A antagonizes the mitogen-activated protein kinases (Erk2 and P38MAPK) in cultured human vascular smooth muscle cells. *Mol Cell Biochem* 233, 165-173.

- Shenker Y, Sider RS, Ostafin EA, Grekin RJ. (1985). Plasma levels of immunoreactive atrial natriuretic factor in healthy subjects and in patients with edema. *J Clin Invest* 76, 1684-1687.
- Shubeita H, McDonough PM, Harris AN, Knowlton KU, Glembotski CC, Brown JH, Chien KR. (1990). Endothelin induction of inositol phospholipid hydrolysis, sarcomere assembly, and cardiac gene expression in ventricular cardiomyocytes. A paracrine mechanism for myocardial cell hypertrophy. *J Biol Chem* 33, 20555-20562.
- Simon AM, Goodenough DA, Paul DL. (1998). Mice lacking connexin40 have cardiac conduction abnormalities characteristic of atrioventricular block and bundle branch block. *Curr Biol* 8, 295-298.
- Singh R, Horsthuis T, Farin HF, Grieskamp T, Norden J, Petry M, Wakker V, Moorman AFM, Christoffels VM, Kispert A. (2009). Tbx20 interacts with smads to confine tbx2 expression to the atrioventricular canal. *Circ. Res.* 105, 442-452.
- Small EM, Krieg PA. (2003). Transgenic analysis of the atrial natriuretic factor (ANF) promoter: Nkx2-5 and GATA-4 binding sites are required for atrial specific expression of ANF. *Dev Biol* 261, 116-131.
- Soriano, P. (1999). Generalized lacZ expression with the ROSA26 Cre reporter strain. *Nature Genetics*, 21, 70–71.
- Spater D, Abramczuk MK, Buac K, Zangi L, Stachel MW, Clarke J, Sahara M, et al. (2013). HCN4+ cardiomyogenic progenitor derived from the first heart field and human pluripotent stem cells. *Nat Cell Biol* 15, 1098-1106.
- Srivastava D, Olsen En. (2000). A genetic blueprint for cardiac development. *Nature* 407, 221-226.
- Stanley EG, Biben C, Elefanty A, Barnett L, Koentgen F, Robb L, Harvey RP. (2002). Efficient Cre-mediated deletion in cardiac progenitor cells conferred by a 3'UTR-ires-Cre allele of the homeobox gene Nkx2-5. *Int J Dev Biol* 46, 431-439.
- Stastna M, Chimenti I, Marban E, Van Eyk JE. (2010). Identification and functionality of proteomes secreted by rat cardiac stem cells and neonatal cardiomyocytes. *Proteomics* 10, 245-253.
- Steinhilber ME, Cochrane KL, Field LJ. (1990). Hypotension in transgenic mice expression atrial natriuretic factor fusion genes. *Hypertension* 16, 301-307.
- Stollberger C, Finsterer J. (2004). Left ventricular hypertrabeculation/noncompaction. *J Am Soc Echocardiogr Off Publ Am Soc Echocardiogr* 17, 91-100.

- Subramanyan R, Joy J, Venugopalan P, Sapru A, Khusaiby SM. (2000). Incidence and spectrum of congenital heart disease in Oman. *Ann Trop Paediatr* 20, 337-341.
- Suenobu N, Shichiri M, Iwashina M, Marumo F, Hirata Y. (1999). Natriuretic peptides and nitric oxide induce endothelial apoptosis via a cGMP-dependent mechanism. *Atheroscler Thromb Vasc Biol* 19, 140-146.
- Suga S, Nakao K, Hosoda K, Mukoyama M. (1992). Receptor selectivity of natriuretic peptide family, atrial natriuretic peptide, brain natriuretic peptide, and CNP. *Endocrinology* 130, 229-239.
- Sun M, Yan X, Bian Y, Caggiano AO, Morgan JP. (2011). Improving murine embryonic stem cell differentiation into cardiomyocytes with neuregulin-1: differential expression of microRNA. *Am J Physiol Cell Physiol* 301, C21-C30.
- Takahashi K, Sasano T, Sugiyama K, Kurokawa J, Tamura N, Soejima Y, Sawabe M et al. (2016). High-fat diet increases vulnerability to atrial arrhythmia by conduction disturbance via miR-27b. *Journal of Molecular and Cellular Cardiology* 90, 38-46.
- Takebayashi-Suzuki K, Pauliks LB, Eltsefon Y, Mikawa T. (2001). Purkinje fibers of the avian heart express a myogenic transcription factor program distinct from cardiac and skeletal muscle. *Developmental Biology* 234, 390-401.
- Takebayashi-Suzuki K, Yanagisawa M, Gourdie RG, Kanzawa N, Mikawa T. (2000). In vivo induction of cardiac Purkinje fiber differentiation by coexpression of preproendothelin-1 and endothelin converting enzyme-1. *Development* 127: 3523–3532.
- Tam PP, Parameswaran M, Kinder SJ, Weinberger RP. (1997). The allocation of epiblast cells to the embryonic heart and other mesodermal lineages: the role of ingression and tissue movement during gastrulation. *Development* 124, 1631-1642.
- Tamaddon HS, Vaidya D, Simon AM, Paul DL, Jalife J, Morley GE. (2000). High-resolution optical mapping of the right bundle branch in connexin40 knockout mice reveals slow conduction in the specialized conduction system. *Circ Res* 87, 929-936.
- Tanaka M, Chen Z, Bartunkova S, Yamasaki N, Izumo S. (1999). The cardiac homeobox gene *Csx/Nkx2.5* lies genetically upstream of multiple genes essential for heart development. *Development* 126, 1269-1280.
- Thattaliyath BD, Firulli BA, Firulli AB. (2002). The basic-helix-loop-helix transcription factor *HAND2* directly regulates transcription of the atrial natriuretic peptide gene. *J Mol Cell Cardiol* 34, 1335-1344.

Thomas PS, Kasahara H, Edmonson AM, Izumo S, Yacoub MH, Barton PJ, Gourdie RG. (2001). Elevated expression of Nkx-2.5 in developing myocardial conduction cells. *Anat Rec* 263, 307–313.

Toshimori H, Toshimori K, Oura C, Matsuo H. (1987). Immunohistochemical study of atrial natriuretic polypeptides in the embryonic, fetal and neonatal rat heart. *Cell Tissue Res* 248, 627-633.

Tripathi S, Pandey KN. (2012). Guanylyl cyclase/natriuretic peptide receptor-A signalling antagonizes the vascular endothelial growth factor-stimulated MAPKs and downstream effectors AP-1 and CREB in mouse mesangial cells. *Mol Cell Biochem* 368, 47-59.

Tsuruda T, Boerrigter G, Huntley BK, Noser JA, Cataliotti A, Costello-Boerrigter LC, Chen HH, Burnett JC. (2002). Brain natriuretic peptide is produced in cardiac fibroblasts and induces matrix metalloproteinases. *Circ. Res.* 91, 1127–1134.

Van Rijen HVM, van Veen TA, van Kempem MJ, Wilms-Schopman FJ, Potse M, Krueger O, Willecke K, et al. (2001). Impaired conduction in the bundle branches of mouse hearts lacking the gap junction protein connexin40. *Circulation* 103, 1591-1598.

Viragh S, Challice CE. (1977). The development of the conduction system in the mouse embryo heart. II. Histogenesis of the atrioventricular node and bundle. *Dev Biol* 56, 397-411.

Viragh S, Challice CE. (1982). The development of the conduction system in the mouse embryo heart IV. Differentiation of the atrioventricular conduction system. *Developmental Biology* 89, 25-40.

Von Geldern TW, Budzik GP, Dillon TP, Holleman WH, Holst MA, Kiso Y, Novosad EI, et al. (1990). Atrial natriuretic peptide antagonists: biological evaluation and structural correlations. *Molecular Pharmacology* 38, 771-778.

Wadugu B, Kuhn B. (2012). The role of neuregulin/ErbB2/ErbB4 signalling in the heart with special focus on effects of cardiomyocyte proliferation. *Am J Physiol Heart Circ Physiol* 302, H2139-H2147.

Wahid F, Shehzad A, Khan T, Kim YY. (2010). MicroRNAs: synthesis, mechanism, function and recent clinical trials. *Biochimica et Biophysica Acta* 1803, 1231-1243.

Wang Z, Xu G, Wu Y, Guan Y, Cui L, Lei X, Zhang J, et al. (2009). Neuregulin-1 enhances differentiation of cardiomyocytes from embryonic stem cells. *Med Biol Eng Comput* 47, 41-48.

Weerd JH, Christoffels VM. (2016). The formation and function of the cardiac conduction system. *Development* 143, 197-210.

- Wei YF, Rodi CP, Day ML, Wiegand RC, Needleman LD, Cole BR, Needleman P. (1987). Developmental changes in the rat atriopeptin hormonal system. *J Clin Invest* 79, 1325–1329.
- Weidmann P, Hasler L, Gnadinger MP, Lang RE, Uehlinger DE, Shaw S, Rascher W, et al. (1986). Blood levels and renal effects of atrial natriuretic peptide in normal men. *J Clin Invest* 77, 734-742.
- White TW, Bruzzone R, Paul DL. (1995). The connexin family of intercellular channel forming proteins. *Kidney Int* 48, 1148-1157.
- Woodard GE, Rosado JA. (2008). Natriuretic Peptides in Vascular Physiology and Pathology. *International Review of Cell and Molecular Biology* 468, 59-93.
- Wu CF, Bishopric NH, Pratt RE. (1997). Atrial natriuretic peptide induces apoptosis in neonatal rat cardiac myocytes. *J Biol Chem* 272, 14860-14866.
- Wu SM, Fujiwara Y, Cibulsky SM, Clapham DE, Lien CL, Schultheiss TM, Orkin SH. (2006). Developmental origin of a bipotential myocardial and smooth muscle cell precursor in the mammalian heart. *Cell* 127, 1137–1150.
- Xie GX, Palmer PP. (2007). How regulators of G protein signalling achieve selective regulation. *J Mol Biol* 366, 349-365.
- Yahuaca P, Ek-Vitorin JF, Rush P, Delmar M, Taffet SM. (2000). Identification of a protein kinase activity that phosphorylates connexin43 in a pH-dependent manner. *Braz J Med Biol Res* 33, 399-406.
- Yamaguchi TP. (2001). Heads or tails: Wnts and anterior-posterior patterning. *Current Biology* 11, R713-R724.
- Yang-Feng TL, Floyd-Smith G, Nemer M, Drouin J, Francke U. (1985). The pronatriodilatin gene is located on the distal short arm of human chromosome 1 and on mouse chromosome 4. *Am J Hum Genet* 37, 1117-1128.
- Yasoda A, Ogawa Y, Suda M, Tamura N, Mori K, Sakuma Y, Chusho H, et al. (1998). Natriuretic peptide regulation of endochondral ossification. *The Journal of Biological Chemistry* 273, 11695-11700.
- Yasui K, Liu W, Opthof T, Kada K, Lee JK, Kamiya K, Kodama I. (2001). If current and spontaneous activity in mouse embryonic ventricular myocytes. *Circ Res* 88, 536-542.
- Yin H, Li X, Jiang Z, Zhou MD. (2015). Progress in neuregulin/ErbB signalling and chronic heart failure. *World J Hypertens* 5, 63-73.

- Yoshizumi M, Tsuchiya K, Kirima K, Kyaw M, Suzaki Y, Tamaki T. (2001). Quercetin inhibits Shc- and phosphatidylinositol 3-kinase-mediated c-Jun N-terminal kinase activation by angiotensin II in cultured rat aortic smooth muscle cells. *Mol Pharmacol* 60, 656-665.
- Zeller R, Bloch KD, Williams BS, Arceci RJ, Seidman CE. (1987). Localized expression of the atrial natriuretic factor gene during cardiac embryogenesis. *Genes Dev* 1, 693–698.
- Zhang F, Feridooni T, Hotchkiss A, Pasumarthi KB. (2015). Divergent cell cycle kinetics of midgestation ventricular cells entail a higher engraftment efficiency after cell transplantation. *Am J Physiol Cell Physiol* 308, C220-C228.
- Zhang F, Pasumarthi KBS. (2007). Ultrastructural and immunocharacterization of undifferentiated myocardial cells in the developing mouse heart. *J Cell Mol Med* 11, 552-560.
- Zhang J, Zhao Z, Zu C, Hu H, Shen H, Zhang M, Wang J. (2013). Atrial natriuretic peptide modulates the proliferation of human gastric cancer cells via KCNQ1 expression. *Oncol Lett* 6, 407-414.
- Zhang S, Weinheimer C, Courtois M, Kovacs A, Zhang CE, Cheng AM, Wang Y, et al. (2003). The role of Grb2-p38 MAPK signalling pathway in cardiac hypertrophy and fibrosis. *J Clin Invest* 111, 833-841.
- Zhao Y, Ransom JF, Li A, Vedantham V, von Drehle M, Muth AN, Tsuchihashi T, et al. (2007). Dysregulation of cardiogenesis, cardiac conduction, and cell cycle in mice lacking miRNA 1-2. *Cell* 129, 303-317.
- Zhao Y, Samal E, Srivastava D. (2005). Serum response factor regulates a muscle-specific microRNA that targets Hand2 during cardiogenesis. *Nature* 436, 214-220.
- Zhao Y, Srivastava D. (2007). A developmental view of microRNA function. *Trends Biochem Sci* 32, 189-197.
- Zhao YY, Sawyer DR, Baliga RR, Opel DJ, Han X, Marchionni MA, Kelly RA. (1998). Neuregulins promote survival and growth of cardiac myocytes. *J Biol Chem* 273, 10261-10269.
- Zhu WZ, Xie Y, Moyes KW, Gold JD, Askari B, Laflamme MA. (2010). Neuregulin/ErbB signalling regulates cardiac subtype specification in differentiating human embryonic stem cells. *Circ Res* 107, 776-786.

APPENDIX I

Note: The following copyright permissions are for **Figure 1.1.*

Development

Billing Status: **N/A**

Order detail ID: 70590728

ISSN: 1477-9129

Publication Type: e-Journal

Volume:

Issue:

Start page:

Publisher: COMPANY OF BIOLOGISTS,

Author/Editor: Company of Biologists

Permission Status:  **Granted**

Permission type: Republish or display content

Type of use: Republish in a thesis/dissertation

Order License Id: 4138840384988

Order ref number: N/A

Requestor type	Author of requested content
Format	Print, Electronic
Portion	chart/graph/table/figure
Number of charts/graphs/tables/figures	1
Title or numeric reference of the portion(s)	Figure 1
Title of the article or chapter the portion is from	Fashioning the vertebrate heart: earliest embryonic decisions
Editor of portion(s)	Fishman MC, Chien KR
Author of portion(s)	Fishman MC, Chien KR
Volume of serial or monograph	124
Issue, if republishing an article from a serial	11

Page range of portion	2100
Publication date of portion	June 1997
Rights for	Main product
Duration of use	Life of current and all future editions
Creation of copies for the disabled	no
With minor editing privileges	yes
For distribution to	Worldwide
In the following language(s)	Original language of publication
With incidental promotional use	no
Lifetime unit quantity of new product	Up to 499
Made available in the following markets	University Education
The requesting person/organization	Arun Govindapillai/ Dalhousie University
Order reference number	N/A
Author/Editor	Arun Govindapillai/Dalhousie University
The standard identifier of New Work	Dalhousie University
Title of New Work	Characterizing the role of atrial natriuretic peptide signalling in the development of the embryonic ventricular cardiac conduction system
Publisher of New Work	Dalhousie University
Expected publication date	Aug 2017
Estimated size	250

(pages)

**WOLTERS KLUWER HEALTH, INC. LICENSE
TERMS AND CONDITIONS**

Jul 05, 2017

This Agreement between Arun Govindapillai ("You") and Wolters Kluwer Health, Inc. ("Wolters Kluwer Health, Inc.") consists of your license details and the terms and conditions provided by Wolters Kluwer Health, Inc. and Copyright Clearance Center.

License Number	4138810360570
License date	Jun 30, 2017
Licensed Content Publisher	Wolters Kluwer Health, Inc.
Licensed Content Publication	Circulation Research
Licensed Content Title	The Multiple Phases and Faces of Wnt Signalling During Cardiac Differentiation and Development
Licensed Content Author	Susanne Gessert,Michael Kühl
Licensed Content Date	Jul 23, 2010
Licensed Content Volume	107
Licensed Content Issue	2
Type of Use	Dissertation/Thesis
Requestor type	Individual
Portion	Figures/table/illustration
Number of figures/tables/illustrations	1
Figures/tables/illustrations used	Figure 2
Author of this Wolters Kluwer article	No
Title of your thesis / dissertation	Characterizing the role of atrial natriuretic peptide signalling in the development of the embryonic ventricular cardiac conduction system
Expected completion date	Aug 2017
Estimated size(pages)	270
Total	0.00 CAD
Terms and Conditions	

APPENDIX II

Note: The following copyright permission is for **Figure 1.2.*

Development

Billing Status: **N/A**

Order detail ID: 70590724

ISSN: 0950-1991

Publication Type: Journal

Volume:

Issue:

Start page:

Publisher: COMPANY OF BIOLOGISTS,

Author/Editor: COMPANY OF BIOLOGISTS

Permission Status:  **Granted**

Permission type: Republish or display content

Type of use: Republish in a thesis/dissertation

Order License Id: 4138840382992

Order ref number: N/A

Requestor type	Author of requested content
Format	Print, Electronic
Portion	chart/graph/table/figure
Number of charts/graphs/tables/figures	2
Title or numeric reference of the portion(s)	Figure 1, Figure 2
Title of the article or chapter the portion is from	The Formation and Function of the Cardiac Conduction System
Editor of portion(s)	van Weerd JH, Christoffels VM
Author of portion(s)	van Weerd JH, Christoffels VM
Volume of serial or monograph	143
Issue, if republishing an article from a	2

serial	
Page range of portion	198
Publication date of portion	Jan 15 2016
Rights for	Main product
Duration of use	Life of current and all future editions
Creation of copies for the disabled	no
With minor editing privileges	yes
For distribution to	Worldwide
In the following language(s)	Original language of publication
With incidental promotional use	no
Lifetime unit quantity of new product	Up to 499
Made available in the following markets	University Education
The requesting person/organization	Arun Govindapillai/ Dalhousie University
Order reference number	N/A
Author/Editor	Arun Govindapillai/Dalhousie University
The standard identifier of New Work	Dalhousie University
Title of New Work	Characterizing the role of atrial natriuretic peptide signalling in the development of the embryonic ventricular cardiac conduction system
Publisher of New Work	Dalhousie University
Expected publication date	Aug 2017

Estimated size
(pages)

270

APPENDIX III

Note: The following copyright permission is for **Figure 1.3.*

ELSEVIER LICENSE TERMS AND CONDITIONS

Jul 05, 2017

This Agreement between Arun Govindapillai ("You") and Elsevier ("Elsevier") consists of your license details and the terms and conditions provided by Elsevier and Copyright Clearance Center.

License Number	4138810761269
License date	Jun 30, 2017
Licensed Content Publisher	Elsevier
Licensed Content Publication	Trends in Cardiovascular Medicine
Licensed Content Title	Insights into cardiac conduction system formation provided by HCN4 expression
Licensed Content Author	Xingqun Liang,Sylvia M. Evans,Yunfu Sun
Licensed Content Date	Jan 1, 2015
Licensed Content Volume	25
Licensed Content Issue	1
Licensed Content Pages	9
Start Page	1
End Page	9
Type of Use	reuse in a thesis/dissertation
Intended publisher of new work	other
Portion	figures/tables/illustrations
Number of figures/tables/illustrations	1
Format	both print and electronic

Are you the author of this Elsevier article?	No
Will you be translating?	No
Order reference number	
Original figure numbers	Figure 4
Title of your thesis/dissertation	Characterizing the role of atrial natriuretic peptide signalling in the development of the embryonic ventricular cardiac conduction system
Expected completion date	Aug 2017
Estimated size (number of pages)	270
Elsevier VAT number	GB 494 6272 12
Total	0.00 USD
Terms and Conditions	

APPENDIX IV

Note: The following copyright permission is for **Figure 1.4.*

OXFORD UNIVERSITY PRESS LICENSE TERMS AND CONDITIONS

Jul 05, 2017

This Agreement between Arun Govindapillai ("You") and Oxford University Press ("Oxford University Press") consists of your license details and the terms and conditions provided by Oxford University Press and Copyright Clearance Center.

License Number	4138810890870
License date	Jun 30, 2017
Licensed content publisher	Oxford University Press
Licensed content publication	Cardiovascular Research
Licensed content title	Genetically modified mice: tools to decode the functions of connexins in the heart—new models for cardiovascular research
Licensed content author	Gros, Daniel; Dupays, Laurent
Licensed content date	May 1, 2004
Type of Use	Thesis/Dissertation
Institution name	
Title of your work	Characterizing the role of atrial natriuretic peptide signalling in the development of the embryonic ventricular cardiac conduction system

Publisher of your work	n/a
Expected publication date	Aug 2017
Permissions cost	0.00 CAD
Value added tax	0.00 CAD
Total	0.00 CAD
Publisher Tax ID	GB125506730
Billing Type	Invoice
Total	0.00 CAD

[Terms and Conditions](#)

APPENDIX V

Note: The following copyright permission is for **Figure 1.7.*

ELSEVIER LICENSE TERMS AND CONDITIONS

Jul 05, 2017

This Agreement between Arun Govindapillai ("You") and Elsevier ("Elsevier") consists of your license details and the terms and conditions provided by Elsevier and Copyright Clearance Center.

License Number	4138811029226
License date	Jun 30, 2017
Licensed Content Publisher	Elsevier
Licensed Content Publication	Developmental Cell
Licensed Content Title	Coordinating Tissue Interactions: Notch Signalling in Cardiac Development and Disease
Licensed Content Author	José Luis de la Pompa,Jonathan A. Epstein
Licensed Content Date	Feb 14, 2012
Licensed Content Volume	22
Licensed Content Issue	2
Licensed Content Pages	11

Start Page	244
End Page	254
Type of Use	reuse in a thesis/dissertation
Intended publisher of new work	other
Portion	figures/tables/illustrations
Number of figures/tables/illustrations	1
Format	both print and electronic
Are you the author of this Elsevier article?	No
Will you be translating?	No
Order reference number	
Original figure numbers	Figure 5
Title of your thesis/dissertation	Characterizing the role of atrial natriuretic peptide signalling in the development of the embryonic ventricular cardiac conduction system
Expected completion date	Aug 2017
Estimated size (number of pages)	270
Elsevier VAT number	GB 494 6272 12
Total	0.00 CAD
Terms and Conditions	